Review

Design and Applications of Water-Soluble Coordination Cages

Edmundo G. Percástegui, Tanya K. Ronson, and Jonathan R. Nitschke*

Read Online

ACCESS | Metrics & More | Article Recommendations

ABSTRACT: Compartmentalization of the aqueous space within a cell is necessary for life. In similar fashion to the nanometer-scale compartments in living systems, synthetic water-soluble coordination cages (WSCCs) can isolate guest molecules and host chemical transformations. Such cages thus show promise in biological, medical, environmental, and industrial domains. This review highlights examples of three-dimensional synthetic WSCCs, offering perspectives so as to enhance their design and applications. Strategies are presented that address key challenges for the preparation of coordination cages that are soluble and stable in water. The peculiarities of guest binding in aqueous media are examined, highlighting amplified binding in water, changing guest properties, and the recognition of specific molecular targets. The properties of WSCC hosts associated with biomedical applications, and their use as vessels to carry out chemical reactions in water, are also presented. These examples sketch a blueprint for the preparation of new metal−organic containers for use in aqueous solution, as well as guidelines for the engineering of new applications in water.

CONTENTS

1. INTRODUCTION

Life consists of highly interconnected networks of aqueous chemical transformations occurring independently, in cascades, or in a periodic fashion along specific physiological pathways. One of the methods that nature uses to control these processes is to employ confined spaces that select, sort, and spatially

segregate individual tasks.[1] Selective encapsulation of substrates within the confined pockets of enzymes,[2,3] protein receptors,[4−6] or the vesicles that compartmentalize the aqueous medium of living cells,[7,8] prevents crosstalk between subsystems. Accordingly, the fundamental functions of life, ranging from binding regulation,[9] transmembrane communication,[10] metabolic conversions,[11] gene expression,[12] to neurotransmission,[13] can be adjusted in response to the needs of the entire organism. Artificial encapsulants with the ability to express these recognition and catalytic functions in water, the medium of life, open up many potential applications in medicine, biology, industrial processes, and the resolution of environmental problems.[14,15]

This review describes one such class of container molecule, the water-soluble coordination cages (WSCCs). In similar fashion to the nanoenvironments in natural systems, the well-defined hydrophobic inner spaces of WSCCs provide a suitable confined space isolated from the aqueous environment that allows guests to be selectively trapped, sequestered, and released, with consequent control over their chemical reactivity.[16] Likewise, these confined spaces may increase the local concentration of reactants, leading to dramatic enhancements of reaction rates and different product distributions.[17−19] For these reasons, synthetic WSCCs can serve as high-level conceptual models for their biological counterparts.

1.1. Scope and Structure of the Review

This review will explore synthetic methods for the construction of water-soluble metal−organic cages and the aqueous applications of these cages. These aspects will be discussed in the context of the peculiarities of supramolecular chemistry in water,[20,21] where the hydrophobic effect is a key protagonist.[22−25] The cages in question are molecular architectures enclosing three-dimensional cavities, assembled *via* multiple donor→metal coordination bonds.

Points of view may differ as to what constitutes an aqueous solvent mixture; the discussion in this review is limited to cages that can be formed or solubilized in pure water as well as to selected cage exemplars that dissolve in solvent mixtures containing at least 50% H$_2$O. Other reviews cover cases on the borderline or outside of our scope.[26−28] Purely organic molecular containers soluble in water are also excluded from discussion under the above definition; examples of such systems have been the subject of several excellent reviews[29−31] and recent publications.[32,33]

The review is divided into sections covering the synthesis of WSCCs, and then their applications to binding guests and carrying out chemical reactions. In the first section of this review, we briefly touch upon foundational work and key examples of water-soluble discrete coordination assemblies. Discussion is focused on highlighting the strategies that allow the synthesis of such cage species in forms that are soluble and stable in water. The host−guest chemistry of WSCCs is then treated. We next describe the use of WSCCs for the binding of neutral and charged guests in aqueous media, as well as the consequences of binding on either the guest (solubilization or modulation of properties) or the host (structural transformations) before examining biomedically relevant applications. The application of WSCCs to promote stoichiometric and catalytic chemical reactions in aqueous media is finally examined.

We hope that the principles behind the design and functioning of WSCCs compiled in this review may provide a guide to enhancing their properties, the design of new functions, and the development of new technologies based on WSCCs. Beyond WSCCs, we anticipate that these design principles may be extended to other metallosupramolecular systems and stimulate further design of new aqueous metallacycles, self-healing coordination polymers, rotaxanes and catenanes.

2. STRATEGIES FOR AQUEOUS SOLUBILITY AND STABILITY OF COORDINATION CAGES

2.1. General Considerations

Over the last three decades, the construction and chemistry of three-dimensional (3D) coordination cages has been developed extensively.[34] These discrete coordination constructs provide inner nanospaces useful for a wide range of applications.[35] The principles that underpin the assembly of polyhedral coordination cages may also help build our understanding of natural 3D self-assembled structures, for example, viral capsids with octahedral or icosahedral symmetries.[36]

Three-dimensional coordination cages form as the thermodynamically favored product from the spontaneous organization of metal ions and organic ligands. Given that reversible ligand→metal dative bonds are the key motif for the formation of these metal−organic assemblies, this synthetic approach is referred to as *coordination-driven self-assembly*.[37,38] The energies of metal−ligand bonds (15−50 kcal mol^{-1}) are intermediate between the energies of organic covalent bonds (*ca.* 60−120 kcal mol^{-1}) and weaker dispersive interactions (*ca.* 0.5−10 kcal mol^{-1}). This intermediate strength enables self-repair and corrections of kinetic mistakes to achieve thermodynamic control over the formation of superstructures.[39] Moreover, the well-defined coordination geometries of metal ions and the use of rigid donor ligands allow for the prediction of structural outcomes, as the geometries of ligands and metal ions come together to define the symmetry axes of polyhedra.[37] Pioneering work by Lehn,[40,41] Stang,[42,43] Fujita,[44] and Raymond[45] established the utility of this directional bonding approach. Following the formative stages of this field, many 3D metal−organic architectures of varied topologies and geometries have been developed using these principles, prepared by groups around the world. The products thus prepared have been called coordination cages, metal−organic polyhedra (MOPs),[46,47] and capsules.[48] *Coordination cages* herein refers to all such 3D structures built using metal coordination.

Most coordination cages have been prepared and studied in organic solvents. The design of water-soluble and -stable cages has been challenging for three reasons. First, many of the ligands employed are poorly soluble in aqueous solution because they incorporate nonpolar aromatic backbones. These moieties enable the ligands to maintain the rigidity required to minimize the entropic cost of bringing many components together into a large assembly. As more intricate and functional assemblies have been created, more elaborate organic building blocks have been crafted and functionalized with photoactive,[49,50] redox active,[51,52] charged,[53] or chiral[54] groups. These groups thus lend new functionality to the final assembly, but many such functionalized ligands are based on extended aromatic scaffolds which are detrimental to water solubility. Second, because of its coordinating ability, water may also compete as a ligand to bind with the cage metal centers, precluding cage formation.[55] Third, the hydrophobic effects
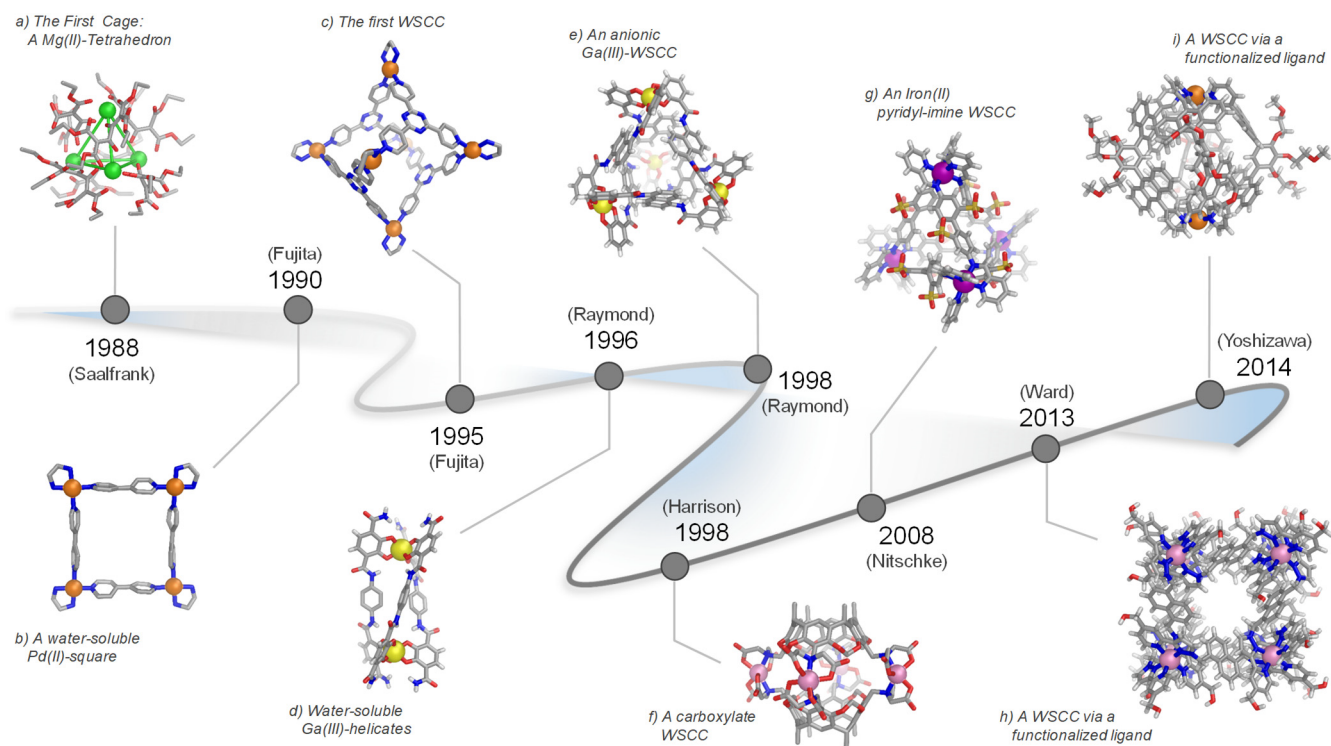
Figure 1. Timeline showing major advances in supramolecular coordination chemistry that have led from (a) the first cage complex to (b−f) early water-soluble complexes in the 1990s, and to (g−i) recent examples of WSCCs synthesized from ligands functionalized with solubilizing functional groups. The name of the group for each work is shown for reference.

engendered by water may alter the way aromatic ligands organize around metal ions, leading to stacking as opposed to the formation of hollow cages.

2.2. A Brief History of Water-Soluble Coordination Cages

This section touches upon key advances in metallosupramolecular chemistry, which have led to the emergence and development of WSCCs (Figure 1), with an emphasis on the synthetic strategies that allow solubility and stability in water. Since the first reported coordination cage,[56] there has been rapid progress in the design of 3D cages, including those that show widespread aqueous applications. Some of the early coordination assemblies turned out to be soluble and stable in water due to the combination of charge and polar functional groups within their structures. Subsequent progress has built upon these early successes to expand the range and size of water-soluble architectures available, a few of which are depicted in Figure 1.

In 1988, Saalfrank and co-workers serendipitously obtained the first self-assembled tetrahedral coordination cage (Figure 1a).[56] While intending to prepare allene compounds, they generated magnesium-malonate structure **1** through the condensation of diethyl malonate with oxalyl chloride in the presence of methylmagnesium iodide as a base. The NMR and X-ray diffraction characterization of the product indicated a high-symmetry structure, the ammonium salt of a tetramagnesium chelate complex (Figure 2). This unprecedented anionic structure consisted of a tetrahedron defined by four magnesium(II) corners and six bis-bidentate organic edges. Although complex **1** was obtained by serendipity and not reported to be soluble in solvents other than methanol, its discovery opened the door to the development of discrete water-soluble metal−organic assemblies.
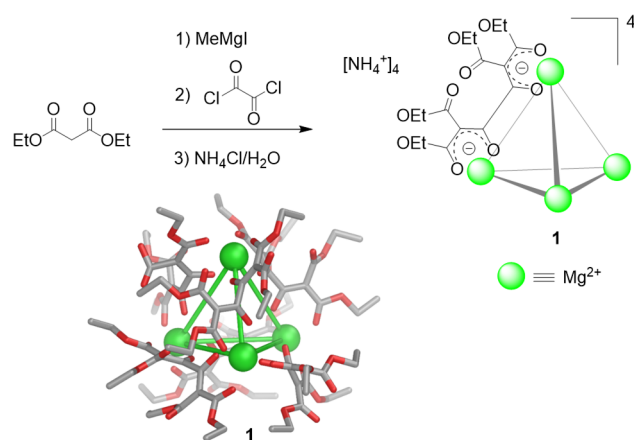
Figure 2. Synthesis of the Mg[II]-based cage (**1**) obtained by Saalfrank.[56] The X-ray crystal structure of anionic $[Mg_4L_6]^{4-}$ (**1**) is shown.

Two years later, Fujita's group prepared square **4**, arguably the most complex water-soluble self-assembled coordination architecture prepared until then (Figure 1b). The hydrogen-bond-donating ability of the capping $[(en)Pd]^{2+}$ units (en = ethylenediamine) (**2**) and the use of hydrophilic nitrate counterions were instrumental in solubilizing this structure in water, despite its hydrophobic 4,4′-bipyridine (**3**) structural elements (Figure 3).[44] This two-dimensional macrocycle also proved capable of incorporating hydrophobic molecules such as 1,3,5-trimethoxybenzene within its interior.

The fundamental concepts uncovered during the preparation of square **4** paved the way for the development of 3D water-soluble coordination cages (Figure 1c). In 1995, the Fujita group revealed that the reaction of $[(en)Pd]^{2+}$ units (**2**)
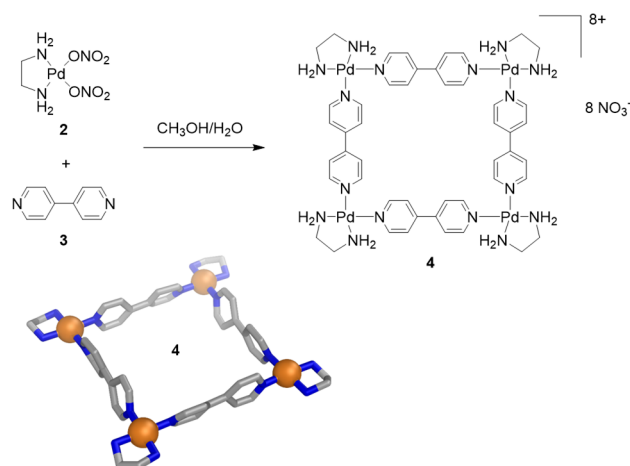
Figure 3. Synthesis of Fujita's water-soluble square (**4**) and the cationic portion of its X-ray crystal structure.[44]

and 1,3,5-tris(4-pyridyl)triazine (**5**) ligands in a 6:4 ratio assembled to produce the first water-soluble molecular cage (**6**) displaying a large enough central void to accommodate guest molecules (Figure 4).[57] The ten-component $[Pd_6L_4]^{12+}$
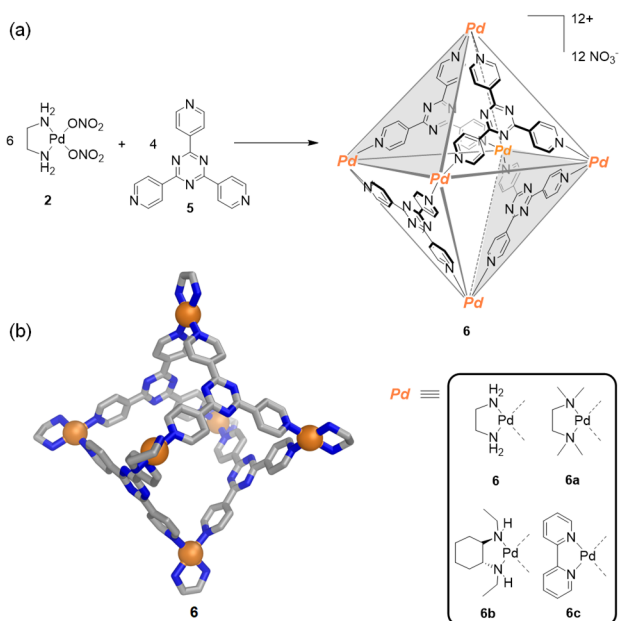
Figure 4. (a) Self-assembly of water-soluble octahedron **6** reported by Fujita.[57] Analogous octahedra can be prepared using different *cis*-capped metallic corners in place of the $[(en)Pd]^{2+}$ units. (b) The X-ray crystal structure of **6**.

molecular structure of **6** was confirmed by X-ray crystallographic analysis. Its four triazine (**5**) panels are held together by six palladium(II) centers, forming what may be considered a truncated tetrahedron, or more usefully, a molecular octahedron with alternate closed and open faces. The Fujita group has explored the use of octahedron **6** for encapsulating guests ranging in size and chemical nature as well as its role in mediating chemical reactions; its many uses have made this cage a milestone in metallosupramolecular chemistry. Likewise, other palladium(II) or platinum(II) complexes with two accessible *cis*-oriented coordination sites (similar to the end-capping $[(en)Pd]^{2+}$ units) have been used to assemble

isostructural analogues of $[Pd_6L_4]^{12+}$ octahedron (**6**). These include $[(tmeda)Pd]^{2+}$ (tmeda = *N,N,N',N'*-tetramethylethylenediamine) (**6a**),[58] chiral $[(EtCyhex)Pd]^{2+}$ (EtCyhex = *cis*-(1*R*, 2*R*)-*N,N'*-diethyl-1,2-diaminocyclohexane) (**6b**), and $[(bipy)Pd]^{2+}$ (bipy = 2,2'-bipyridine) (**6c**)[59] derivatives. This family of $[M_6L_4]^{12+}$ octahedral analogues of **6** display nearly the same shape, size, and binding capabilities regardless of the end-capping groups or the metal employed.

At around the same time, Raymond and co-workers developed the self-assembly of water-soluble dinuclear helicates using C_2-symmetric bis(bidentate) catecholamide ligands. The reaction of three equivalents of ligand **7** with two equivalents of $[M(acac)_3]$ (M = Ga^III, Al^III, Fe^III; acac = acetylacetonate) produced the triple helical complex **8**, which was soluble and stable in water (Figure 5a).[60]

Upon the basis of concepts used in the preparation of **8** (the formation of O−M^III catecholate connections and the overall negative charge of the assembly), they next prepared a new type of water-soluble anionic $[M_4L_6]^{12-}$ tetrahedron (Figure 5b)[45] akin to the $[M_4L_6]^{4-}$ cage reported by Saalfrank. The geometry of bis-catechol ligand **9** (L = 1,5-bis(2,3-dihydroxybenzoylamino)-naphthalene) was designed to avoid M_2L_3 helicate formation while favoring the self-assembly of a M_4L_6 tetrahedron. The naphthalene spacer caused the two catechol binding units to be offset from one another, preventing helicate formation and guiding the system to form cage **10**.

Single-crystal X-ray diffraction studies corroborated the *T*-symmetric structure of **10**, where the four metals defined the vertices of the tetrahedron and the six naphthalene-based bis-catecholate ligands spanned its edges. In this case, one of the Et_4N^+ counterions was located inside the cage cavity. Cage **10** was obtained as a racemic mixture of tetrahedra that contained homochiral (all Δ or Λ) metal centers.

In 1998, Harrison et al. introduced carboxylate coordinating groups into the design of WSCCs. A water-soluble capsule based on a resorcinarene ligand equipped with iminodiacetate chelating groups (**11**), shown in Figure 6,[62] was observed to self-assemble to produce cobalt(II)-capsule **12** when treated with $Ba(OH)_2$ in the presence of potassium carbonate (pH ≈ 6) and cobalt(II) chloride. Crystallographic analysis showed that **12** possessed approximate D_{4h} symmetry, with two cup-shaped resorcinarenes held together by four pseudooctahedral cobalt(II) ions, each coordinated to two doubly deprotonated iminodiacetates. The charge of the octaanionic cage was balanced by barium(II) and cobalt(II) countercations. Although cage **12** readily assembled at pH 6, lowering the pH to 1 triggered cage disassembly and concomitant carboxylate protonation. However, the capsule was observed to reform upon raising the pH.

The advent of these cages and other new molecular containers[63] paved the way for the development of new functions and applications. It was recognized that their well-enclosed interiors could trap chemicals, safeguard guests from reacting, and conversely provide a new medium to carry out reactions. The field of coordination cages has prospered as chemists have come to an understanding of how organic and metallic building units link together. The result has been a collection of complex molecules of varying structures and applications.

Despite key early work by the Fujita and Raymond groups on water-soluble cages, most cage work since has been in organic solution. The time is thus ripe to come back to water, to see what might be done now that had been difficult before.
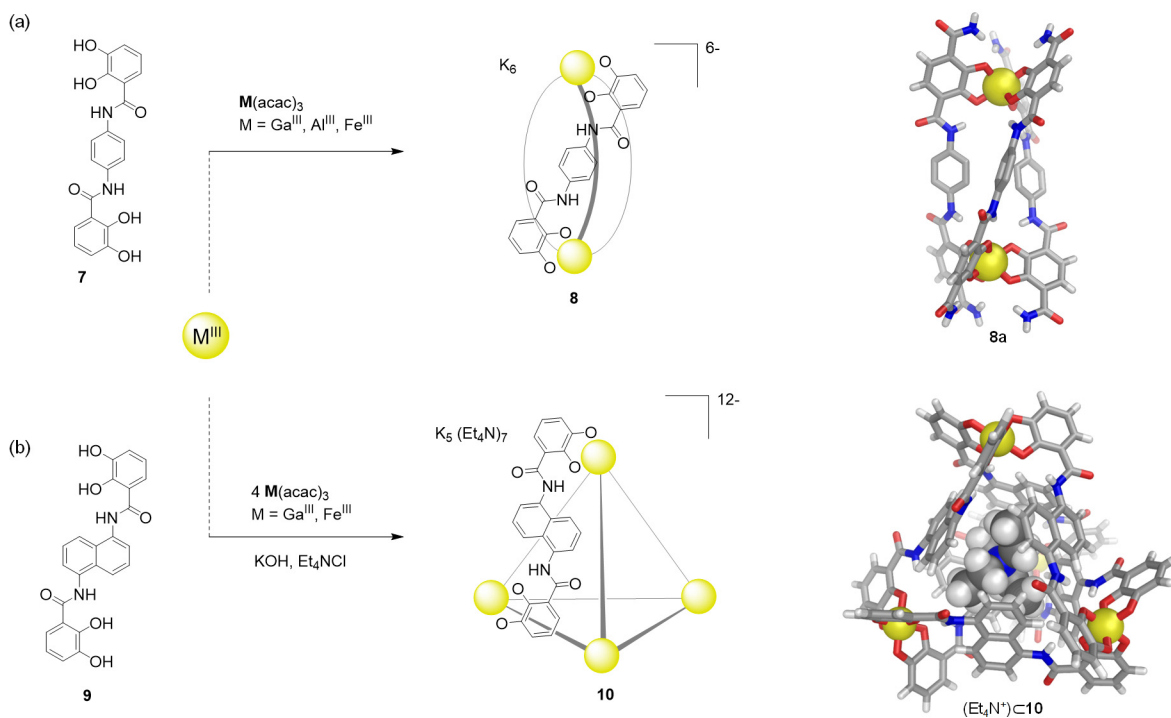
Figure 5. (a) The C_2-symmetric catechol ligand **7** combined with trivalent metal ions to yield dinuclear helicates[60] of type **8**; the anionic part of the X-ray crystal structure of a gallium(III) helicate (**8a**)[61] obtained from a modified version of ligand **7** is shown. (b) The similar ligand **9**, based on a naphthalene spacer, selectively self-assembles with Ga^{III} or Fe^{III} to afford water-soluble tetrahedron **10**;[45] the anionic part of the X-ray structure of complex $K_5(Et_4N)_7[Fe_4L_6]$ containing an encapsulated Et_4N^+ is shown.
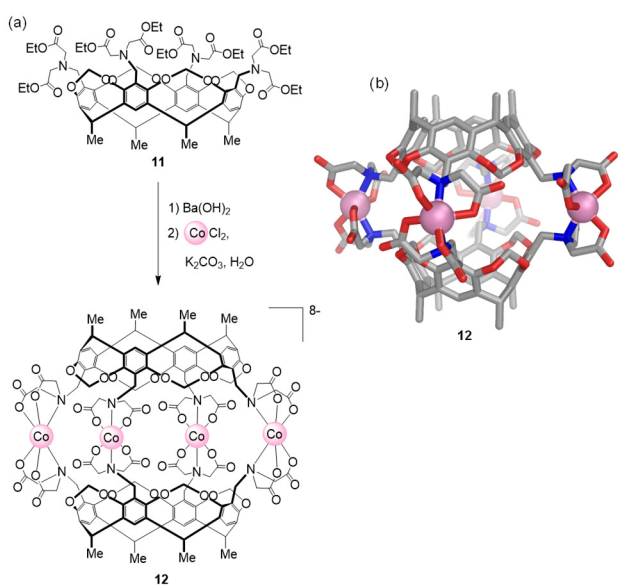
Figure 6. (a) Synthesis of capsule **12** built from two **11** ligands and Co^{II} ions.[62] (b) X-ray structure of **12** showing the four cobalt(II) ions around the periphery.

2.3. Strategies to Prepare Water-Soluble Cages

One of the first general strategies for the preparation of WSCCs was demonstrated by the Fujita group. As an extension of their original work leading to square **4** and octahedron **6** (Figures 3 and 4), they showed that the simple combination of *cis*-capped $[(en)Pd(NO_3)_2]$ complex **2** with rigid pyridine/pyrimidine molecular panels (*e.g.*, **13**–**23**) resulted in the self-assembly of a variety of elegant polyhedral architectures, some of which (**14**–**24**) are shown in Figure 7.[64]

The authors point out that although these cages have hydrophobic cavities, they are water-soluble due to the cationic charges associated with their palladium(II) centers. Their nitrate counterions also augment the water solubility of these structures.[65,66] Likewise, the $[(en)Pd]^{2+}$ units are crucial for successful self-assembly. Whereas the pyridine-containing bridging ligands undergo substitution at the Pd^{II} centers, allowing for thermodynamically disfavored intermediate structures to rearrange to generate the polyhedral thermodynamic products, the ethylenediamine ligand is kinetically inert due to its five-membered *cis*-chelating configuration.[67] Thus, the multiple $[(en)Pd]^{2+}$ corners also provide structural stability, and may be regarded as solubilizing groups, because ethylenediamine itself is highly soluble in water. The generality of this approach is further demonstrated by examples from the Mukherjee[68] and Klajn[69] groups, who also showed that it is possible to employ imidazole-containing ligands in place of the pyridines originally used by the Fujita group to efficiently form WSCCs (*vide infra*).

Most coordination cages have cationic or anionic overall charge, and as noted above, they are insoluble in water but dissolve in organic solvents such as acetonitrile (MeCN), dimethyl sulfoxide (DMSO), nitromethane, methanol, or dichloromethane. Possession of an overall charge is thus not sufficient for a cage to be water-soluble. More elaborate organic building blocks, many of which incorporate water-solubilizing polar groups, have therefore been explored.

The Nitschke group introduced a new type of water-soluble Fe$^{II}_4$L$_6$ tetrahedron in 2008.[70] This cage was obtained using the subcomponent self-assembly method developed by this group.[71] This technique involves the simultaneous formation of dynamic coordinative N→M and covalent C=N bonds, in turn leading to the *in situ* construction of pyridyl-imine
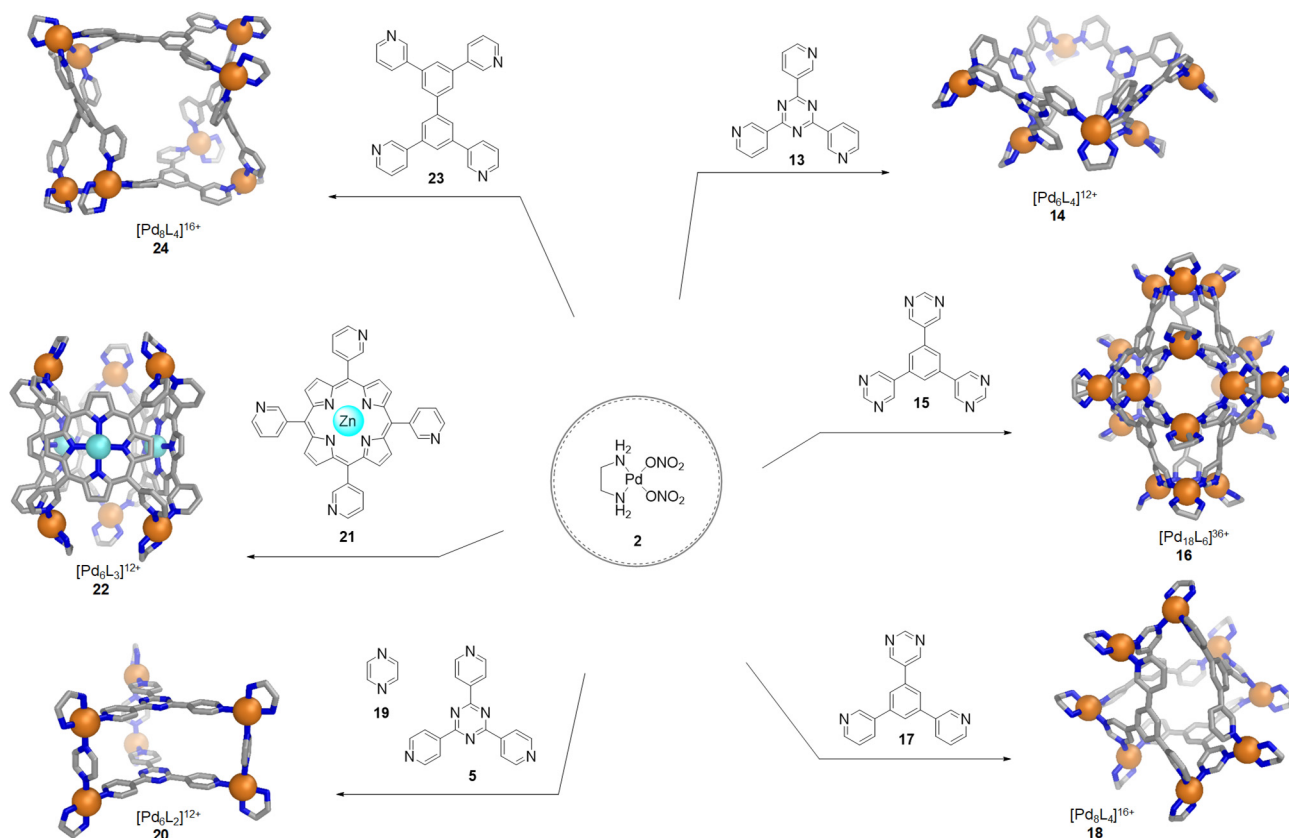
Figure 7. Reactions of $[(en)Pd(NO_3)_2]$ (**2**) with rigid oligo(pyridine/pyrimidine) "panels" enable the formation of WSCCs.[64] Examples of these ligands and the X-ray crystal structures of the corresponding cages are shown.

chelating ligands (L) and their organization around metal ion templates. This method has proven useful for constructing many different water-soluble cages, with examples that are discussed throughout this review.

The subcomponents 2-formylpyridine (**25**) and 4,4′-diaminobiphenyl-2,2′-disulfonic acid (**26**), containing two solubilizing sulfonate groups, were thus selected. Their aqueous reaction with iron(II) and base yielded tetrahedron **27** as the uniquely observed product (Figure 8).

Cage **27** contains exclusively iron(II) ions in the low-spin state, as indicated by its diamagnetic NMR spectrum and intense metal-to-ligand charge transfer transitions, which give rise to a deep-purple coloration. The X-ray structure of **27** confirmed the formation of an anionic tetrahedron with four Fe^{II} vertices and six bis-bidentate ligand edges, which resulted from the condensation of **25** and **26**. The sulfonate groups of **27** are symmetrically arrayed toward the exterior, lending high aqueous solubility to **27** (34 g L^{-1}). Cage **27** is stable in solution due to the strong binding and mutual stabilization between iron(II) and the imine ligands. The water solubility of **27**, together with its hydrophobic internal cavity (141 $Å^3$), have enabled this cage to encapsulate a wide range of guests, as noted below.

On the basis of the successful synthesis of **27**, enantiopure water-soluble cages were later prepared with applications in molecular binding and catalysis.[72] Diamino terphenylene subcomponent **28** was thus prepared, functionalized with chiral glyceryl groups, along with its enantiopure derivatives (S,S)-**28** and (R,R)-**28**. Self-assembly reactions of these subcomponents with 2-formylpyridine (**25**) and iron(II)
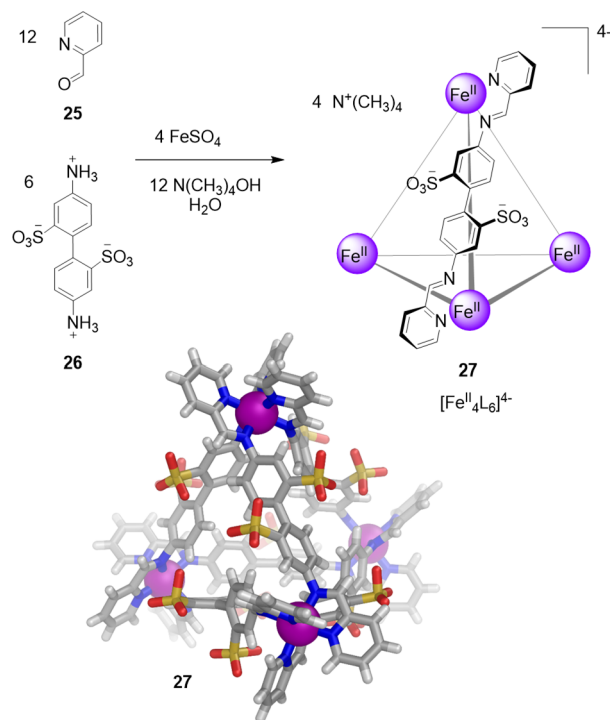
Figure 8. Aqueous subcomponent self-assembly reaction to prepare the tetramethylammonium salt of cage **27**;[70] the anionic portion of its X-ray crystal structure is depicted.

sulfate yielded the corresponding chiral $[Fe^{II}_4L_6]^{8+}$ capsules ΔΔΔΔ-**29** and ΛΛΛΛ-**29** in water (Figure 9a).
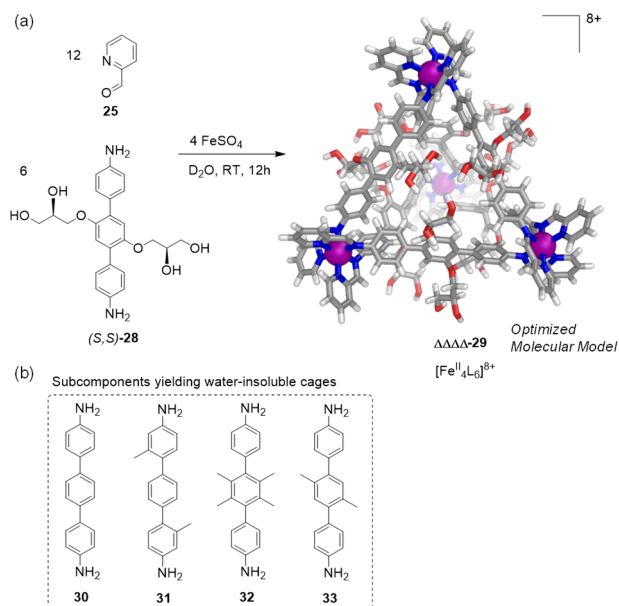
Figure 9. (a) Enantioselective formation of ΔΔΔΔ-**29** from (*S,S*)-**28**;[72] the universal force field (UFF) model of ΔΔΔΔ-**29** is shown. (b) Previously reported 4,4′′-diamino-*p*-terphenyls **30**−**33** led to water-insoluble cages.

Figure 10. (a) Self-assembly of Co[II] ions with **34** led to water-insoluble cube **35**.[74] The analogous reaction using **36**, equipped with hydroxymethyl groups yielded water-soluble cage **37**.[75] (b) View of the X-ray structure of WSCC **37**, emphasizing the windows leading to the central cavity, and the decoration of the external surface with hydroxyl groups.

Previously, a series of related terphenyl-edged $[Fe^{II}_4L_6]^{8+}$ tetrahedra had been prepared, which were only soluble in acetonitrile due to the lack of hydrophilic substituents on their 4,4′-diamino-*p*-terphenyl subcomponents **30**−**33** (Figure 9b).[73] The glycerol groups thus serve not only to render **29** water-soluble but also to dictate the handedness of the iron(II) stereocenters despite the distance between stereochemical elements. Cages ΔΔΔΔ-**29** and ΛΛΛΛ-**29** thus formed enantioselectively from the enantiopure subcomponents (*S,S*)-**28** and (*R,R*)-**28**, respectively.

Ward and co-workers also developed synthetic strategies to enhance the aqueous solubility of coordination cages. In 2008 they established that the self-assembly of cobalt(II) ions with ligand **34**, based on a naphthalene-1,5-diyl spacer with two chelating pyrazolyl-pyridine units, led to the quantitative formation of $[Co^{II}_8L_{12}]^{16+}$ cage **35** (Figure 10a).[74] This cage displayed an approximately cubic arrangement of eight octahedral Co[II] corners, with a bridging ligand spanning each of the 12 edges. This first exemplar **35** was soluble only in polar organic solvents such as acetonitrile, in which it showed the ability to bind diverse molecular guests (see below).

A water-soluble version of cage **35** was subsequently realized.[75] The attachment of hydroxymethyl substituents to the pyridyl-C^4 sites of ligand **34** gave rise to new ligand **36**. The subsequent reaction of **36** with $Co(BF_4)_2$ in a 3:2 ratio yielded cage **37**, isostructural to **35** but water-soluble due to the presence of 24 outward-facing hydroxyl groups (Figure 10a). The internal cavity of the cage is hydrophobic, lined with CH and CH_2 groups from the ligands.

Single crystals of **37** were obtained from MeOH and X-ray crystallographic analysis confirmed that cage **37** was structurally analogous to the parent unsubstituted cage **35** (Figure 10b). Cage **37** exhibited the expected octanuclear core structure, approximating to a cube with (noncrystallographic) S_6 symmetry.

Research from the Yoshizawa group also highlights the benefits of attaching solubilizing groups onto ligands to improve the aqueous solubility of $[Pd_2L_4]^{4+}$ hosts. To obtain molecular hosts combining solubility in protic solvents and photoactive properties, Yoshizawa and co-workers designed ligand **38**, with two anthracene panels and two methoxyethoxy groups on the central *m*-phenylene ring. The combination of Pd[II] ions and **38** in a 1:2 ratio favored the exclusive formation in DMSO of $[Pd^{II}_2L_4]^{4+}$ capsule **39** (Figure 11a).[76] The presence of eight such pendant hydrophilic chains per cage facilitated the dissolution of **39** in DMSO and in 2:1 $CD_3OD:D_2O$.

To render this class of molecular host soluble in pure water, ligand **40** was prepared, containing an additional methoxyethoxy group attached to the *m*-phenylene ring (Figure 11a).[77] Self-assembly of palladium(II) ions with **40** afforded spherical capsule **41**, possessing 12 hydrophilic chains that endowed it with solubility in H_2O and also in 9:1 $D_2O:CD_3CN$ (Figure 11b). A Pt[II] version of **41** has also been prepared by the Yoshizawa group and extensively used for guest binding, as described in subsequent sections.

The same group elucidated that the additional methoxyethoxy groups in going from **42** to **43** (Figure 12) enabled the corresponding double $[Pd^{II}_3L_4]^{6+}$ capsule to become soluble in aqueous solutions.[78] Both capsules **44** (from ligand **42**) and **45** (from **43**) were prepared in DMSO, but only **45**, bearing eight more methoxyethoxy groups than **44**, proved soluble beyond DMSO in CH_3CN (>30 mM) and even 100:1 H_2O/CH_3CN (~30 mM) solutions.

Similarly, research from the Crowley group corroborates the successful use of ligands grafted with hydrophilic groups to obtain water-soluble coordination cages. The combination of 2,6-bis(pyridin-3-ylethynyl)pyridine (**46**) with palladium(II) nitrate yielded the $[Pd^{II}_2L_4]^{4+}$ capsule **47** as a water-insoluble complex (Figure 13a);[79] the use of other anions did not increase water solubility. Only ligands **48**[80] and **49**,[81]
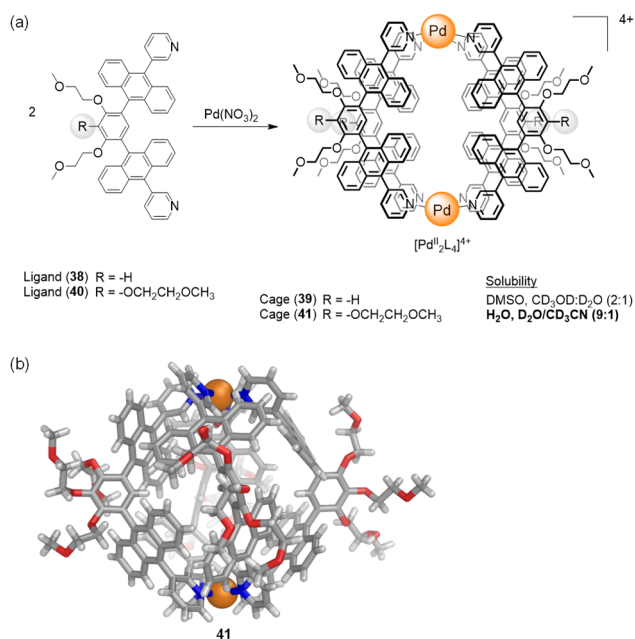
Figure 11. (a) Reaction of Pd^{II} with ligands **38** and **40**, containing a different number of solubilizing chains, led to organic-soluble cage **39**[76] and its water-soluble analogue **41**,[77] respectively. (b) X-ray structure of the water-soluble cage **41** showing its 12 pendant solubilizing chains.[77]
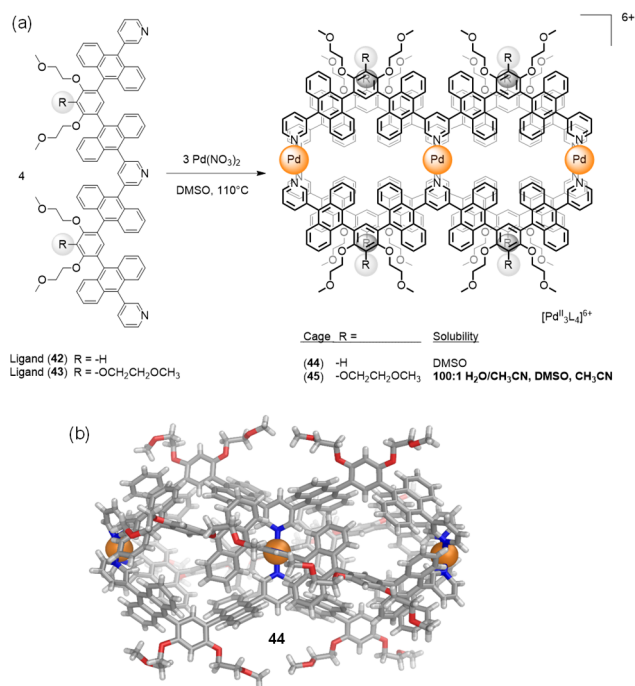
Figure 12. (a) Self-assembly of Pd^{II} ions with W-shaped ligands **42** and **43** (bearing four and six solubilizing chains, respectively) yielded **44** and the more water-soluble **45** dual cavity cages.[78] (b) X-ray structure of the water-insoluble cation **44**.

Figure 13. (a) The self-assembly of Pd^{II} ions with **46** afforded water-insoluble capsule **47**.[79] (b) Water-soluble analogues were obtained using functionalized ligands **48**[80] or **49**[81] instead of **46**.

self-assembly of Pd^{II} ions and bent bis-acridinium ligands (Figure 14).[82] Even without pendant hydrophilic groups, these capsules are soluble in water due to their polycationic shells.
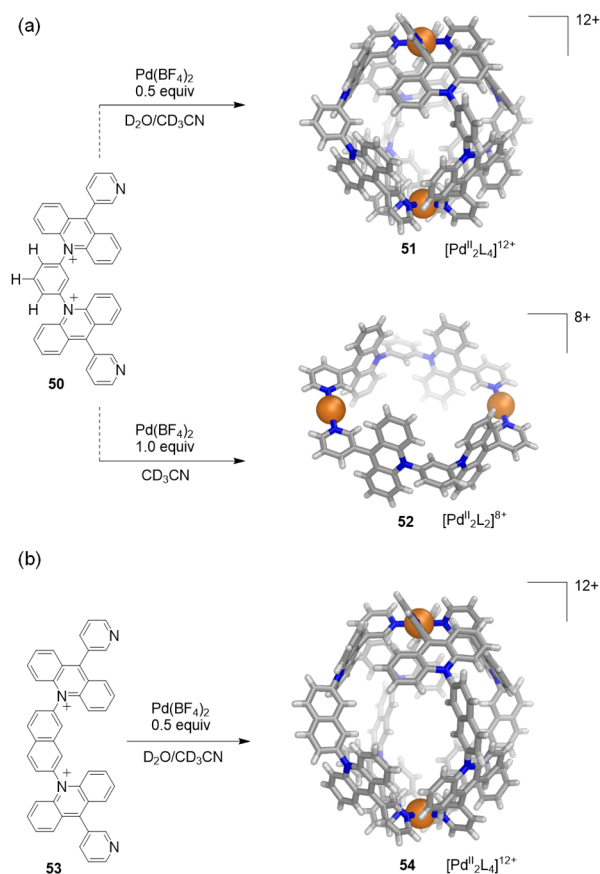
Figure 14. (a) Cationic ligand **50** selectively self-assembles with Pd^{II} ions under different conditions to yield water-soluble capsule **51** or tube **52**. (b) The combination of the elongated cationic ligand **53** with Pd^{II} affords expanded water-soluble capsule **54**. The X-ray structures of the products are depicted.[82]

analogous to **46** but equipped with hydrophilic solubilizing groups (Figure 13b), yielded water-soluble cages.

Organic ligands containing charged groups have also proven valuable for the formation of coordination cages soluble in water. The Yoshizawa group reported the preparation of new polycationic capsular and tubular nanostructures through the

As compared with neutral bis-anthracene ligand **39** with pendant hydrophilic groups (Figure 11), cationic analogue **50** shows higher solubility (>4 mM) in water and selectively forms well-defined capsular or tubular structures depending on the ratio between ligand and metal ion. When ligand **50** (1.6 mmol) and [Pd(CH$_3$CN)$_4$](BF$_4$)$_2$ (0.8 mmol) were mixed in 5:1 D$_2$O:CD$_3$CN at room temperature, [Pd$^{II}_2$L$_4$]$^{12+}$ capsule **51** was formed quantitatively. Conversely, mixing ligand **50** and Pd^{II} ions in a 1:1 ratio in CD$_3$CN resulted in the formation of the octacationic [Pd$^{II}_2$L$_2$]$^{8+}$ tube **52**. The capsule and the tube display closed spherical and open cylindrical cavities surrounded by cationic panels and with ~1 nm diameters. The long-axis expansion of spherical capsule **51** was accomplished through the use of elongated bis-acridinium ligand **53** containing a naphthalene spacer, which enabled preparation of [Pd$^{II}_2$L$_4$]$^{12+}$ capsule **54**, with an open elliptical cavity (Figure 14b).

Other pyridinium-based ligands proved capable of generating water-soluble coordination assemblies. Peinador, Quintela, and co-workers prepared Pd^{II} and Pt^{II} water-soluble metallacycles and 2D receptors using this approach.[83−85] Mukherjee and co-workers presented water-soluble "molecular dice" (**56**) synthesized *via* coordination-driven self-assembly of flexible, cationic, tritopic ligand **55** (Figure 15a).[86] Likewise, Sun and
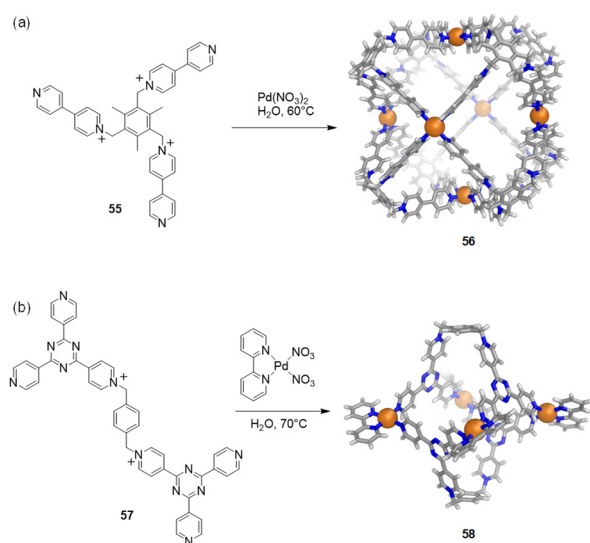
Figure 15. Examples of WSCCs based on palladium(II) ions and pyridinium ligands. (a) Synthesis of Mukherjee's "molecular dice" (**56**)[86] and (b) Sun's nanocapsule **58**.[87] X-ray structures of the cages are depicted.

co-workers reported the self-assembly of photochromic, redox-capable nanocapsule **58** made of four *cis*-blocked palladium corners and two pyridinium-functionalized tetratopic ligands (**57**), which contain two tris(4-pyridyl)-1,3,5-triazine bridged by a *p*-xylene linker (Figure 15b).[87]

So far, we have presented cases of self-assembly reactions that directly yield coordination cages that are soluble in water because the building blocks integrate charge or solubilizing groups into the final structure (*e.g.*, ethylenediamine, glycerol, sulfonate). Sometimes it is not straightforward to integrate all of the structural elements required to directly form a WSCC. This approach often requires the preparation of hydrophilic ligands, whose preparation may be synthetically demanding, necessitating the installation of polar solubilizing groups or

cationic elements. Greater synthetic complexity may hinder widespread uptake of WSCCs for applications.

To circumvent the limitations imposed by synthetic complexity, our group has reported an alternative approach to WSCCs. Starting from the premise that the aqueous solubility of large, cationic cages may be sensitive to the identity of their counteranions, we have developed a simple anion-exchange protocol that allowed the solubilization in water of hydrophobic cages prepared using iron(II)-templated subcomponent-self-assembly.[88]

This method consisted of exchanging the less hydrophilic trifluoromethanesulfonate (triflate, OTf$^-$) counterions of cages, initially formed in acetonitrile and constructed using hydrophobic ligands, for more hydrophilic sulfate (SO$_4^{2-}$). This strategy was applied to a series of capsules representative of those designed by our group.[89] Importantly, none of these capsules could be prepared directly from iron(II) sulfate. Direct preparation worked only when sufficiently water-soluble and hydrophilic subcomponents were involved (*e.g.*, cages **27** and **29**, Figures 8 and 9).

As an example of this anion-exchange method, water-insoluble porphyrin cube **60** (Figure 16) was first obtained
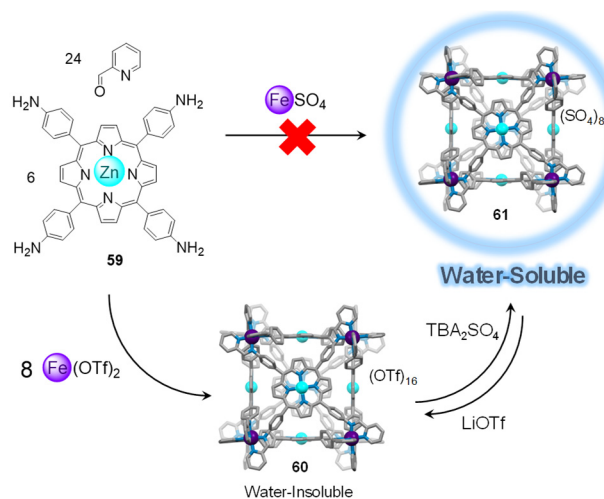
Figure 16. Preparation of water-insoluble cube **60** and reversible anion exchange to obtain water-soluble cube **61**, the direct synthesis of which is not possible. Adapted with permission from ref 88. Copyright 2017 Wiley-VCH.

from the reaction of iron(II) triflate with zinc(II)-porphyrin **59** and 2-formylpyridine **25** in *N,N*-dimethylformamide (DMF).[88] Cube **60** is composed of six faces defined by porphyrin ligands and eight low-spin Fe^{II} corners, and it is soluble in DMF and MeCN but insoluble in H$_2$O. Anion metathesis of **60** with tetrabutylammonium (TBA) sulfate in MeCN led to precipitation of the corresponding octasulfate cube **61** that remained soluble and stable in water over months, even at 0.015 mM concentration.

Attempts to directly prepare sulfate cube **61** from its components and FeSO$_4$ in diverse solvent systems (DMF, MeCN, 1:1 DMF/H$_2$O, 1:1 MeCN/H$_2$O, or 1:1 MeOH/ H$_2$O) were unsuccessful, affording intractable solid products. The anion-exchange strategy, combining subcomponent self-assembly and anion metathesis, thus provides a powerful means of generating WSCCs from highly hydrophobic ligands. Generally, it has been observed that subcomponent self-assembled cages prepared as triflate (TfO$^-$) or triflimide

(Tf_2N^-) salts are soluble in organic solvents. The subsequent addition of excess tetrabutylammonium sulfate induces the spontaneous precipitation of the sulfate salt of the cage in a water-soluble form.[90,91]

2.4. Strategies to Improve Cage Stability in Aqueous Media

The construction of coordination cages that are not only soluble but stable in water can be difficult. Even if the requirements for aqueous solubility are satisfied, water may perturb the reversible ligand→metal connections. Water is a coordinating solvent and a competitive ligand for metal complexes.[55] It may thus act to hinder the formation of a cage, or to compromise the structural integrity of a preformed assembly upon dissolution, by competing with cage ligands.

One strategy to create cages that withstand water involves the use of kinetically inert metal ions. Second- and third-row d-block elements have thus served to generate kinetically robust structures, which may be either insoluble or soluble in aqueous media.[92] For metal ions of similar ionic radii, lability depends strongly on charge, with more highly charged ions having slower water-exchange rates than less highly charged ions.[93,94]

In two separate studies, the Raymond group demonstrated the preparation of a series of catecholamide-based M_4L_6 tetrahedral clusters, isostructural to the well-studied $[Ga^{III}_4L_6]^{12-}$ cage **10** but less kinetically labile due to the presence of tetravalent metal ion vertices (Figure 17).[95] Their
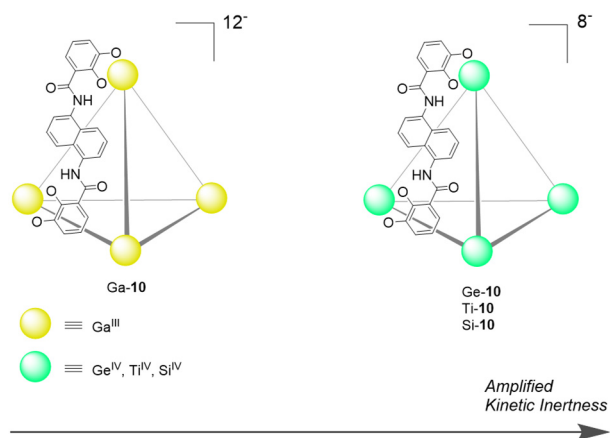
Figure 17. $[Ga_4L_6]^{12-}$ tetrahedron Ga-**10** and its less-labile congeners $[M_4L_6]^{8-}$ (M = Ge^{IV}, Ti^{IV}, Si^{IV}), built using tetravalent metal ions.[95,96]

syntheses required higher temperatures and longer reaction times, a consequence of the lower lability of the M^{IV}–catecholate bonds.[96] Guest templates were also required for their assembly. Ligand exchange studies with mononuclear Ga^{III} and Ge^{IV} analogues of the cage vertices supported the conclusion that there is a significant difference in lability between catecholate complexes of each metal.[95]

Despite the gain in kinetic inertness, it was observed that replacement of Ga^{III} for a tetravalent ion led to decreased aqueous solubility, presumably due to a decrease in the negative charge of the cage framework.

Recently, Zhang and co-workers have reported a water-soluble and stable Ti_4L_6 tetrahedron (**62**) incorporating calixarene-like coordination vertices (Figure 18).[97] This cage is a mixed-valent Ti^{III}/Ti^{IV} complex built using bis-(naphthylene) ligand **63**, the carboxylate and phenolate groups of which bind well to titanium ions. X-ray crystallography of **62**
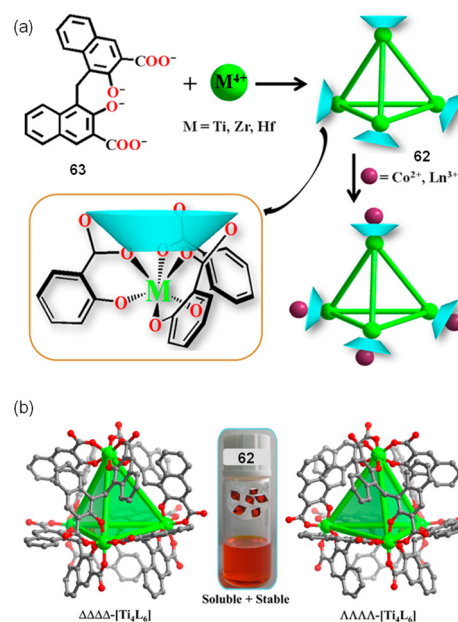
Figure 18. (a) Assembly of tetrahedral Ti_4L_6 cage **62**, the vertices of which bound Co^{II} or Ln^{III} ions. (b) X-ray structures of the ΔΔΔΔ and ΛΛΛΛ enantiomers of **62**. Inset: photo of cage crystals in DMF/H_2O solution. Adapted with permission from ref 97. Copyright 2017 American Chemical Society.

confirmed the *T*-symmetric cage framework, of which both ΔΔΔΔ and ΛΛΛΛ enantiomers were observed in the crystal (Figure 18b). Free carboxylate oxygen atoms from the three different ligands around each Ti center formed a calixarene-like array and proved capable of binding additional Co^{II} and Ln^{III} ions. Cage **62** dissolved in water (2.5 g L^{-1} at 80 °C) and remained stable. The methodology to construct this type of tetrahedral cage proved general, enabling the preparation of Zr^{IV} and Hf^{IV} analogues.

Metal−organic cages built using carboxylate ligands and first-row transition metals often decompose in water. For example, cages incorporating dicopper(II) paddlewheel motifs tend to be readily hydrolyzed,[98] with good aqueous stability rarely observed.[99,100] However, Zhao, Yuan, and co-workers developed a family of stable zirconium metal−organic polyhedra (**64**−**67**), composed of trinuclear zirconium clusters and bridging carboxylate ligands (Figure 19).[101] The authors undertook a systematic study of their stability in aqueous media, using high-resolution electrospray ionization mass spectrometry (ESI-TOF-MS) analyses in H_2O/MeCN. After 1 day in solution, the ESI-TOF-MS spectra showed signals consistent with the presence of undamaged tetrahedral cages in solution over the pH range of 2.0−10.0. Cage decomposition was only detected at pH values above 10.0.

To further probe the stability of these tetrahedra, the authors investigated the covalent postassembly modification (PAM)[102,103] of cage **65** bearing one NH$_2$ group on each of its six carboxylate linkers.[104] The Mannich reaction of **65** with formaldehyde in methanol and water at 25 °C was monitored by ESI-TOF-MS (Figure 19b). After a reaction time of 24 h, mass spectra were dominated by signals corresponding to **65** decorated with five or six CH$_2$OCH$_3$ groups. The observed stability of the Zr^{IV}-tetrahedra in neutral, acidic, and even weakly basic aqueous environments, which is comparable to
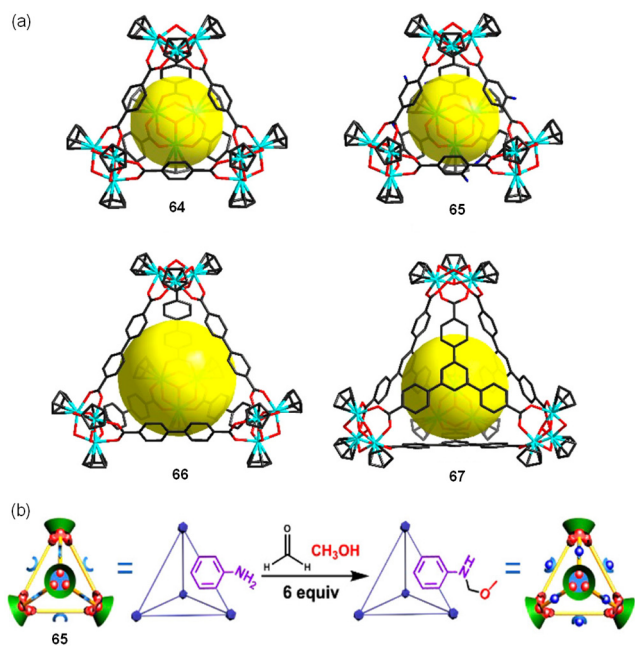
Figure 19. (a) Crystal structures of zirconium tetrahedra **64–67**. Color code: Zr, turquoise; O, red; N, blue; C, black. Yellow balls represent the cage inner void. (b) Scheme for the postassembly modification (PAM) of cage **65** containing up to six functionalized sites per cage. Adapted with permission from ref 101. Copyright 2018 American Chemical Society.

that of their MOF counterparts, is attributed to the strong Zr–O bonds.[105]

Recently, our group developed synthetic conditions for the preparation of water-soluble cationic cages as sulfate salts using diverse metal(II) ions as templates (M = Co^{II}, Ni^{II}, Zn^{II} and Cd^{II}). A collection of M_8L_6 cubes, face-capped M_4L_4 tetrahedra, edge-linked M_4L_6 tetrahedra as well as M_2L_3 triple helicates were obtained despite the hydrophobicity and poor aqueous solubility of their organic subcomponents.[89] Both direct cage formation from the metal(II) sulfate and the corresponding subcomponents, and the exchange of triflate for sulfate (as in Figure 16) worked in different cases to make cages of types **73–77** (Figure 20), although the anion-exchange method was more broadly applicable.

Figure 20 summarizes the structures prepared during the course of our studies.[89] Although all of these new sulfate structures dissolved in water, they exhibited markedly different degrees of kinetic stability in aqueous solution. The greatest number of stable structures formed when Ni^{II} was used as a template (four out of five, **73–76**). Fe^{II} and Co^{II} only afforded two stable cages at room temperature (**73** and **74**), whereas all five frameworks containing Zn^{II} or Cd^{II} templates either failed to form or rapidly disassembled upon dissolution in water, with half-lives <30 min.

The formation of water-stable structures containing the more labile Zn^{II} and Cd^{II} ions was possible when the chelating tris(2-aminoethyl)amine (TREN) (**78**) and tris(3-aminopropyl)amine (TRPN) (**79**) were combined with tritopic (**74**) and ditopic (**72**, **80–82**) formylpyridine subcomponents (Figure 21). Notably, the triple helicates and tetrahedra obtained represent the first pyridyl-imine complexes (**83–90**) containing labile Zn^{II} and Cd^{II} ions that are both soluble and stable in water, complementing rare examples of
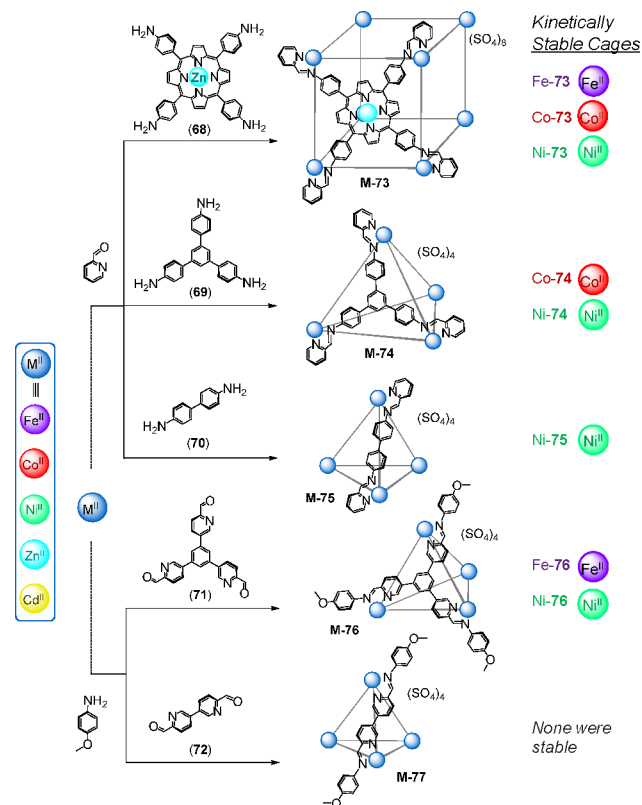
Figure 20. (a) Self-assembly of subcomponents **68–72** with metal(II)-ions (M = Co^{II}, Ni^{II}, Zn^{II}, and Cd^{II}) yielded cages M-**73–77**. Kinetically stable WSCC assemblies were obtained in the cases noted.[89]

aqueous coordination assemblies that incorporate these metal centers.[106–108]

The differences in behavior observed for the architectures shown in Figures 20 and 21 exposed two key factors influencing their kinetic stability in water: (1) stronger metal–ligand bonding led to higher stability, and (2) more dense connections between metals and ligands likewise led to higher stability, considering both ligand topicity (tetratopic > tritopic > ditopic) and degree of chelation.

The stabilizing effects of different metals were evident from the comparison of half-lives ($t_{1/2}$ at 20 °C) and temperatures of decomposition of cubes M-**73** in water (Figure 22). While cubes constructed from Zn^{II} and Cd^{II} survived for only minutes in aqueous solution at room temperature, their Ni^{II}, Fe^{II}, and Co^{II} congeners remained intact for months under identical conditions. Ni-**73** tolerated the highest temperature before decomposing in water. Hence, metal ions stabilize the structures into which they are incorporated following the order $Ni^{II} > Fe^{II} > Co^{II} > Zn^{II} > Cd^{II}$. These observations were found to mirror the trends in the stability constants measured for mononuclear transition metal complexes of 2,2′-bipyridine and 1,10-phenanthroline[109] and the stabilities predicted by the Irving–Williams series.[110] These trends are also reflected in the shorter ionic radii[111] of the metals forming the most stable complexes, and the slower ligand-exchange rate of aqua ligands[112] associated with these complexes. The greater stabilizing effect of Ni^{II} is not exclusive to cube **73**, containing tetratopic ligands; this metal ion also resulted in stable capsules with the tri- and ditopic ligands incorporated into cages **74–76**. These Ni^{II} tetrahedra were stable indefinitely at 298 K, and
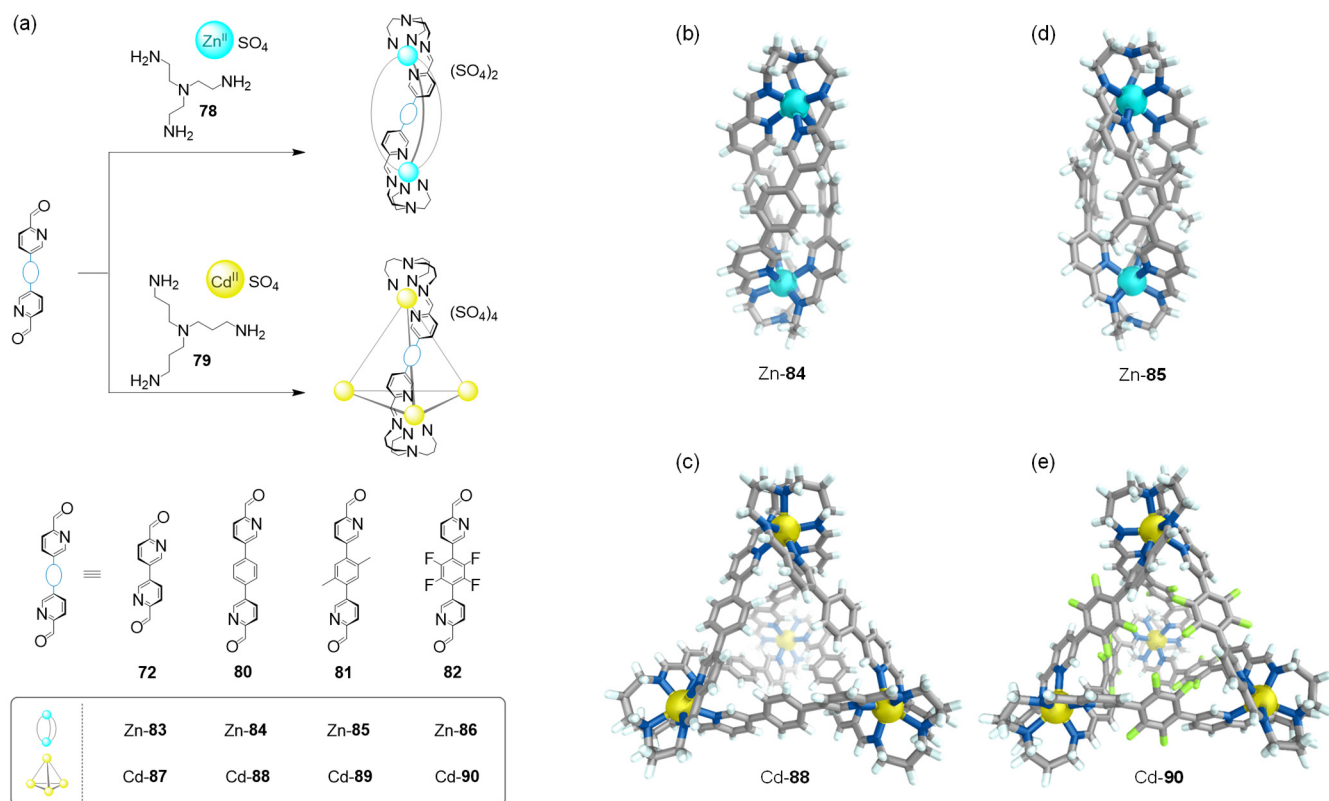
Figure 21. (a) Self-assembly of water-soluble Zn^{II}-helicates and Cd^{II}-tetrahedra from tritopic amines TREN (**78**) and TRPN (**79**) and C_2-symmetric subcomponents **72** and **80**–**82**. Cationic portions of the X-ray structures of (b) helicate Zn-**84**, (c) tetrahedron Cd-**88**, (d) helicate Zn-**85**, and (e) tetrahedron Cd-**90**. Adapted with permission from ref 89. Copyright 2019 Royal Society of Chemistry.
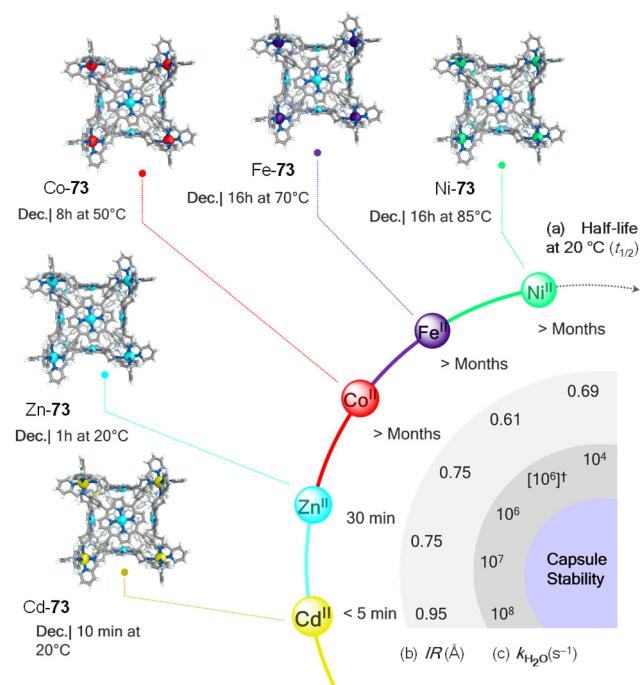
Figure 22. Stability of cubes M-**73** in water noting their decomposition conditions. (a) Half-lives ($t_{1/2}$), (b) ionic radii (*IR*, Å),[111] and (c) ligand-exchange rates for water (k_{H_2O}, s^{-1})[112] for the different metal ions are shown for comparison. †Fe-**76** is low-spin, but k_{H_2O} for high-spin Fe^{II} is given as reference. Adapted with permission from ref 89. Copyright 2019 Royal Society of Chemistry.

disassembly was only observed when aqueous solutions of Ni-**74**, Ni-**75**, and Ni-**76** were heated to 75, 60, and 75 °C, respectively.

An increase in aqueous stability with ligand topicity also clearly emerged from this study. The tetratopic ligands of **73** lend this cubic framework the greatest stability, enabling its formation across the widest range of metal ions. Similarly, the tritopic ligands of tetrahedra **74** and **76** led to stability with a wider range of metal ions than was observed in the cases of their congeners **75** and **77**, which incorporated ditopic ligands. The topicity effect upon stability was inferred to result from the higher degree of binding cooperativity[113,114] imposed by these ligands. For example, it is envisaged that dissociation of a single ligand arm from a tetratopic ligand of cube **73** would require three more arms to disengage in order to free the ligand to precipitate. In contrast, dissociation of one end of a ditopic ligand of tetrahedron **75** would only require the other end to come off for the ligand to be free. Hence, at room temperature, framework **75** disintegrated in water when prepared with iron(II)[88] and cobalt(II) ions; **75** was only stable in water when prepared with the most strongly binding nickel(II) ion.[109]

Similarly, binding cooperativity[113,114] was also essential for the aqueous stabilization of cryptate-like structures **83**–**90** containing the most labile Zn^{II} or Cd^{II} ions and chelating amines (Figure 21). These assemblies must undergo numerous imine hydrolysis steps in addition to deligation in order for their subcomponents to become free to precipitate. A framework containing a single "defect", a free TREN or TRPN amine arm in proximity to an aldehyde would thus experience a high effective molarity[114] for imine condensation,

whereas decomposition would require the two remaining imine arms to hydrolyze. The tightly knit, cooperative construction of these cages thus underpins their aqueous stability. This study thus provides a blueprint not only to prepare water-soluble cages but to render cages stable in aqueous environments, through the choice of the assembling metal ions or ligand topicity.

Although the direct combination of inert metals and ligands is a clear route for the assembly of highly stable WSCCs, as shown above, this strategy can be challenging. In practice, many self-assembly reactions involving inert metals fall into kinetic traps, where oligomeric intermediates forming at initial reaction stages cannot self-repair into the desired structure because of the inertness of their coordinative linkages. The generation of water-soluble cages that integrate inert metals required new methods to be developed.

In 1998, Fujita and co-workers described the conditions required for the self-assembly of a robust WSCC made of platinum(II) ions.[115] This third-row transition metal is more kinetically inert than Pd^{II}, forming Pt−pyridine linkages that are essentially fixed at room temperature. Hence, the authors made use of the thermal labilization of Pt^{II}−N coordinative bonds and the presence of a suitable template for the quantitative formation of platinum(II)-based WSCC Pt-6 (Figure 23), which is isostructural to the octahedron $[Pd_6L_4]^{12+}$ (6) (Figure 4) but displays superior kinetic stability.
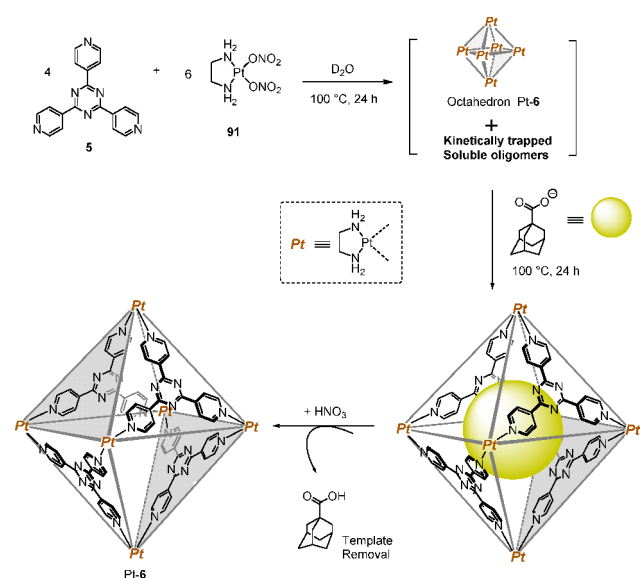
Figure 23. Reaction of 5 with Pt^{II}-complex 91 yielded a kinetic mixture of oligomers containing the target cage Pt-6. Addition and subsequent removal of a template led to the clean formation of the kinetically robust product Pt-6.[115]

The reaction of 1,3,5-tris(4-pyridyl)triazine (5) with bis-(ethylenediamine)platinum(II) nitrate 91 in D_2O at 100 °C yielded a mixture containing kinetic oligomers and the target cage. Addition of a sodium adamantanecarboxylate template and heating to 100 °C for an additional 24 h induced the clean organization of the initial products into octahedron Pt-6. The template was removed in its protonated form by acidification with HNO_3, followed by solvent extraction, without perturbing the cage framework. Nanocage Pt-6 was tolerant to pH < 1 and pH > 11 conditions at room temperature and did not decompose through addition of the nucleophile NEt_3. This

stability toward acidic and basic conditions stands in contrast to that of the palladium(II) counterpart, which was observed to decompose under the same acidic or basic conditions.

Postassembly modification is an alternative strategy to overcome the problem of kinetic traps associated with the use of poorly labile metal ions. In an initial step, labile building blocks self-assemble. Subsequent modification then results in the formation of a kinetically locked state.[92] Taking advantage of the substitutional nonlability of Co^{III} in comparison to Co^{II},[116−118] Lusby and co-workers implemented a postassembly chemical locking protocol to synthesize a water-soluble and robust $[Co^{III}_4L_6]^{12+}$ tetrahedral host (Figure 24).[119] While d^7
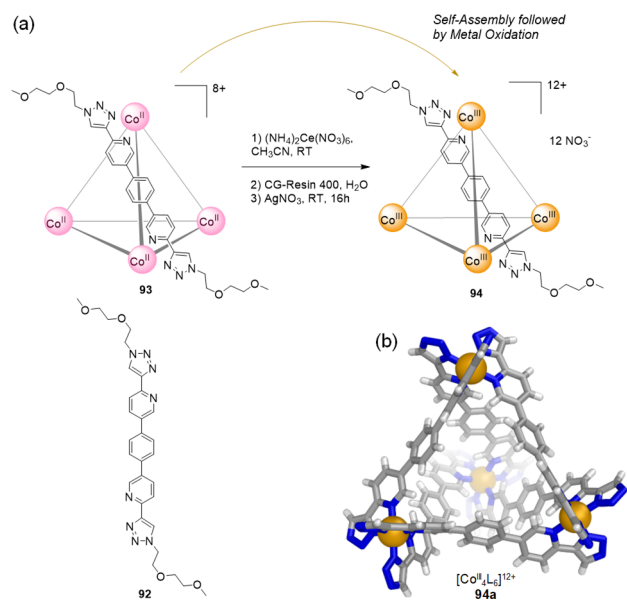
Figure 24. (a) Ligand 92 assembles with Co^{II} to afford cobalt(II) tetrahedron 93, which is transformed into the more robust cobalt(III) tetrahedron 94 through oxidation.[119] (b) X-ray crystal structure of a cobalt(III) cage (94a) obtained from a derivative of ligand 92; peripheral groups are omitted.

Co^{II} has a labile octahedral coordination sphere, Co^{III} has a d^6 electronic configuration and almost always adopts a low-spin, substitutionally inert octahedral configuration.

The reaction of pyridyl-triazole ligand 92 with $Co^{II}(ClO_4)_2$ afforded tetrahedron 93. Subsequent reaction with ceric ammonium nitrate resulted in the formation of oxidized Co^{III} cage 94 with mixed ClO_4^-/NO_3^- counteranions, which was soluble in 1:1 D_2O/CD_3CN. This cage system is constitutionally more robust and less dynamic than 93 due to the inertness of the Co^{III}−N linkages.

To further increase its aqueous solubility, oxidized cage 94 was treated with GC-400 ion-exchange resin and then $AgNO_3$, yielding the water-soluble nitrate salt of the tetrahedron. Cage 94 was indefinitely stable as a 2.5 mM solution in D_2O, even in the presence of 5.0 M $NaNO_3$.

The previous sections summarize the synthetic progress that has led to a better understanding of the elements required to solubilize and stabilize coordination cages in aqueous media. Stable WSCCs have been obtained through the following key strategies: (1) Self-assembly of metal salts containing hydrophilic counterions with organic ligands possessing water-solubilizing polar substituents or charged functional groups. (2) Performing anion-exchange on preformed cages that
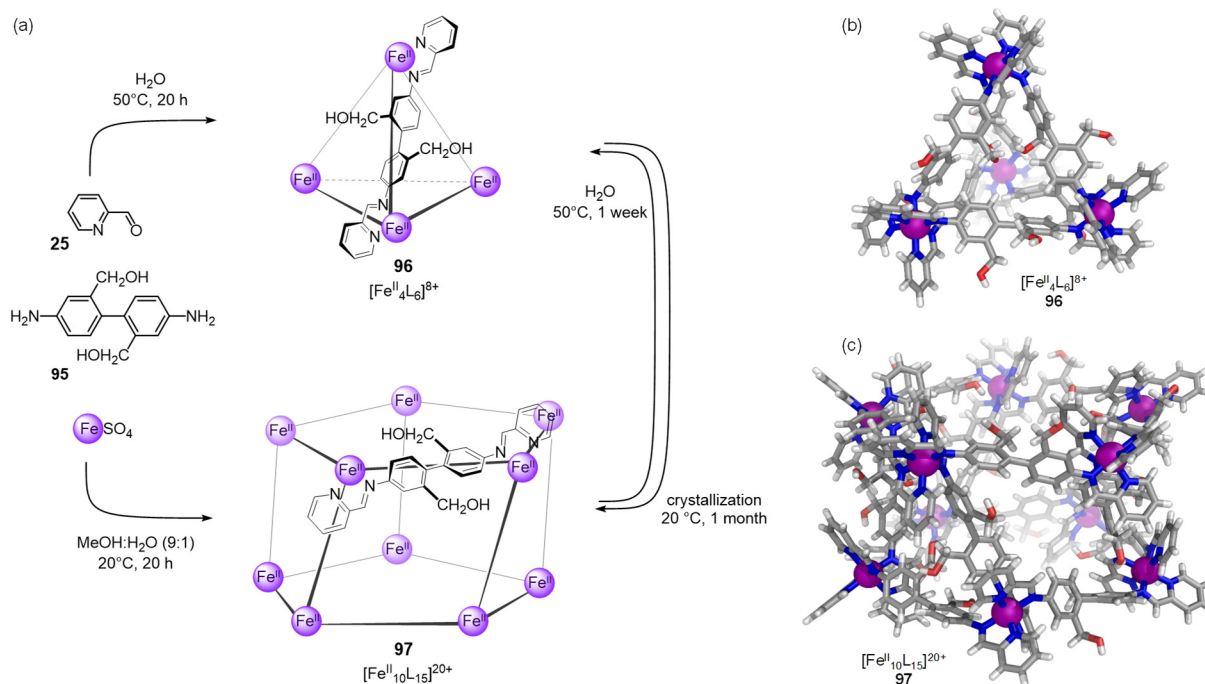
Figure 25. (a) Conditions for the selective preparation of tetrahedron **96** and prism **97** and their interconversion.[120] The cationic parts of the crystal structures of (b) **96** and (c) **97**.
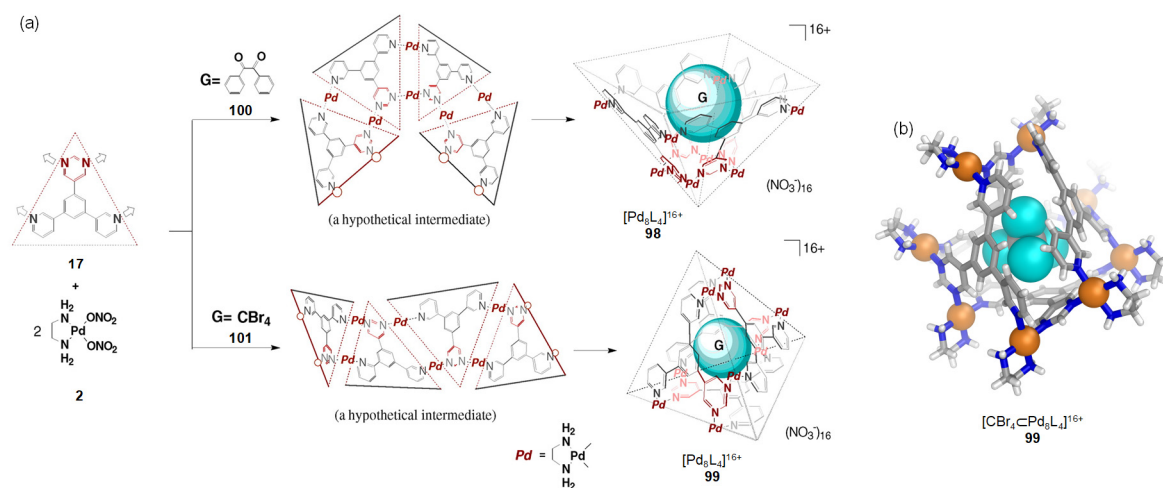
Figure 26. (a) Schematic representation of the template-controlled syntheses of WSCCs **98** and **99**. (b) X-ray structure of tetrahedron **99** with CBr$_4$ in its cavity. (a) Adapted with permission from ref 121. Copyright 2000 American Chemical Society.

cannot be directly prepared using hydrophilic counterions in order to render them water-soluble. (3) Employing metal ions that form strong coordination bonds to produce more robust cages in water. This effect is most pronounced when metal ions that are regarded as kinetically inert (*e.g.*, second- and third-row d−block elements) are employed for self-assembly. (4) Using ligands that contain more chelating groups (higher topicity) to improve the kinetic stability of coordination cages *via* binding cooperativity. (5) Using postassembly modification to further strengthen the aqueous stability of coordination cages, for instance, by increasing the oxidation state and thus the charge and kinetic inertness of a metal ion in a preassembled structure.

2.5. Further Synthetic Considerations

Beyond the geometries and topicities of the ligands, and the preferred coordination environments of the metal ions, other factors may dictate the most stable product formed during aqueous coordination-driven self-assembly. Key factors include the presence of template species, temperature, and solvent composition.

Our group reported that two water-soluble structures, a Fe$^{II}_4$L$_6$ tetrahedron and a Fe$^{II}_{10}$L$_{15}$ prism, can be prepared from the same mixture of starting materials. These products differ based on the adoption of *fac* versus *mer* stereochemistry at the metal centers (Figure 25a).[120] It was observed that the reaction of 2,2′-bis(hydroxymethyl)benzidine (**95**), 2-formylpyridine (**25**), and FeSO$_4$ in water at 50 °C led to the formation of tetrahedron **96**. Crystals of **96** were obtained from slow diffusion of diethyl ether into an acetonitrile solution of the
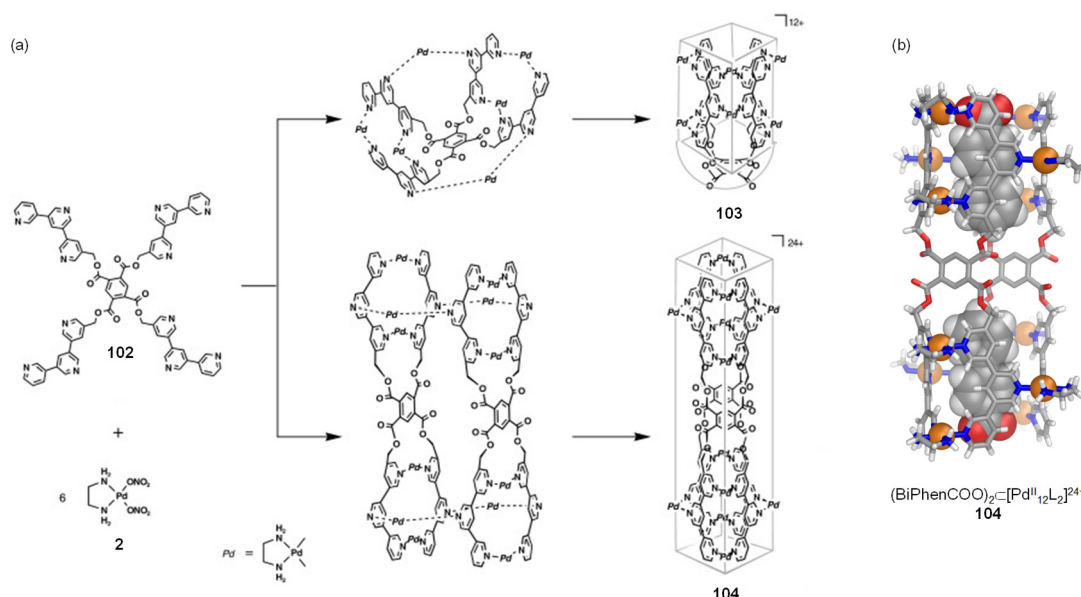
Figure 27. (a) Template-induced self-assembly of monoend-capped tube **103** and dimeric open tube **104**. (b) Crystal structure of **104** with two equivalents of biphenylcarboxylate included. (a) Reproduced with permission from ref 122. Copyright 2003 Wiley-VCH.

PF_6^- salt of **96** and confirmed the tetrahedral assembly, with all metal centers displaying *fac* coordination and the 12 CH_2OH groups directed outward to provide water solubility (Figure 25b).

Crystals of tetrahedron **96** could not be grown from aqueous solution; instead, single crystals of the sulfate salt of prism **97** were obtained. The structure of **97** can be described as a twisted pentagonal prism of D_5 symmetry, with each metal center defining a vertex and adopting *mer* coordination (Figure 25c). This prism is composed of two parallel staggered $Fe^{II}_5L_5$ pentagonal rings, linked at their iron(II) vertices by five bridging axial ligands. Prism **97** was inferred to be a minority product, crystallizing from water due to its lower solubility.

The use of 9:1 methanol/water as reaction solvent allowed for the selective preparation of **97**. Isolated prism **97** did not convert into tetrahedron **96** in solution in either water or 9:1 methanol/water at room temperature, which suggested that **97** was kinetically trapped at this temperature owing to the cooperative locking effect of its 60 Fe^{II}–N bonds. However, complete prism-to-tetrahedron conversion occurred when a solution of **97** was heated to 50 °C for 1 week in either water or 9:1 methanol/water. The selectivity for the synthesis of **97** in 9:1 methanol/water also decreased from >95% to 60% (over 20 h) on raising the reaction temperature from 20 to 50 °C, after 1 week, **97** converted fully into tetrahedron **96**. These findings indicated that both structures exist in an equilibrium that shifts depending on the solvent and temperature employed.

Within a dynamic self-assembling system, different structures may coexist in equilibrium, with molecular templates serving to stabilize and select one from the mixture. For example, the Fujita group observed that the addition of template guests[121] could help select one WSCC from among a library of such cages. In this study, the C_2-symmetric molecular panel **17** could bridge palladium centers (from **2**) in either parallel or antiparallel fashion in D_2O, yielding the open cone **98** or the closed tetrahedron **99**, respectively (Figure 26a).

Both assemblies have the same $[Pd_8L_4]^{16+}$ composition and, therefore, constitute a dynamic receptor library from which

each receptor is selected by its optimal template. Whereas the larger dibenzoyl template (**100**) induced the assembly of open form **98**, the smaller tetrahedral CBr_4 (**101**) templated the formation of closed cage **99**. The structure of **99** was confirmed by X-ray crystallographic analysis, which showed the entrapment of CBr_4 (Figure 26b).

In the absence of a template and at 25 mM concentration, **2** and **17** were observed to assemble into a 3:2 mixture of two products. The minor product was identified as open cone **98**. The proportion of the major product increased at lower concentrations, indicating that this product contained fewer components than **98**. Fujita and co-workers tentatively assigned the major product to a trimeric open-cone structure of $[Pd_6L_3]^{12+}$ composition.

The Fujita group also observed that one template induced the formation of two different assemblies at different concentrations (Figure 27a).[122] The combination of palladium(II) complex **2** and ligand **102**, bearing four terpyridine moieties on a benzenetetracarboxylate scaffold, was expected to yield the monoend-capped nanotube **103** in the presence of a suitable template. With no template, the combination of **2** and **102** in D_2O resulted in the formation of a complex mixture. In the presence of biphenylcarboxylate and at lower concentration ($[102] = 2.1$ mM), the self-assembly reaction afforded only the isomer of **103**, in which the hydrophobic biphenyl group was included within the tube and the hydrophilic carboxylate group was exposed outside, as confirmed by ^1H NMR spectroscopy.

At higher concentrations ($[102] > 8$ mM), inclusion complex **103** self-assembled together with a second, minor product. X-ray crystallographic analysis of this second product revealed an open tubular array (**104**) containing two molecules of ligand **102** held together by 12 $[(en)Pd]^{2+}$ units and including two template molecules, whose carboxylate groups were again exposed to the aqueous exterior (Figure 27b). Concentration proved to have an important effect on the system because the conversion of the smaller tube **103** into the larger structure **104** occurred slowly at high concentrations and it was further facilitated by removing the complex **104** through

crystallization. Surprisingly, **104** was not observed to convert into **103**. The authors concluded that **103** and **104** were not thermodynamic products but rather kinetically trapped local minima of a potential energy surface for this system.

In natural systems, hydrophobic interactions can drive the organization of structural subunits in water into higher-order structures (*e.g.*, protein folding).[123,124] In synthetic systems, the hydrophobic effect can lead to the aggregation of small molecules[125] and drive the self-assembly of complex arrays, including supramolecular polymers[126] and organic capsules.[127,128] For instance, Rebek,[129] Ramamurthy,[130,131] Gibb,[132−135] and more recently Yoshizawa[136] have carried out elegant work on organic containers, which form and bind guests in water *via* the hydrophobic effect.

Most WSCCs have been synthesized in pure water or in aqueous solvent mixtures using nonpolar organic ligands possessing extended aromatic regions. This feature deserves attention; it then becomes pertinent to consider that hydrophobic effects may also impact the association of ligands during aqueous self-assembly and possibly shape the distribution of products.

In a domain adjacent to cages, one of the first examples of this effect in coordination-driven systems was the catenation of palladium(II) macrocycles.[137] The [2]catenane (**105**) and its individual rings (**106**) exist in equilibrium in D_2O at room temperature (Figure 28). At low concentration, the equilibrium lies toward the free metallacycles **106**, but at higher concentrations catenane **105** is the dominant species in solution.
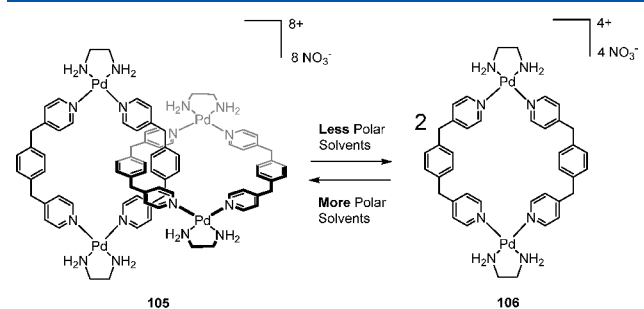
Figure 28. Equilibrium between catenane **105** and monomeric ring **106** shifts to either side depending on the polarity of the solvent employed.[137]

The polarity of the solvent significantly impacted the equilibrium between the interlocked and unlocked states. Increasing the ionic strength, and thus the polarity, through use of a $NaNO_3$ solution increased the proportion of catenane **105** to >99%; conversely, the formation of the catenane was suppressed (<1%) in less polar CD_3OD/D_2O (1/1) or D_2O/glycerol (1/1) media. Fujita and co-workers concluded that the catenane formation was driven by favorable hydrophobic interactions promoted by more polar media.

In a related study, the hydrophobic effect was confirmed as the driving force leading to the aggregation of coordination metallacycles into [2]catenanes. While a set of diverse palladium(II) macrocycles formed quantitatively from hydrophobic ligands in DMF, the gradual addition of water triggered their catenation, maximizing the yield of catenane (>90%) at 2:1 D_2O:DMF.[138] In the domain of WSCCs, the same authors observed the formation of a catenane in water composed not of two interlocking rings but of two interlocking cages made of

hydrophobic panels. The hydrophobic effect would appear to play a key role in this outcome.[139]

More recently, Ward and co-workers described a more elaborate equilibrium where three cobalt(II) assemblies coexist and interconvert in water in an equilibrium governed by the hydrophobic effect.[140] The self-assembly of naphthalene-1,8-diyl spaced bis-bidentate ligand **107** and cobalt(II) afforded a $[Co^{II}_2L_3]^{4+}$ cylindrical mesocate (**108**), a tetrahedral cage $[Co^{II}_4L_6]^{8+}$ (**109**), and a dodecanuclear truncated-tetrahedron $[Co^{II}_{12}L_{18}]^{24+}$ (**110**) in water, all of which were crystallized and structurally characterized: in **108**, all three bridging ligands span both metal ions, whereas **109** and **110** are cages with a metal ion at each vertex and a ligand bridging every edge (Figure 29).

The equilibrium between the three complexes occurred on a time scale of hours or days and was influenced by temperature, concentration, and solvent in favor of one structure or another due to hydrophobic effects. NMR studies showed that increasing temperature and dilution favored the smaller assemblies for entropic reasons. Conversely, the largest cage **110** dominated at higher concentrations and lower temperatures.

The authors suggested that the hydrophobic effect was responsible for the formation of the larger structures: reorganization of several smaller complexes into a larger one results in a smaller proportion of the hydrophobic ligand surface being exposed to solvent, with a larger proportion of the ligand surface being shielded in the cage interior. The solvent-accessible surface areas of the $[Co^{II}_4L_6]^{8+}$ (**109**) and the $[Co^{II}_{12}L_{18}]^{24+}$ (**110**) cages were determined to be 2076 and 4885 $Å^2$, respectively. Hence, three equivalents of **109** correspond to a solvent-exposed surface area of *ca.* 6200 $Å^2$, whereas reorganizing them into a single **110** reduces the hydrophobic surface area by *ca.* 1300 $Å^2$.

Corroboration of the effect of water on self-assembly was obtained from the measurement of the product distribution in $MeNO_2$. Only the smallest structure **108** could be detected by NMR and ESI-MS, with no traces of the larger assemblies. This outcome was inferred to result from the absence of the hydrophobic effect as a driving force for their formation. This study highlights that self-assembly in water can be an exceptional situation, where the hydrophobic effect can outweigh entropic and electrostatic factors to enforce the construction of larger assemblies over lower-order structures.

3. REPERCUSSIONS AND APPLICATIONS OF THE AQUEOUS HOST−GUEST CHEMISTRY OF COORDINATION CAGES

Host−guest chemistry is a key feature of coordination cages.[141] Guest encapsulation within the internal cavity of such cages hinges on the operation of dispersive or polar noncovalent forces,[142,143] which may alter guest properties and result in their chemical transformations.[144] Much of the success of metal−organic hosts relies on the rich variety of geometries and sizes that their inner pockets can adopt. The synthesis and characterization of complex container structures is increasingly focusing upon cavity design in order to target specific guests with high affinity and selectivity.

Past studies have evidenced that molecular recognition through encapsulation is governed by the size and shape match between cavity and guest, as well as favorable Coulombic attractions. These precepts provide a valuable starting point for the design of host−guest systems. Similarly, volume consid-
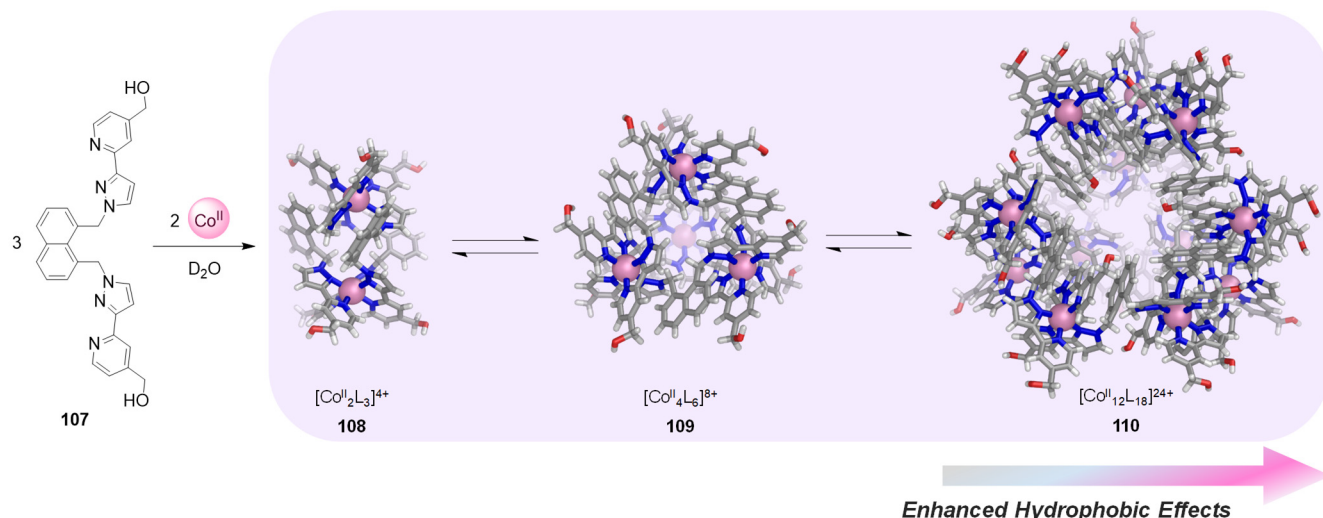
Figure 29. Self-assembly of ligand **107** with Co[II] ions results in an equilibrium between three assemblies **118**, **109** and **110** in D$_2$O.[140] The X-ray crystal structures of each assembly are shown.

erations are useful to determine the suitability of guests. As first noted by Rebek, a 55% void occupancy by a guest provides an optimal situation for many host−guest pairs in solution.[145] Although the preceding concepts are universal to molecular recognition and thus apply in aqueous solution, the hydrophobic effect lends unique features to host−guest chemistry in water.[16,20,29]

3.1. Neutral Guests and Influence on Guest Properties

A detailed description of the hydrophobic effect in aqueous binding and the thermodynamic factors involved is beyond the scope of this review. However, it is pertinent to note studies that seek to shed light on guest recognition by WSCCs in water. Ligands with extended rigid aromatic regions have been extensively employed to enclose the molecular cavities of WSCCs, thus rendering their interiors hydrophobic and suitable to host neutral organic molecules aided by the hydrophobic effect.

"Empty" hosts contain solvent molecules, in this case, water. This encapsulated water is distinct from the outer bulk solvent. The hydrophobic cavities of water-soluble hosts, both purely organic and metal−organic, are filled with "high-energy" water.[146] The liberation of this cavity-bound water contributes both entropically and enthalpically to the binding of a hydrophobic guest.

These effects were detailed in the context of host−guest complexes of cyclodextrins, cyclophanes, and cucurbiturils.[147] Unless trapped water molecules are able to engage in hydrogen-bonding with bulk water inside a poorly shielding container, or are hydrogen-bonded to functional groups within the host interior, they are frustrated from forming an optimal number of hydrogen bonds. The release of high-energy water molecules to the bulk, where they may form four hydrogen bonds, can provide an important favorable enthalpic contribution to binding.

The ordering of water molecules in cavities (see below) also leads to an entropically less-favorable state in comparison to the relative freedom of the bulk.[148] Keeping these ideas in mind, throughout this review, "empty" cages thus do not contain a specific guest but may be inferred to bind water.

Strong evidence of the existence of water molecules within the pocket of WSCCs was obtained from Fujita's Pd$_6$L$_4$

octahedron **6c**. X-ray crystallography and neutron diffraction studies revealed a T_d-symmetric adamantoid cluster of 10 water molecules, which was referred to as "molecular ice" because of its structural similarity to naturally occurring I$_c$-type ice (Figure 30a).[149] Remarkably, this molecular ice does not "melt" even at
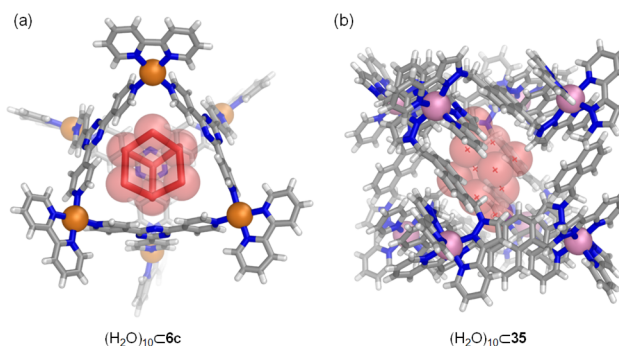
Figure 30. Crystal structures of coordination cages containing water clusters in the central cavity. (a) Fujita's Pd$^{II}_6$L$_4$ octahedron **6c**[149] and the (b) Co$^{II}_8$L$_{12}$ cube **35** made by Ward.[150]

room temperature; the water cluster could be located by diffraction even at room temperature. Neutron diffraction showed unusual D$_2$O•••π (lone pair−π electron) interactions between the host and the cluster, which may contribute to the stability of the cluster. The authors suggested that molecular recognition by this type of cage can be driven by entropy, whereby the encapsulation of hydrophobic guests can be driven by the "melting" of the molecular ice and displacement of the free water molecules.

Recently, the Ward group reported insights that deepen understanding of how the presence of water within coordination cages influences guest binding in aqueous solution.[150] A combined crystallographic and NMR spectroscopic study showed that the binding of guests within Co$^{II}_8$L$_{12}$ cube **37** has a substantial enthalpic component related to the liberation of "high-energy water". By soaking crystals of the isostructural water-insoluble cube **35** in water and then determining the single-crystal X-ray structure, it was found that this type of cavity accommodated a (H$_2$O)$_{10}$ cluster where
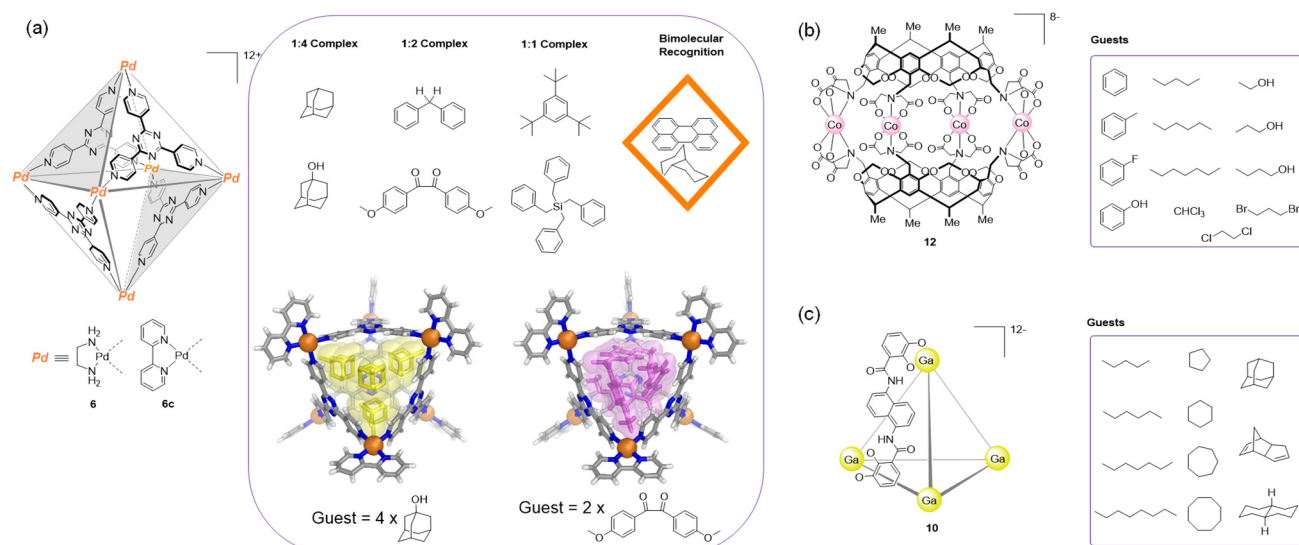
Figure 31. Initial WSCCs as examples of binding of hydrophobic neutral organic molecules. (a) Fujita octahedra can bind up to four identical guests[59] or two different ones.[155] Cages reported by (b) Harrison[156,157] and (c) Raymond[158] also bind hydrophobic molecules in water.
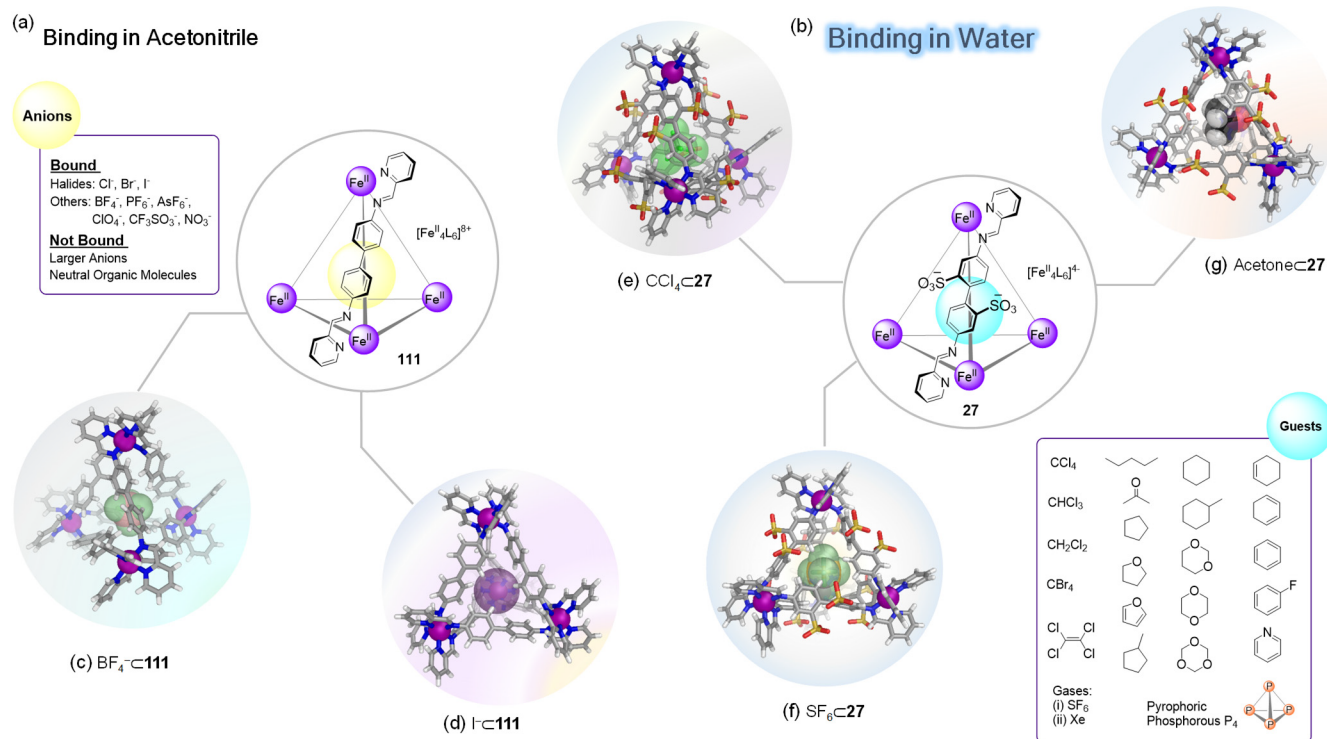
Figure 32. Contrasting binding ability of two isostructural $Fe^{II}_4L_6$ tetrahedra. (a) Cage **111** binds only small inorganic anions in acetonitrile but not larger anions or neutral organic molecules.[159] (b) Analogous cage **27** binds a wide variety of neutral organic molecules, some gases, and P_4 in water.[160−165] (c−g) X-ray crystal structures of selected host−guest complexes of each cage are depicted.

each trapped water molecule forms an average number of 0.5 fewer hydrogen bonds than it would in bulk solution (Figure 30b).

Aqueous guest binding studies with **37** indicated that freeing the cavity-water enthalpically drives hydrophobic guest binding. This dominance of ΔH is consistent with the view that guest binding is dominated by the freeing of "high-energy" water into the bulk, a conclusion contrasting with the classical view of the hydrophobic effect, dominated by the favorable entropy change associated with the release of ordered molecules from hydrophobic surfaces.

The question of "high-energy" water is still a matter of debate,[21] and there is much to learn about the fundamentals of aqueous binding thermodynamics.[20] The Hofmeister,[151] reverse Hofmeister,[152] and chaotropic[153] effects influence the properties of aqueous salt solutions, and greater insights into these phenomena are needed.[20,154]

3.1.1. Hydrophobic Effects. The ability of WSCCs to host neutral molecules within their hydrophobic interiors has been investigated in water since the development of the first cages (Figure 31). Fujita's M_6L_4 octahedra of type **6** encapsulate hydrophobic guests in three distinct ways.[59]

First, 1:4 host–guest complexes have been observed for small molecules such as substituted benzenes, adamantane derivatives, or o-carborane. Second, medium-sized bent molecules, such as cis-stilbene and cis-azobenzenes, associate into roughly spherical dimers inside the cage, yielding 1:2 host–guest adducts. Third, still larger molecules form 1:1 complexes, examples being tri-tert-butylbenzene or tetrabenzylsilane (Figure 31a).

Octahedron **6** is also capable of bimolecular recognition. Two different hydrophobic guests may be simultaneously encapsulated to form a stable ternary complex. Such complexes may form even in cases where the two guests cannot be recognized individually by the cage.[155]

Similarly, the hollow interior of Harrison's capsule **12** bound organic molecules in water (Figure 31b).[156,157] Raymond's tetrahedron **10** also bound organic molecules, including alkanes, in aqueous solution, with size and shape selectivity.[158] The driving force for these binding events is attributed to the hydrophobic effect, the strength of which is an advantage of WSCCs (Figure 31c).

Hydrophobic effects may be gauged through comparison between the binding of guests by coordination cages in water and in other solvents. Using cages that can dissolve in different solvents, our group has investigated the effect of the medium on guest-binding with respect to both preferences and affinity.

An example is the case of two isostructural $Fe^{II}_4L_6$ tetrahedra, which depending on nature of the diamino subcomponent employed for their preparation, are soluble in either acetonitrile or water. Acetonitrile-soluble cage **111**, based on 4,4′-diaminobiphenyl, exists as a mixture of three diastereomers, the T, C_3, and S_4 symmetric isomers.[159] This structure encapsulated small inorganic anions such as Cl^-, I^-, BF_4^-, or ClO_4^-. Larger anions and neutral organic molecules were not bound in MeCN (Figure 32a).

In contrast, the structurally analogous but water-soluble cage **27** (built on 4,4′-diaminobiphenyl-2,2′-disulfonic acid) exhibited different guest preferences in water (Figure 32b). A wide variety of neutral organic molecules: hydrocarbons, halocarbons, and heterocyclic compounds were bound within this cage.[160] A study of a set of these guest molecules examined the strength as well as the kinetics of their binding to **27**.[161] The effects of different guest properties upon the binding strength and kinetics were elucidated by a systematic analysis of the binding data through principal component analysis, thus allowing structure–property relationships to be determined. Guest size was the most important factor in determining whether or not a molecule could be accommodated within the host's cavity and has a strong influence upon the uptake rate, with smaller guests entering the cavity faster than larger ones. The shape of the guest also affected the uptake rate, with flat molecules being encapsulated more rapidly than similarly sized less flat ones. Finally, the measured binding constants correlated with the hydrophobicity of the guest. These insights served as a foundation for the construction of complex systems, in which multiple guests were sequentially bound and released by the host in a controlled time-dependent manner, thus allowing multiple states of the system to be accessed sequentially. Cage **27** also proved capable of binding gases such as the most climate-heating greenhouse gas SF_6,[162] and xenon,[163,164] as well as solid white phosphorus (P_4),[165] which was also bound by this cage.

Solvent-dependent binding was also observed for $Fe^{II}_4L_4$ tetrahedron **113** (Figure 33).[166] The acetonitrile-soluble
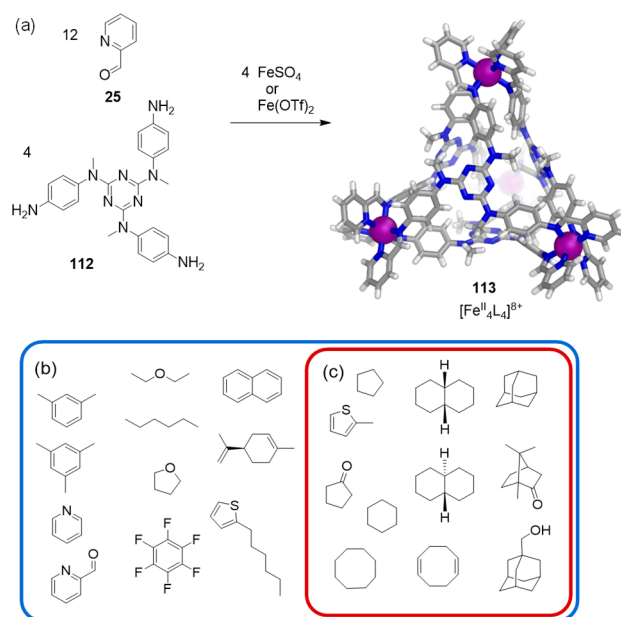
Figure 33. (a) Subcomponent self-assembly of cage **113** and its crystal structure.[166] Guest molecules for **113**. In D_2O (b) all molecules shown were encapsulated (outer blue box) in **113**, whereas in CD_3CN (c) only a subset (inner red box) were bound.

triflate salt of **113** was prepared from the triamine **112**, 2-formylpyridine (**25**), and iron(II) triflate via subcomponent self-assembly. Cage **113** could also be prepared in water-soluble form by employing iron(II) sulfate in place of iron(II) triflate. The crystal structure of **113** confirmed that four octahedral iron(II) centers are bridged by four ligands, each of which caps a face of the tetrahedron and adopts a C_3-symmetric propeller-like configuration. The cavity of **113** is almost completely enclosed and displays a volume of ca. 233 $Å^3$.

Cage **113** bound a variety of guests in water, both aromatic and aliphatic (Figure 33b), whereas only a subset of these, mainly aliphatic species, were bound in acetonitrile (Figure 33c). Moreover, it was observed that the cage walls flex in such a way as to allow the cage to expand for larger guests or contract for smaller ones.

The behavior of some of the guests was also altered in subtle ways upon encapsulation. Large guests, such as 2-hexylthiophene, reorganized to adopt coiled conformations that are thermodynamically disfavored in their free states. In addition, the chirotopic inner phase of the cage rendered enantiotopic guest proton signals diastereotopic in specific cases.

Similar behavior was observed for the porphyrin-faced $Fe^{II}_8L_6$ cubes **60** and **61** (Figure 34). As noted above, the acetonitrile-soluble triflate salt **60** converted into water-soluble **61** through anion metathesis (Figure 16).

Biologically-relevant products, such as caffeine, inosine, and an antibiotic macrolide, were bound by **61** in water, along with steroids of biological and therapeutic relevance. None of these guests showed evidence of binding to cube **60** in acetonitrile, however.[88]

The counterion-induced solubility-switching of theses cubes also offers the opportunity to use such cubes as vectors to transport water-insoluble cargoes from organic to aqueous phases. An $Fe^{II}_8L_6$ cube analogous to **60**, assembled using free base porphyrins, was able to accommodate either one fullerene
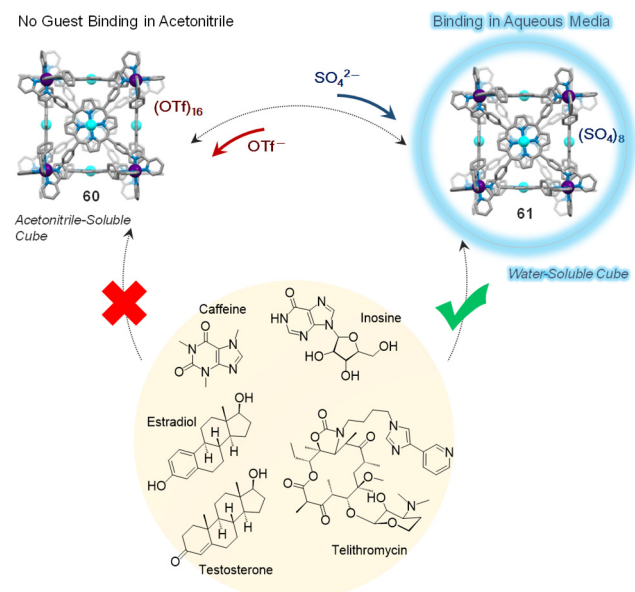
Figure 34. Binding of biologically relevant guests was only observed in aqueous solution using the water-soluble cube **61** obtained upon anion exchange from the MeCN-soluble cube **60**.[88]

Figure 35. Guests used to compare binding between hosts **35** and **37** in acetonitrile and water, respectively.[167] The highest binding association was observed between host **37** and 2-hydroxyquinoline (amide tautomer) in water.

C_{60} or three molecules of coronene in DMF. Anion-exchange with sulfate rendered this cube and its hydrophobic cargoes water-soluble despite guest insolubility in water.[88]

The examples noted above suggest that aromatic guests experienced a greater driving force for encapsulation in water than in acetonitrile, whereas aliphatic guests did not.[167] Ward, Hunter, and co-workers quantified the effect of acetonitrile and water on the recognition of a family of small organic molecules within MeCN-soluble (**35**) and water-soluble (**37**) cubic cage congeners, with a central cavity volume of *ca.* 407 Å³ (Figure 35). By comparing ΔG° values for host−guest complex formation in the two solvents, using pairs of related guests differing only in the presence or absence of a fused aromatic ring, the authors constructed thermodynamic models that allowed quantification of the solvophobic contribution to binding. The most stable host−guest complex among the series was formed by **37** binding the amide tautomer of 2-hydroxyquinoline in water ($\Delta G^\circ = -22.6 \pm 0.5$ kJ mol^{-1}). For **35** binding this guest in MeCN, the major contribution to binding came from electrostatic interactions and H-bonding between the guest and the cage cavity because the solvent is noncompetitive.

In MeCN, a contribution of *ca.* 10 kJ mol^{-1} was found for the binding of bicyclic guests within **35**, which was associated with interactions of the fused aromatic ring with the cage interior. In contrast, recognition by **37** in water proved to be dominated by the hydrophobic effect, with no contribution to ΔG° from polar interactions because the aqueous solvent provided a better H-bonding environment than the cage interior. The ΔG° values showed that the binding of bicyclic guests in water was also favored over the monocyclic ones by *ca.* 20 kJ mol^{-1} due to the presence of the fused aromatic ring. Although the same trend was observed in MeCN, this energetic difference is 10 kJ mol^{-1} higher in water than in MeCN, clearly reflecting the larger hydrophobic contributions to ΔG° induced by water.

Subsequent studies using aliphatic ketone guests indicated that binding by cube **37** in water was dominated by the
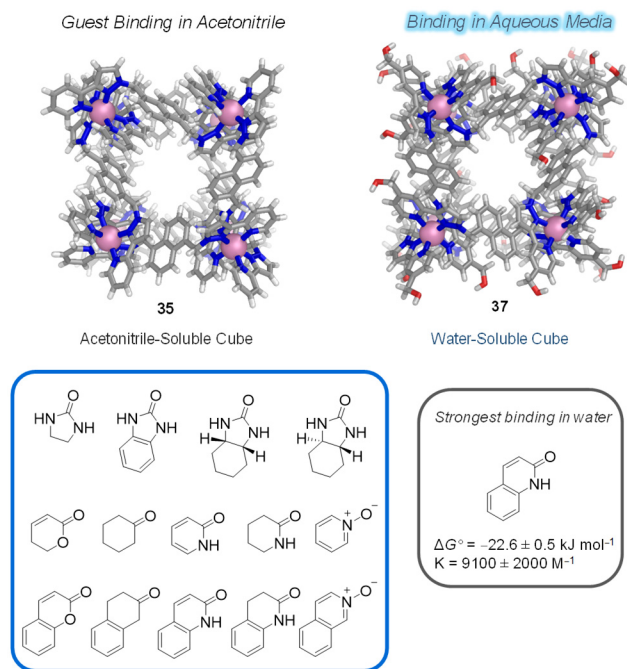
hydrophobic effect, elucidating the dependence of binding affinity on size and shape.[168] Two series of guests showed distinct behavior (Figure 36a).

For guest series A (Figure 36a), consisting of cyclic aliphatic ketones of varying size, binding affinity increased with the surface area of the hydrophobic guest, gaining 5 kJ mol^{-1} for each additional guest CH_2 group (plot in Figure 36a) up to the point where the steric bulkiness became limiting. This peak was reached with cycloundecanone, yielding the host−guest complex with the highest affinity ($K = 1.2 \times 10^6$ M^{-1}). This complex was characterized by X-ray crystallographic studies, showing how the alkyl backbone of the guest formed close contacts with the cavity, whereas the carbonyl group is hydrogen-bonded to one of the two *fac*-tris-chelate vertices (Figure 36a).

Guest series B (Figure 36a) showed no simple correlation between surface area and binding affinity. These guests, consisting of cyclic ketones with C_{10} skeletons, were all close to the size limit that the cage cavity can accommodate. Steric issues became dominant, and guests with more elongated shapes presented a poor fit for the pseudospherical cavity, with linear ketones not binding at all.

The crucial role of the hydrophobic effect in aqueous binding by host **37** was further established using a pH swing experiment, which enabled the selection of one of three different guests from aqueous solution. Acidic adamantane-1,3-dicarboxylic acid (**114**), cyclononanone (**115**), and basic 1-aminoadamantane (**116**) were utilized as guests.

Depending on guest protonation state, these molecules exhibited variable binding affinity for the host cage (Figure 36b). A D_2O solution containing cage **37** and prospective guests **114**, **115**, and **116** was prepared, and ^{1}H NMR spectra were measured over the pH range 3−12. Complex **114⊂37** was dominant at low pH, but was successively replaced by
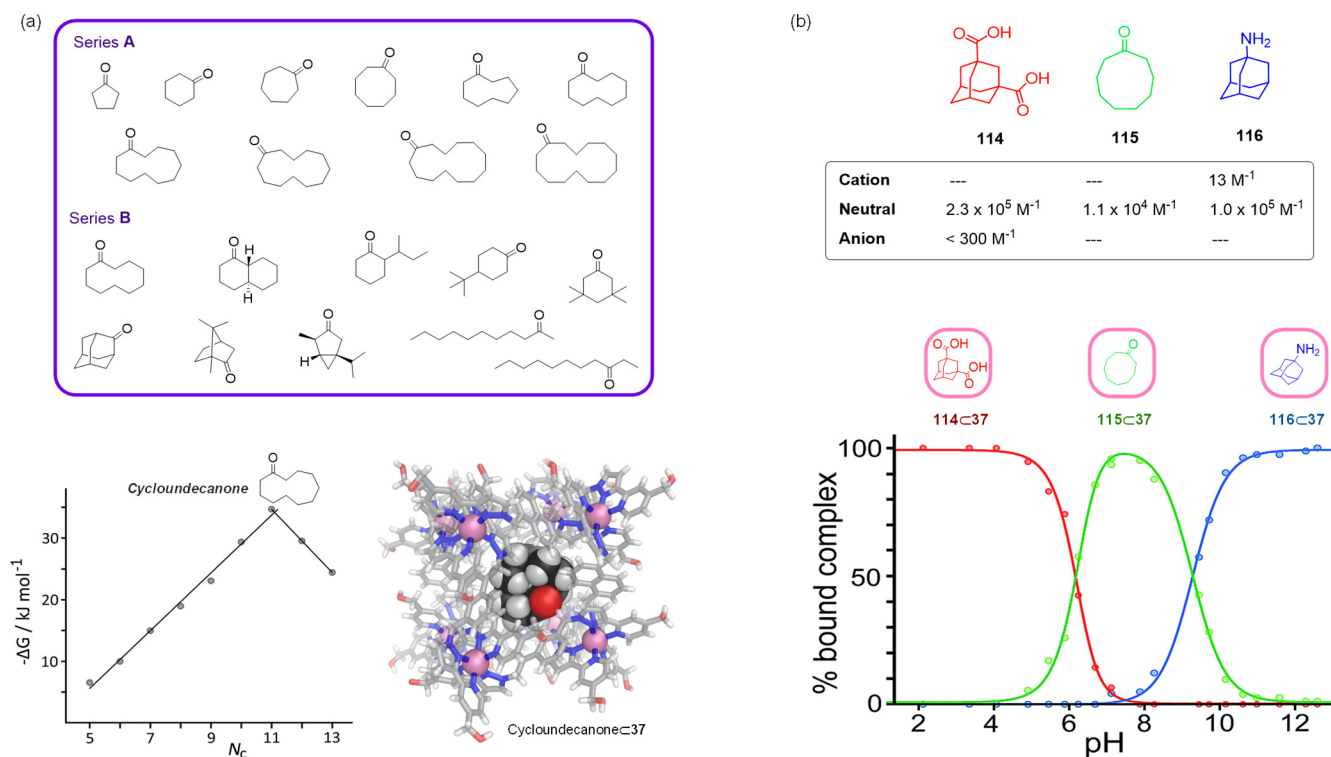
Figure 36. (a) Ketone guests for **37** in water. The plot of binding free energy vs number of C atoms for guest series A, and the X-ray crystal structure of the cycloundecanone⊂**37** complex are shown.[168] (b) The three guests used in the pH-swing experiment and their binding constants within cage **37** as a function of protonation state,[169] together with a diagram showing which host−guest species predominates as a function of pH.

115⊂37 complex as the pH was neutralized and then by **116⊂37** at high pH.

The proportions of each complex throughout the pH range, expressed as a fraction of total complex concentration, are summarized in Figure 36b. Switching between different guests occurred because neutral organic guests bind strongly in the cage due to the hydrophobic effect, whereas charged (protonated or deprotonated) forms are hydrophilic and thus did not bind.[169]

In follow-up work, the useful potential of the pH-dependent binding of guests was further demonstrated with molecules of biological relevance.[170] The Parkinson's drug amantadine (1-aminoadamantane) binds with an association constant of $K = 1.0 \times 10^4$ M^{-1} in the neutral form (pH > 11), but the stability of the complex is reduced by 3 orders of magnitude when the guest is protonated at lower pH. Although the association constants were lower, aspirin and nicotine guests showed similar binding behavior, with a substantial difference between neutral (stronger binding) and charged (weakly binding) forms, irrespective of the sign of the charged species.

A recent investigation involving **35** has revealed that guests such as coumarins and saturated analogues unexpectedly bind in the solid-state as pairs with up to 87% of the cavity volume being occupied. Aqueous solution studies using **37** also suggested that the multiple guest binding may occur in the presence of high guest concentrations.[171]

Work from the Crowley group also corroborates that binding within a series of large $[\text{Pd}_6\text{L}_8]^{12+}$ octahedra is more effective in aqueous solutions.[172] They first observed that in DMSO, anionic *p*-toluensulfonate effectively binds within these cages, but no binding was observed when anthracene, pyrene, or 1,8-naphthalimide were mixed with the cages in DMSO. To probe the importance of the hydrophobic effect in

binding, a mixed water−DMSO solvent system was used to reexamine binding. Increasing the amount of water to 50% (1:1 D$_2$O/DMSO) promoted encapsulation of all of these prospective guests, as the hydrophobic effect drove binding. NMR spectroscopy and molecular modeling suggested that between 3−6 guest molecules per cage were bound simultaneously.

3.1.2. Influence on Guest Stability and Conformation.

Molecules can behave differently when they are isolated from their surroundings. Within a cage, interactions between guests and the bulk solvent and with other solutes are inhibited.[173] The hydrophobic cavities of WSCCs are spatially confined and shielded by aromatic rings. Reactive molecules can be stabilized and protected from undesired reactions or from attack by water. Guests may adopt otherwise unfavorable conformations within WSCCs. Furthermore, many WSCCs are capable of binding multiple guests simultaneously, in either homotropic (same guests) or heterotropic (different guests) fashion. New modes of guest−guest interactions and unusual guest behaviors may thus be engendered.[174]

WSCCs thus enable the observation and study of these phenomena in aqueous solution with molecules that are otherwise not soluble in water. One such example is white phosphorus, tetrahedral P$_4$, which is pyrophoric and thus spontaneously combusts upon exposure to atmospheric oxygen. Our group demonstrated that tetrahedral container **27** encapsulates P$_4$, thus rendering it water-soluble and air-stable.[165] The corresponding host−guest complex was characterized by X-ray crystallography, which showed stabilizing van der Waals contacts between P$_4$ and the hydrophobic phenylene groups lining the cage interior (Figure 37a).

Although the pores of the cage are large enough to allow the passage of oxygen, the highly exothermic phosphorus oxidation
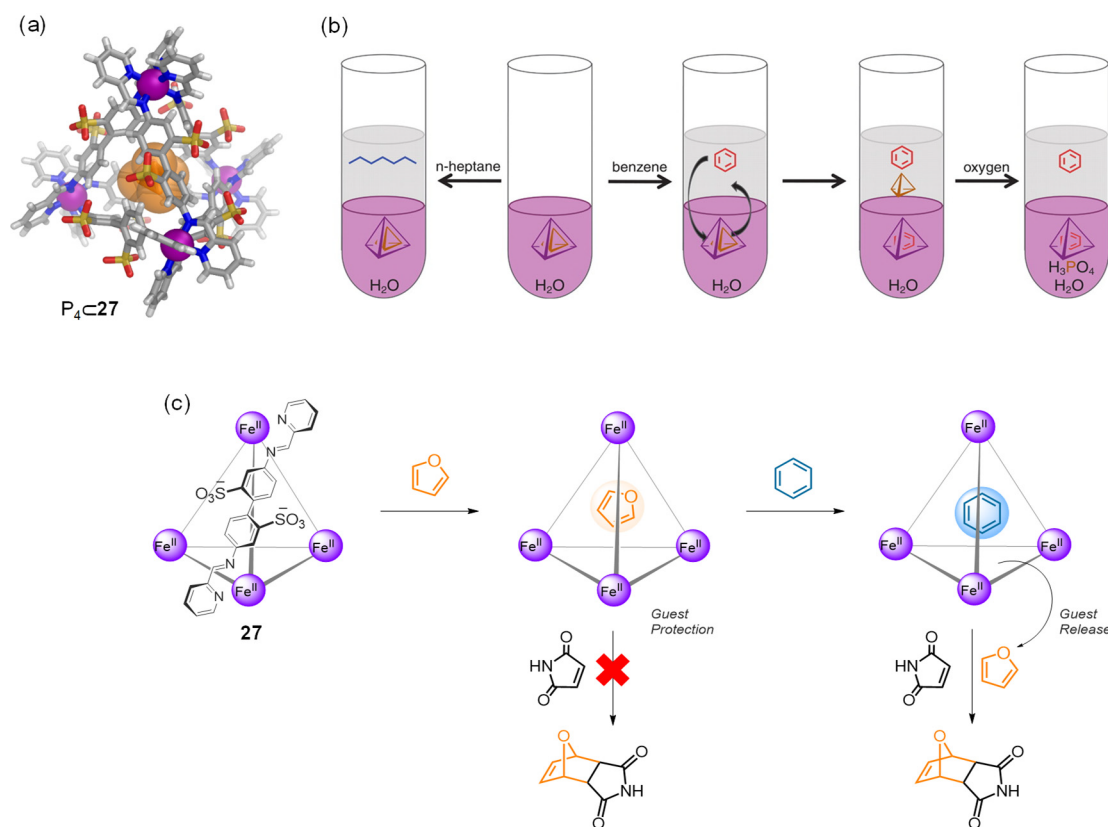
Figure 37. Cage **27** as a protective environment for guests. (a) Crystal structure of $P_4 \subset 27$.[165] (b) Extraction of P_4 from **27** by *n*-heptane was not possible, whereas replacing P_4 with benzene results in phosphorus release into the organic phase. (b) Reproduced with permission from ref 165. Copyright 2009 American Association for the Advancement of Science. (c) Schematic representation of a cage-controlled Diels−Alder reaction: encapsulation of furan by **27** prevented its reaction with maleimide. Addition of benzene released furan, triggering reaction.[175]
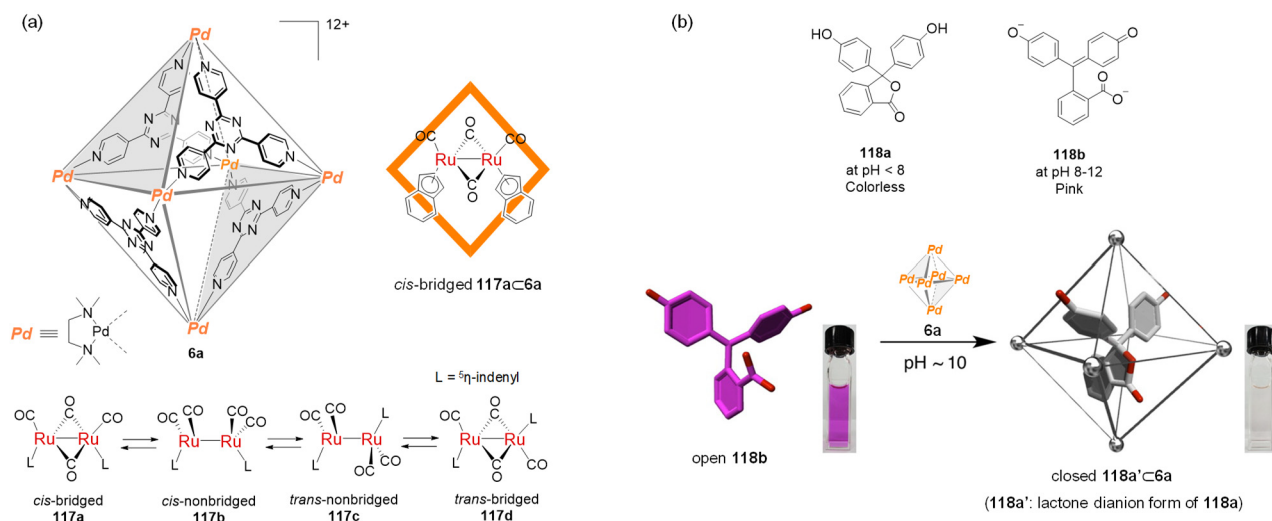
Figure 38. Stabilization of otherwise unfavorable guest configurations by cage **6** in aqueous media. (a) Ruthenium(II) complex **117** exists in equilibrium among four isomers; cage **6** stabilizes the **117a** form upon encapsulation.[178] (b) Chemical structures of the lactone (**118a**) and the quinone (**118b**) forms of phenolphthalein, along with a cartoon representation of the cavity-directed stabilization of the ordinarily unstable lactone dianion.[179] (b) Adapted with permission from ref 179. Copyright 2015 American Chemical Society.

reaction is prevented. We proposed that stabilization of P_4 resulted from constriction: although this guest fits well, the intermediates of the oxidation reaction are too large to fit within the cavity.

Although P_4 appeared to be stable within **27**, its extraction from the host through the addition of a competing guest

proved straightforward (Figure 37b). The addition of benzene to an aqueous solution of $P_4 \subset 27$ resulted in the extraction of P_4 from **27** into the benzene layer, with concomitant formation of aqueous $C_6H_6 \subset 27$. When *n*-heptane was used instead, no extraction of P_4 from **30** was observed, despite the solubility of P_4 in this solvent. Heptane is not bound by **27**, whereas
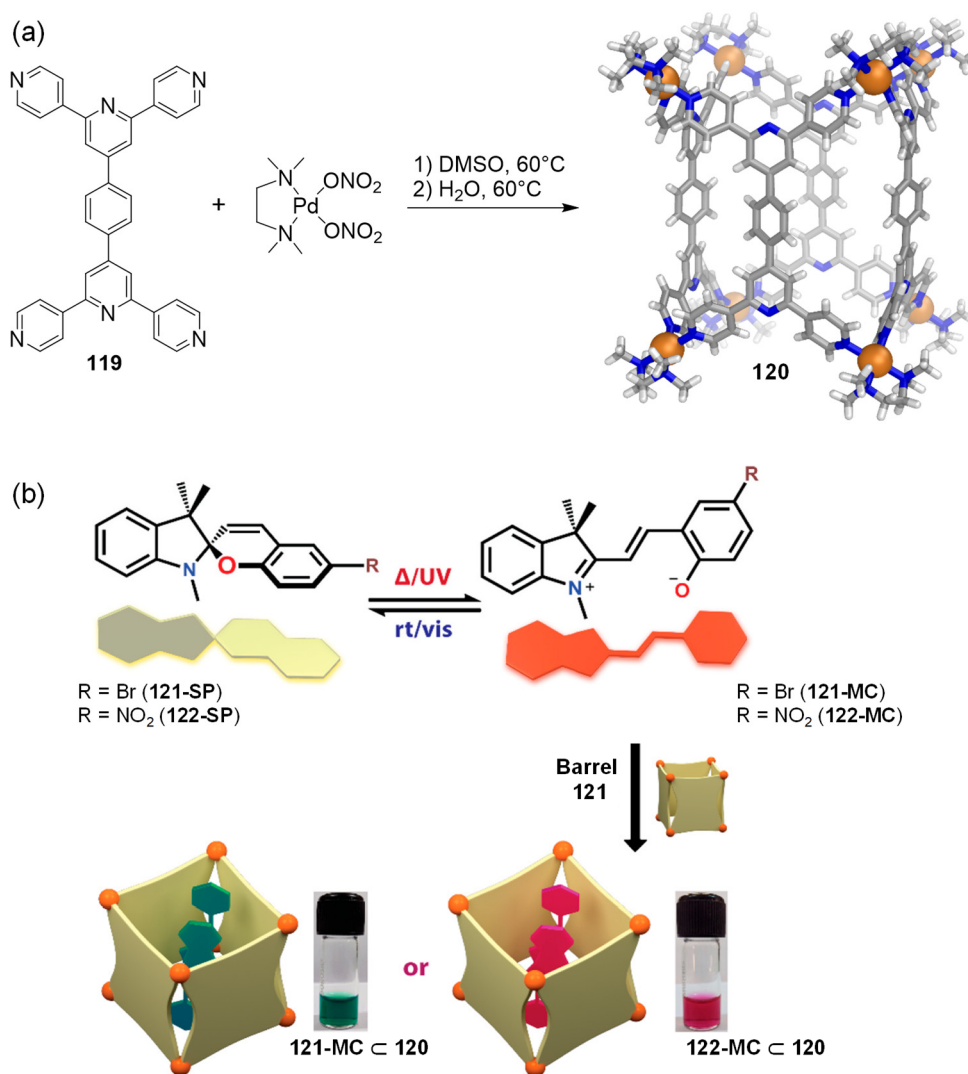
Figure 39. (a) Self-assembly of barrel **120** from ligand **119** and *cis*-[(tmeda)Pd(NO₃)₂]; the X-ray structure of **120** is shown. (b) Encapsulation of **121**-MC and **122**-MC into the cavity of **120** led to stable green and pink aqueous solutions of the host−guest complexes. (b) Adapted with permission from ref 183. Copyright 2018 American Chemical Society.

benzene is a good guest. Extraction of P₄ thus requires not only the "pull" of a solvent that can extract P₄ but also the "push" of a competing guest capable of displacing it.

Cage **27** also served as a "whole-molecule protecting group" in the Diels−Alder reaction between furan and maleimide (Figure 37b).[175] Hiding the diene furan in the cage prevents its reaction with the dienophile maleimide, which remains free in solution. Upon addition of a competing guest that binds more strongly (benzene) to an aqueous solution of furan⊂**27**, furan was released and its reaction with the complementary substrate maleimide immediately started.

The Fujita group's M₆L₄ octahedra of type **6** (M = Pd^II, Pt^II) have also proven useful at preventing reactions of encapsulated guests in water. For instance, cyclic trimers of siloxanes are short-lived products of polycondensation of trisilanols that rapidly convert into a thermodynamically favored cyclic tetramer and higher condensed products; however, cyclic siloxane trimers remain stable within this cage.[176] Likewise, it was observed that the homolytic photocleavage of α-diketones was suppressed within the cavity of the octahedron, leading

instead to cyclization products *via* pathways that were otherwise kinetically unfavorable.[177]

In a recent example, the stabilization of an unstable form of an organometallic complex was demonstrated (Figure 38a).[178] Dinuclear ruthenium complex [(η⁵-indenyl)Ru(CO)₂]₂ **117** exists as a mixture of four *cis* and *trans* bridged and nonbridged isomers in rapid equilibrium. Upon inclusion into **6a**, complex **117** freezes into the CO-bridged *cis* configuration **117a**, whereby confinement in the cage prevents *cis*-to-*trans* conversion. Moreover, complex **117** is photosensitive and undergoes facile photoinduced Ru−Ru bond cleavage and CO dissociation within a few days under ambient light. However, encapsulation of complex **117a** within the cage enhanced its photostability in water: no decomposition was observed in solution over several months under ambient light.

The rigid tetrahedral cavity of **6a** also changed the behavior of the dye phenolphthalein (Figure 38b).[179] Phenolphthalein exists as the colorless lactone **118a** (closed form) at low pH (pH < 8) but as the colored quinone dianion **118b** (open form, pink) at high pH (pH 8−12). Upon encapsulation, the quinone dianion **118b** was transformed into the lactone

dianion **118a′** (colorless). The shape compatibility between the lactone **118a′** and the rigid cavity pushed the equilibrium toward lactonization, preventing its isomerization even at pH 10. The colored form of the phthalein dye was recovered when the dye was ejected from the cavity. An opposite effect was observed by Klajn when using a flexible M_6L_4 cage[180,181] originally reported by Mukherjee.[182] The more flexible cavity adapted to encapsulate azo-benzenes and spiropyran guests and permitted the reversible photoisomerization of the bound guests.

Mukherjee and co-workers also employed WSCCs as containers to store the planar, unstable merocyanine isomers of spiropyran molecules for several days in aqueous solution (Figure 39).[183] Spiropyran-based compounds are generally stable in the closed spiro form (SP) under visible light and readily convert to the merocyanine (MC) form upon UV irradiation in solution. The transient MC form readily converts back to the stable spiro form under visible light or upon standing at room temperature.

The treatment of ligand **119** with cis-[(tmeda)Pd(NO_3)_2] in DMSO afforded a mixture of two isomeric Pd_8L_4 barrels, an approximately D_{2d}-symmetric Gyrobifastigium-type solid (Johnson solid J_{26}), and barrel **120** with distorted D_{4h}-symmetry. Symmetrical barrel **120** was obtained exclusively when the mixture of barrels was isolated from DMSO and heated in water. Treatment of an aqueous solution of **120** with solid 6-bromospiropyran (**121**-SP) or 6-nitrospiropyran (**122**-SP) yielded the corresponding host−guest complexes. The metastable merocyanine forms (**121**-MC and **122**-MC) were observed to form inside **120** and remained stable under visible and UV-light and upon heating.

A related carbazole-based molecular barrel also showed similar stabilization of transient MC forms under visible light at room temperature.[183] Such structural transformations of photochromic spiropyrans in the solid state are unusual. Remarkably, upon UV irradiation even the solid mixture of barrel and spiro compound **122** produced merocyanine forms that were stable in the solid state under visible light. These properties were employed in the development of a "magic ink".[183]

The Mukherjee group also reported a self-assembled Pd_8 molecular vessel that can stabilize and store the open form of donor−acceptor Stenhouse adducts (DASAs) in aqueous solution.[184] The reaction of the tetraimidazole ligand **123** with cis-[(tmeda)Pd(NO_3)_2] in DMSO produced the barrel-like cage **124**. After isolation, cage **124** dissolved in water, where it bound and stored two equivalents of DASAs **125** or **126** in their open forms (Figure 40a).

DASA molecules photoisomerize from blue/violet neutral open forms to yellow/colorless zwitterionic cyclic forms following the absorption of green light in toluene or dioxane. In water, the open form is not stable and converts to the cyclic zwitterionic form irreversibly (Figure 40b).

Although **125** and **126** exist in the cyclic zwitterionic form in water in the absence of the cage, the open structures **125** and **126** were stabilized within the hydrophobic cavity of the barrel in water. In aqueous solutions of the host−guest complexes, the open DASA forms remained stable even upon visible light irradiation. The conversion of the open form to the cyclic form is irreversible in water; however, the confined nanospace of **124** enabled the slow conversion of the cyclic form to the open form in aqueous solution when the cage was present in excess. This behavior of DASA compounds in water contrasts with
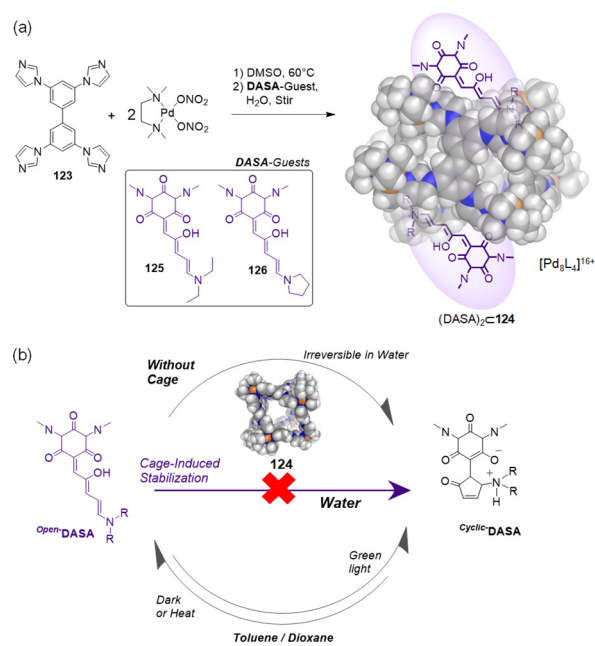
Figure 40. (a) Self-assembly of barrel **124** and the unusual stabilization of the open forms of DASA molecules **125** and **126**;[184] the X-ray crystal structure of **124** is depicted. (b) Photoswitching behavior of DASA molecules in organic solvents or water in the presence and absence of **124**.

what is observed in organic solvents and was only possible because of the operation of the WSCC.

The protection of light-sensitive guests can be effected within cavities enclosed by moieties capable of absorbing visible or ultraviolet light. Su and co-workers introduced a new heterometallic Pd^{II}−Ru^{II} cage framework built on a prede-signed triangular C_3-symmetric Ru^{II}-metalloligand (Figure 41a).[185] Triangular Ru^{II}L$_3$ metalloligand **127**, containing three coordinated phenanthroline moieties and three pendent uncoordinated pyridines, assembled with Pd^{II} at 80 °C resulting in formation of cage **128**. X-ray diffraction studies confirmed that the cage consists of six Pd^{II} ions and eight ligand **127** units bridging the six metal vertices (Figure 41b). This cage also displays 12 rhombic windows at the octahedron edges. The cage possesses a cavity of 5350 Å^3. NMR binding studies in 2:1 D$_2$O:DMSO-d_6 evidenced the inclusion of variable amounts of phenanthrene, pyrene, or anthracene, driven by the hydrophobic effect. NMR titrations using phenanthrene as the guest suggested that 18 ± 2 guest molecules were bound per cage in a stepwise manner. Molecular dynamic simulations revealed that a maximum of seven phenanthrene guest molecules may reside in the cavity of **128**, another 17 guests can be accommodated in the 12 cage windows, for a maximum of 24 phenanthrene guests in total.

The trapping and stabilization of photosensitive molecules within **128** was also demonstrated for three photoinitiators: 2,2-dimethoxy-2-phenylacetophenone (DMPA), 1-hydroxycy-clohexyl phenyl ketone (HCPK), and 2-hydroxy-2-methyl-propiophenone (HMPP), which are light-curing agents used in inks and paints (Figure 41c). Upon radiation with 365 nm UV light for 12 h, the free molecules underwent photolysis while the trapped ones remained intact. Although the pure Ru^{II}L$_3$ metalloligand itself was also observed to shield these photosensitive molecules from UV radiation, the cage system protected the photosensitive guests on a much longer time
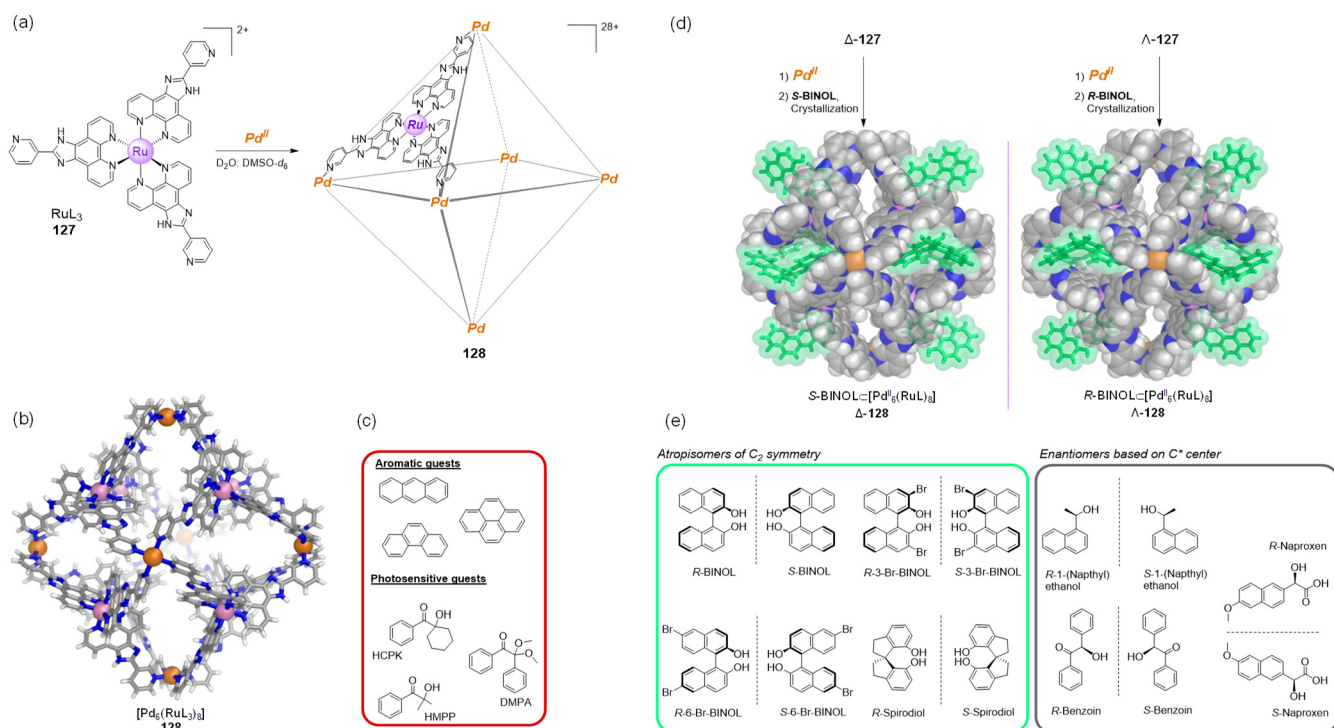
Figure 41. (a) Self-assembly of heterometallic cage **128** from ruthenium(II)-ligand **127** and palladium(II). (b) The X-ray structure of **128**, and (c) the aromatic and photosensitive guests bound by **128** are shown.[185] (d) Preresolved ligands Δ/Λ-**127** assemble with Pd^{II} to yield WSCCs Δ/Λ-**128**, which crystallized in the presence of *S*- or *R*-BINOL. The crystal structures of Δ/Λ-**128** showing *S*-/*R*-BINOL guests residing in the window pockets. (e) Chiral guests tested for enantioselective resolution.[186]

scale. While photolysis was observed after 24 h in the presence of the Ru^{II}L$_3$ ligand, it was suppressed for up to 120 h by using cage **128**.

Cage **128** was initially obtained as a racemate. Su, Pan, and co-workers reported a general approach to enantiopure versions of cage **128** and demonstrated the ability of these cages to separate atropisomeric compounds.[186] Enantiopure Δ-**128** and Λ-**128** were obtained by resolution of the Δ/Λ-Ru^{II}-metalloligand precursors (**127**) and their subsequent assembly with Pd^{II} ions.

Single crystals of Δ-**128** and Λ-**128** were grown from their MeCN solutions in the presence of *S*-BINOL and *R*-BINOL, respectively (Figure 41d). No racemization of Δ/Λ-**128** occurred on heating at 373 K. Given this stereochemical retention and the high solubility in water (26.0 g L^{-1}), these cages were investigated as platforms for enantioseparation.

A series of chiral guests were tested for enantioselective binding (Figure 41e). This study revealed limited stereoselectivity toward binding of chiral compounds with point stereocenters. However, the cages could achieve modest enantiomeric excesses (*ee*), ranging from 34−62%, in the separation of BINOL atropisomers. After separation, extraction of the resolved chiral guests from the water phase of Δ/Λ-**128** enabled the recovery of the empty cages, which could be reused for further runs of chiral resolution without loss of their enantioseparation ability.

The same group expanded this stepwise strategy to the assembly of configurationally stable [Pd$_6$(FeL$_3$)$_8$]$^{28+}$ (Δ/Λ-Fe-**128**) homochiral octahedral cages from the stereolabile metalloligand Fe-**127**.[187] This ligand is analogous to **127** but contains a Fe^{II} center in place of Ru^{II}. Although this more labile ligand is more convenient for synthesis, tris-chelate-Fe^{II} complexes exhibit less stereoconfigurational stability, under-

going more rapid racemization than their Ru^{II} congeners. Kinetic studies revealed that the iron(II)-phenanthroline dissociation rate of the Δ/Λ-Fe-**128** cages is 100-fold slower than that of the free Fe-**127** metalloligand, enabling the cages to retain their stereochemical configuration over >5 months at room temperature.

Photoshielding by a cage can be useful in preserving photosensitive reagents and controlling their photocatalytic reactions in aqueous media; for instance, by delaying photopolymerization and smoothing initiation through controlled release. This concept was elegantly demonstrated by the Yoshizawa group, who reported the stabilization of 2,2′-azobis(isobutyronitrile) (AIBN) and its derivatives toward light and heat on encapsulation by the water-soluble Pd$_2$L$_4$ nanocapsule **41** (Figure 42a).[77]

When AIBN was suspended in a 9:1 D$_2$O/CD$_3$CN solution of capsule **41** at room temperature, the AIBN⊂**41** complex formed quantitatively. Crystallographic analysis confirmed a single AIBN guest shielded within the anthracene panels of **41** (Figure 42a). UV irradiation of an aqueous solution of AIBN⊂**41** for 10 h at room temperature did not damage the radical initiator. Free AIBN, on the other hand, completely decomposed into tetramethylsuccinonitrile and other by-products under similar conditions. The estimated half-lives for the free and bound AIBN were 1.8 and 690 h, respectively, indicating that the bound radical initiator was 380-fold more stable than the free one.

The stabilization of AIBN by **41** was attributed to optical shielding by the shell of eight anthracene panels. Similarly, the radical initiators AMBN and AMMVN were encapsulated quantitatively and stabilized against UV-driven decomposition. Remarkably, AMMVN remained intact in the polyaromatic shell of capsule **41** after heating at 50 °C for 10 h. AMMVN is
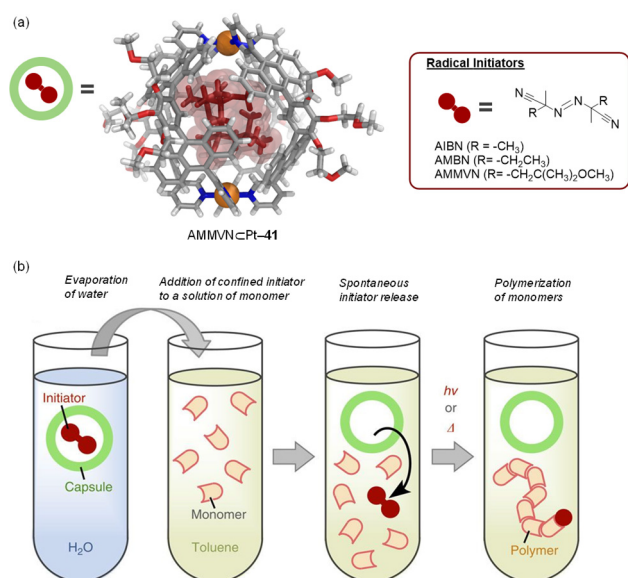
Figure 42. (a) X-ray crystal structure of AMMVN⊂Pt-**41** and diagram of encapsulated radical initiators. (b) Addition of the confined initiator (red) to an organic solution of monomers induces the spontaneous release of the initiator from the capsule and the polymerization initiates by light or thermal stimuli. (b) Adapted with permission from ref 77. Copyright 2014 Springer Nature.

one of the most reactive initiators among reported AIBN derivatives, whose decomposition usually occurs at room temperature.

Crystallographic analysis of AMMVN⊂Pt-**41** (which is an analogue of AMMVN⊂**41**, where the Pd^{II} ions are replaced by Pt^{II}) revealed that the AMMVN guest occupies 64% of the cavity volume (Figure 42a).

Encapsulated AIBN⊂**41** and AMMVN⊂**41** retained their reactivity as initiators for radical polymerization through photo- or thermally-induced release of the initiators from the capsule (Figure 42b). For instance, a toluene solution of methyl methacrylate (MMA, 1.9 mmol) was mixed with solid AIBN⊂**41** (0.75 μmol) and heated to 80 °C for 24 h. The initiator was spontaneously released, and the resultant solution solidified due to poly(methyl methacrylate) (PMMA) formation.

Water-soluble host **41**, constructed using either Pd^{II} or Pt^{II}, displays an isolated spherical cavity 1 nm in diameter and *ca.* 480 Å^3 in volume. In addition to azobis(isobutyronitrile)s, methylated benzenes and xanthine derivatives[188] as well as hydrophobic S$_6$ and S$_8$ molecules[189] have been encapsulated due to the hydrophobic effect.

Capsules of type **41** bind not only hydrophobic species but biologically relevant hydrophilic ones, too. Amphiphilic molecules have also been encapsulated. The binding of hydrophilic and amphiphilic substances is challenging because these compounds are effectively hydrated, and water of hydration must be removed for binding to occur. To effect host−guest binding, unusual conformations of more hydrophilic guests have been observed within **41**.

In an initial study,[190] it was observed that cage Pt-**41** did not bind natural monosaccharides, such as D-glucose, D-fructose, and D-mannose, in water. However, pentamethylated α-D-glucose was quantitatively encapsulated within Pt-**41** with an association constant (K$_a$) > 10^8 M^{-1}. Monomethylated α-D-glucose was also bound by Pt-**41**.

The host−guest interactions between the aromatic capsule walls and natural disaccharides were then examined (Figure 43). It was discovered that D-sucrose (**129**), a highly hydrated
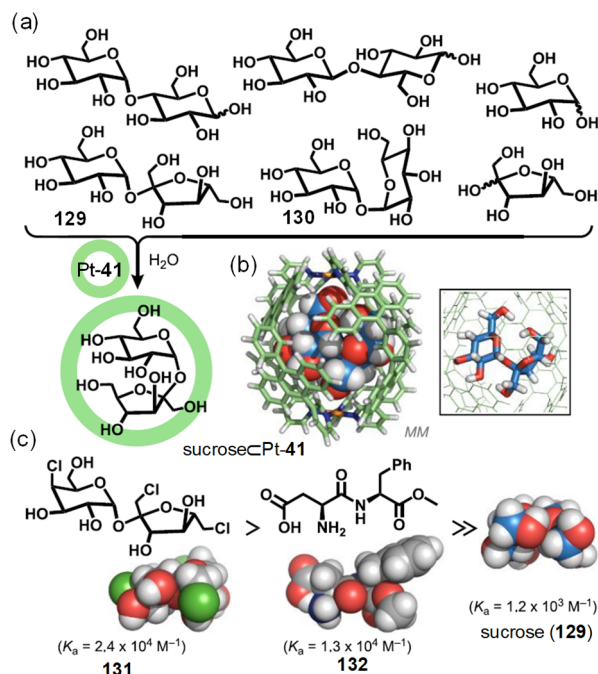
Figure 43. (a) Selective sucrose recognition by Pt-**41** in water and (b) the X-ray crystal structure of sucrose⊂Pt-**41**. (c) Hierarchy of binding affinity of artificial and natural sweeteners by Pt-**41**.[190] Reproduced with permission from ref 136. Copyright 2019 American Chemical Society.

biomolecule, was selectively encapsulated by Pt-**41** from mixtures of other natural disaccharides in water. In a competitive binding experiment, cage Pt-**41** was mixed with equivalent amounts of D-sucrose and D-trehalose (**130**) in aqueous solution, leading to the exclusive formation of the D-sucrose⊂Pt-**41** host−guest complex.

Capsule Pt-**41** also bound the sugar substitutes sucralose (**131**) and aspartame (**132**) in water. Competitive encapsulation experiments revealed the binding preference follows the order of sucralose (K$_a$ = 24,000 M^{-1}) > aspartame (K$_a$ = 13,000 M^{-1}) > D-sucrose (K$_a$ = 1,200 M^{-1}). The lower hydrophilicity of sucralose, which has three hydrophobic chloro substituents, enhances its affinity for the hydrophobic cavity of Pt-**41**. Interestingly, the observed order of binding affinity mirrors the relative sweetness perceived in these compounds.

In a subsequent study,[191] the encapsulation of hydrophilic lactic acid oligomers in water by **41** was demonstrated. The cavity captured tetra(lactic acid) **132** preferentially from a mixture of other oligomers, from dimer to octamer, with a binding constant of 3.3 × 10^5 M^{-1}. In the crystal, the encapsulated tetra(lactic acid) contacts the shell of **41** (Figure 44), and no interactions between the Pd^{II} centers of **41** and the carboxy or hydroxy termini of the guest were observed.

In the above examples, calculations, X-ray crystallographic and ITC analyses indicated that this ability of **41** to trap hydrophilic molecules derives from enthalpic stabilization through multiple and effective C−H•••π interactions with the host anthracene panels and from hydrogen-bonding with its pyridine rings.
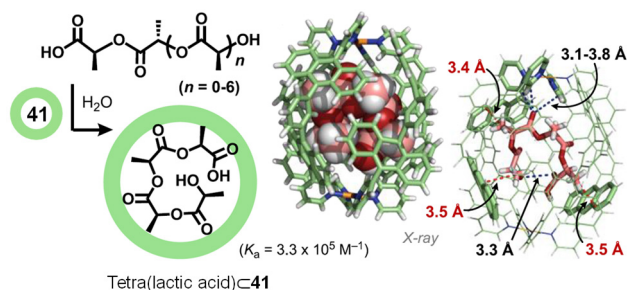
Figure 44. Preferential binding of lactic acid tetramer by **41**.[191] The X-ray crystal structure and specific host−guest interactions are shown. Reproduced with permission from ref 136. Copyright 2019 American Chemical Society.

Capsule Pt-**41** also proved capable of binding amphiphilic oligo(ethylene glycol)s in water in two distinct ways, depending on the chain length (Figure 45a).[192] First, one
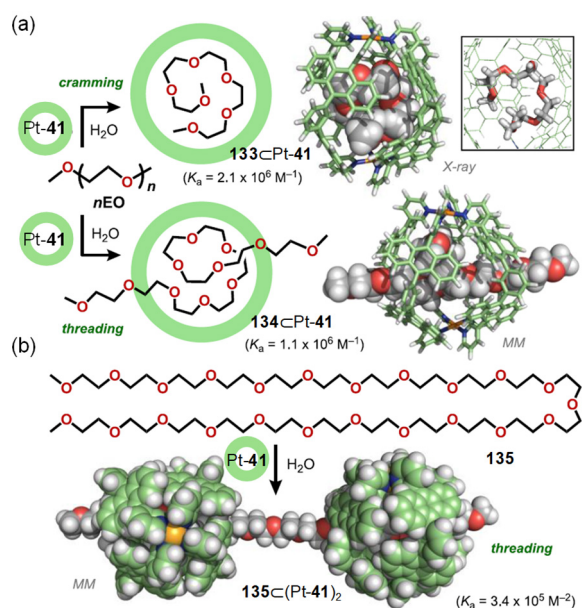
Figure 45. (a) Coiling of **133** and threading of **134** into Pt-**41** in water, showing the X-ray and computationally optimized structures of **133**⊂Pt-**41** and **134**⊂Pt-**41** complexes, respectively.[192] (b) Formation of pseudorotaxane complex **135**⊂(Pt-**41**)$_2$. Reproduced with permission from ref 136. Copyright 2019 American Chemical Society.

molecule of shorter penta(ethylene glycol) (**133**) was quantitatively encapsulated by Pt-**41** in a coiled conformation, as confirmed by X-ray crystallographic analysis. The series from tetramer to octamer folded similarly within Pt-**41**. The larger decamer **134**, in contrast, threaded through the capsule to form a 1:1 **134**⊂Pt-**41** pseudorotaxane host−guest complex. These binding events proceeded with relatively high binding constants ($K_a > 10^6$ M^{-1}). Interestingly, longer poly(ethylene oxide)s of ~7 nm such as **135** also threaded through Pt-**41** to give 2:1 host−guest complex **135**⊂(Pt-**41**)$_2$ in water (Figure 45b). As with other hydrophilic guests, ITC studies revealed enthalpic stabilization to be the dominant driving force, with C−H•••π and hydrogen-bonding interactions playing important roles.

A similar cavity-induced guest coiling underpinned the recognition of natural fatty acids by receptor Pt-**41**.[193] In water, cage Pt-**41** exclusively recognizes monounsaturated

natural fatty acids from a mixture of unsaturated and corresponding saturated substrates (*e.g.*, oleic and stearic acids). Pt-**41** also binds multiply unsaturated fatty acids, which are stabilized within the cage against degradation in the presence of air, light, and heat. The selective recognition of fatty acids is challenging due to their long, flexible, and weakly interacting hydrocarbon chains; their inclusion within receptor Pt-**41** is possible, however, because of the synergy of hydrophobic effects and multiple C−H•••π and π•••π host−guest interactions.

3.1.3. Heterotropic Guest Binding within WSCCs.

The selective formation of complexes of more than one distinct guest has been of great interest because new behavior and functions are expected to emerge as a result of interguest communication.[174] It is challenging to engineer such interactions in bulk aqueous solution, however. The probability of specific ensembles of guest molecules coming together is low due to their limited concentrations in solution. However, the encapsulation of poorly soluble molecules within WSCCs brings guests into solution and close proximity. Palladium(II) octahedron **6** served as a vehicle for the Fujita group to explore the binding of different guests together in water.[155]

Yoshizawa's Pt-**41** enabled preparation of emissive ternary aqueous host−guest complexes and modulation of guest photophysical behavior through the coencapsulation of different fluorescent dyes.[194] The boron dipyrromethene (BODIPY, **136**), coumarin 153 (**137**), and Nile red (**138**) were quantitatively encapsulated by Pt-**41** in water through the hydrophobic effect (Figure 46a). Studies of the corresponding host−guest complexes revealed that guests **136**−**138** retained their intrinsic emissivities of ~60% within capsule Pt-**41** in water. Long-lived fluorescence (7.4 ns) was observed at $\lambda >$ 585 nm from BODIPY in the complex **136**⊂Pt-**41** when the guest was excited at 525 nm in water; this lifetime is comparable to that of free BODIPY (**136**) (5.7 ns) in CH$_3$CN.

Capsule (**136**⊂Pt-**41**) containing only one molecule of BODIPY emits green fluorescence with a quantum yield Φ_F = 0.5. The color of emission of the host−guest complex changes, however, upon coencapsulation with an additional molecule of a planar aromatic (Figure 46b). In aqueous solution, 9-methylanthracene **139** within (**136**•**139**⊂Pt-**41**) emitted orange fluorescence with Φ_F = 0.36 and showed a broad emission band around λ_{max} = 577 nm, which is shifted toward the red ($\Delta\lambda$ = 42 nm) as compared with that of (**136**⊂Pt-**41**).

Confined in the capsule, the emission color of BODIPY is sensitive to the identity of the coencapsulated guest. While the (**136**•**140**⊂Pt-**41**) complex containing anthracene (**140**) exhibited strong yellow emission (Φ_F = 0.42 and λ_{max} = 554 nm), the phenanthrene-containing ternary complex (**136**•**141**⊂Pt-**41**) displayed strong green fluorescence (Φ_F = 0.58) with a sharp emission band at λ_{max} = 538 nm. Insertion of pyrene derivatives also modulated the fluorescent properties of BODIPY (**136**) within the capsule, leading to aqueous solutions with yellow and orange emissions (Φ_F = 0.36−0.48).

These new emissive host−guest complexes thus enable new applications of organic dyes as chemosensors, biological labels, and light-emitting materials in aqueous media, as would be limited by the poor solubility and the usual tendency of these dyes to self-quench emission *via* the formation of nonemissive aggregates. WSCCs can enable the solubilization of large hydrophobic dyes and pigments in water without chemical modifications, engendering photophysical properties that are otherwise available only in organic solvents. The examples
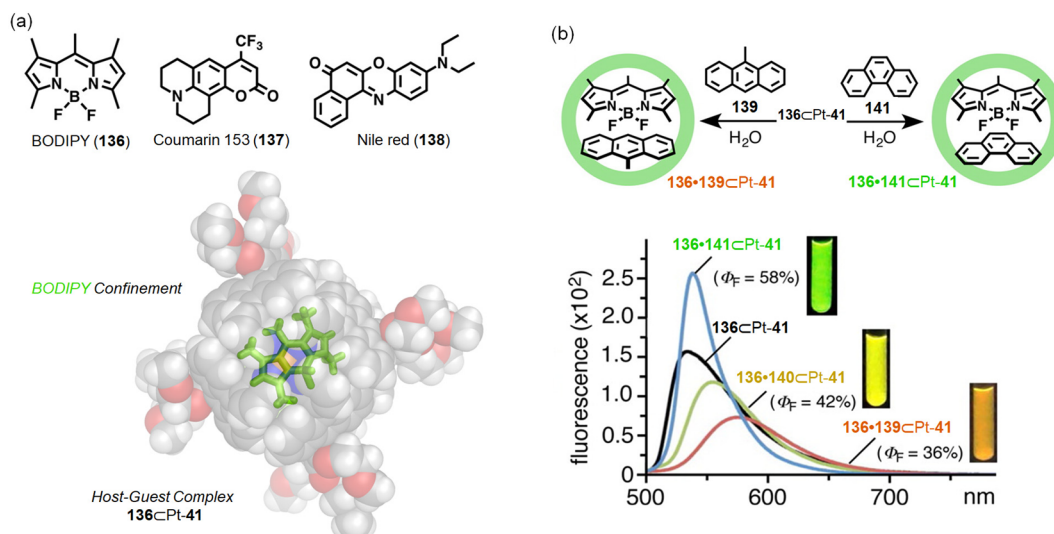
Figure 46. (a) Fluorescent guests **136**−**138** for Pt-**41** and the X-ray crystal structure of **136**⊂Pt-**41** with the cage represented as transparent spheres and the included BODIPY in green. (b) Schematic representation of the formation of **136•139**⊂Pt-**41** and **136•141**⊂Pt-**41** along with the fluorescence spectra (H_2O, λ_{ex} = 495 nm, rt) of **136•139**⊂Pt-**41**, **136•140**⊂Pt-**41**, **136•141**⊂Pt-**41**, and **136**⊂Pt-**41**. (b) Adapted with permission from ref 194. Copyright 2015 American Chemical Society.

shown above thus elucidate how WSCCs may allow for the development of new photofunctional materials for aqueous applications.

The Fujita group has demonstrated the aqueous solubilization of poorly soluble organic molecules and the selective creation of stable heterotropic guest combinations within the water-soluble prisms **142**−**147** (Figure 47).[195] The general
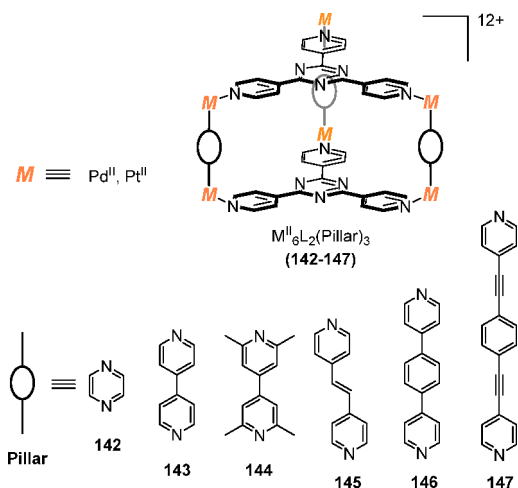
Figure 47. Water-soluble triangular prisms **142**−**147** prepared through the use of different bipyridyl pillars.[195]

$M^{II}_6L_2Pillar_3$ structure of these cages combines triazine panels (**5**), M^{II} ions (M = Pd^{II}, Pt^{II}) with chelating ancillary ligands, and ditopic pyridyl-based pillars. By choosing different pillars, the height of the host, as well as the type and number of guests that bind, can be adjusted.

In an example of the use of these hosts for enhancing the effective aqueous solubility and photo-optical properties of hydrophobic aromatics, the red-fluorescent dye tetraazaporphyrin **148** was bound within coordination cage **142**, which endowed the dye with water solubility and prevented its aggregation in solution and the solid state (Figure 48a).[196]

Electron-deficient **148** does not form a charge-transfer complex with cage **142** and fluoresces when bound. Additionally, encapsulation within the highly cationic host enhances the acidity of the interior protons, such that addition of NEt_3 quenches the emission of **148** *via* deprotonation.

Taller prismatic hosts were used to template the endohedral formation of heterotropic aromatic stacks with specific heights and ordering in aqueous solution. These box-shaped cavities can be also used to engineer pairwise aromatic stacks even if the host−guest complexes exhibit unfavorable interactions.

For example, the D−A inclusion complex (**149•150**)⊂**144** selectively formed from a 1:1 mixture of donor **149** and acceptor **150**, triazine **5**, the pillar ligand (2,2′,6,6′-tetramethyl-4,4′-bipyridine), and [(en)Pd(NO_3)_2] in D_2O at 100 °C (Figure 48b).[197] The exclusive formation of (**149•150**)⊂**144** highlights the greater stability of the heterotropic D−A complex over either of the homotropic complexes, (**149**)_2⊂**144** or (**150**)_2⊂**144**. Treatment of cage **144** only with donor **149** resulted in the formation of D−D complex (**149**)_2⊂**144**, but when treated with **150**, one equivalent of **149** was displaced to give the heterotropic (**149•150**)⊂**144** complex.

The inner spaces of these pillared cages also enabled the formation of stacked heterometallic clusters containing soft d^{10} metal ions. Within cage **146**, the trinuclear Au^I_3 complex **151** takes up additional Ag^I ions to form a triple-decker heterometallic cluster (**151•Ag^I•151•Ag^I•151**) (Figure 48c).[198] The inclusion complex (**151•5•151**)⊂**146**, in which electron-deficient triazine **5** was sandwiched between molecules of electron-rich **151**, was a suitable precursor for this triple-decker complex. When (**151•5•151**)⊂**146** was treated with additional **151** (1 equiv) and $AgNO_3$ (2 equiv) at 40 °C for 12 h, the replacement of guest **5** with **151** occurred smoothly and was accompanied by Ag^+ ion uptake to form the (**151•Ag^I•151•Ag^I•151**)⊂**146** triple-decker ion cluster inside **146**, whose structure was determined by X-ray crystallography. Formation of this heterometallic cluster was specific to Ag^I ions as a consequence of favorable $Au^I \cdots Ag^I$ interactions (Au−Ag distances = 2.694−2.823 Å). The authors emphasized that this
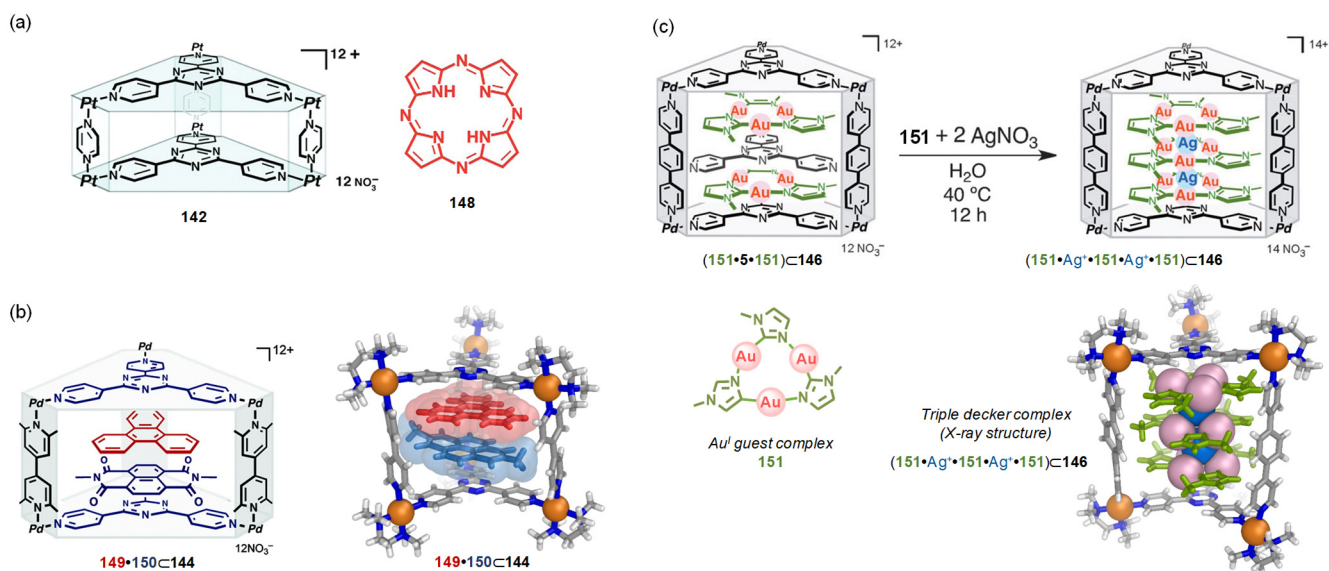
Figure 48. (a) Prism **142** encapsulates tetraazaporphyrin **148**, preserving its red emission.[196] (b) Electrostatic interactions in discrete stack **144**; the D−A heterocomplex (**149•150**)⊂**144** is shown along with its X-ray crystal structure.[197] (c) Formation of triple-decker cluster (**151•Ag^I•151•Ag^I•151**)⊂**146**; the X-ray crystal structure is shown.[198] Structural formulas of pillared cages shown in (a, b, and c) are reproduced with permission from refs 196, 197, and 198, respectively. Copyrights 2009 and 2010, American Chemical Society, and 2012 Wiley-VCH.

triple-decker complex remains stable in aqueous solution because it is tightly encapsulated by the box-shaped cage, and it could not have been synthesized without the help of the WSCC.

The same group also reported base pair formation of mononucleotides within pillared cages.[199] In water, anti-Hoogsteen hydrogen bonding between 5′-adenosine (**152**) and 5′-uridine (**153**) monophosphates formed within the cavity of a platinum(II) analogue of cage **142** as was confirmed by X-ray analysis (Figure 49a).

When platinum(II) prism **143** with an expanded cavity was used, the cavity selectively bound and stabilized a dinucleotide base-pair duplex. An aqueous solution of thymidylyl-(3′-5′)-2′-deoxyadenosine (**154**) was stirred with **143** to give the host−guest complex (**154**)$_2$⊂**143**. The crystal structure of the host−guest complex showed two hydrogen-bonded adenosine−thymidine pairs connected by anti-Hoogsteen-type pairing (Figure 49b). Short nucleotide fragments are not able to form stable hydrogen-bonded base pairs or duplexes in water; however, they form within the hydrophobic environment of these pillared hosts and remain stable because the hydrogen bonds are protected from competition by water.

3.2. Charged Guest Molecules

Aqueous media are competitive environments for the recognition of ions. While hydrophobic effects, and an optimal shape and size match between cage cavity and guest, satisfy the conditions for binding neutral molecules in water, effective electrostatic host−guest attractions often contribute to the recognition of charged guests. Because of the challenging nature of binding charged guests in water, few WSSCs have successfully been employed for this purpose to date.

3.2.1. Cation Binding. Making use of the hydrophobicity and the anionic charge of host assembly **10**, Raymond, together with Bergman and Toste for some studies, have extensively studied the encapsulation of cationic guests in aqueous media, ranging from simple organic ammonium species to more complex organometallic complexes. Early
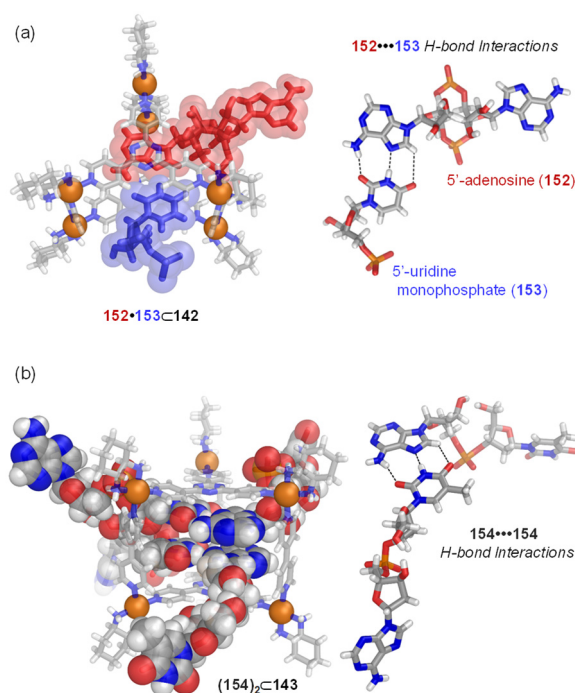
Figure 49. Crystal structures of (a) the (**152•153**)⊂**142** inclusion complex, highlighting H-bonds between nucleotides, and (b) the (**154**)$_2$⊂**143** duplex formed in a taller cage.[199]

reports on cage **10** investigated the binding of alkyl ammonium cations, revealing that the strength of the host−guest interactions is dependent on the size of the cation. Cage **10** exhibited a preference for the inclusion of Et$_4$N$^+$ (**155**) over the smaller Me$_4$N$^+$ (**156**) or the larger Pr$_4$N$^+$ (**157**) (Figure 50a).[45]

A range of reactive cations have been kinetically stabilized by encapsulation, which decompose in water in the absence of **10**. For instance, the condensation of pyrrolidine and ketones in
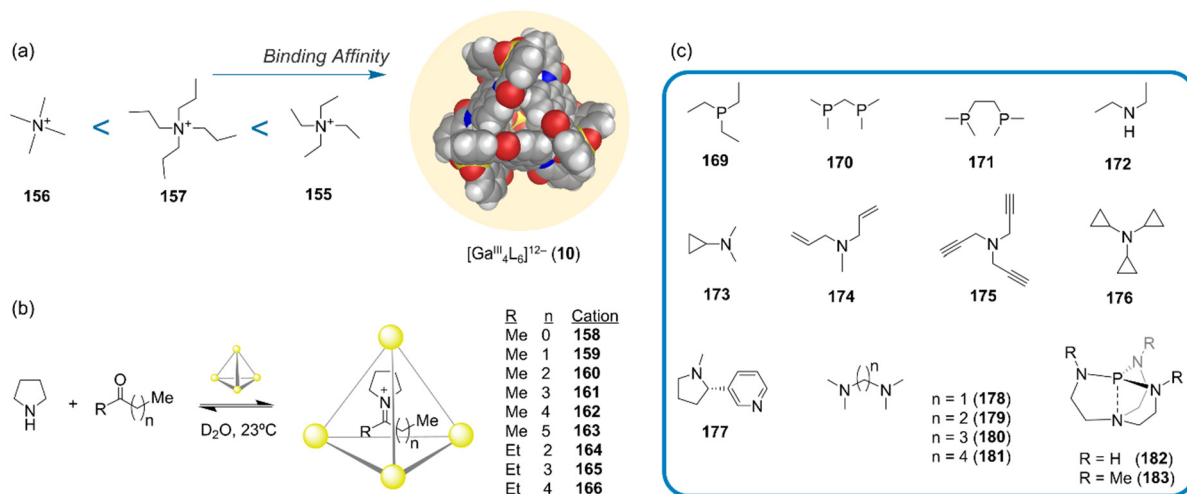
Figure 50. Cation binding within cage **10**. (a) Cage **10** exhibits a preference for the inclusion of Et_4N^+ over the smaller Me_4N^+ and larger Pr_4N^+.[45] (b) Stabilization of iminium ions generated in water from pyrrolidine and various ketones.[200] (c) Examples of amines and phosphines that bind within **10** upon protonation.[201]

water at basic pH in the presence of tetrahedron **10** resulted in the quantitative formation and stabilization of inclusion adducts of the corresponding iminium ions **158**−**166** (Figure 50b).[200] The binding affinities of these cations varied according to the size of the guest and was maximized for pentanone and hexanone derivatives. In the absence of cage **10**, no iminium ion was detected. In aqueous solution, iminium ions usually exist only transiently due to their high reactivity toward hydrolysis, but once encapsulated, these cations remained intact for months at room temperature.

Amines and phosphines **169**−**183** were also observed to bind in the interior of **10** upon protonation (Figure 50c). Interestingly, the basicity of many of these amines was increased by encapsulation,[201] with shifts observed of up to 4.5 pK_a units.

Because of its affinity for cationic species, tetrahedron **10** could also stabilize reactive organometallic intermediates in aqueous solution through encapsulation.[202] Cage **10** was shown to encapsulate the *in situ* generated $[Cp^RRu(cis\text{-}1,3,7\text{-}octatriene)]^+$ cationic species **186** or **187** generated from $[Cp^RRuCl(COD)]$ (R = H (**184**) or Me (**185**); COD = 1,5-cyclooctadiene) (Figure 51a).

Notably, the unbound cationic ruthenium complexes decomposed within hours in organic solution and within
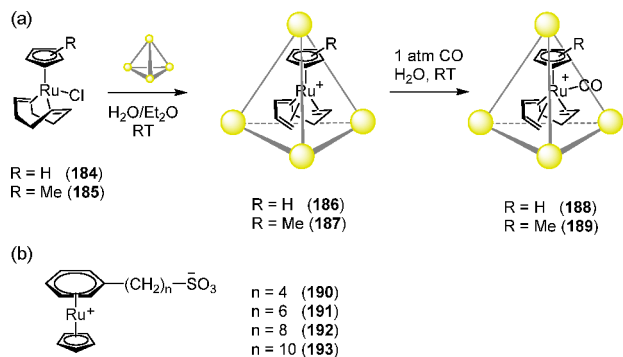
minutes in water; however, the corresponding host−guest complexes proved stable in aqueous solution for weeks. Despite their stabilization, the guest molecules were still able to react inside the cage cleanly and stoichiometrically with CO to yield the new $[CpRu(COD)(CO)]^+$ cations **188**−**189**, which also remained stable in aqueous solution. When the aryl ligand of the ruthenium guest was functionalized with a sulfonate-terminated alkyl chain, the cationic part of the complexes **190**−**193** were encapsulated in the cavity, but the negatively charged alkylsulfonate group protruded out of one of the openings due to electronic repulsion (Figure 51b).[203]

Investigations on cation binding using Raymond's $[M^{III}_4L_6]^{12-}$ host **10** indicate that guest ingress and egress does not require a ligand dissociation step.[95] Small apertures exist in the triangular faces of the host, and a concerted cluster distortion is inferred to enlarge these gaps for guests to pass through.

Raymond, Bergman, and co-workers have explored the concept of external guest binding with WSCC **10**. These investigations revealed that cationic guest molecules interact with both the exterior of host **10** in water, through ion-association, and its interior, through encapsulation.[204] These cation-binding studies indicate that the driving force for encapsulation is the entropy-driven desolvation of the host interior and the guest, whereas external cation association is enthalpy driven and mainly due to attractive interactions between the guests and the exterior surface of the assembly.[205]

Our group also observed that guanidinium cations (**194**) bind to the exterior of the $[Fe^{II}_4L_6]^{4-}$ cage **27** in water, bridging between three sulfonate groups through six hydrogen bonds (Figure 52).[206] The presence of guanidinium on the faces of **27** blocks guest exchange between bulk solution and the host's cavity. Kinetic studies on the uptake of cyclohexane into host **27** in the presence of guanidinium cations showed a decrease in the uptake rate constant (k_{up}) as a function of the guanidinium concentration in D_2O. The k_{up} value in the presence of nonbinding $[Me_4N]^+$ was $(2.73 \pm 0.07) \times 10^{-6} s^{-1}$, but in the presence of an equivalent concentration of guanidinium, it decreased to $(1.81 \pm 0.02) \times 10^{-6} s^{-1}$.

3.2.2. Anion Binding. Receptors that bind anions in water have potential applications in the biological, medical,

Figure 51. (a) The organometallic intermediates **186**−**189** are stabilized in water within **10**.[202] (b) Structural formula of Ru^{II} complexes **190**−**193** that are partially encapsulated.[203]
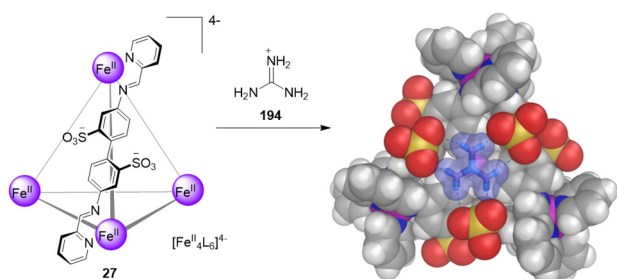
Figure 52. Binding of guanidinium to the faces of **27**.[206] A space-filling representation is shown of the crystal structure of host **27**, as viewed perpendicular to a face capped by one guanidinium ion (**194**, depicted in blue).

industrial, and environmental areas. For example, many therapeutic molecules and pollutants found in water are anionic. The design of receptors for anions in water remains a challenge.[207−210] The metal-cation frameworks of WSCCs render them electronically complementary to anions, facilitating binding.

Cationic coordination cages have been observed to act as receptors for many different anions in polar organic solvents.[211] Fewer examples of coordination cages that encapsulate anions in water have been reported, however.[212,213] In addition to being soluble and stable under aqueous conditions, the design of such WSCCs has required the incorporation of specific recognition sites that promote anion anchoring and electrostatic attraction.

The success of this approach was illustrated by Custelcean and Hay, who prepared a metal−organic tetrahedral host that specifically binds sulfate in water.[214] Sulfate is highly hydrophilic and structurally similar to other members of the series of tetrahedral oxoanions.

The computer-aided design of their host **195** (Figure 53a) led to two key design features. First, the incorporation of inward-facing urea functional groups capable of forming a
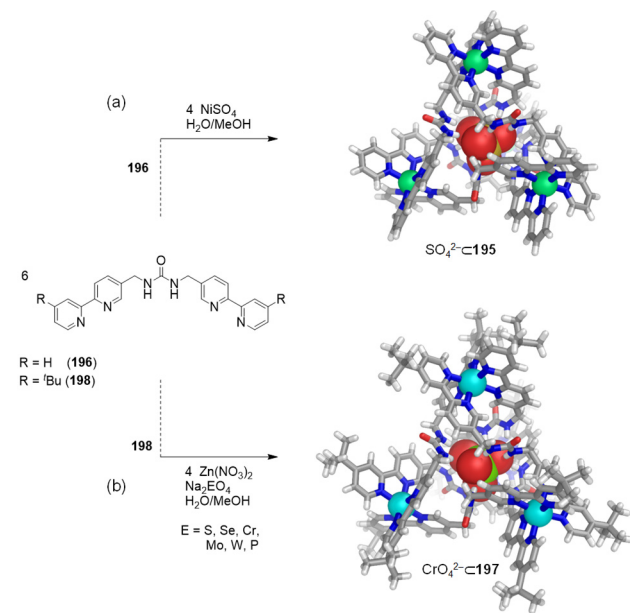
dense set of hydrogen bonds with sulfate in the cavity. Second, for aqueous stability, the cage vertices were chosen to be $[Ni(bpy)_3]^{2+}$ (bpy = 2,2′-bipyridine) complexes, which have exceptionally high stability.[215]

This design process resulted in the synthesis of ligand **196**. Mixing **196** with $NiSO_4$ in $H_2O/MeOH$ yielded the complex $[Ni^{II}_4L_6(SO_4)](SO_4)_3$ ($SO_4 \subset$**195**). A homochiral metal−organic tetrahedral cage encapsulating one sulfate anion was formed, where the internal hexa-urea arrangement anchors the sulfate through 12 hydrogen bonds, the maximum number that sulfate may accept. To estimate the sulfate binding strength, precipitation experiments were carried out using Sr^{II} and Ba^{II} salts. The results converged to an estimated sulfate binding constant K_{app} of 6.0×10^6 M^{-1}, an exceptionally high value for a hydrophilic anion in water.

Extending these results, $Zn^{II}_4L_6$ tetrahedron **197** was prepared from ligand **198** and $Zn(NO_3)_2$ (Figure 53b). External functionalization with ${}^tBu$ groups led to enhanced solubility of **197** in aqueous methanol solutions. This new cage proved capable of selectively encapsulating tetrahedral oxoanions EO_4^{n-} (E = S, Se, Cr, Mo, W, n = 2; E = P, n = 3) from aqueous solutions, based on shape, size, and charge recognition (Figure 53b).[216]

The selectivity among the series of oxoanions investigated showed the following trend: $PO_4^{3-} \gg CrO_4^{2-} > SO_4^{2-} > SeO_4^{2-} > MoO_4^{2-} > WO_4^{2-}$. A detailed solution investigation (D_2O/CD_3OD) combined with solid-state studies indicated that self-assembly of the urea-containing cages **195** and **197** is templated by the oxoanions. Upon removal of the templating anion, these tetrahedra rearrange into different coordination assemblies.

In a related approach, Kaifer and co-workers further illustrated the utility of urea groups and their affinity for sulfate anions (Figure 54).[217] Using subcomponent self-
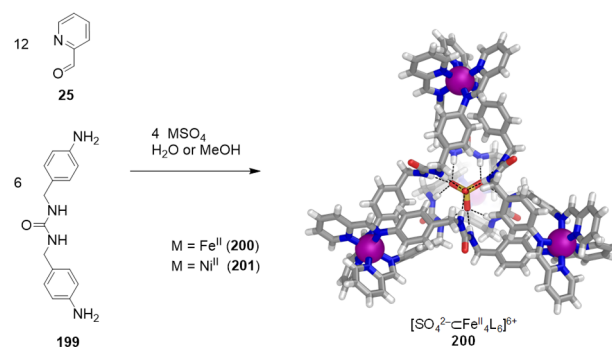
Figure 54. Subcomponent self-assembly of cages **200** and **201**.[217] The X-ray crystal structure of **200** is shown along with the hydrogen bonding between the central SO_4^{2-} and the urea functions.

Figure 53. Self-assembly of the urea-functionalized anion hosts constructed from (a) nickel(II)[214] and (b) zinc(II).[216] Representative X-ray structures of the host−guest complexes are depicted.

assembly, a combination of six equivalents of bis-urea subcomponent **199**, 12 equivalents of 2-formylpyridine (**25**), and four equivalents of $FeSO_4$ or $NiSO_4$, yielded the tetrahedral cages **200** and **201**, respectively. X-ray analyses confirmed that each cage envelops a single sulfate anion through 12 hydrogen bonds. As in the previous examples, sulfate served as a template for the assembly of these cages. Templation attempts using PF_6^-, ClO_4^-, Cl^-, and PO_4^{3-} failed to form discrete hosts.

WSCCs built on aromatic shells with multiple positive charges provide suitable inner spaces for the selective recognition of anions in aqueous solution. In contrast to

other WSCCs reported by the Yoshizawa group, the polycationic capsule 51 did not bind neutral compounds (*e.g.*, cyclophane, pyrene, and fullerene C_{60}).[82] On the contrary, cycloalkanes with anionic trifluoroborate substituents, such as cycloheptyltrifluoroborate 202, are encapsulated by cage 51 (Figure 55).
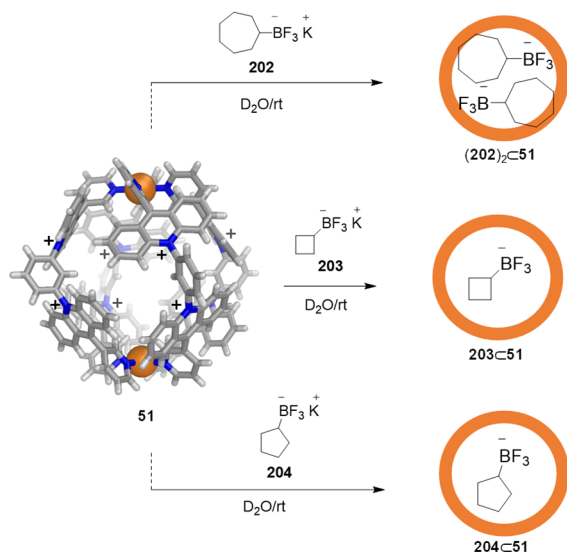
Figure 55. Schematic representation of the encapsulation of trifluoroborates by capsule 51 in water.[82]

For the formation of stable host−guest complexes with capsule 51 in water, the guest must possess both anionic and hydrophobic character. Neither neutral hydrophobic cycloheptane, nor anionic hydrophilic sodium *p*-toluenesulfonate were encapsulated within 51. Conversely, trifluoroborates 203 and 204, with smaller hydrophobic cyclobutyl and cyclopentyl groups, respectively, were also bound in the polycationic cavity of 51 to give 1:1 host−guest complexes.

The subcomponent self-assembly method has also enabled the use of cationic panels to build hosts for binding anions in water. Our group prepared the azaphosphatrane-functionalized tetrahedron 205 from cationic triamine 206 (Figure 56a).[218] Subcomponent 206 contains a P^+−H moiety, which was anticipated to provide water solubility as well as enhancing the electrostatic attraction and hydrogen bonding between the host and anionic guests. The MeCN-soluble $Fe^{II}_4L_4$ cage was prepared as shown in Figure 56a. X-ray crystallographic analysis confirmed that the $Fe^{II}_4L_4$ structure has a face-capped tetrahedral framework with approximate *T*-symmetry, in which the P^+−H groups of the azaphosphatrane units point inward (Figure 56b). The central cavity has a volume of *ca.* 166 Å^3, which is occupied by a disordered TfO^-.

The reaction of the sulfate salt of ligand 206 with $FeSO_4$ in water failed to give the corresponding water-soluble version of cage 205, probably due to the hydrophilic character of SO_4^{2-}, preventing it from acting as a template for cage formation. A series of other anions with volumes ranging from 35 Å^3 (I^-) to 219 Å^3 ($CB_{11}H_{12}^-$) were thus screened by adding each to the
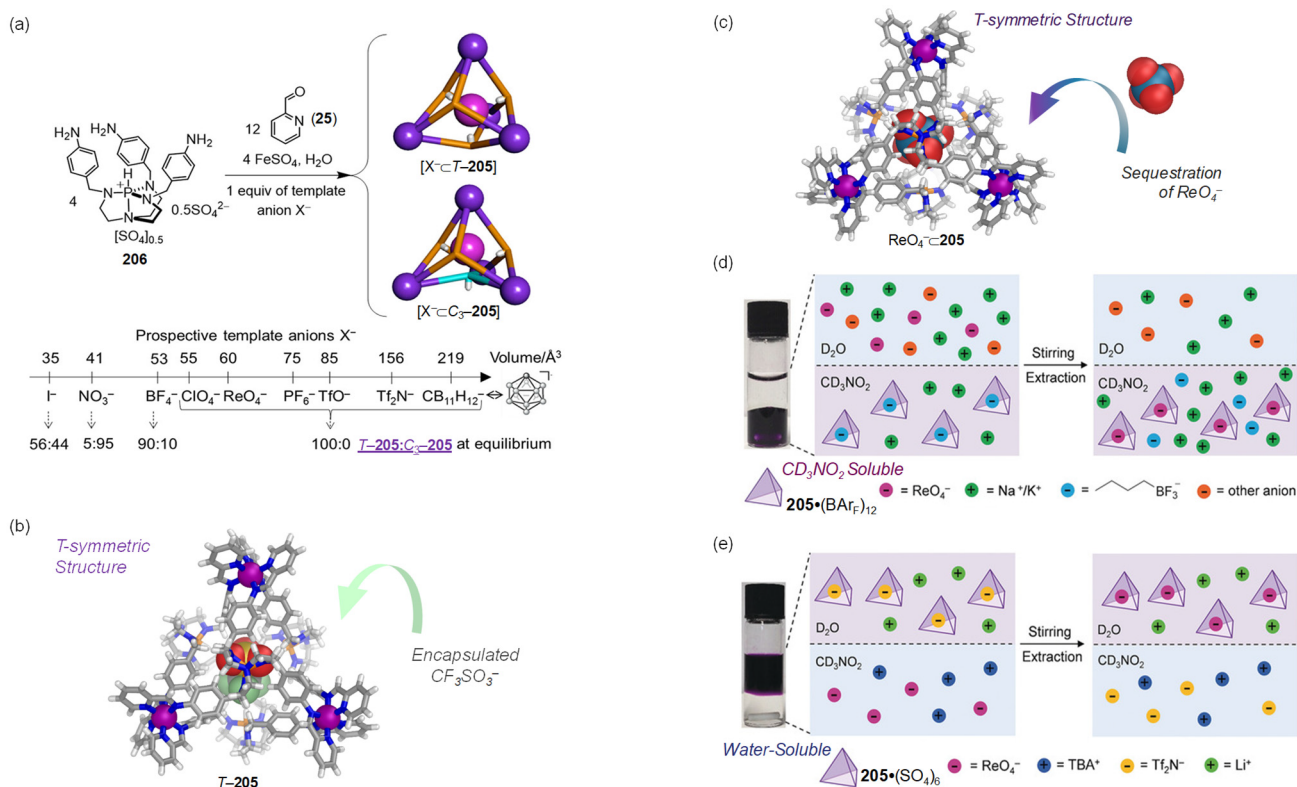
Figure 56. (a) Schematic representation of the cage isomers $X^-⊂T$-205 and $X^-⊂C_3$-205 obtained by aqueous self-assembly in the presence of template anions. Adapted with permission from ref 218. Copyright 2017 American Chemical Society. (b) X-ray structure of the $OTf^-⊂T$-205 complex. (c) X-ray crystal structure of $ReO_4^-⊂205$. (d) Selective extraction of ReO_4^- from water into an organic phase in the presence of competing anions. (e) Liquid−liquid extraction of ReO_4^- from an organic phase into water. Adapted with permission from ref 219. Copyright 2018 Wiley-VCH.

Figure 57. (a) Self-assembly reaction to form fluorescent tetrahedron **208**; an MM3-optimized molecular model of the cage is depicted. (b) While neutral molecules and nucleobases were not encapsulated, their anionic congeners, including nucleotides, were bound in fast exchange; affinity constants were measured from NMR titration experiments.[220]
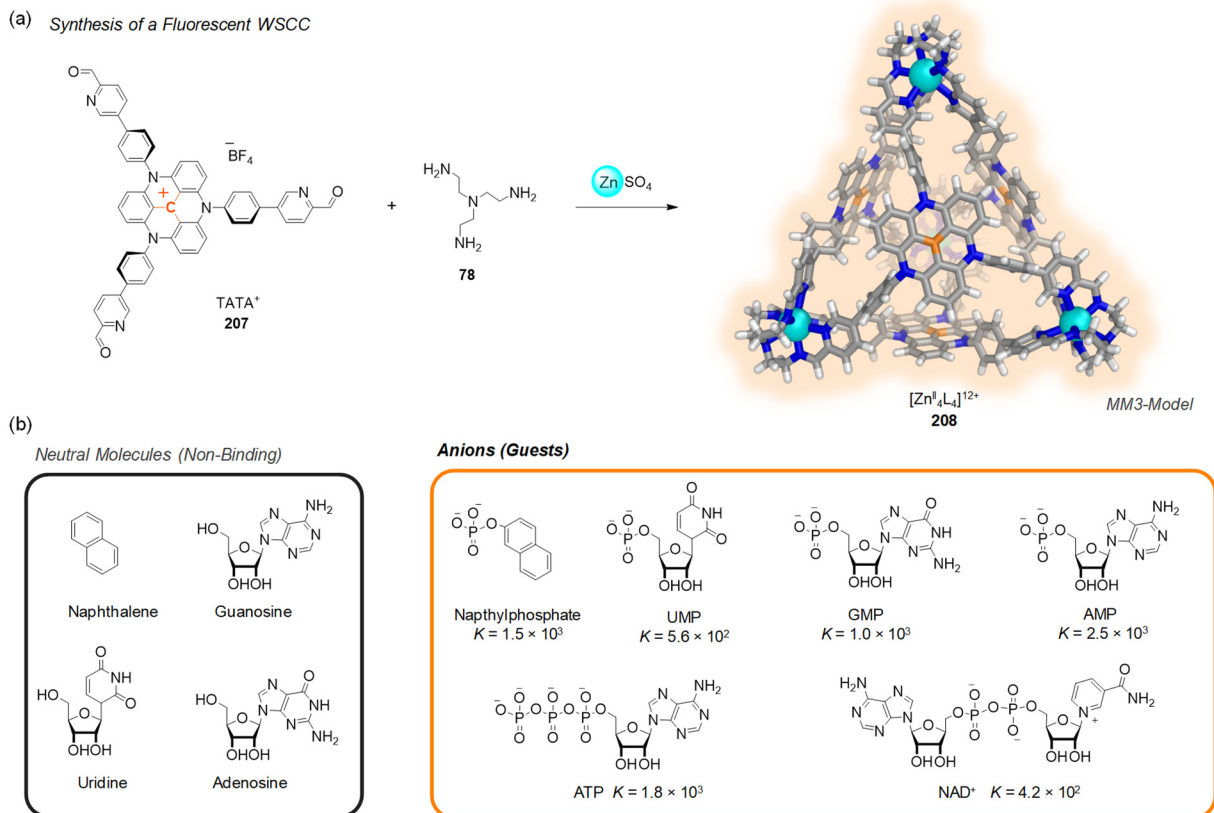
aqueous reaction mixture; all proved to be competent templates for **205** in water.

The designed flexibility of **205** enabled the aqueous binding of these anions *via* hydrogen bonding and electrostatic interactions, triggering structural adaptation of the cage framework in response to the sizes and shapes of template anions. Cage **205** manifested this adaptability in a novel way: for the smaller template anions, with volumes ≤53 Å^3, part of the population of **205** consisted of a C_3-symmetric isomer (C_3-**205**) in which one of the azaphosphatrane P$^+$−H groups was oriented away from the inner cavity (*exo*) with the other three pointing inward (*endo*). A T-symmetric isomer (T-**205**), containing four *endo* P$^+$−H groups, constituted the other part of the population. For the larger anionic templates, having volumes ≥55 Å^3, the T-**205** isomer was observed exclusively.

Although the cage was unstable in water in the absence of a template anion, competitive guest exchange offered a way of measuring the relative binding affinities of the different anions, revealing the following anion binding hierarchy: PF$_6^-$ > ReO$_4^-$ > OTf$^-$ > ClO$_4^-$ > CB$_{11}$H$_{12}^-$ > NTf$_2^-$ > BF$_4^-$ > I$^-$ > NO$_3^-$.

Selective anion extraction is desirable for the recovery and purification of valuable chemicals and in the removal of pollutants from the environment. Taking advantage of the anion-binding ability of the Fe$^{II}_4$L$_4$ cage **205**, we developed a method to selectively extract rhenium as perrhenate (ReO$_4^-$), a high-value anion and a nonradioactive surrogate of TcO$_4^-$, from water into nitromethane.[219] To this end, a water-insoluble version of the azaphosphatrane cage **205** was first prepared, having tetrakis[3,5-bis(trifluoromethyl)phenyl]-borate (BAr$_F^-$) counteranions and one encapsulated *n*-

butyltrifluoroborate (^{n}BuBF$_3^-$) anion. The ^{n}BuBF$_3^-$ anion templated the cage while still being readily replaced by other anions. The resultant ^{n}BuBF$_3^-$⊂**205**•(BAr$_F$)$_{11}$ cage salt was readily soluble and stable in CD$_3$NO$_2$.

Competitive guest exchange yielded the following hierarchy of anion-binding affinities in CD$_3$NO$_2$: CB$_{11}$H$_{12}^-$ > ReO$_4^-$ > OTf$^-$ > PF$_6^-$ > ClO$_4^-$ > NTf$_2^-$ > BF$_4^-$ > I$^-$ > NO$_3^-$. This ordering differs from the one observed in water, given above. In both solvents, however, ReO$_4^-$ binds more strongly than other common anions. The crystal structure of **205** containing ReO$_4^-$ was obtained and confirmed the T-symmetric cage array (Figure 56c).

When the extractant ^{n}BuBF$_3^-$⊂**205**•(BAr$_F$)$_{11}$ in CD$_3$NO$_2$ was mixed with an equimolar amount of NaReO$_4$ in D$_2$O, ReO$_4^-$⊂**205**•(BAr$_F$)$_{11}$ was exclusively observed after separation of the two layers, indicating complete removal of ReO$_4^-$ from water. The selectivity of **205** toward ReO$_4^-$ was evaluated in the presence of 10 other different anions simultaneously in water: F$^-$, Cl$^-$, Br$^-$, I$^-$, SO$_4^{2-}$, ClO$_4^-$, NO$_3^-$, BF$_4^-$, H$_2$PO$_4^-$, and AcO$^-$ (1 equiv per ReO$_4^-$ in each case) (Figure 56d). Under these conditions, the extraction efficiency for ReO$_4^-$ by **205** was 97%, with ClO$_4^-$ comprising the other 3% extracted. The high charge density of cage **205** renders it unstable in ethyl acetate (EtOAc). This feature was exploited to establish a mechanism to release and separate the extracted ReO$_4^-$ guest while recovering the cage extractant. After extraction from water, the nitromethane layer was first separated and the solvent evaporated. The isolated cage was then redissolved in degassed EtOAc, where it disassembled into its constituents. Consequently, the extracted ReO$_4^-$ guest moved to the water

phase, allowing its removal as the phases were separated. Regeneration of $^nBuBF_3^-\subset\mathbf{205}\bullet(BAr_F)_{11}$ was then realized by evaporating the EtOAc and adding $^nBuBF_3K$ in acetonitrile. In this manner, the cage extractant could be reused for further extraction sequences.

Perrhenate could also be extracted from an organic phase into water, in the opposite direction to the process described above. The water-soluble $NTf_2^-\subset\mathbf{205}\bullet(SO_4)_{5.5}$ was used as extractant, completely removing ReO_4^- from CD_3NO_2 into D_2O (Figure 56e). Control experiments revealed that without cage $\mathbf{205}$, ReO_4^- did not transfer to the aqueous layer, thus confirming the necessity of the WSCC.

In a few of the examples discussed above, the WSCCs were only stable in the presence of an anionic template (e.g., cages $\mathbf{197}$, $\mathbf{200}$, and $\mathbf{205}$), which might at first glance appear to limit their practical applications as ion receptors or transporters. However, this limitation can be overcome through the use of weakly binding anion templates, which can then be selectively replaced by a stronger-binding high-value target anion. This phenomenon can provide a means to control the lifetime of cages for prospective applications, for example, cage disassembly may be induced to recover the relevant cargo and the cage components recycled for reassembly, as was recently demonstrated using cage $\mathbf{205}$.[219]

The design of aqueous probes and sensors for complex, biologically relevant anions demands the preparation of more advanced and selective receptors. We recently developed a fluorescent tetrahedral assembly equipped with cationic faces that is capable of discriminating between anionic and neutral guests in water, while allowing fluorometric detection at micromolar concentrations in water at neutral pH.[220]

The reaction of tris-formylpyridine-TATA$^+$ (triazatriangulenium) subcomponent $\mathbf{207}$ with $ZnSO_4$, and TREN ($\mathbf{78}$) in 1:1 $H_2O:CH_3CN$ resulted in the quantitative formation of the WSCC $\mathbf{208}$. Within the luminescent TATA$^+$ panels that form the cage walls, tetrahedron $\mathbf{208}$ has an interior cavity of ca. 940 $Å^3$ (Figure 57a). Additionally, the presence of highly chelated Zn^{II} corners provides micromolar stability in water (see section 2.4) and preserves the TATA$^+$ emission because of the closed-shell ground state of zinc(II) ions. Upon photo excitation of $\mathbf{208}$ in H_2O at λ_{ex} = 520 nm, a single emission band was observed at λ_{max} = 570 nm.

A series of neutral molecules and anions were screened as guests for $\mathbf{208}$ (Figure 57b). The NMR and fluorescence studies revealed that $\mathbf{208}$ binds anions in preference to neutral molecules. Whereas naphthalene was not observed to bind, 2-naphthyl phosphate bound in fast exchange on the NMR time scale. A similar trend of neutral nonbinding and anion binding was observed among the uridine/uridine monophosphate (UMP), guanosine/guanosine monophosphate (GMP), and adenosine/adenosine monophosphate (AMP) pairs. Phosphate guests with higher charges, such as adenosine diphosphate (ADP) and adenosine triphosphate (ATP), were also bound by $\mathbf{208}$. The binding strengths were on the order of 10^3 M^{-1} for all phosphate nucleotides.

The fluorescence of the TATA$^+$ panels was quenched upon anion binding in water, thus confirming the ability of cage $\mathbf{208}$ to sense, via fluorescence, phosphorylated biomolecules over their unphosphorylated counterparts. For nonbinding neutral substrates, emission quenching of the TATA$^+$ panels was not observed, even after addition of a 100-fold excess of the neutral species.

Interestingly, nicotinamide adenine dinucleotide (NAD$^+$) was also observed to bind in D_2O. NMR studies showed that only the AMP portion of NAD$^+$ is bound and the positively charged nicotinamide fragment is repelled. Selective supramolecular encapsulants, such as $\mathbf{208}$, could thus enable new biomolecular sensing applications under biological conditions.

3.3. Guest-Induced Cage Transformations in Water

Discussion has so far mostly been limited to cases in which guest-binding brings about alterations in guest properties. As discussed in section 2.5, the size and shape of a WSCC can also be influenced by the action of templates, the concentration of reactants, or solvent composition. Guest encapsulation may also trigger structural transformations on a preformed host, resulting in the formation of a more energetically favored state.[221]

In 1999, Raymond and co-workers observed a guest-induced transformation from a triple helicate to a tetrahedral cluster due to host−guest interactions (Figure 58).[222] Ligand $\mathbf{209}$,
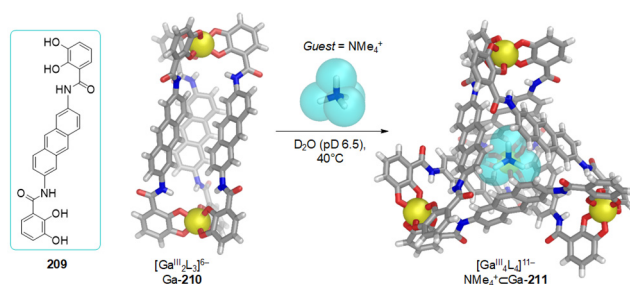
Figure 58. Helicate Ga-$\mathbf{210}$ transforms into tetrahedron Ga-$\mathbf{211}$ following the addition of Me_4N^+.[222]

built on a 2,6-diaminoanthracene backbone, reacted with $[TiO(acac)_2]$ in two different ways depending on the base employed. The use of KOH as the base afforded the helicate Ti-$\mathbf{210}$, whereas Me_4NOH produced the tetrahedral cluster Ti-$\mathbf{211}$. Both structures were characterized by X-ray crystallography. The Ti-$\mathbf{210}$ tetraanion displayed a chiral triple helical array, with either Δ or Λ stereochemistry at both metal centers and approximate D_3 symmetry. The structure of the tetranuclear complex Ti-$\mathbf{211}$ has idealized T symmetry, with one Me_4N^+ cation encapsulated within its cavity.

The hypothesis that Me_4N^+ might bring about the guest-induced interconversion between these two structures was investigated. To test this hypothesis, the gallium(III) analogues were prepared because of the greater lability of Ga^{III} ions compared to Ti^{IV}.

Addition of 20 equiv of Me_4NCl to a solution of $K_6[Ga_2L_3]$ (Ga-$\mathbf{210}$) in D_2O induced the quantitative transformation of the helicate to the tetrahedral cluster $Me_4N^+\subset$Ga-$\mathbf{211}$ over the course of 5 days at pD = 6.5, 40 °C (Figure 58). Although this transformation also took place at higher pD values (pD 7.5) and lower temperatures (room temperature), the conversion rates were lower due to the slower kinetics of metal−ligand rearrangement under these conditions. The formation of the tetrahedral product is inferred to be controlled by favorable interactions between the anionic host and the cationic guest.

The Fujita group reported the conceptually similar guest-induced $Pd_{18}L_6$ ($\mathbf{212}$) → $Pd_{24}L_8$ ($\mathbf{213}$) cage−cage conversion in water (Figure 59).[223] Both cages are closed-shell structures with large hydrophobic inner spaces composed of $[Pd(en)]^{2+}$ linking units bridged by 1,3,5-tris(3,5-pyrimidyl)pyrimidine
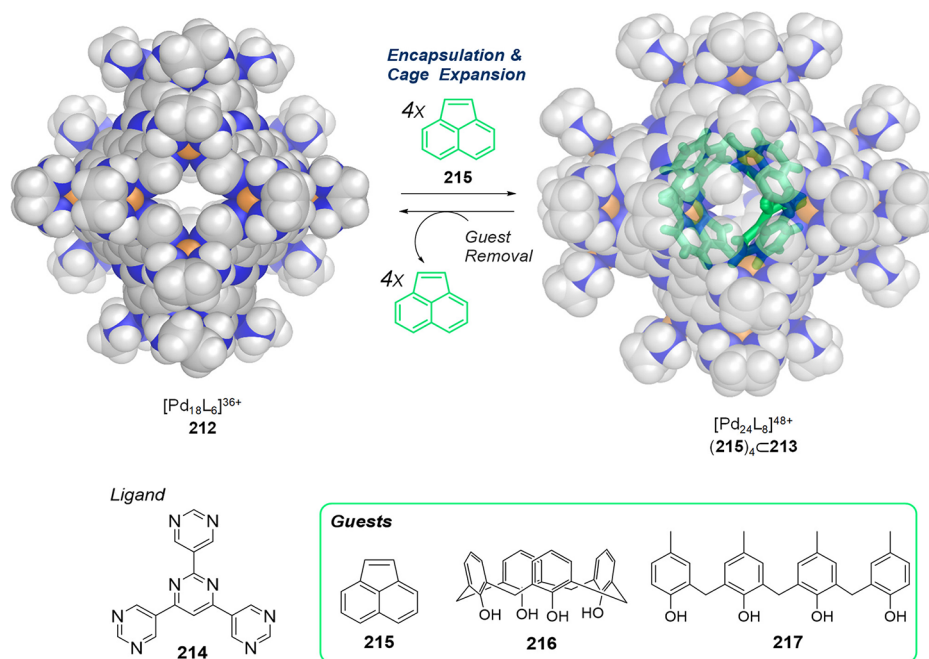
Figure 59. Guest-induced $Pd_{18}L_6-Pd_{24}L_8$ cage−cage conversion. X-ray structures of **212** and $(215)_4 \subset 213$ complexes as well as structural formulas of the ligand and guests are shown.[223]

ligands **214**. By mixing $[(en)Pd(NO_3)_2]$ and **214** in water, $Pd_{18}L_6$ trigonal bipyramidal cage **212** was obtained quantitatively; its composition and approximate D_{3h} symmetry were confirmed by crystallographic analysis. Cage **213** was capable of encapsulating acenaphthylene (**215**), calix[4]arene **216** as well as the linear phenol tetramer **217** in D_2O as followed by NMR.

The encapsulation of large hydrophobic guests triggered the conversion of $Pd_{18}L_6$ cage **212** (D_{3h} symmetry) into $Pd_{24}L_8$ octahedron **213** with a concurrent cavity expansion. The volume of **213** (943 Å^3) is three times larger than that of **212** (381 Å^3). X-ray analysis unambiguously confirmed the pseudo-octahedral structure of $Pd_{24}L_8$ (**213**), which encapsulated four molecules of acenaphthylene (**215**). Despite the dynamic nature of the host, the encapsulated guests are isolated from the external environment. The interior of the closed-shell structure of the host-guest complexes of **213** only becomes accessible upon heating to *ca.* 60 °C, which brought about guest release. Without the stabilizing guests, the octahedral structure converted to cage **212**.

Similarly, the $Pd_{20}L_8$ host **218** structurally adapted to the size and form of hydrophobic guests in water. Cage **218** converted into Pd_8L_4 open-bowl **219** upon large guest inclusion (Figure 60).[224] Cage **218** formed in water upon reaction of $[(en)Pd(NO_3)_2]$ and ligand **220**, structurally similar to **214** but with one fewer nitrogen donor per ligand.

Pseudo-octahedral capsular structure **218** was confirmed by crystallographic studies. This cage showed the ability to encapsulate hydrophobic molecules such as dihaloalkanes or ferrocene. Likewise, one molecule of calix[4]arene (**216**) was bound within **218** while still leaving substantial void. However, when binding occurred in the presence of excess **216**, the cage split into two equivalents of bowl-shaped **219** to maximize host−guest interactions.

Interestingly, the cage−bowl conversion was also triggered by the reaction of an entrapped guest. Excess phenyl trimethoxysilane **221** was suspended in a D_2O solution of
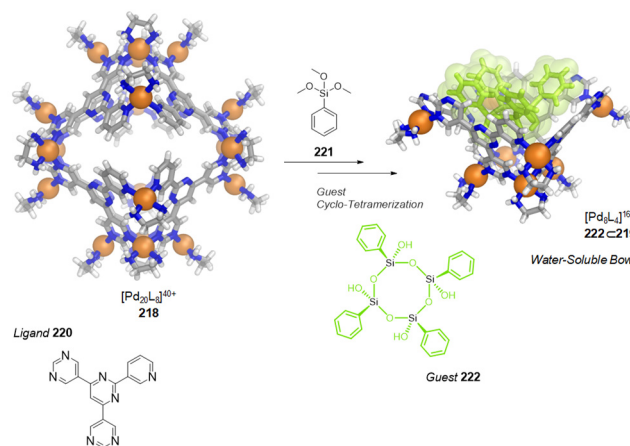
Figure 60. Cage−Bowl conversion driven by encapsulation of hydrolyzed guest **222**.[224] X-ray structures of **218** and $222 \subset 219$ are shown.

218 and hydrolyzed upon heating (100 °C for 15 min). Crystallographic analysis of the host−guest product revealed that substrate **221** condensed to form the cyclic tetrasiloxane **222**, whose structure was stabilized within bowl **219** (Figure 60).

4. BIOMEDICAL APPLICATIONS OF WSCCS

Recent efforts have sought to employ WSCCs for biomedical purposes.[225] The realization of some of these applications has required the ability to control guest uptake and release by external stimuli.[226] For WSCCs in aqueous media, the most straightforward way to release cargo involves partial or full cage disassembly. Other approaches, relying on varying pH or the addition of competing guests, have also been implemented to induce guest discharge without cage destruction.

4.1. Drug Delivery, Imaging, and Chemotherapy

Recent efforts in biology and medicine have focused upon the development of intracellular probes for drug delivery, imaging, and chemotherapy, capable of improving efficacy and selectivity while keeping side effects to a minimum.[227] Poor solubility limits the utility of many drugs and fluorescent probes, as does difficulty in controlling the release of therapeutic payloads, and the lack of selectivity toward targets. Recently, supramolecular materials,[228] including WSCCs,[229,230] have emerged as promising solutions to address some of these limitations.

Besides WSCCs, several synthetic nanoscale systems hold potential as intracellular transportation vectors. Metal nanoparticles,[231] metal–organic frameworks (MOFs),[232,233] peptides,[234,235] and dendrimers[236] have proven useful as delivery platforms. WSCCs complement these other platforms, featuring structural diversity and variable forms that lead to different functions. They may be as small as 2 nm in diameter, rendering them able to cross barriers within the cell and target sites that larger materials may not reach. Hence, WSCCs have potential in applications that require cellular uptake, including cell imaging, drug delivery, photodynamic therapy, and chemotherapy.[237] In addition, WSCCs hold the potential to interact with peptides and proteins as well as recognize DNA by electrostatic interactions in aqueous environments, as noted in the following examples.

Therrien and co-workers focused on the design and use of prismatic hexa-ruthenium WSCCs to facilitate the delivery of drugs and photosensitizers to cancer cells.[238,239] The cationic hexanuclear metalloprism **223**, which incorporates 2,5-hydroxyl-1,4-benzoquinolate-bridged diruthenium pillars (**224**) and 1,3,5-tris(4-pyridyl)triazine (**5**) linkers, encapsulated the water-insoluble acetylacetonate (acac) derivatives [Pd(acac)$_2$] (**225**) and [Pt(acac)$_2$] (**226**) (Figure 61a).[240] The molecular structure of **226⊂223** was determined by X-ray
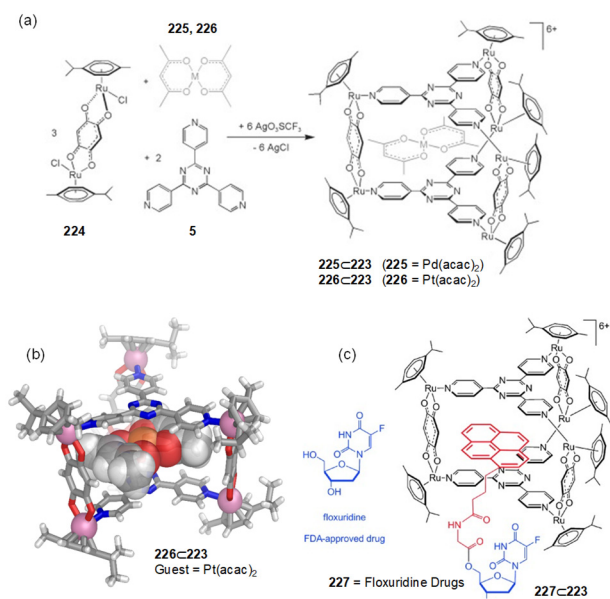
crystallography (Figure 61b). The resultant "complex-in-a-complex" cations proved toxic to ovarian cancer cells (A2780), whereas the free complexes **225** and **226** were inactive due to their insolubility in water.

Although the empty metalloprism **223** was moderately cytotoxic, the **225⊂223** and **226⊂223** systems were more active, with the platinum-containing species being about twice as active as the empty host and the palladium congener being more than an order of magnitude more cytotoxic, displaying an IC$_{50}$ value of 1 μM (IC$_{50}$ = drug concentration necessary for 50% inhibition of cell viability).

The authors proposed that the host–guest complex acts as a "Trojan horse", with the hexa-ruthenium cage opening and releasing the [M(acac)$_2$] agent upon entry to a diseased cell. The drug delivery ability of ruthenium–arene metallacage **223** was confirmed by encapsulating and transporting a series of pyrenyl-functionalized floxuridine conjugates of type **227** (Figure 61c).[241]

Floxuridine treats solid tumors but exhibits limited water solubility. In contrast to the floxuridine compounds in current clinical use, the host–guest complex **227⊂223** is water-soluble. During testing on human ovarian cancer cells (A2780 and A2780cisR), this complex proved more cytotoxic than the empty cage alone, showing excellent uptake of floxuridine derivatives into cancer cells with IC$_{50}$ as low as 0.3 μM.

Therrien and co-workers have employed the hydrophobic cavities of trigonal-prismatic ruthenium WSCCs to protect and shield photosensitizers as a strategy in photodynamic therapy. The porphyrin photosensitizer **228** binds within metallacages **223** and **229** (Figure 62).[242] With the smaller **223**, **228** formed
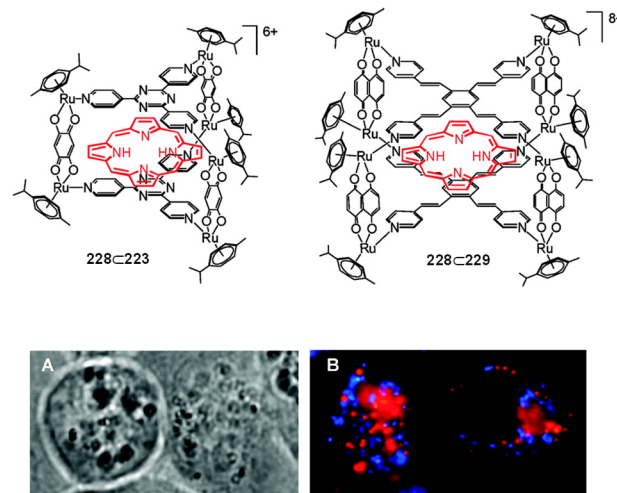
Figure 62. Structural formula of hexa- (**223**) and octa-ruthenium (**229**) cages encapsulating porphyrin **228**. Fluorescence microscopy of HeLa cells incubated with [**228⊂229**]$^{8+}$: (A) white light and (B) fluorescence. Reproduced with permission from ref 242. Copyright 2012 American Chemical Society.

Figure 61. (a) Synthesis of hexaruthenium prism **223** for transporting M(acac)$_2$ (M = Pd^{II}, Pt^{II}) complexes into cells. Reproduced with permission from ref 240. Copyright 2008 Wiley-VCH. (b) Crystal structure of the platinum containing adduct **226⊂223**. (c) A pyrenyl-floxuridine derivative encapsulated within **223**.[241]

the carceplex **228⊂223**, in which it is permanently trapped. Conversely, when the more spacious octanuclear metallacage **229** was used, the host–guest system **228⊂229** was formed and the release of porphyrin occurred without rupturing the cage. Both complexes are stable at physiological pH 6–8 at 37 °C. No degradation of the host–guest systems was observed in the presence of oxidative (H$_2$O$_2$) or reductive (dithiothreitol) reagents.

In solution, both host–guest adducts showed hypochroism with respect to the free photosensitizer, resulting in the absence of photoactivity. Cell internalization was nonetheless inferred to result in the discharge of porphyrin from the cages, whereupon its photoactivity is regained. This on–off photoactivity was also used to follow the uptake and accumulation of the photosensitizer in cancer cells.

Fluorescence microscopy revealed that the larger system **228⊂229** produced a stronger emission response compared to the carceplex system **228⊂223**. Cells incubated with **228⊂223** did not fluoresce enough to be detected, while incubation with **228⊂229** revealed strong red and blue fluorescence signals corresponding to porphyrin molecules and empty cages, respectively, thus confirming intracellular release of porphyrin from the cage (Figure 62).

The higher fluorescence observed in cancer cells also correlated well with the observed phototoxicity. The most phototoxic system was the octanuclear **228⊂229** complex with a LD_{50} (LD_{50} = light dose necessary for 50% inhibition of cell viability) of 0.2 J cm^{-2} on HeLa cells. This value is 10 times lower than what was observed with carceplex **228⊂223** (LD_{50} = 2.1 J cm^{-2}). The differing photoactivities of these host–guest complexes may arise from either better uptake of the octanuclear metallacage or more facile release of the guest following internalization.

Using dicopper(II)-containing cuboctahedron **230**, Zhou, Wang, and co-workers developed a delivery system for the anticancer drug 5-fluorouracil (**231**).[243] Cage **232**, a PEG-substituted, water-soluble derivative of **230**, was first prepared (Figure 63a). TEM images of **232** revealed the formation of
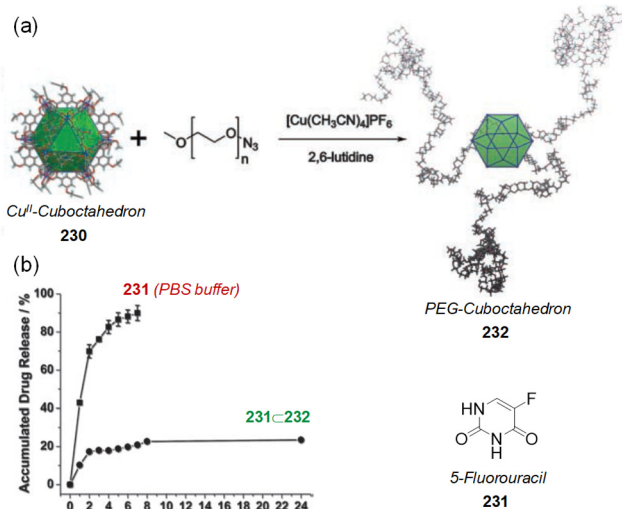
Figure 63. (a) Scheme of click reaction to obtain **232**. (b) Chemical structure of 5-fluorouracil (**231**) and the release of **231** from control (square) and cage **232**. Adapted with permission from ref 243. Copyright 2011 Wiley-VCH.

nanoparticles much larger (diameter of *ca.* 20 nm) than a single PEG-functionalized nanocage, attributed to intermolecular aggregation.

Cage **232** proved stable in water. This stability may result from the outer polymeric shell and intermolecular aggregation, which protected the dicopper paddlewheel clusters by blocking water access.

Drug release experiments were carried out by dialyzing **231⊂232** against PBS buffer solution (pH = 7.4) at room temperature. Pure 5-fluorouracil (**231**) was also dialyzed against PBS buffer as a control experiment, in which close to 90% of the drug was released within 7 h. In contrast, it was found that 20% of the drug was liberated from **231⊂232** during an initial burst release (2 h), followed by a flat release curve up to 24 h (Figure 63b). The authors suggested that this slow release is due to the slow diffusion rate of drug **231**, caused by the strong interaction between Lewis acid sites in cage **232** and the basic site in **231**.

Lippard and co-workers described a delivery system for cisplatin based on the combination of WSCCs and Pt^{IV} prodrugs.[244] The platinum(II)-octahedron Pt-**6**, reported by Fujita (Figure 23), was employed as the delivery vehicle. Pt-**6** simultaneously encapsulates four equivalents of the adamantyl-appended Pt^{IV} prodrug **233** (host–guest complex (**233**)$_4$⊂Pt-**6**). Prodrug **233** has low solubility in water (<500 mM) but becomes readily soluble when encapsulated.

A release mechanism for cisplatin was first established. The host–guest complex is reduced by ascorbic acid at neutral pH, thus releasing cisplatin (**234**), 1-adamantylamine (**235**), and succinic acid (**236**) (Figure 64). The anticancer activity of the
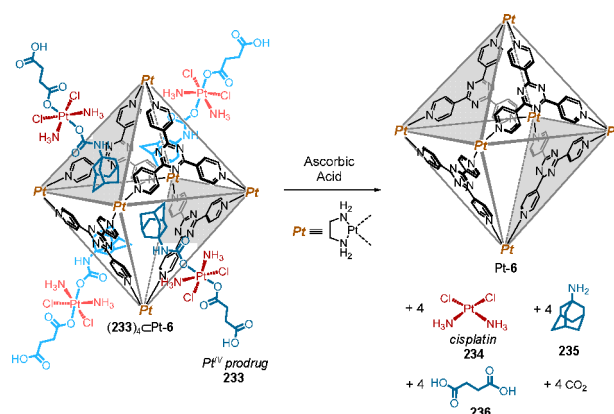
Figure 64. Representation of the release of cisplatin upon reduction of (**233**)$_4$⊂Pt-**6** by ascorbic acid.[244]

host–guest complex (**233**)$_4$⊂Pt-**6** was explored in a group of human cancer cell lines. Cytotoxicity profiles of the Pt^{IV} prodrug (**233**), the empty cage Pt-**6**, and the combined system (**233**)$_4$⊂Pt-**6** were evaluated against A549 (lung carcinoma), A2780 (ovarian carcinoma), and A2780CP70 (ovarian carcinoma resistant to cisplatin) cells.

Complex (**233**)$_4$⊂Pt-**6** displayed micromolar potency against all cancer cell lines tested, comparable to that of cisplatin, and superior efficacy to the prodrug or cage alone. The mechanism of action of (**233**)$_4$⊂Pt-**6** is by triggering programmed cell death *via* intracellular release of cisplatin.

The proficient cytotoxicity of (**233**)$_4$⊂Pt-**6** was attributed to the high cellular uptake of the cationic cage. Both Pt-**6** and (**233**)$_4$⊂Pt-**6** have 10 times greater uptake than either cisplatin or the Pt^{IV} prodrug **233**. Interestingly, subsequent efforts from the Lippard group also indicated that octahedron Pt-**6** is capable of noncovalently interacting with DNA by intercalation, thus promoting DNA condensation. In cancer cells, this interaction induces DNA damage and triggers apoptosis and senescence.[245]

Also using the Pt-**6** WSCC, Zheng presented a strategy to encapsulate Pt-based anticancer agents for delivery.[246] Octahedron Pt-**6** formed a host−guest complex upon encapsulation of a fluorescein-conjugated Pt^{IV} prodrug for cisplatin. Subsequent treatment of the complex with an anionic block copolymer resulted in the formation of 80 nm drug-loaded nanoparticles, which released their therapeutic cargo at a controlled rate and showed higher efficacy compared to that of cisplatin *in vitro*.

Live cell imaging is an essential tool for medical diagnosis and for understanding cellular dynamics. Hydrophobic dyes feature prominently as probes; however, their low aqueous solubility and self-aggregation-induced quenching are challenges to their use. The Mukherjee group described the use of a WSCC as an aqueous carrier for the transportation of water-insoluble fluorophores for live cell imaging.[247] The self-assembly of tetraimidazole donor **237** with the 90° linker $[Pd(tmeda)(NO_3)_2]$ led to the water-soluble tetragonal barrel **238**. The polycyclic aromatic hydrocarbons (PAH) naphthalene, anthracene, pyrene, perylene, perylene tetracarboxylic acid dianhydride, and coronene were encapsulated within the hydrophobic pocket of **238** in water. Crystallographic analysis of the (coronene)$_2$⊂**238** inclusion complex confirmed the cage structure and a 2:1 host−guest stoichiometry (Figure 65a).
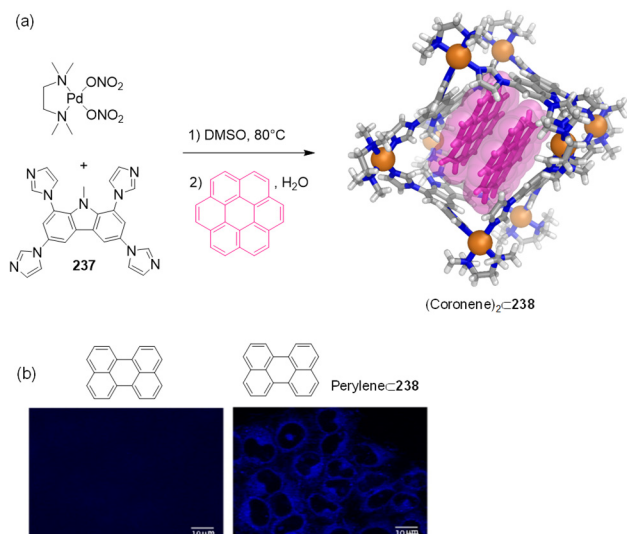
Figure 65. (a) Synthesis of WSCC **238** and encapsulation of coronene; the X-ray structure of the (coronene)$_2$⊂**238** complex is shown. (b) Micrographs reveal that perylene does not enter the cell on its own (no fluorescence) but that blue emission corresponding to perylene was observed from the cytoplasm of HeLa cells after the incubation with an aqueous solution of perylene⊂**238**. (b) Adapted with permission from ref 247. Copyright 2015 American Chemical Society.

Perylene was delivered into HeLa cells and used as a cell imaging agent upon incubation. The perylene⊂**238** complex readily entered the cells without killing them. Micrographs of the treated cells showed brilliant blue emission from the cytoplasm without alteration of cell morphology; on the contrary, no fluorescence was detected upon treatment of the cells with perylene itself due to its lack of solubility (Figure 65b).

The same team later reported the synthesis of Pd$_8$L$_4$ water-soluble molecular barrel **239** that forms from tetrapyridyl

donor **240** and *cis*-capped palladium(II) precursor **2** (Figure 66a).[248] In water, barrel **239** was found to encapsulate anticancer drug curcumin **241**, protecting this photosensitive compound from photodegradation.
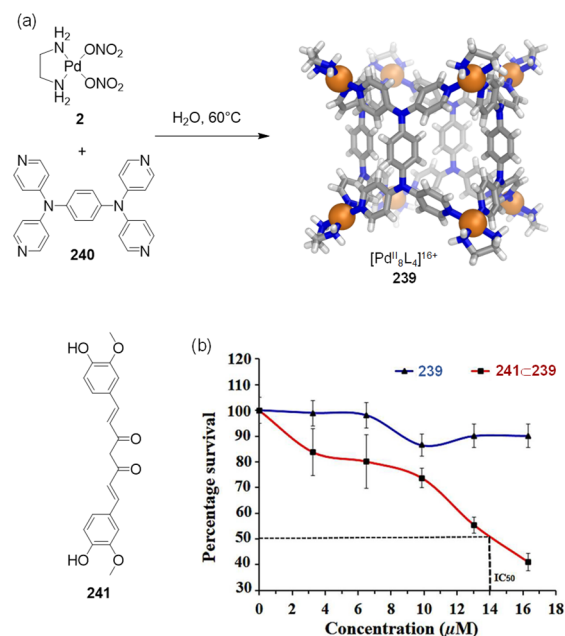
Figure 66. (a) Synthesis of barrel **239**. The crystal structure of **239** and structural formula of cucrumin guest **241** are shown. (b) Plot showing the decrease in cancer cell growth when treated with **241**⊂**239** as compared to **239** alone. (b) Reproduced with permission from ref 248. Copyright 2017 American Chemical Society.

Encapsulation of **241** within **239** rendered curcumin soluble in water. The antiproliferative activity of host−guest complex **241**⊂**239** was tested on HeLa cancer cells. Fluorescence imaging confirmed that curcumin was delivered into the cells by the water-soluble barrel with its anticancer activity preserved (IC$_{50}$ value of *ca.* 14 μM) (Figure 66b). Conversely, free curcumin proved inactive toward cancer cells in water due to its negligible solubility; it was only effective when dissolved in the toxic solvent DMSO.

In a sophisticated approach to drug delivery, Isaacs and co-workers prepared water-soluble metal−organic polyhedron (MOP) **242** from self-assembly of the bent dipyridyl ligand **243** and palladium(II) ions (Figure 67).[249] Polyhedron **242** bears 24 covalently attached methyl viologen units on its external surface. The strong binding affinity of viologens toward cucurbit[n]urils (CB[7] and CB[8]) was exploited to construct CB[7]- and CB[8]-capped MOPs containing a total of 24 CB[n] units on the cage surface.

The CB[8]-capped polyhedron was loaded with naphthol-derivatized doxorubicin (DOX) prodrug **244**, yielding the drug-loaded WSCC **245**. The hydrazone linkage of prodrug **244** is acid sensitive, enabling selective delivery of doxorubicin in a pH-responsive manner at the slightly acidic pH of tumors.

Cell viability assays demonstrated that water-soluble polyhedron **245** is 10-fold more cytotoxic toward HeLa cells than equimolar quantities of DOX prodrug **244**. The enhanced cytotoxicity is attributed to a combination of enhanced cellular uptake and improved doxorubicin release from cage **245**, as demonstrated by flow cytometry experiments and confocal fluorescence microscopy. Importantly, the cytotoxicity of **245**
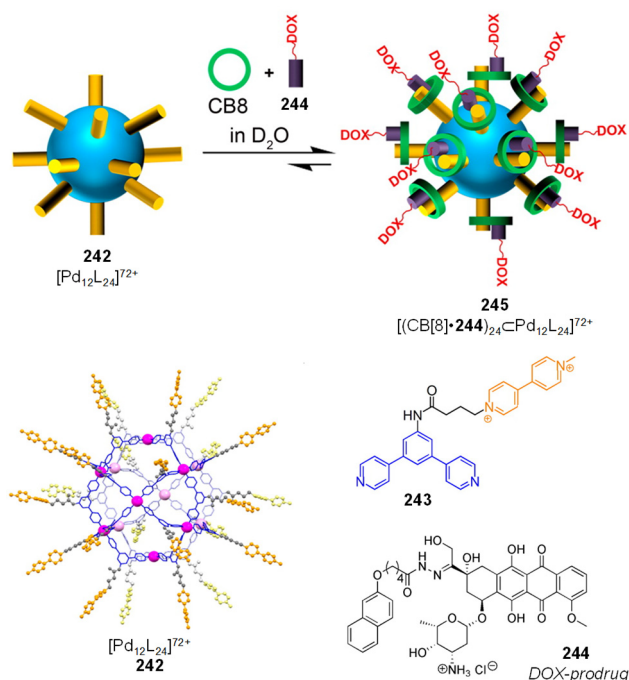
Figure 67. Cage **242**, assembled from **243** and Pd^{II} ions, forms the heteroternary complex **245** with CB[8] and prodrug **244** for the delivery of doxorubicin. Adapted with permission from ref 249. Copyright 2016 American Chemical Society.

Figure 68. Self-assembly of cages **246** and **251** and schematic representation of the stimuli-responsive release of guests from the hydrophobic cavity of **251** by **252**. Chemical structures of compounds used are shown. Adapted with permission from ref 250. Copyright 2017 American Chemical Society.

(IC$_{50}$ = 48 nM) is comparable to that of free DOX (IC$_{50}$ = 34 nM), thus showing that the polycationic nanoscale architecture of **245** imparts improved cytotoxic features without diminishing the inherent activity of the drug.

Isaacs and co-workers also developed a stimuli-responsive nanocarrier based on a Pd-MOP that releases doxorubicin or the dye Nile red in response to the chemical stimuli of a competitive guest or pH change.[250] Cuboctahedral cage **246** was prepared by self-assembly of Pd^{II} ions, bent dipyridyl ligand **247**, cucurbit[7]uril-containing ligand **248**, and hexanediammonium guest **249** (HAD). The surface of coordination sphere **246** is thus decorated with 18 CB[7] units that each contain a HAD guest (**249**).

When amphiphilic C$_{18}$H$_{37}$−HAD guest **250** was used for cage self-assembly, polyhedron **251** was obtained. Unlike MOP **246**, **251** possess a more hydrophobic environment within the dodecanuclear core promoted by the long alkyl chains noncovalently attached to the CB[7] units, which are able to penetrate and densely pack within the cage core.

Adamantylammonium **252** (ADA) was observed to displace the amphiphilic C$_{18}$H$_{37}$−HAD guest (**250**) from the CB[7] arms, leading in turn to destruction of the hydrophobic environment to give structure **253** (Figure 68). ADA **252** was thus used as a chemical stimulus to discharge the Nile red and doxorubicin (DOX) hydrophobic guests.

To determine the suitability of this class of polyhedra for delivery to eukaryotic cells, the toxicity of **251** was evaluated. HeLa cells were incubated with increasing concentrations of **251** for 24 h. Increased toxicity was observed at **251** concentrations higher than 3.12 μM.

Following the uptake of the complex [Nile red⊂**251**] by HeLa cells, the release of Nile red from the complex was assessed. Cells were treated with [Nile red⊂**251**] or free Nile red and visualized by fluorescence microscopy. Red fluo-

rescence staining patterns in both samples showed selective staining of lipid bodies in the cytosol as well as diffuse staining of the cellular membrane. The staining patterns seen with free Nile red and [Nile red⊂**251**] were identical, which indicates that the dye undergoes passive release from the cage without requiring an external additive such as ADA (**252**). Unfortunately, this passive release process precluded study of the triggered release of Nile red intracellularly.
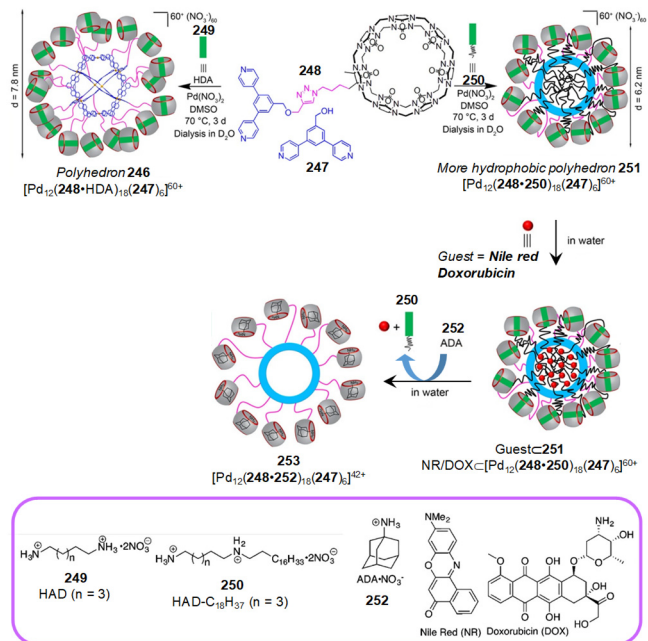
The same group has demonstrated more recently that cucurbit[7]uril-functionalized Pd$_{12}$L$_{24}$ polyhedra can be postfunctionalized with cell-targeting small molecules and peptides as a means to tune their capabilities in targeted drug delivery and imaging applications.[251]

As discussed in section 2.4, current synthetic approaches to WSCCs allow for the development of highly robust ensembles or the strengthening of existing constructions to increase their structural integrity and broaden their applications. In this vein, Zhao, Liu, and co-workers described the self-assembly of highly stable zirconium(IV)-based coordination cages with aggregation induced emission (AIE) molecular rotors and their use for *in vitro* bioimaging.[252] The two coordination cages, **254** and **255**, are assembled from high-stability trinuclear zirconium vertices and the carboxyl-terminated tetraphenylethylene spacers **256** and **257**, respectively (Figure 69a).

Extensive experimental and theoretical studies showed that the emissive intensity of these coordination cages can be controlled by restricting the dynamics of the AIE-active molecular rotors using external stimuli (viscosity and temperature). Both cages displayed excellent chemical stability in aqueous solutions from pH 2−10. Likewise, bright AIE fluorescence was displayed by both cages; the quantum yields of **254** and **255** in neutral aqueous solutions were determined to be 19.0% and 28.8%, respectively. Because of these qualities and the low cage cytotoxicity, their imaging capabilities were
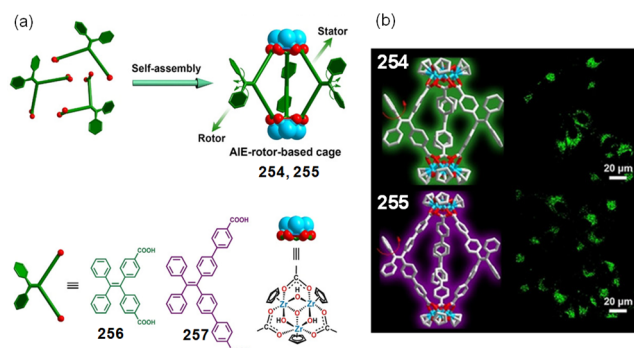
Figure 69. (a) Self-assembly of zirconium(IV) cages **254** and **255** from carboxylate molecular rotors **256** and **257**. (b) Cell imaging of **254** (top) and **255** (bottom) in HeLa cells. Adapted with permission from ref 252. Copyright 2020 Wiley-VCH.

evaluated in HeLa cells, showing strong signals from inside the cytoplasm (Figure 69b).

Recently, Lusby, Archibald, and co-workers demonstrated the feasibility of using the kinetically robust $Co^{III}_4L_6$ tetrahedra **258** and **259** for encapsulating a widely used precursor in clinical nuclear diagnostic imaging, the γ-emitting $^{99m}TcO_4^-$ anion, under conditions compatible with *in vivo* administration (Figure 70a).[253] Initially, they chose tetrahedron **258** (built
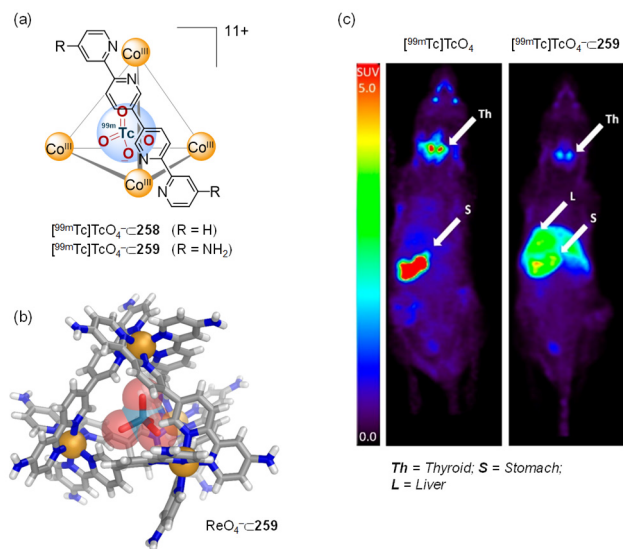
Figure 70. (a) Chemical structure of $^{99m}TcO_4^- \subset$**258/259** complexes. (b) X-ray crystal structure of $ReO_4^- \subset$**259**. (c) Comparison of $^{99m}TcO_4^-$ uptake in mice (left) vs $^{99m}TcO_4^- \subset$**259** (right). (c) Reproduced with permission from ref 253. Copyright 2018 American Chemical Society.

using inert Co^{III} ions) to guarantee the structural integrity required for safe *in vivo* applications. Besides pertechnetate, SO_4^{2-}, BF_4^-, PF_6^-, ClO_4^-, and ReO_4^- bound within **258** in D_2O. Notably, the pertechnetate analogue, perrhenate (ReO_4^-), bound in slow exchange on the ^1H NMR time scale and with high affinity (61 000 M^{-1}).

For the $^{99m}TcO_4^- \subset$**258** host–guest system, full anion encapsulation was achieved at 100 μM and with an EC_{50} of 14 μM (cage concentration required for 50% radiochemical yield, RCY). Complex stability was maintained even after the addition of competing NO_3^-, Cl^-, HPO_4^{2-}, and PO_4^{3-} anions. However, a steady decrease in stability was observed in serum

after 24 h, possibly due to cage disassembly induced by biological reductants.

Reasoning that a cage built on a stronger σ-donor ligand would afford a more stable host–guest complex, cage **259**, was prepared from a ligand bearing free amino groups (Figure 70b). The introduction of 12 amino groups had a positive impact on $^{99m}TcO_4^-$ encapsulation. The concentration of **259** required to achieve >95% RCY was reduced to 1.9 μM, nearly 50-fold lower than **258**, with an EC_{50} value of just 0.05 μM. In this case, the presence of serum resulted in no discernible drop in radiochemical stability over 24 h.

Given the improved serum stability and the lower dose required to fully encapsulate $^{99m}TcO_4^-$, **259** was selected for *in vivo* SPECT (single-photon emission computed tomography) imaging experiments with animals. The utilization of cage **259** resulted in a difference of the $^{99m}TcO_4^-$ biodistribution. When $^{99m}TcO_4^- \subset$**259** was administered and imaged, reduced thyroid and stomach uptake was observed, with significant uptake noted in the liver (Figure 70c). It was inferred that the well-defined shape and positive charge (+12) of tetrahedron **259** promoted binding to proteins and liver uptake.

Observation of liver uptake also indicated that the cage remained intact during imaging. In the presence of excess biological cations, isolated samples of cage were observed to disassemble and destroy the high-affinity cavity that keeps the anion associated with the cage, but cage destruction was not observed *in vivo*. Moreover, extraction of liver tissue gave a sample with *ca.* 30% of the $^{99m}TcO_4^-$ anion associated with the host, with the remainder released during the extraction process. While the (pre)clinical use of self-assembled carrier systems is still in its infancy, this study illustrates the potential of WSCCs to be used as clinical agents for *in vivo* applications.

4.2. Recognition and Detection of Biomolecules

Metal–organic cages bind a wide range of molecules of biological and medical importance. A step toward their implementation in, for example, sensitive analytical devices, requires the cage to express selectivity and affinity for substrates at a level that mimics the sensitivity and discrimination of protein receptors.

The Yoshizawa group reported that polyaromatic capsule Pt-**41** can be used to detect a single molecule of androgen in the presence of progestogens and estrogens in water.[254] Steroid sex hormones are biochemical signals essential for animal life. Human androgen receptors routinely distinguish and bind "male" (♂) steroid sex hormones over "female" (♀) hormones with high selectivity. However, the design of artificial molecular receptors able to distinguish between male and female hormones in water is challenging.

Capsule Pt-**41** binds testosterone (TES) with >98% selectivity from a 1:1:1 as well as a 1:100:100 mixture of TES and female progesterone (PRG) and β-estradiol (ESD) in water (Figure 71a). Competitive binding studies further elucidated the affinity of Pt-**41** toward various hormones: TES ≈ dihydrotestosterone (♂) > androstenedione (♂) > androsterone (♂) ≫ PRG > 17α-hydroxyprogesterone (♀) > ESD (♀) > estriol (♀).

Lastly, a prototype detection system for testosterone was set up based on the displacement of a fluorescent dye from Pt-**41**. When bound within Pt-**41**, hydrophobic coumarin 153 (**137**) emits bluish-green fluorescence in water upon excitation at 423 nm. The emission of **137**⊂Pt-**41** decreased as the dye guest was displaced by a more hydrophobic hormone guest in water.

Figure 71. (a) Selective testosterone binding by Pt-**41** and X-ray structure of TES⊂Pt-**41**. (b) Schematic representation of nanogram-scale fluorescent detection of TES with one drop of **137**⊂Pt-**41** solution on a Petri dish. (c) Fluorescence spectra and pictures of a H₂O solution of **137**⊂Pt-**41** before and after addition of TES. Adapted with permission from refs 136 and 254. Copyright 2019 American Chemical Society. Copyright 2019 American Association for the Advancement of Science.

When 100 μL of an aqueous solution of **137**⊂Pt-**41** (8 μM) was added to testosterone (TES, 230 ng, 0.80 nmol), the bluish-green emission was weakened after brief sonication (20 s) at room temperature. The displaced dye is nonemissive due to the formation of aggregated precipitates. Thus, the visual detection of a nanogram-scale quantity of testosterone could be carried out on a small Petri dish (Figure 71b). In fluorescence spectra, the emission intensity of **137**⊂Pt-**41** (78 μM, 0.5 mL) in water was largely decreased (−85%) upon addition of the hormone (45 nmol) at room temperature within 10 min (Figure 71c).

The Fujita group has demonstrated that the inner pockets of WSCCs can recognize and accommodate peptides up to nine residues in length in water, changing the peptide conformation. For instance, within the protected environment of a porphyrin-based WSCC, the interference of water in hydrogen-bond formation was suppressed, stabilizing intrapeptide hydrogen-bonding and favoring different modes of folding. Peptides that typically display a pure α-helix conformation in the nonbound state exhibited hybrid β-turn (3₁₀)/α-helix (4₁₃) conformations.[255]

The encapsulation of larger biomolecules can be more challenging. However, by taking advantage of the modularity of self-assembly, the same group engineered the first encapsulation of a small protein, ubiquitin, within synthetic Pd₁₂L₂₄ coordination nanocages **260a–c** in aqueous media.[256] The protein was attached to one ditopic ligand (**262a–c**) and, upon addition of further ligands (**261a–c**) and Pd(NO₃)₂ in

D₂O/CD₃CN, hosts self-assembled around the protein (Figure 72).

Figure 72. Aqueous self-assembly of ubiquitin-containing spheres **260a–c**. Reproduced with permission from ref 256. Copyright 2012 Springer Nature.

The **260a–c** cages displayed nanometer-sized cavities that were expanded up to 7.3 nm in diameter, simply by lengthening the ligand arms. Because of the well-defined host framework, the protein-encapsulated Ubiquitin⊂**260a–c** could be characterized by NMR spectroscopy, ultracentrifugation, and X-ray crystallography (for Ubiquitin⊂**260c**) coupled with the maximum entropy method (MEM), which clearly mapped the electron density of the protein in the coordination cage. In this case, the covalent, irreversible attachment of ubiquitin to the inside of the cage prevents its release or exchange.

Synthetic self-assembled cages may regulate the properties of biomolecules and their susceptibility to enzymatic degradation. Our group reported that porphyrin-faced Feᴵᴵ₈L₆ cube **263**, based on metalloporphyrin **264**, is capable of binding and protecting peptide guests up to 23 residues in length from degradation (Figure 73).[257] This cube is flexible and compatible with aqueous media (1:1 H₂O/MeCN).

Cube **263** exhibited specific binding toward guests bearing imidazole motifs via coordination to its internal zinc(II)-porphyrin faces. For instance, Ritonavir is an antiretroviral medication used to treat HIV/AIDS that contains two thiazole moieties; it binds with a dissociation constant of 104 μM in a 1:3 host–guest binding stoichiometry. Clavanin A, obtained from the marine organism *Styela Clava*, is a peptide widely used as an antibiotic that consists of 23 amino acids, four of which are histidines. Clavanin A binds to cube **263** with a dissociation constant of 80 nM according to a 1:2 host–guest binding model, thus suggesting that each peptide interacts through three histidines. Other peptides without histidines did not bind **263**.

Abiological peptide **265**, containing three histidine residues, was bound within **263** and protected from enzymatic degradation by the protease trypsin. Incubation of **265** with trypsin in a mixture of phosphate buffer (pH = 7.5) and MeCN led to the cleavage of **265** in 76% yield. When the same reaction was run in the presence of 0.6 equiv of cube **263**, the

Figure 73. (a) Self-assembly of **263** from porphyrin **264**.[257] (b) Trypsin treatment of peptides **265** and **266** in the presence and absence of **263**. Red arrows indicate the cleavage positions of peptides: Abz, 2-aminobenzoic acid; Dnp, 2,4-dinitrophenyl.

Figure 74. Self-assembly of cages **267a−d** with (b) the crystal structure of complex **267a** shown. (c) Illustration of the end-stacking binding of cage **267** to two G-quadruplexes. (c) Reproduced with permission from ref 265. Copyright 2016 Royal Society of Chemistry.

extent of cleavage was only 9%. When the same experiment was carried out with the nonbinding peptide **266**, which does not contain histidine, in place of **265**, with or without cube **263**, quantitative cleavage of **266** was observed. Further evidence of the protective role and selectivity of this cube was demonstrated when a mixture of cube **263**, binding **265**, nonbinding **266**, and trypsin was incubated. In this case, the selective hydrolysis of **266** was observed with only 11% of **265** being hydrolyzed (Figure 73b). Cage **263** thus represents a rare example of an artificial host able to bind large and complex biomolecular guests in aqueous media, altering their reactivity in fundamental ways.

Synthetic constructs able to recognize and interact with DNA are useful in biomedicine, clinical diagnosis, and gene regulation.[258] In aqueous metallosupramolecular chemistry, research into nucleic acid binders has often focused upon M_2L_3 helical complexes, whose size, shape, and complementary charge enable them to interact with the native DNA double helix as well as other structural forms such as quadruplexes and three- and four-way DNA junctions. Elegant examples are the molecular cylinders[259,260] and the flexicates[261,262] reported by Hannon and Scott, respectively, and more recently, the helicates prepared by Qu.[263,264] Although these structures lack an inner cavity for binding, these families of helical compounds have exhibited biological activity arising from their interaction with DNA structures in aqueous media.

The ability of WSCCs to recognize specific DNA structures has also been demonstrated. Gu and co-workers reported the synthesis of four pairs of enantiomers of water-stable tetrahedral metal−organic $Ni^{II}_4L_6$ cages **267a−d**, which stabilized antiparallel G-quadruplex DNA with moderate enantioselectivity.[265] Cages were prepared through the subcomponent-self-assembly reaction of Ni^{II} ions, 1,8-di(2-formylimidazole)octane **268**, and different optically pure amine components, which were used to control the absolute configuration of the metal centers (Figure 74a). These complexes were crystallographically characterized (Figure
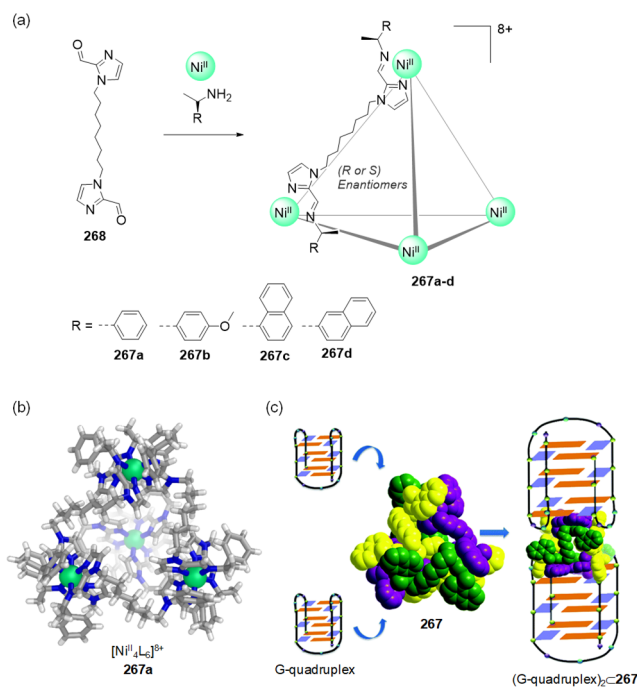
74b). The chloride salts of the cages were soluble and stable in water, with minimal decomposition under acidic conditions. Enantiomeric cages **267a−d** showed affinity toward G-quadruplex DNA with binding constants (K_b) ranging from 1.13×10^5 M^{-1} to 5.66×10^5 M^{-1}. Likewise, complexes **267a−d** stabilized G-quadruplex DNA in solution. The stabilizing effect became stronger as the concentration of cage increased. On the basis of a Job plot analysis, the authors proposed that the tetrahedral cages bind to G-quadruplexes with a 1:2 binding stoichiometry through an end-stacking binding mode to form the (G-quadruplex)$_2$⊂**267** complex (Figure 74c). Later work from this group has shown that analogous nickel(II) tetrahedral cages $[Ni^{II}_4L_6]^{8+}$, but built from biphenyl-containing ligands, stabilized G-quadruplex DNA to a greater extent, likely due to the increased structural rigidity of the cages.[266]

The Keyser and Nitschke groups described the use of subcomponent self-assembled $Fe^{II}_4L_4$ tetrahedron **269** as a site-selective binder for three-way junction DNA (3WJ) and base-pair mismatches. The binding of water-soluble **269** quenches the fluorescence of a proximate fluorophore, the dye 6-carboxy fluorescein (FAM) attached to the different DNA strands, enabling optical readout for the sensing of these DNA structures (Figure 75).[267] Initially, cage **269** was treated with four different kinds of DNA structures, each labeled with FAM: single-stranded (ssDNA), double-stranded (dsDNA), three-way junction (3WJ), and four-way junction (4WJ) DNA. Fluorescence monitoring of these interactions showed that cage **269** quenched FAM emission in the samples containing ssDNA and 3WJ by 69% and 75%, respectively.

Thus, **269** showed higher affinities for these structures, as compared to dsDNA and 4WJ, for which only 40% and 38% quenching were observed. Only the complete cage caused fluorescence quenching; addition of either Fe^{II} or the organic
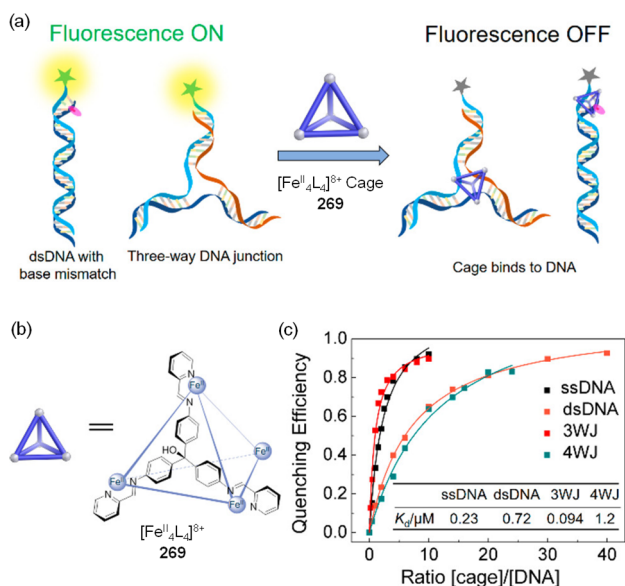
Figure 75. (a) Schematic representation of the fluorescence quenching of DNA structures upon binding with cage **269**. (b) Molecular structure of cage **269**. (c) Quenching efficiency based on the ratio of **269** to the DNA. Adapted with permission from ref 267. Copyright 2019 American Chemical Society.

cage subcomponents to the 3WJ had a minimal effect on fluorescence intensity.

Interaction studies revealed that **269** binds at the central branch point of a 3WJ, where base-pairings are loose or absent. Given that the DNA-cage binding occurred specifically at unpaired bases, cage **269** was also used to detect and sense base-pair mismatches in DNA double strands (dsDNA).

The fluorescence quenching property of cage **269** thus enabled straightforward optical detection of a variety of base mismatches at low concentrations. This approach opens up opportunities for the design of DNA probes, including the possibility of incorporating encapsulated guests to be released in the vicinity of specific DNA sequences.

5. CHEMISTRY WITHIN WATER-SOLUBLE CAGES

The development of WSCCs has been driven by both fundamental interest in understanding molecular recognition processes in water, and by practical uses, such as the biomedical applications discussed in the previous section. One of these applications is the ability of WSCCs to catalyze reactions in a manner reminiscent of enzymes.[18,268] These natural catalysts employ hydrophobic pockets separated from the bulk cytosol to accelerate transformations with high specificities and rates, via the stabilization of specific transition states.[269,270]

Since the first reports of guest binding by WSCCs, it was recognized that their confined, hydrophobic cavities may be able to mimic the functions of enzyme active sites.[17,271] Great strides have been made toward achieving this goal, although there is still much scope for optimization of their catalytic performance.[272] While enzymes employ secondary non-covalent interactions such as hydrogen bonds or ionic interactions to control substrate access to the active site, such functionality has only in a few noteworthy cases[216–219] been incorporated into the cavities of WSSCs, with substrate specificity in most cases controlled by the size and shape of the cavity instead. Some of the most attractive aspects of catalysis

with WSCCs are the potential to combine the most desirable attributes of biological catalysts with the scope of reactivity developed by synthetic chemists[273] and the potential for interfacing biological and supramolecular catalytic processes within a single aqueous medium to achieve multistep catalytic relays.[274]

The use of WSCCs as catalysts is also guided by a move toward developing greener industrial processes. Water is an environmentally friendly alternative to organic solvents for such processes, although problems associated with disposal and purification of contaminated water still need to be addressed before a catalytic process may be considered "green".[275]

WSCCs can bring insoluble substrates into water and render them reactive, greatly expanding the scope for reactions that can take place in aqueous environments. Such cages can also act as phase transfer catalysts, to bring organic substrates into proximity with other reagents dissolved in water, and transport products back to organic phases for isolation.[276,277]

The central theme of this section is the use of WSCCs for controlling the aqueous reactivity of bound guests. Catalysis by metal−organic cages has been widely reviewed,[19,26,278−281] as well as supramolecular catalysis[282−285] more generally, hence this review will focus on key examples of altered reactivity by WSCCs in aqueous media. Readers are directed to the abovementioned thorough and thoughtful reviews for a more comprehensive treatment of these topics, including more detailed mechanistic discussions.

Fundamental investigations into understanding host−guest binding in water have paved the way for using WSCCs to influence the reactivity of guests and the promotion of reactions inside their cavities. The selective binding of multiple guests in WSCCs can lead to acceleration of intermolecular chemical reactions of two or more encapsulated substrates as well as the generation of unique products in some cases.[286] The confined environments within the cavities of WSCCs are able to raise the effective concentration of guests or force reactive sites into close proximity, as well as stabilizing unusual orientations within the cavity. Conformational restriction can protect otherwise reactive functional groups[287] or increase the reactivity of usually unreactive functional groups.[288]

Some of the effects discussed below, such as those reliant upon substrate confinement, were first[289,290] demonstrated for other supramolecular hosts such as cavitands[30,291,292] and other organic container molecules.[283,293] Other effects rely on specific structural features of the WSCC, such as photoactive ligand panels or redox-active metal centers. The synthetic accessibility of WSCCs and relative ease of tailoring their cavity size and shape render them attractive hosts for exploring these applications.

In many examples discussed below, the hydrophobic effect is key to enforcing the strong and selective guest binding necessary for the observed reactivity. This effect explains why many reports of catalytic coordination cages involve WSCCs, with notable exceptions.[26,294−299] Several early examples of WSCCs, such as Fujita's M_6L_4 octahedra[17] of type **6** and Raymond's $[Ga^{III}_4L_6]^{12−}$ tetrahedra **10**,[300,301] have been especially fruitful in this regard.

More recent strategies for rendering organic-soluble cages water-soluble enabled the Ward group[302] to develop new reactivity for existing coordination cage types, signaling a large scope for new reactivity to be discovered because only a minority of reported coordination cages have been investigated for these applications so far. The small number of WSSCs
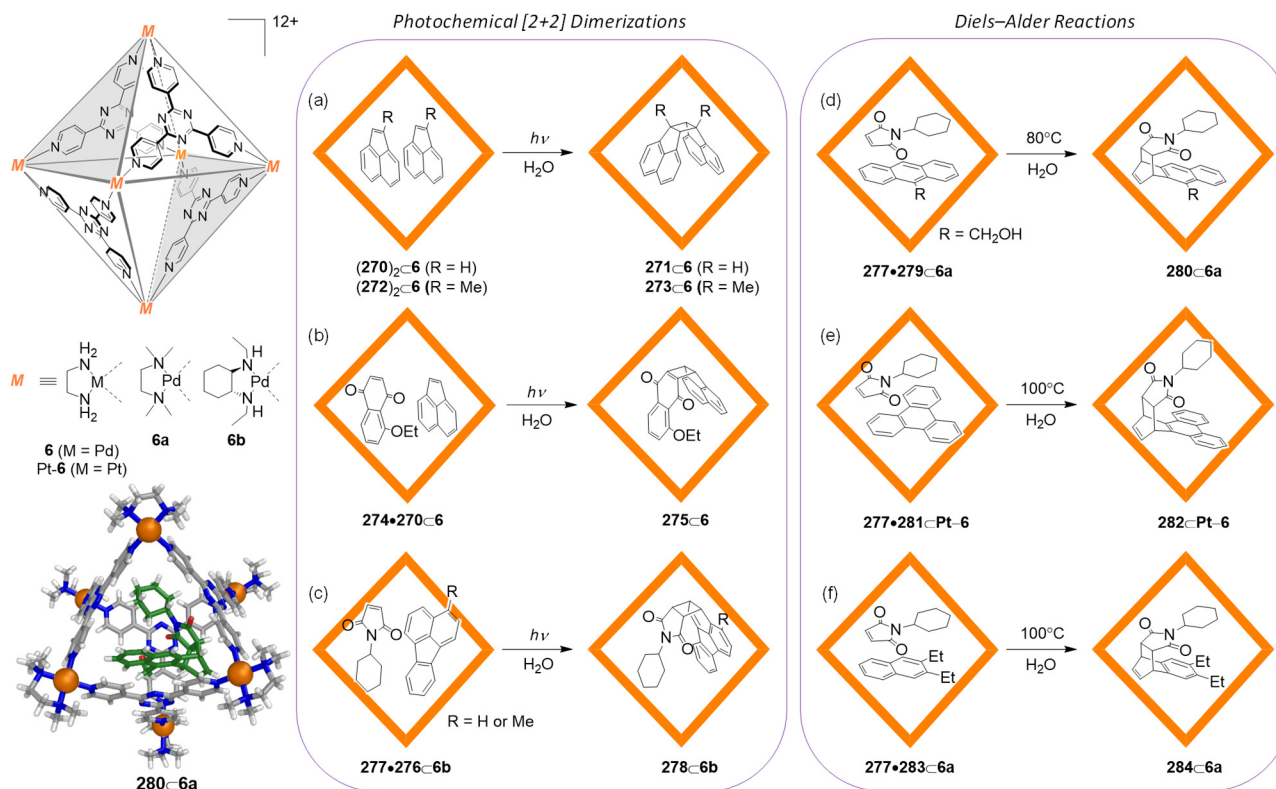
Figure 76. Examples of pericyclic reactions mediated by Fujita's Pd[II] and Pt[II] octahedral cages. (a) [2 + 2] Photodimerization of acenaphthylenes.[303] (b) [2 + 2] Cross-photoaddition of acenaphthylene and 5-ethoxy-1,4-naphthoquinone.[304] (c) Asymmetric [2 + 2] cross-photoaddition of fluoranthenes and *N*-cyclohexylmaleimide.[58] Diels−Alder reactions of *N*-cyclohexylmaleimide with (d) 9-hydroxymethylan-thracene[305] to give a 1,4-adduct and with normally unreactive (e) triphenylene[306] and (f) 2,3-diethylnaphthalene.[307] The X-ray structure of Diels−Alder adduct **280⊂6a** is shown.

utilized as catalysts to date thus reflects a field still under rapid development, with much potential for the rational design of new catalytic cages, alongside the development of new applications for the library of cages already reported.

5.1. Chemical Reactions Promoted by Coordination Cages in Water

A key initial demonstration of altered reactivity within the cavity of a WSCC was reported by Fujita in 2002, when **6** was shown to alter both the rate and stereoselectvity of the [2 + 2] photodimerization of olefins.[303] Two molecules of acenaph-thylene (**270**) were bound in the cavity of **6**, producing exclusively the *syn*-dimer **271** (Figure 76a) in near-quantitative yield upon photoirradiation, in contrast to the mixture of *syn*- and *anti*-dimer produced in low yields in the absence of the cage. Normally, unreactive 1-methylacenaphthylene (**272**) also underwent efficient photodimerization in regioselective fashion to form only the head-to-tail *syn*-dimer **273** (R = Me). In addition to increasing the effective concentration of the encapsulated guests, the aromatic walls of **6** also filter out light of wavelengths below 310 nm, thus preventing the back reaction from dimer to monomer. Bowl-shaped cage **14**, with an open hydrophobic pocket, was also able to facilitate stereoselective [2 + 2] photodimerization reactions.

The selective pairwise encapsulation of two different guests within the cavity of **6** enabled more challenging selective cross-photodimerizations of olefins to be achieved, which are normally difficult to realize in bulk solution as both substrates often have comparable reactivity, leading to mixtures of products.[304] The encapsulation of acenaphthylene (**270**) and

5-ethoxy-1,4-naphthoquinone (**274**) in selective, pairwise fashion led to formation of the hetero *syn*-dimer **275** in >90% yield upon photoirradiation (Figure 76b). This strategy was extended to incorporate otherwise unreactive olefins, such as bulky *N*-substituted maleimide derivatives.[304] Simple chiral modification at the periphery of the cage to produce enantiopure host **6b** enabled a degree of stereocontrol over the asymmetric [2 + 2] cross-photoaddition of fluoranthenes (**276**) and *N*-cyclohexylmaleimide (**277**) to give **278** with up to 50% *ee* (Figure 76c).[58] The observed *ee* values were sensitive to the steric bulk on the chiral auxiliaries, which were proposed to induce subtle chiral deformation of the cage triazine panels.

The selective bimolecular guest recognition[155] by **6** also inspired its investigation as a molecular flask for thermally induced Diels−Alder reactions, with precise spatial organ-ization of substrates often facilitating reactions with unusual regio- and stereoselectivity to generate products that could not be obtained in the absence of the host.

An example is the Diels−Alder addition of *N*-cyclo-hexylmaleimide **277** to 9-hydroxymethylanthracene **279** to give *syn*-1,4-adduct **280** (R = CH$_2$OH) in 98% yield, as reported by the Fujita group (Figure 76d).[305] Typically, anthracenes selectively react with dienophiles at the central ring (9,10-position) as a consequence of the localization of π-electron density at that site. Confinement in the cavity of **6a** preorganizes the maleimide dienophile above a terminal anthracene ring, thus favoring the 1,4-adduct.

The steric bulk of the *N*-cyclohexyl substituent on the maleimide was found to be essential both to pairwise recognition and 1,4-regioselectivity, with the 9,10-adduct

forming when a less bulky *N*-propylmalimide dienophile was used. The reaction is stoichiometric in host **6a** due to the product binding tightly within the cavity, as revealed by X-ray crystallographic analysis of **280⊂6a**, which showed stacking between the aromatic rings of **280** and the host walls (Figure 76). The reaction was rendered catalytic in a more open Pd$_6$L$_4$ cage[182] or in bowl-shaped host **14**, as the bent product showed less efficient π-stacking with the host panels compared to the anthracene substrate. However, in both catalytic cases, the more common 9,10-adduct was obtained.[305]

Confinement inside the cavity of **6** not only induced new regioselectivity but also new reactivity. Typically inert triphenylene (**281**) reacted with *N*-cyclohexylmaleimide (**277**) inside the cavity of **6** or its more stable Pt^{II} analogue Pt-**6** to give the corresponding *syn* Diels−Alder adduct **282** (Figure 76e); perylene also afforded Diels−Alder adducts under similar conditions.[306] Even unreactive naphthalene derivative **283** was able to undergo Diels−Alder reaction with **277** to give **284**. The alkyl chains of **283** were necessary to ensure preorganization of the substrates within the cavity of **6a** (Figure 76f).[307]

Alternatively, the cavity of the cage could be tuned through the use of bulky ancillary ligands on the Pd^{II} vertices, which compress the cage cavity and induce reaction of unsubstituted naphthalene.[308] The cavity of **6** was also able to promote [2 + 2] olefin photodimerization of otherwise unreactive polycyclic aromatic hydrocarbons.[306,309]

The hydrophobic effect is crucial for the promotion of the thermal [2 + 4] and photochemical [2 + 2] cycloadditions of the inert aromatic molecules shown in Figure 76. The strong binding of these nonpolar substrates within the hydrophobic cavity of **6** is central to their greatly enhanced reactivity, resulting from the increased local concentration and preorganization of the substrate pair within the cage. The unfavorability of the entropy of activation of these reactions is thus reduced, and the reaction profile switches from a bimolecular to a pseudointramolecular reaction pathway.[286] The role of the bulky substituents on the substrates in many of the examples discussed further highlights the role of confinement in forcing substrates into specific orientations. Little or no reactivity was observed in the absence of the WSCC due to the poor solubilities and reactivities of the substrates.

Geometric restriction of substrates within the cavity of **6** could also be used to control the pathway of the bimolecular radical reaction of *o*-quinone **285** and bulky toluene derivative **286** to form unusual 1,4-adduct **287**, which was not detected in the absence of the cage (Figure 77).[310] The reaction was proposed to proceed *via* 1,4-addition of the benzylic radical, formed by photoexcitation of the *o*-quinone and subsequent hydrogen abstraction from the nearby methyl group of **286**. The orientation of the substrates within the cage, observed *via* X-ray crystallography, disfavors otherwise predominant reaction pathways. In this way, the WSCC acts in an analogous manner to enzymes, where the specific orientation of substrates within the active site forces them to react *via* pathways that differ from those favored in bulk solution.[311]

In addition to promoting reactions through spatial confinement of substrates within its cavity, **6** can also actively participate in transformations, as shown schematically in Figure 78a. In the photoexcited state, its electron-deficient triazine panels can function as electron acceptors, leading to the regioselective photooxidation of alkanes[312] and triquinacene[313] guests.
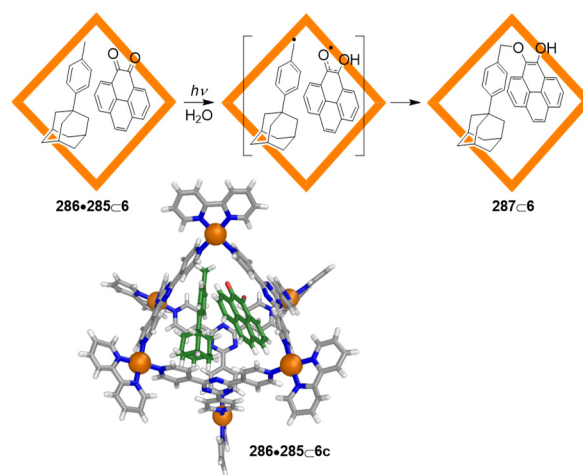
Figure 77. Regio- and stereoselective light-mediated 1,4-radical addition within **6**. The crystal structure of **286•285⊂6c** is shown.[310]
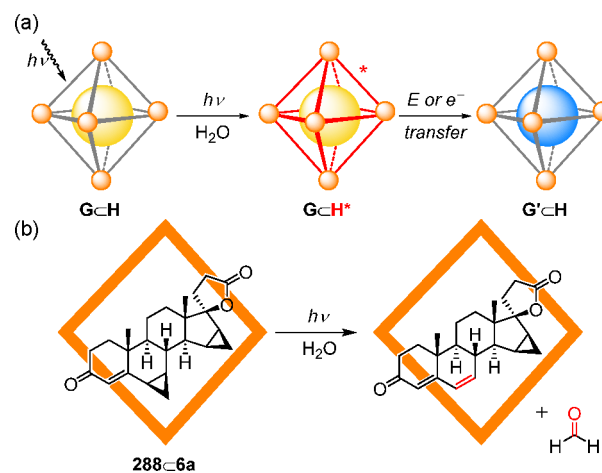
Figure 78. (a) Schematic representation showing WSCCs as photosensitizers for reactions. (b) Example showing demethylenation of **288** *via* photoinduced guest-to-host electron transfer in cage **6a** under UV radiation.[315]

The same cage also enabled the selective anti-Markovnikov hydration of internal arylalkynes *via* cage-mediated, photoinduced electron transfer from alkyne to cage.[314] Following the reaction, the benzyl ketone product, usually unstable to light, was stabilized within the cage. Photoinduced guest-to-host electron transfer was also able to promote unusual demethylenation reactions of cyclopropanes within the cavity of **6a**, including that of structurally complex steroid derivative **288** (Figure 78b).[315]

Another WSCC that has been shown to function as an effective photosensitizer is naphthalene-edged tetrahedron **10**. Raymond, Bergman, and Toste used this cage to photochemically promote the 1,3-rearrangement of encapsulated cationic cinnamylammonium guests from the linear isomer to the higher-energy branched isomer, a transformation not observed in bulk solution.[316] Photophysical studies implicated a photoinduced electron transfer (PET) mechanism for this process, whereby the [Ga$^{III}_4$L$_6$]$^{12−}$ cage absorbs light and transfers an electron to the encapsulated cinnamylammonium ion, which undergoes C−N bond cleavage, followed by back electron transfer to the cage and recombination of the guest fragments.

The photoredox-active Ru^{II}-metalloligands of Su's [Pd$_6$(RuL$_3$)$_8$]$^{28+}$ cage **128** were employed for regio- and enantioselective photodimerization of naphthols.[317] The racemic and enantiopure forms of the cage both encapsulated naphthol guests **289**, which then underwent a regiospecific 1,4-coupling to form 4-(2-hydroxy-1-naphthyl)-1,2-napthoqui-nones **290** (Figure 79a). This reaction outcome contrasts with the conventional 1,1-coupling observed in the absence of the cage.
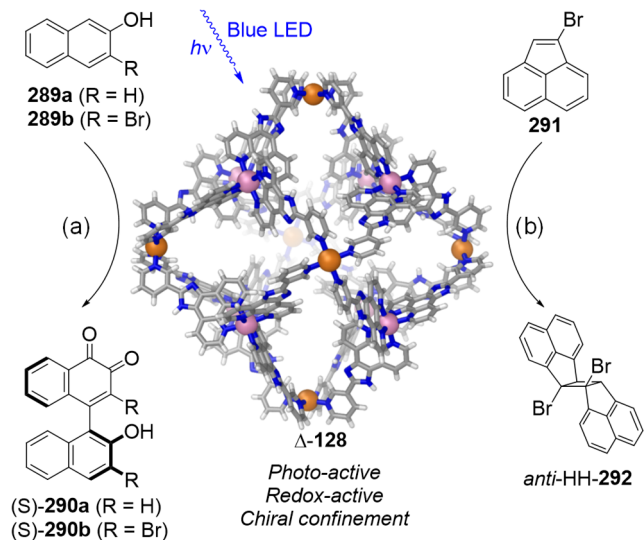
Figure 79. Regio- and stereoselective reactions mediated by Δ-**128**.[317] (a) Photoinduced biaryl coupling of **289** to give **290**. (b) Photodimerization of **291**.[318]

The authors propose that encapsulation prearranges the substrates close to the photo- and redox-active Ru^{II} sites, simultaneously rendering electron transfer more efficient and stabilizing reactive radical intermediates. Dimerization of **289a** thus proceeded in near quantitative yields in water, while that of **289b** required 1:1 CH$_3$CN/H$_2$O and proceeded in lower yields due to the poor aqueous solubility of the substrate. Some stereochemical control was also imposed when enantiopure **128** was employed, with observed enantioselec-tivities of up to 58% for the dimerization of **289b**.

The same cage also mediates the stereo- and regioselective photodimerization of 1-bromoacenaphthylene **291** in 1:1 H$_2$O/DMSO. The *anti*-head-to-head dimer **292** was produced in 94% yield, with none of the five other possible isomers observed (Figure 79b).[318] The product is chiral and a single enantiomer was favored with up to 88% *ee* in the presence of Δ-**128** or Λ-**128**.

This reaction was rendered catalytic by precipitation of the insoluble product **292**, which is a less effective guest than the planar substrates. Confinement also led to 75-fold rate acceleration vs the uncatalyzed reaction or 34-fold compared to the reaction mediated by mononuclear RuL$_3$ complex **127**. The important role played by the hydrophobic effect in catalysis was elucidated by the reduction in selectivity observed when a less hydrophobic CH$_3$CN/H$_2$O solvent mixture was employed, leading to less effective guest inclusion.

The favored *anti*-stereoselectivity contrasts with the preference for *syn*-dimerization of related substrates inside Fujita's smaller Pd$_6$L$_4$ octahedron **6**.[303] In the case of **6**, guests were confined in the central pseudospherical cavity prior to

reaction, favoring the more spherical *syn*-dimer. In contrast, **128** is proposed to bind guests in its 12 rhombic portals in the surface of the cage which are bound by two planar phenanthroline motifs from adjacent ligands. Two **291** guests bind inside a portal through aromatic stacking interactions, preorganizing the two substrates in an offset head-to-tail fashion with their 1,2-ethylene segments in proximity to each another, thus giving rise to *anti*-dimer **292**. Dipolar interactions between the Br atoms and Ru^{II} centers also play a role in substrate preorganization, favoring the in head-to-head isomer over the head-to-tail one.

Organometallic photochemical reactions can also take place in the cavities of WSCCs, including reactions that do not normally happen in water. Diruthenium complex [(Me$_4$Cp)-Ru(CO)$_2$]$_2$ (**293**; Cp = cyclopentadienyl) within cage **6a** undergoes photosubstitution of a CO ligand for an alkyne, without the cleavage of the Ru−Ru bond that would occur in the absence of the cage (Figure 80).[319] The resulting π-

Figure 80. Organometallic transformation of dinuclear ruthenium complex **293** encapsulated in **6a**.[319] The complex undergoes photosubstitution of a CO ligand by an alkyne, followed by rearrangement upon extraction from the cage.

complex **294** was stabilized within the cage. Following extraction into organic solvent, however, **294** underwent rearrangement to give final product **295**. This unusual product is not observed in the absence of the cage due to fragmentation pathways predominating in solution.

Raymond and Bergman's observation of cationic organo-metallic complex encapsulation in the cavity of **10**,[320] including species such as [Cp$_2$Fe]$^+$, [Cp$_2$Co]$^+$, and [CpRu(C$_6$H$_6$)]$^+$, prompted them to investigate the encapsulation of more reactive organometallic half-sandwich compounds. The coencapsulation of Ir^{III} complex [Cp*(PMe$_3$)Ir(Me)(C$_2$H$_4$)]-[OTf] **296** and an aldehyde promoted C−H activation of the aldehyde (Figure 81a).[321] Only aldehyde substrates capable of fitting within the cage cavity were observed to react, providing evidence that C−H activation occurs inside the cavity. This selectivity is reminiscent of the behavior of metalloenzymes, although the reaction was stoichiometric in this case due to encapsulation of the product by **10**.

A detailed follow-up study explored the scope and mechanism of the reaction.[322] Binding of the Ir^{III} complexes was found to be enthalpically disfavored but entropically favored, suggesting that the hydrophobic effect plays a dominant role despite the potential for favorable electrostatic interactions.

The Fujita group reported the coencapsulation of square planar complex *trans*-[PdCl$_2$(PEt$_3$)$_2$] (**297**) and terminal alkyne **298** by **6a**, thus promoting C(sp)−H activation to form a σ-alkynylpalladium(II) complex **299** in the cavity (Figure 81b).[323] The cage exhibited shape selection in terminal alkyne activation. This activation occurs without the help of a Brønsted base and even under acidic conditions, excluding a
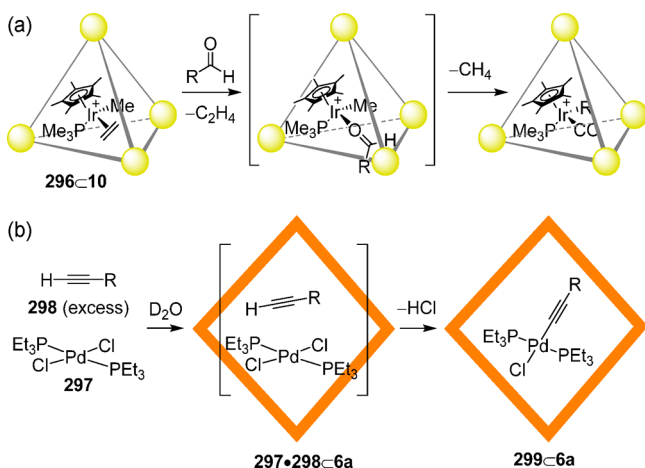
Figure 81. Cavity-promoted C−H activation by WSCCs. (a) C−H activation of aldehydes, where R is a short alkyl group, by an encapsulated Ir^III host−guest complex.[321] (b) C−H activation of a terminal alkyne, where R = ^nBu or ^iBu, by an encapsulated Pd^II complex. In both, the cavities of the WSCCs exhibited shape selectivity for their substrates.[323]

base-mediated deprotonation mechanism. No reaction was observed in a control reaction without the cage.

More recently Raymond, Bergman, and Toste used the ability of **10** to stabilize reactive cationic organometallics to promote the oxidative addition of aryl halides to Cu^I and Pd^II metal centers under mild conditions in water, a process that did not take place at all in the absence of the cage.[324]

Complementing the utilization of WSCCs as whole-molecule protecting groups is the protection of specific reactive groups in molecules with multiple reactive sites. This concept was elegantly demonstrated by the Fujita group through the site-selective electrophilic addition to linear diterpenoids (**300**) within octahedron **6a** (Figure 82).[287] The flexible linear substrates folded into a U-shaped
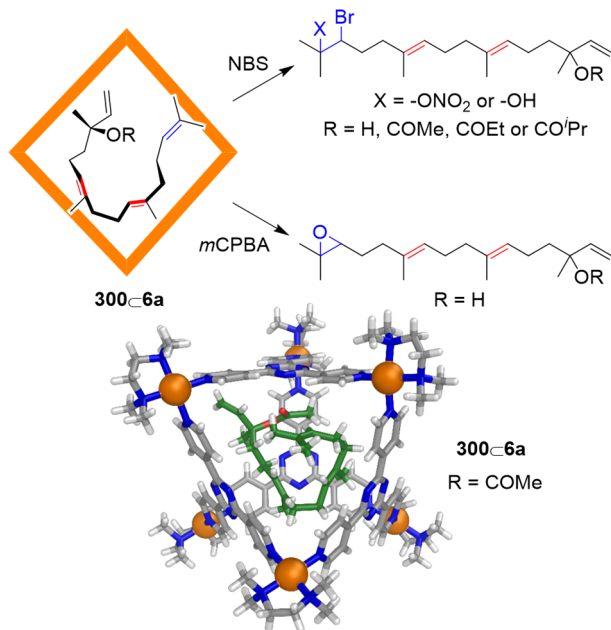
Figure 82. Site-selective electrophilic addition reactions of diterpenoids within **6a**. The crystal structure of **300⊂6a** is shown.[287]

conformation within the cavity, resulting in noncovalent protection of internal C=C bonds and enhanced selectivity for reaction at the terminal site, which is exposed through the portal of the cage.

The folded arrangement of the diterpenoids was revealed through NOESY correlations in solution and X-ray crystallography in the solid state. The conformations of the flexible diterpenoids are cooperatively fixed within the cavity of **6a** by multiple noncovalent interactions. These interactions include C=O···π interactions between the ester carbonyl group and one of the triazine rings of the ligand and stacking between the trisubstituted olefin moieties and the ligand panels.

The folding of the diterpenoid substrates contrasts with previously investigated linear hydrocarbons,[325] which do not fold within the cavity of **6a** but instead adopted the inherently most stable zigzag conformation as a consequence of binding being driven by hydrophobic effects alone. Control experiments confirmed that conformational constriction inside cage **6a** was vital for the observed high degree of site selectivity. Analogous conformational restrictions of related polyisoprenoids in the active sites of enzymes is a key step for the construction of natural product frameworks, suggesting potential for WSCCs to be used for the synthesis of new natural product-like compounds.

As well as suppressing the reactivity of encapsulated functional groups, the constriction of substrates can enhance the reactivity of normally unreactive moieties. The Fujita group reported that the inclusion of two molecules of aromatic secondary amides **301**−**302** in the cavity of **6a** favors the cis-twisted conformation over the usually observed trans-planar one, as revealed by NMR and X-ray crystallographic studies of (**301**)$_2$⊂**6c**, which showed that the amides twist by up to 34° from planarity (Figure 83).[288]

Distortion from a planar conformation disrupts conjugation between the nitrogen lone pair and the π* orbital of the carbonyl, leading to enhanced reactivity toward nucleophiles and accelerated hydrolysis of the encapsulated amides in basic solution. The magnitude of guest twisting could be tuned by coencapsulation of appropriate second guests to form ternary host−guest complexes, leading to enhancements of up to 14 times compared to the rates in the absence of the cage. A steric shielding effect was observed for substrate **303** (Figure 83b), where the amide conjugation was relatively weak due to delocalization of the amide nitrogen lone pair into an indole ring.

The structure of the cage cavity was vital for conformational constriction, with neighboring ligands providing a V-shaped region sandwiched between two electron-accepting triazine ligand panels. The cage ligands thus stacked with the aromatic rings of the twisted amides, with the strength of this interaction enhanced via hydrophobic effects. The importance of these stacking interactions is supported by the observation that only electron-rich amides were encapsulated.

The size and shape match between substrate and host were also vital, as smaller substrate **302** formed a mixed cis−trans dimer in the cavity compared to the cis−cis dimer observed for the larger substrate **301**. The enhanced hydrolysis of the twisted amides mimics the strain-induced hydrolysis mechanism proposed for the cleavage of specific peptide bonds in proteins, pointing to the potential for WSCCs to perform complex biomimetic functions.

(301)$_2$⊂6a

Amide guests

301 k_{cage}/k_{bulk} = 5.1

302 k_{cage}/k_{bulk} = 6.1

303 k_{cage}/k_{bulk} = 0.11

k_{cage}/k_{bulk} up to 14 with modulator guest

(301)$_2$⊂6c
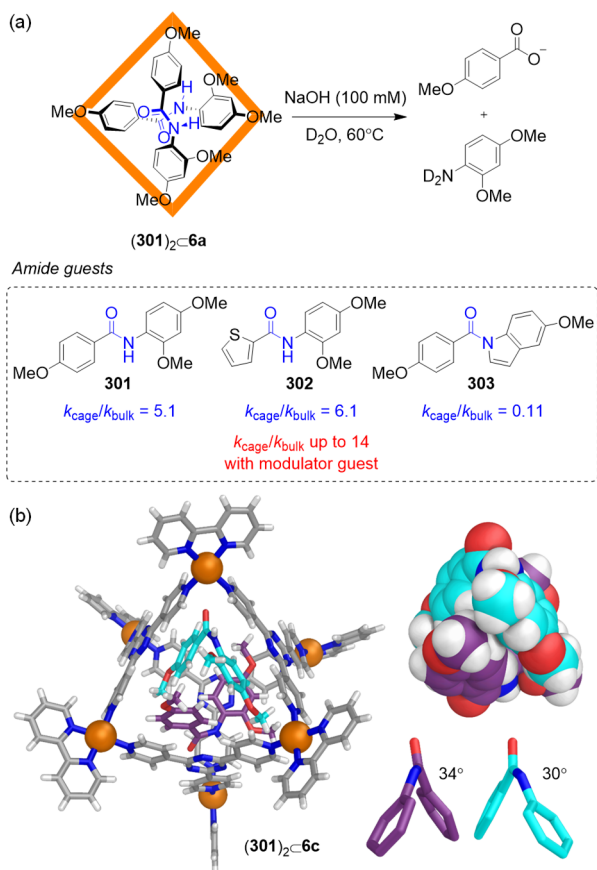
Figure 83. (a) Hydrolysis of twisted amides in the cavity of **6a**. (b) X-ray structure of (**301**)$_2$⊂**6c** with cutout of the dimer composed of two inequivalent amides, which are twisted by 34° and 30° around their C−N−C(O)−C bonds.[288]

5.2. Catalytic Reactions within Cages in Aqueous Media

5.2.1. Catalysis by Substrate Confinement. Although striking rate enhancements were sometimes observed for pericyclic reactions in the cavity of WSCCs, catalytic turnover was often inhibited by encapsulation of the product in the cage cavity due to the similarity in transition state and product geometries. Raymond and Bergman overcame this problem to achieve catalytic turnover in the aza-Cope electrocyclization of allylenammonium salts inside the cavity of tetrahedron **10**, with rate enhancements of up to 850-fold compared to the uncatalyzed reaction (Figure 84).[326,327]

Cationic substrate **304** bound inside the cage and underwent a [3,3] sigmatropic rearrangement to form iminium cation **305**, aided by preorganization of the substrate into a reactive chairlike conformation (Figure 84). Subsequent hydrolysis to the corresponding γ,δ-unsaturated aldehyde **306** led to ejection of the product from the cavity of the cage in favor of binding more substrate, as the neutral product is a poorer guest for the negatively charged cage.

The scope of the reaction was expanded to include less reactive enammonium cations[328] and enantioselective catalysis, with up to 78% ee using enantiomerically resolved **10**.[329]

The remarkable stabilization of protonated guests within the cavity of **10** prompted Raymond and Bergman to investigate the cage as a catalyst for reactions that take place *via* positively charged transition states, which are stabilized by encapsulation.[330] Host-induced shifts in effective basicity promoted the
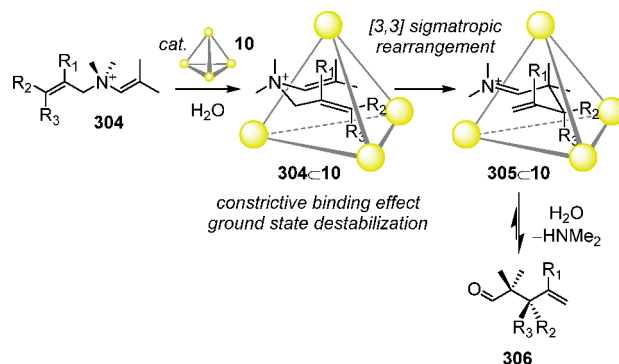
Figure 84. Catalytic acceleration of the aza-Cope rearrangement of allyl enammonium ions, promoted by constrictive binding effects within **10**.[326,327]

normally acidic hydrolysis of orthoformates in basic solution (Figure 85a).

Stabilization of the protonated transition state in the host interior led to rate accelerations of up to 890-fold.[331,332] The intermediate formate ester product was rapidly hydrolyzed to the formate anion, which is not bound by the cage.

Competitive inhibition by a more strongly binding guest and the observed substrate size selectivity confirmed that catalysis occurs in the cavity. Similarly, **10** also catalyzed the hydrolysis of acetals and ketals in basic solution.[328,333] The acid-catalyzed hydrolyses in basic solution by **10** are reminiscent of the action of enzymes,[334−336] which exploit pK_a shifts that occur as a result of hydrogen-bonding or electrostatic interactions to activate otherwise unreactive substrates.

Raymond and Bergman achieved even higher rate enhancements for the Nazarov cyclization, an acid-catalyzed reaction in which a 1,4-dien-3-ol forms a cyclopentadiene (Figure 85b).[337] Rate enhancements of up to 2×10^6 resulted from a combination of enhancement of the basicity of the alcohol group of the bound substrate and preorganization of the substrate in the reactive U-shaped conformation through confinement in the cavity of **10**.[338] The role of charge stabilization in the rate acceleration was validated by the observation of a 680-fold decrease in reaction rate upon reducing host charge from 12− in Ga-**10** to 8− in Si-**10**.[96]

As well as achieving rate enhancements similar to those obtained by biological catalysts, enzyme-like mechanistic control by WSCCs has also been observed. Biologically relevant terpene cyclizations were catalyzed by **10** at physiological pH.[339] The hydrophobic interior of **10** directs the Prins cyclization of monoterpene (±)-citronellal **307** toward deprotonation to give **308** instead of nucleophilic capture by water (Figure 86a). In the absence of the cage, reaction only occurs in acidic solution, with the predominant reaction pathway involving hydration of the carbocation intermediate produced by cyclization to give cyclic diol product **309**.

The observed catalysis thus relies on both conformational control and the exclusion of water from reactive intermediates in an analogous manner to terpene synthases. Use of the WSCC also avoids the dehydration and dimerization by-products often observed when the reaction was carried out using organic solvents and Lewis acids.[340,341]

Functionalization of the Raymond group's ligand with amide-containing chiral groups resulted in the formation of enantiopure cage **310** (Figure 86b), which exhibited increased
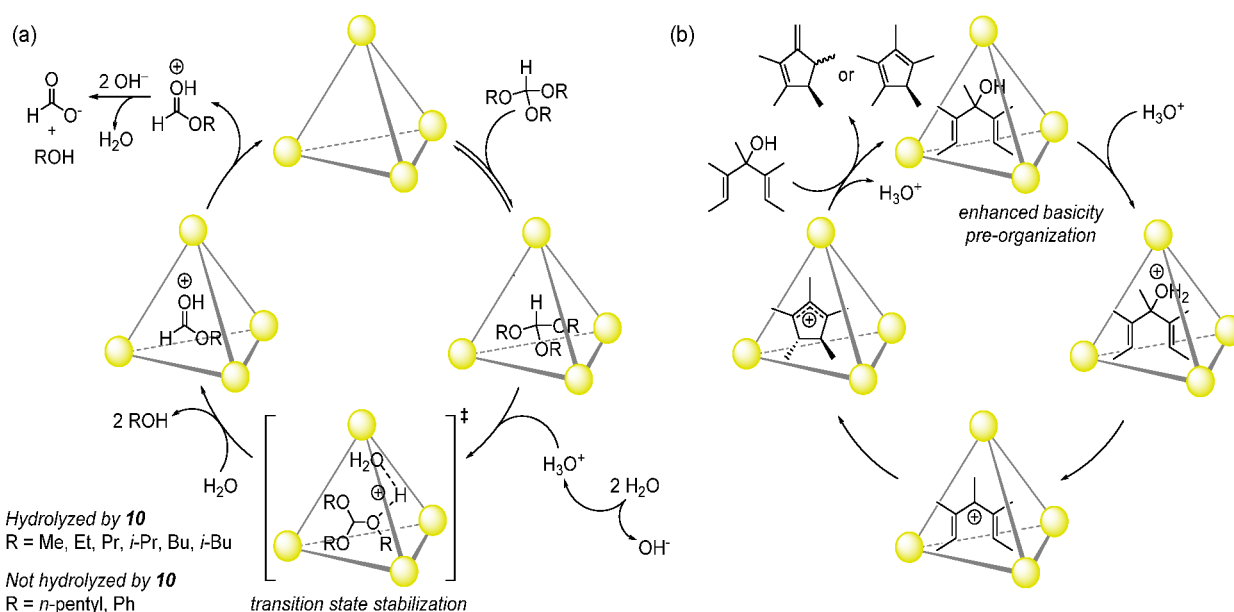
Figure 85. Examples of catalysis *via* enhancement of substrate basicity through encapsulation within **10**. (a) Hydrolysis of orthoformates in basic solution.[331,332] (b) Nazarov cyclization, which also benefits from conformational restriction.[337]
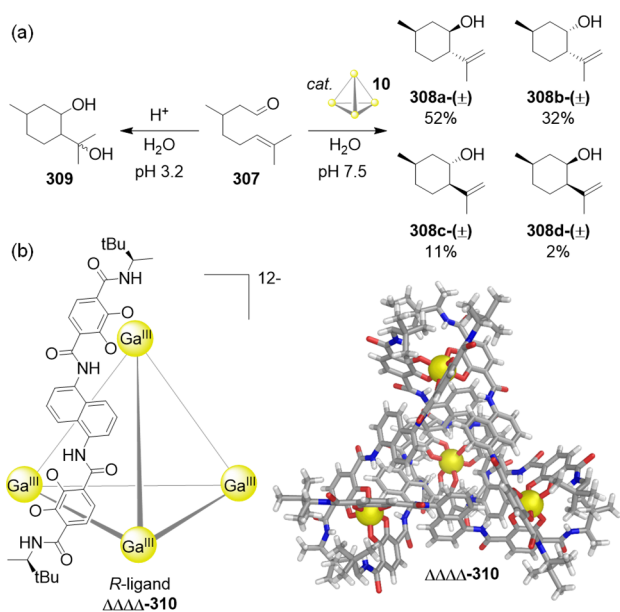
Figure 86. (a) Cyclization of monoterpene (±)-citronellal (**307**) catalyzed by **10** gives alkene **308a** as the major product, whereas diol **309** is obtained for the acid catalyzed reaction in bulk solution.[339] (b) Structure of water-soluble enantiopure tetrahedron **310** used as an enantioselective catalyst, showing the X-ray structure of ΔΔΔΔ-**310**.[342]

stability to oxidation due to hydrogen bonding between the amides and catecholates at the cage vertices.[342] Cage **310** enabled enantioselective catalysis of related Prins cyclization reactions. A subsequent study further investigated the effect of host structure on the selectivity and mechanism of intramolecular Prins cyclizations.[343]

The propensity of **10** to catalyze cyclization reactions and its ability to promote iminium ion formation led Raymond, Bergman, and Toste to investigate the catalysis of aza-Prins reactions, as shown in Figure 87a. Unexpectedly, the reaction of amine-tethered olefin **311** with excess formaldehyde and a

catalytic amount of **10** yielded dealkylated piperidine **312**, rather than the expected product **313**, formed in the absence of the cage under acidic conditions (Figure 87a).[344]

The authors proposed a transannular 1,5-hydride shift mechanism, which has never been observed in bulk solution. This reaction pathway occurs through a more spherical transition state, which is favored in the constricted cavity of the cage but too high in energy to be accessed in bulk solution. This study demonstrates how constrictive binding in WSCCs can redirect the pathway of a reaction, opening up pathways that yield new products.

The iminium-stabilizing ability of **10** also enabled a three-component Aza-Darzens reaction of anilines, aldehydes, and α-diazo esters (Figure 87b).[345] The *trans* isomer of the disubstituted *N*-phenylaziridine product was obtained in contrast to the *cis* isomer generated in bulk solution.

Cage **10** catalyzed the solvolysis of benzyl derivatives (**314**) in buffered 1:1 CD_3OD/D_2O to give **315** or **316** with retention of absolute stereochemistry, whereas reaction of the same substrates in bulk solution gave products with inverted stereochemistry through a classical S_N2 mechanism (Figure 88).[346] The authors proposed that the electron density of the naphthalene walls stabilizes the developing positive charge at the benzylic carbon atom in the transition state through cation−π interactions, resulting in one face of the carbocation intermediate being blocked from nucleophilic attack. The nucleophile is then bound with retention of configuration before the cation has a chance to rotate in the confined environment of the cavity. The reaction proceeded with stereochemical retention when either enantiomer of chiral cage **310** was used, suggesting that the intermediate is not influenced by the stereochemistry of the host complex cavity.

As a counterpart to the catalysis of reactions with cationic transition states by anionic WSCCs, cationic WSCCs have been used for the catalysis of reactions with anionic transition states. Fujita's octahedron **6** catalyzes the Knoevenagel condensation of aromatic aldehydes in water.[347] Naphthalene and anthracene-based aldehydes such as **317** are bound by **6** and undergo dehydrative condensation with Meldrum's acid
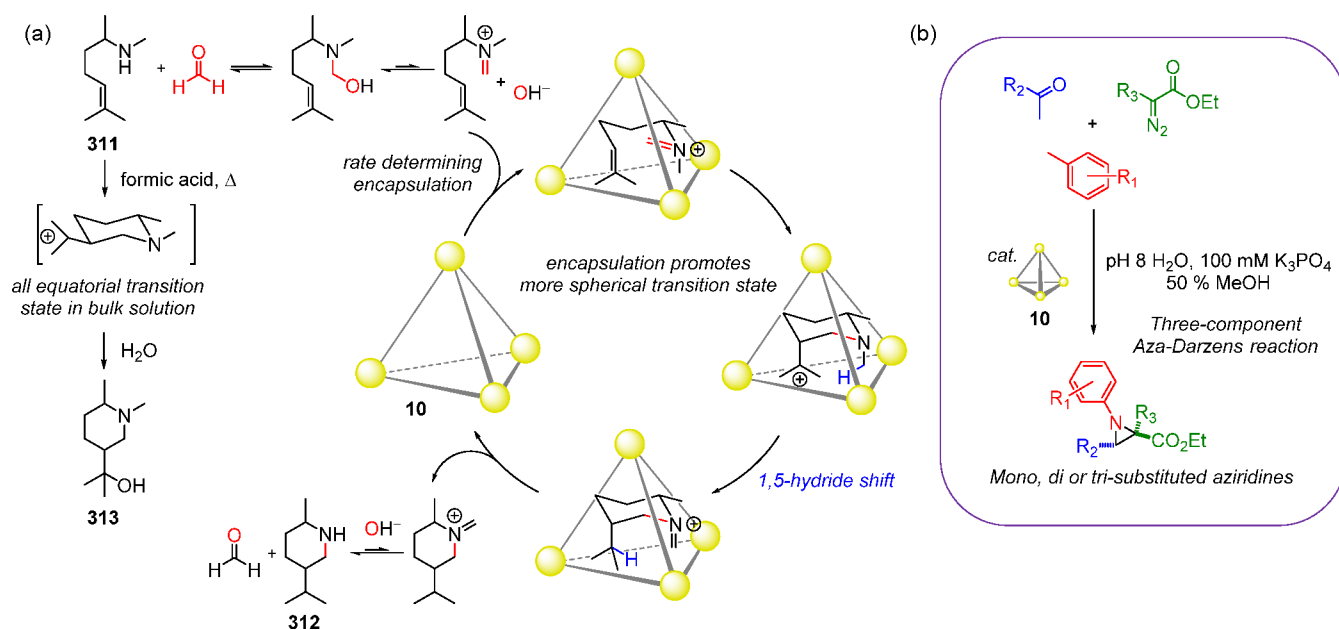
Figure 87. (a) Aza-Prins reaction catalyzed by **10** to give a different product to the one observed in bulk solution as a result of stabilization of a more spherical transition state in the cage cavity.[344] (b) Three-component Aza-Darzens reaction catalyzed by **10**.[345]
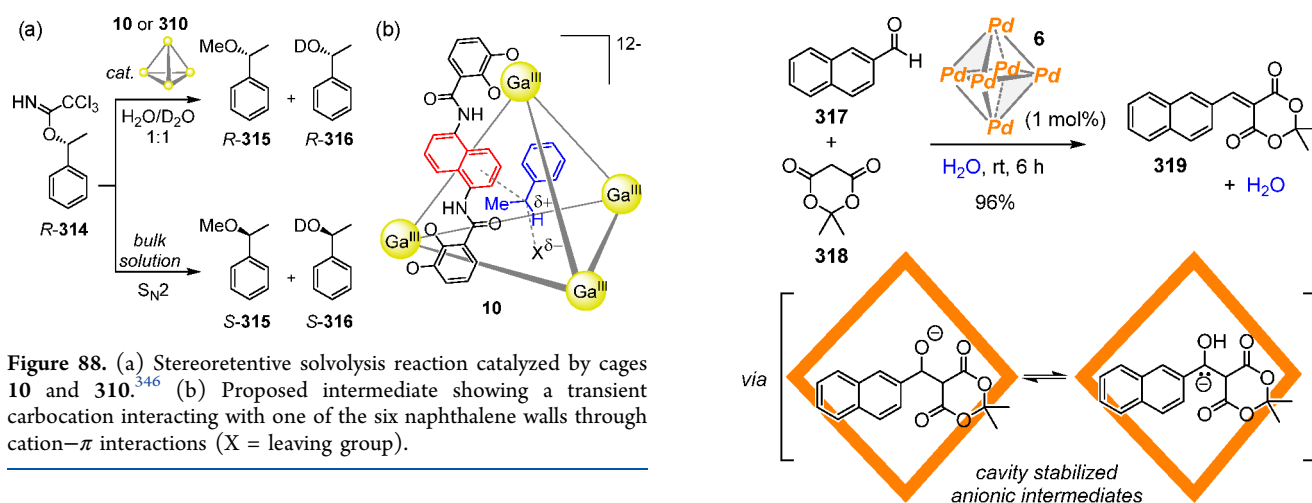
Figure 88. (a) Stereoretentive solvolysis reaction catalyzed by cages **10** and **310**.[346] (b) Proposed intermediate showing a transient carbocation interacting with one of the six naphthalene walls through cation−π interactions (X = leaving group).

Figure 89. Knoevenagel condensation of an aromatic aldehyde with Meldrum's acid in cage **6** showing the structure of the cage-stabilized anionic intermediates formed during the reaction, which then undergo dehydration in the hydrophobic cavity.[347]

318 *via* an anionic intermediate that is stabilized in the cage (Figure 89). The products (**319**) are ejected from the cage, as a result of the host−guest size discrepancy allowing catalytic turnover.

Other positively charged WSCCs have been shown to catalyze Knoevenagel condensations of hydrophobic aldehydes in water and more complex two-step dehydrations to form xanthenes despite such reactions usually being disfavored in water due to the formation of water during the reaction.[182,348]

A larger $[Pt_{12}L_4]^{24+}$ WSCC **320** prepared by the Mukherjee group catalyzes the Michael addition reactions of a series of nitrostyrene derivatives with indole in 9:1 H_2O:MeOH.[349] The cage assembled from chiral *cis*-[(cyhex)Pt(NO$_3$)$_2$] (cyhex = *cis*-(1S, 2S)-N,N′-diethyl-1,2-diaminocyclohexane) corners and tris(4-(pyrimidin-5-yl)phenyl)amine **321** in a 3:1 ratio (Figure 90a). The tetrahedral cage possesses an interior hydrophobic cavity of volume 860 Å^3 surrounded by four hexadentate ligands paneling the faces of a tetrahedron with open windows of 5.7 × 5.4 Å^2 along the edges of the tetrahedron.

The cavity of **320** encapsulates two water insoluble aromatic nitroalkene (**322**) guests. Michael addition of indole **323** to these guests proceeded with greater conversion to the Michael

adduct **324** (Figure 90b) relative to the uncatalyzed reaction. No enantioselectivity was observed in this case despite the enantiopure nature of the cage.

The authors propose that the cationic cage activates the nitro groups of the β-nitrostyrene systems through electrostatic interactions, which facilitate its electrophilic substitution reaction with **323**. The kinetic inertness of the Pt−N bonds enables the cage to catalyze reactions of coordinating Michael donors such as indole, overcoming a common problem of catalysis with WSCCs, whereby strong nucleophiles or bases disrupt the coordinative bonds holding the cage together. This study exemplifies a wider effort to designing catalytic cages with large windows for easy ingress of substrates and exit of products from the cavity.[348,350−352]

The examples discussed so far in this section illustrate how highly charged WSCCs provide a means to stabilize transition
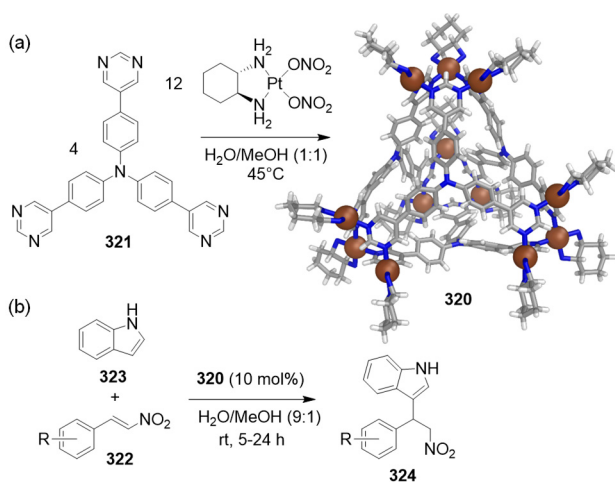
Figure 90. (a) Self-assembly of tetrahedron **320** from ligand **321** and *cis*-[(cyhex)Pt(NO$_3$)$_2$]; the X-ray structure of **320** is shown. (b) Michael addition of aromatic nitroalkene guests with indole promoted by cage **320**.[349]

states with complementary charges, leading to rate enhancements. Charged WSCCs can also be used to enhance the local concentration of ionic reagents through ion pairing effects. This concept was explored by Ward, Hunter, and Williams during their investigation of the Kemp elimination of benzisoxazole **325** to form 2-cyanophenolate **326** in the cavity of water-soluble Co$_8$L$_{12}$ cage **37** (Figure 91a), which accelerated the reaction by up to 2×10^5 at pD 8.5.[353]

Above pD 7, the product exists as the 2-cyanophenolate anion which was not bound by the cage, enabling efficient catalytic turnover. In bulk solution, the Kemp elimination is first-order in hydroxide over a wide pH range, with the rate increasing 10-fold for every unit increase in pH above 7. The

rate of the cage-catalyzed reaction, in contrast, was constant over the pD range 8.5–11.4, below which product inhibition started to occur and above which the cage decomposed.

The uncatalyzed reaction achieved the same rate as the catalyzed reaction at pD 13.8. Thus, even at pD 8.5, the encapsulated benzisoxazole reacts as if experiencing a pD of 13.8. The authors proposed that the surface of the positively charged cage attracts partially desolvated hydroxide ions through ion pairing effects, positioning the hydroxide ions close to the C–H groups of the encapsulated substrate. The observations of anions bound in windows in the surface of the cage in X-ray structures supports this hypothesis (see Figure 91c,d).[302]

The catalysis observed is thus based on two distinct binding events: (i) hydrophobic binding of benzisoxazole in the cavity, and (ii) polar binding of hydroxide ions to specific sites on the cage surface. The importance of both interactions was confirmed by competition experiments. The catalytic reaction was inhibited independently by either the addition of cycloundecanone, which binds more strongly in the cavity of **37** than the substrate **325**, or chloride anions, which compete with hydroxide for the sites on the cage surface.

Although this example of a base-catalyzed reaction mediated by a cationic cage offers some parallels with the promotion of acid-catalyzed reactions by Raymond and Bergman's anionic cage **10**, there are also distinct differences. Notably, no transition state stabilization effect is invoked for the system of Figure 91a, and the cavity of **37** is actually thought to destabilize the buildup of negative charge on oxygen in the transition state relative to pure water. This catalytic mechanism provides a contrast to other modes of catalysis by confinement in WSCCs, which arise from stabilization of transition states *via* electrostatic and constrictive binding effects.

The inhibition studies led to the discovery of an autocatalytic pathway where the 2-cyanophenolate product
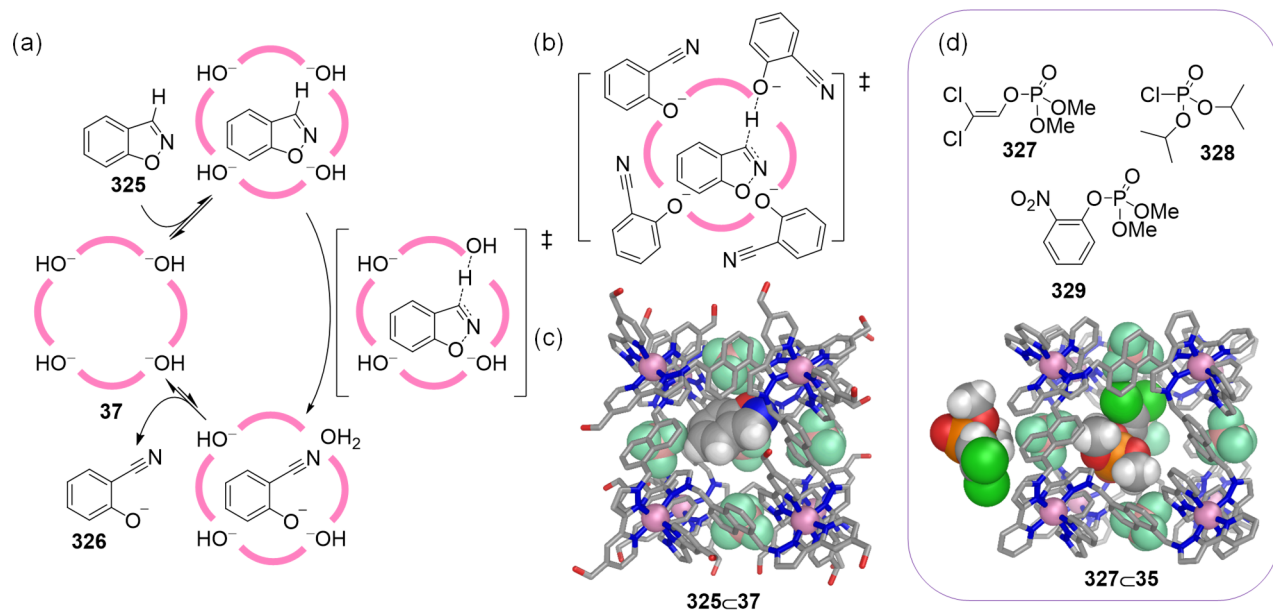
Figure 91. (a) Catalytic reaction cycle for the Kemp elimination catalyzed by cage **37**.[353] (b) Autocatalysis of this reaction occurs in cage **35** in the presence of chloride.[354] (c) X-ray structure of **325⊂37**.[302] (d) Structure of phosphoester guests bound by the chloride salt of cage **35** and X-ray structure of the BF$_4^-$ salt crystallized with dichlorvos **327**, showing both the internally and externally interacting guests.[355] In both structural representations the guests are shown in space-filling mode, and the tetrafluoroborate anions that occupy the cage windows are shown with the frontmost anion omitted for clarity in both cases.

catalyzes the reaction as it accumulates at the cage surface (Figure 91b).[354] This pathway is not normally visible as the reaction with hydroxide is faster, but it dominates when hydroxide binding is switched off by the presence of chloride. These results led the authors to explore the generality of the phenomenon of WSCCs as catalysts for bimolecular reactions between cavity-bound guests with surface-bound anions.

The hydrophobic cavity of **35** (solubilized in water as its chloride salt) was found to bind in water a range of phospho-diester and phospho-triester[107] guests such as the insecticide dichlorvos (**327**) (2,2-dichlorovinyl dimethyl phosphate), the chemical warfare agent simulant di(isopropyl) chlorophosphite (**328**), and 2-nitrophenyl dimethyl phosphate (**329**) and catalyze their hydrolysis (Figure 91d).[355] Unexpectedly, the catalytic hydrolysis persisted even in the presence of competing guests, suggesting that catalysis occurs on the exterior surface of the cage. Supporting this hypothesis, catalysis was observed even with a much smaller $Co^{II}_4L_6$ tetrahedral cage which was unable to accommodate the organophosphate guests internally.

A similar exterior binding mechanism was invoked to explain the catalysis of aldol condensation of indane-1,3-dione to give "bindone" in water by **37**. Here, the surface of the cage is proposed to bring the neutral substrate together with its enolate anion.[356]

These studies point to a general mode of aqueous catalysis whereby surfaces with cationic character are driven into contact with substrates by hydrophobicity. The high surface concentration of anions, due to electrostatic effects, then accelerates a reaction. Highly charged WSCCs, constructed from aromatic-paneled ligands, are ideal candidates for future exploration of this mode of catalysis. The broader applicability of this approach is however balanced by the potential loss of substrate selectivity often observed in catalysis within the cavities of WSCCs. Externally bound guests may also experience a lower local concentration of anions compared to internally bound ones.[355]

The Nitschke group had previously demonstrated catalytic hydrolysis of dichlorvos (**327**) by glycerol substituted cage **29**.[72] In this case, the cavity was implicated in the catalysis, which was inhibited by a more strongly binding guest such as cyclooctane. The hydrolysis products dimethyl phosphate and dichlorovinylmethyl phosphate were not encapsulated by the cage. We hypothesized that dichlorvos may be polarized cooperatively by the positively charged cage framework and the glycerol hydroxyl groups, facilitating nucleophilic attack at phosphorus.

5.2.2. Catalyst Encapsulation.
A complementary strategy to using the cavities of WSCCs to catalyze reactions of bound guests is the encapsulation of active transition metal catalysts as the guests,[291,357] thus allowing control of substrate selectivity as well as potentially stabilizing the active species.[358]

Having achieved selective stoichiometric C−H bond activation by Ir^{III} complexes inside the cavity of **10**,[321,322] Raymond and Bergman were able to obtain similar selectivity in the catalytic isomerization of allylic alcohols by encapsulating a cationic rhodium precatalyst $[(PMe_3)_2Rh(COD)]^+$ (COD = 1,5-cyclooctadiene), which was then activated through hydrogenation.[359] Encapsulation of a related Rh hydrogenation catalyst enabled selective olefin hydrogenation, even in the presence of multiple sites of unsaturation.[360] Although the reaction required at least one sterically nondemanding alkene substituent, complete encapsulation of the substrate in the host cavity was not required to achieve

hydrogenation, as confirmed by the successful hydrogenation of a negatively charged carboxylate substrate which was not encapsulated in the negatively charged cage. This site selectivity allowed for the selective monohydrogenation of lineolenic acid derivative **330** at its least sterically hindered alkene site to form **331** when the larger pyrene-edged tetrahedron **332** was employed in place of **10** (Figure 92).
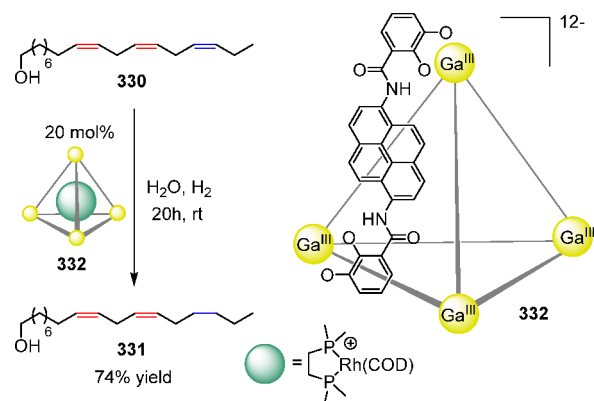
Figure 92. Selective monohydrogenation of **330** using cage **332** and an encapsulated rhodium catalyst.[360]

The larger cage was inferred to allow enough of the guest to enter and undergo hydrogenation at the metal center, with some portion of the large substrate remaining outside of the host cavity. In the absence of the cage, selective hydrogenation of any of the three sites of unsaturation of **330** is challenging due to a lack of directing groups.

Encapsulation of metalloporphyrin catalysts has also been pursed in a strategy to increase their selectivity and to prevent commonly encountered deactivation pathways such as the formation of μ-O-bridged dimers.[26] The de Bruin group observed that the cyclopropanation activity of cobalt−porphyrin catalyst **333** was enhanced through encapsulation in $Fe^{II}_8L_6$ face-capped cubic cage **334** (Figure 93).[361,362] A change of the cage counterion from triflate ($OTf^−$) to triflimide ($NTf_2^−$) allowed catalysis to proceed in aqueous media, rather than toxic DMF, which was used in their initial report.[361]

An unexpected beneficial effect of water on the rate and selectivity of cobalt−porphyrin catalyzed cyclopropanation reactions was observed. The caged catalyst showed enhanced activity in 1:5 acetone/water compared to pure acetone.[362] The hydrophobic cavity of **333⊂334** is proposed to pull substrates into the aqueous phase, or alternatively it may migrate into the water-insoluble substrate phase, thus acting as a phase-transfer catalyst.

Cage **334** also exhibited substrate selectivity, with smaller styrene substrates passing through the cage pores more readily and reacting more rapidly than larger substrates. The observed size selectivity contrasts with the nonselective reactions of similar nonencapsulated catalysts and is only possible due to the use of the WSCC. In a follow-up report, encapsulation of manganese porphyrin **335** inside the same cage framework enabled catalytic epoxidation of various substrates in 1:1 water/acetonitrile mixtures, with improved reactivity and altered selectivity.[363] The cage acts as a phase-transfer agent, creating a protective environment for the catalyst and improving its stability by preventing common deactivation pathways.
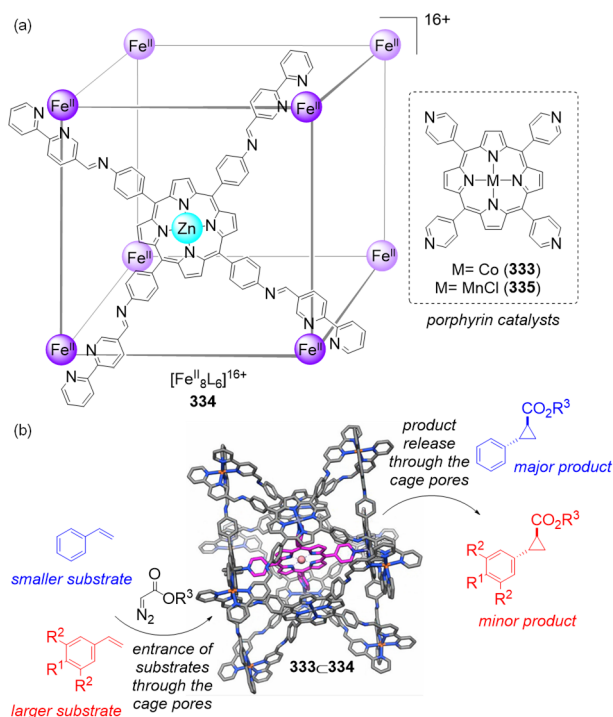
Figure 93. (a) Structure of porphyrin-based cage **334** and encapsulated porphyrin catalysts. (b) Size-selective cyclopropanation catalyzed by **333⊂334** controlled by the pore size of the cage. Adapted with permission from ref 362. Copyright 2014 Wiley-VCH.

5.2.3. Multicatalyst Tandem Reactions. One of the most appealing aspects of catalysis by WSCCs is the prospect of performing chemically incompatible synthetic steps sequentially in one pot, in similar fashion to biological systems where the product from one enzymic transformation may act as a substrate for the next. The cavities of WSCCs offer the potential to separate individual reaction steps without interference from other species present in the system, as well as reducing unwanted side reactions and safely storing reagents until they are required. To date, small steps have been taken toward mimicking more complex biosynthetic pathways by using WSCCs in catalytic processes, together with other biological or synthetic catalysts.

In 2013, our group developed a self-organizing chemical assembly line which was capable of directing the multistep transformation of a simple substrate furan into the more structurally complex 5-hydroxy-3-(nitromethyl)dihydrofuran-2(3H)-one **336** (Figure 94).[364] The initial state of the system consisted of all the subcomponents necessary to assemble [Fe$^{II}_4$L$_6$]$^{4-}$ cage **27**, together with furan, nitromethane, L-proline, methylene blue, and dioxygen.

Catalytic action of the sensitizer methylene blue generated singlet oxygen (^{1}O$_2$), which underwent hetero-Diels−Alder cycloaddition with furan (Figure 94, cycle A) to generate high-energy endoperoxide intermediate **337**. Cage **27**, which self-assembles in situ, catalyzes the subsequent transformation of this intermediate to yield fumaraldehydic acid **338** (cycle B), which feeds into cycle C to afford the final product **336** through the L-proline-catalyzed 1,4-addition of nitromethane to **338** followed by cyclization.

Notably, the orthogonal reactivities of the three catalytic cycles avoid interference between the different catalysts and reagents brought together by the system. The important role of **27** was confirmed by control experiments, which showed that nonselective pathways, whereby the high-energy intermediate **337** reacted to give alternative products, dominated in the absence of the cage.

The ability of WSCCs to protect reactive organometallic complexes, and to promote reactions in water that are usually only possible in organic solvents, greatly increases the scope of synthetic reactions that are compatible with enzymic catalysis, enabling new one-pot transformations to be achieved in water. These principles were illustrated by Raymond, Bergman, and Toste through the elegant combination of reactions catalyzed by Au^I or Ru^{II} complexes encapsulated in tetrahedral host **10** and natural enzymes including esterases, lipases, or alcohol dehydrogenases.[274] The same group had previously shown that encapsulation of the Au^I complex [Me$_3$PAu]$^+$ by **10** enhanced its reactivity in the hydroalkoxylation of allenes as well as increasing its lifetime by inhibiting decomposition.[365] A tandem catalytic process was achieved whereby allenic acetate **339** hydrolyzed enzymatically to form alcohol **340**, which was then cyclized by [Me$_3$PAu]$^+$⊂**10** to give substituted tetrahydrofuran **341** (Figure 95a). The tandem reaction was slower when the free Au^I catalyst was used instead of the bound one, leading the authors to propose that encapsulation may prevent undesirable direct interactions between the enzyme and gold catalysts, thus preserving the activity of both.

In a second example, the order of enzyme-mediated and supramolecular catalysis was reversed. An encapsulated Ru^{II}
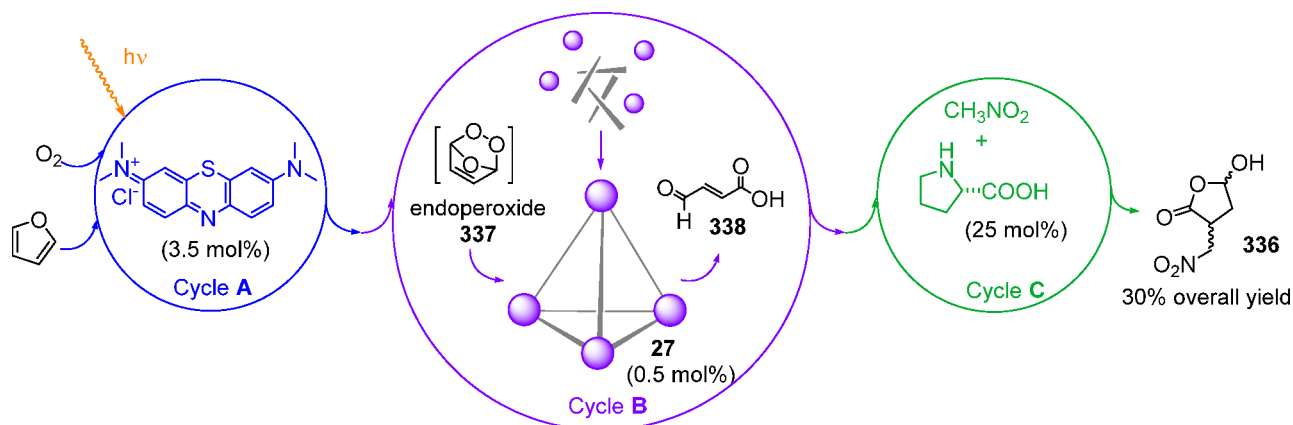
Figure 94. One-pot multicatalytic relay system, in which all steps take place in water at room temperature at pH 4.0.[364]
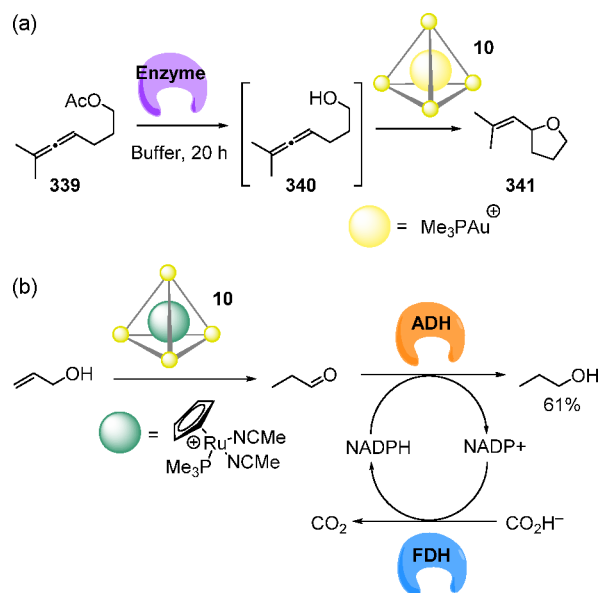
Figure 95. Tandem enzymatic and transition-metal catalysis sequences mediated by **10**. (a) Esterase- or lipase-mediated acetate hydrolysis followed by Me₃PAu⁺⊂**10**-catalyzed hydroalkoxylation.[365] (b) Ru^{II}-mediated olefin isomerization of allyl alcohol to give propanal followed by reduction to propanol via ADH.[274]

complex $[CpRu(PMe_3)(NCMe)_2]^+⊂$**10** catalyzed the isomerization of allyl alcohol to give propanal, which was then reduced by alcohol dehydrogenase (ADH) to give propanol (Figure 95b). The reduction was coupled to the oxidation of sodium formate by formate dehydrogenase (FDH), such that the nicotinamide adenine dinucleotide phosphate (NADPH) cofactor could be regenerated *in situ*, enabling a catalytic amount of it to be used. Neither the enzyme couple nor the encapsulated Ru^{II} catalyst alone could carry out both reactions in the sequence.

6. CONCLUSIONS AND PERSPECTIVES

This review has attempted to span the scope of three-dimensional water-soluble metal−organic cages and summarize the strategies required to render them soluble and stable in aqueous media, where they may find their widest scope of application. Chemists have begun to endow such cages with photoactive and luminescent features, chiral attributes, and the capacity for highly selective recognition. These attributes enable the solubilization of hydrophobic molecules in water, the safeguarding of reactive guests, encapsulation of highly solvated molecules (*e.g.*, hydrophilic cations and anions), the transport of chemicals into cells, and the realization of chemical transformations with improved rates or unexpected product distributions.

The systems discussed herein represent steps toward mimicking the way nature exploits hydrophobic nanospaces for the protection, transport, and transformation of biochemical cargoes to where they are needed under controlled conditions. Living systems also pass information so that the effect of one stimulus can be amplified along signaling cascades to bring about a complex response. A challenge thus exists in creating complex cage consortia that mimic the complexity observed in natural cascade systems, which respond to an initial input by causing an output event that becomes the input for another process within the same system in aqueous

solution. Such investigations may also prompt the use of WSCCs as components in the design of molecular machines, logic gates, and new adaptive materials.

Fruitful future work on WSCCs may also target medical, biological, and environmental applications. Cages better able to selectively recognize biologically relevant molecules at low concentrations in water would find many such uses. Although WSCCs are excellent platforms to recognize biomolecules, the ability to discriminate and distinguish between structurally similar compounds would enable new applications in biosensing, chemical detection, and clinical diagnosis.

Because many biomolecules are hydrophilic and have intricate structures, frequently differing only in subtle regiochemical or stereochemical ways, it is necessary to engineer WSCCs bearing binding sites tailored to recognize specific substrates with the high level of selectivity observed in natural receptors. Although WSCCs show great promise for biomedical applications, their practical use is at an early stage. Before WSCCs may become usable parts of medical treatments, for example, in drug delivery or clinical imaging, it will be necessary to extensively demonstrate their *in vivo* feasibility, establish cage structure−activity correlations, and explore clinical trials.

Supramolecular catalysis within WSCCs also shows great promise. As noted in this review, the hollow interiors of WSCCs can work as enzyme-like catalytic nanoreactors, directing the chemical transformations of guests and enhancing selectivity and rates. Reaching the performance of enzymes, however, requires further progress. For a WSCC to be a competent catalyst, it needs to bind to the transition state of a reaction more strongly than either reactants or products; designing the binding of such an inherently unstable structure remains a major challenge. In practice, many reaction products strongly interact with the cage interior and reside within the host, leading to product inhibition and limiting catalytic turnover. The hydrophobic effect influences both the encapsulation of substrates and the release of products. This effect thus can be a blessing and a curse, enabling the rapid binding of nonpolar substrates but also promoting retention of hydrophobic products.

There is much scope, thus, for improving the catalytic performance of cages, potentially through the use of high-level computational approaches. Such approaches may allow more effort to be focused upon the design of new cages to catalyze reactions of targeted substrates, rather than seeking suitable substrates for existing cages. To date the catalytic applications of WSCCs have been explored with a limited number of highly stable and soluble cages. We anticipate that the strategies discussed for rendering normally organic soluble cages water-soluble will enable a wider exploration of these applications and for new reactivity to be discovered. Beyond the realm of WSCCs, these strategies could also be applied for the development of higher-order materials built from biologically relevant building blocks. For instance, recent examples of coordination cages constructed from protein subunits demonstrated the crucial role of metal ions in determining the geometry of the assembly and its aqueous stability.[366,367]

The field of WSCCs is a flourishing area of research with far-reaching implications, which will continue offering bespoke tools for developing practical applications in the biological, environmental, industrial, and chemical synthesis areas.

AUTHOR INFORMATION

Corresponding Author

Jonathan R. Nitschke − *Department of Chemistry, University of Cambridge, Cambridge CB2 1EW, United Kingdom;* Email: jrn34@cam.ac.uk

Authors

Edmundo G. Percástegui − *Department of Chemistry, University of Cambridge, Cambridge CB2 1EW, United Kingdom; Instituto de Química, Ciudad Universitaria, Universidad Nacional Autónoma de México, Ciudad de México 04510, México; Centro Conjunto de Investigación en Química Sustentable, UAEM-UNAM, Toluca 50200, Estado de México, México*

Tanya K. Ronson − *Department of Chemistry, University of Cambridge, Cambridge CB2 1EW, United Kingdom;* orcid.org/0000-0002-6917-3685

Complete contact information is available at:
https://pubs.acs.org/10.1021/acs.chemrev.0c00672

Notes

The authors declare no competing financial interest.

Biographies

Edmundo G. Percástegui received his Ph.D. degree from Hidalgo State University (Mexico). During his doctoral studies, he spent one year (2011) in the group of Darren W. Johnson at the University of Oregon (USA), investigating self-assembled main-group complexes. He was a DGAPA postdoctoral fellow in Ivan Castillo's group (2013−2015) at the National Autonomous University of Mexico, developing calixarene-based metallomacrocycles and catalysts. He also carried out postdoctoral studies at the University of Cambridge with Jonathan Nitschke (2016−2018), working on the subcomponent self-assembly of molecular cages. In late 2018, he joined the Institute of Chemistry at the National Autonomous University of Mexico as an Assistant Professor. His research interests focus on the self-assembly of functional metal−organic containers and supramolecular compounds.

Tanya K. Ronson received a Bachelor of Science with Honours from the University of Otago, New Zealand. She then went on to complete a Ph.D. in metallo-supramolecular chemistry under the supervision of Michael Ward at the University of Sheffield. Subsequently, she moved on to carry out postdoctoral work on metallo-supramolecular assemblies with stellated polyhedral structures in the group of Michaele Hardie at the University of Leeds before joining the group of Jonathan Nitschke as a postdoctoral research fellow in 2011. Her research interests focus on the self-assembly of complex metal−organic architectures and X-ray crystallography of supramolecular assemblies.

Jonathan R. Nitschke was born in Syracuse, New York, USA. He received his Bachelor of Arts in chemistry from Williams College in 1995, remaining confused to this day as to whether chemistry is an art, and his doctorate from the University of California, Berkeley, in 2001, under the supervision of T. Don Tilley. He then undertook postdoctoral studies with Jean-Marie Lehn in Strasbourg, and in 2003 he started his independent research career as a *Maître-assistant* (fixed-term PI) in the Organic Chemistry Department of the University of Geneva. In 2007, he was appointed University Lecturer at Cambridge, where he has been a full professor since 2014. His research program investigates the self-assembly of complex, functional structures from simple molecular precursors and metal ions.

ABBREVIATIONS

Φ_F = fluorescence quantum yield
acac = acetylacetonate
ADA = adamantane ammonium
ADP = adenosine diphosphate
ADH = alcohol dehydrogenase
AIBN = 2,2′-azobisisobutironitrile
AIE = aggregation induced emission
AMBN = 2,2′-azobis(2-methylbutyronitrile)
AMMVN = 2,2′-azobis(4-methoxy-2,4-dimethylvaleronitrile)
AMP = adenosine monophosphate
ATP = adenosine triphosphate
$BArF^-$ = tetrakis[3,5-bis(trifluoromethyl)phenyl]borate
BINOL = 1,1′-bi-2-naphthol
BODIPY = 4,4-difluoro-4-bora-3a,4a-diaza-*s*-indacene
CB[n] = cucurbit[n]uril
CD_3OD = deuterated methanol-d_4
CD_3CN = methyl-d_3 cyanide/deuterated acetonitrile
COD = 1,5-cyclooctadiene
cp = cyclopentadienyl
cp* = pentamethylcyclopentadiene
D_2O = deuterium oxide
DASA = donor−acceptor Stenhouse adducts
DMF = *N,N*-dimethylformamide
DMPA = 2,2-dimethoxy-2-phenylacetophenone
DMSO = dimethyl sulfoxide
DOX = doxorubicin
ee = enantiomeric excess
en = ethylenediamine
equiv = molar equivalent
ESD = β-estradiol
ESI-MS = electrospray ionization mass spectrometry
Et = ethyl
FDA = U.S. Food and Drug Administration
FDH = formate dehydrogenase
GMP = guanosine monophosphate
HAD = hexanediammonium
HCPK = 1-hydroxy-cyclohexyl phenyl ketone
HMPP = 2-hydroxy-2-methylpropiophenone
IC_{50} = drug concentration necessary for 50% inhibition of cell viability
IR = ionic radii
ITC = isothermal titration calorimetry
LD_{50} = light dose necessary for 50% inhibition of cell viability
MeCN = acetonitrile
MEM = maximum entropy method
MMA = methyl methacrylate
MOF = metal−organic framework
MOP = metal−organic polyhedra
MS = mass spectrometry
MTT = 3-(4,5-dimethylthiazol-2-yl)-2,5-diphenyltetrazolium bromide
NADPH = nicotinamide adenine dinucleotide phosphate
NMR = nuclear magnetic resonance

NTf$_2^-$ = bis(trifluoromethane)sulfonamide/triflimide
OTf$^-$ = trifluoromethanesulfonate/triflate
PAM = postassembly modification
PAH = polycyclic aromatic hydrocarbons
PEG = polyethylene glycol
PET = photoinduced electron transfer
PMMA = poly(methyl methacrylate)
PRG = progesterone
RCY = radiochemical yield
rt = room temperature
SPECT = single-photon emission computed tomography
$t_{1/2}$ = half-life
TATA$^+$ = triazatriangulenium
TEM = transmission electron microscopy
TES = testosterone
THF = tetrahydrofuran
tmeda = N,N,N',N'-tetramethylethylenediamine
TOF-MS = time-of-flight mass spectrometry
TREN = tris(2-aminoethyl)amine
TRPN = tris(3-aminopropyl)amine
UMP = uridine monophosphate
UV = ultraviolet
WSCC = water-soluble coordination cage

REFERENCES

(1) Szostak, J. D.; Bartel, D. P.; Luisi, P. L. Synthesizing Life. *Nature* **2001**, *409*, 387−390.

(2) Radzicka, A.; Wolfenden, R. A Proficient Enzyme. *Science* **1995**, *267*, 90−93.

(3) Appleby, T. C.; Kinsland, C.; Begley, T. P.; Ealick, S. E. The Crystal Structure and Mechanism of Orotidine 5′-Monophosphate Decarboxylase. *Proc. Natl. Acad. Sci. U. S. A.* **2000**, *97*, 2005−2010.

(4) Rosenbaum, D. M.; Rasmussen, S. G. F.; Kobilka, B. K. The Structure and Function of G-Protein-Coupled Receptors. *Nature* **2009**, *459*, 356−363.

(5) Stank, A.; Kokh, D. B.; Fuller, J. C.; Wade, R. C. Protein Binding Pocket Dynamics. *Acc. Chem. Res.* **2016**, *49*, 809−815.

(6) Dorsam, R. T.; Gutkind, J. S. G-Protein-Coupled Receptors and Cancer. *Nat. Rev. Cancer* **2007**, *7*, 79−94.

(7) Elani, Y.; Law, R. V.; Ces, O. Vesicle-Based Artificial Cells as Chemical Microreactors with Spatially Segregated Reaction Pathways. *Nat. Commun.* **2014**, *5*, 5305.

(8) Buddingh', B. C.; van Hest, J. C. M. Artificial Cells: Synthetic Compartments with Life-like Functionality and Adaptivity. *Acc. Chem. Res.* **2017**, *50*, 769−777.

(9) Barton, G. M.; Kagan, J. C. A Cell Biological View of Toll-like Receptor Function: Regulation through Compartmentalization. *Nat. Rev. Immunol.* **2009**, *9*, 535−542.

(10) Ikonen, E. Cellular Cholesterol Trafficking and Compartmentalization. *Nat. Rev. Mol. Cell Biol.* **2008**, *9*, 125−138.

(11) Agapakis, C. M.; Boyle, P. M.; Silver, P. A. Natural Strategies for the Spatial Optimization of Metabolism in Synthetic Biology. *Nat. Chem. Biol.* **2012**, *8*, 527−535.

(12) Francastel, C.; Schübeler, D.; Martin, D. I. K.; Groudine, M. Nuclear Compartmentalization and Gene Activity. *Nat. Rev. Mol. Cell Biol.* **2000**, *1*, 137−143.

(13) Singh, S. K.; Yamashita, A.; Gouaux, E. Antidepressant Binding Site in A Bacterial Homologue of Neurotransmitter Transporters. *Nature* **2007**, *448*, 952−956.

(14) Oshovsky, G. V.; Reinhoudt, D. N.; Verboom, W. Supramolecular Chemistry in Water. *Angew. Chem., Int. Ed.* **2007**, *46*, 2366−2393.

(15) Taylor, L. L. K.; Riddell, I. A.; Smulders, M. M. J. Self-Assembly of Functional Discrete Three-Dimensional Architectures in Water. *Angew. Chem., Int. Ed.* **2019**, *58*, 1280−1307.

(16) Laughrey, Z.; Gibb, B. C. Water-Soluble, Self-Assembling Container Molecules: An Update. *Chem. Soc. Rev.* **2011**, *40*, 363−386.

(17) Yoshizawa, M.; Klosterman, J. K.; Fujita, M. Functional Molecular Flasks: New Properties and Reactions within Discrete, Self-Assembled Hosts. *Angew. Chem., Int. Ed.* **2009**, *48*, 3418−3438.

(18) Brown, C. J.; Toste, F. D.; Bergman, R. G.; Raymond, K. N. Supramolecular Catalysis in Metal-Ligand Cluster Hosts. *Chem. Rev.* **2015**, *115*, 3012−3035.

(19) Zhao, L.; Jing, X.; Li, X.; Guo, X.; Zeng, L.; He, C.; Duan, C. Catalytic Properties of Chemical Transformation within the Confined Pockets of Werner-Type Capsules. *Coord. Chem. Rev.* **2019**, *378*, 151−187.

(20) Ernst, N. E.; Gibb, B. C. In *Supramolecular Chemistry in Water*; Wiley-VCH: Weinheim, Germany, 2019; Chapter 1.

(21) Cremer, P. S.; Flood, A. H.; Gibb, B. C.; Mobley, D. L. Collaborative Routes to Clarifying the Murky Waters of Aqueous Supramolecular Chemistry. *Nat. Chem.* **2018**, *10*, 8−16.

(22) Chandler, D. Hydrophobicity: Two Faces of Water. *Nature* **2002**, *417*, 491.

(23) Chandler, D. Interfaces and the Driving Force of Hydrophobic Assembly. *Nature* **2005**, *437*, 640−647.

(24) Granick, S.; Bae, C. S. A Curious Antipathy for Water. *Science* **2008**, *322*, 1477−1478.

(25) Pratt, L. R.; Pohorille, A. Hydrophobic Effects and Modeling of Biophysical Aqueous Solution Interfaces. *Chem. Rev.* **2002**, *102*, 2671−2692.

(26) Percástegui, E. G.; Jancik, V. Coordination-Driven Assemblies Based on *Meso*-Substituted Porphyrins: Metal-Organic Cages and a new Type of Meso-Metallaporphyrin Macrocycles. *Coord. Chem. Rev.* **2020**, *407*, 213165.

(27) Debata, N. B.; Tripathy, D.; Sahoo, H. S. Development of Coordination Driven Self-Assembled Discrete Spherical Ensembles. *Coord. Chem. Rev.* **2019**, *387*, 273−298.

(28) Saha, S.; Regeni, I.; Clever, G. H. Structure Relationships between Bis-Monodentate Ligands and Coordination Driven Self-Assemblies. *Coord. Chem. Rev.* **2018**, *374*, 1−14.

(29) Biros, S. M.; Rebek, J., Jr. Structure and Binding Properties of Water-Soluble Cavitands and Capsules. *Chem. Soc. Rev.* **2007**, *36*, 93−104.

(30) Murray, J.; Kim, K.; Ogoshi, T.; Yao, W.; Gibb, B. C. The Aqueous Supramolecular Chemistry of Cucurbit[n]urils, Pillar[n]-arenes and Deep-Cavity Cavitands. *Chem. Soc. Rev.* **2017**, *46*, 2479−2496.

(31) Liu, Z.; Nalluri, S. K. M.; Stoddart, J. F. Surveying Macrocyclic Chemistry: From Flexible Crown Ethers to Rigid Cyclophanes. *Chem. Soc. Rev.* **2017**, *46*, 2459−2478.

(32) Liu, W.; Bobbala, S.; Stern, C. L.; Hornick, J. E.; Liu, Y.; Enciso, A. E.; Scott, E. A.; Stoddart, J. F. XCage: A Tricyclic Octacationic Receptor for Perylene Diimide with Picomolar Affinity in Water. *J. Am. Chem. Soc.* **2020**, *142*, 3165−3173.

(33) Liu, W.; Lin, C.; Weber, J. A.; Stern, C. L.; Young, R. M.; Wasielewski, M. R.; Stoddart, J. F. Cyclophane-Sustained Ultrastable Porphyrins. *J. Am. Chem. Soc.* **2020**, *142*, 8938−8945.

(34) Cook, T. R.; Stang, P. J. Recent Developments in the Preparation and Chemistry of Metallacycles and Metallacages via Coordination. *Chem. Rev.* **2015**, *115*, 7001−7045.

(35) Amouri, H.; Desmarets, C.; Moussa, J. Confined Nanospaces in Metallocages: Guest Molecules, Weakly Encapsulated Anions, and Catalyst Sequestration. *Chem. Rev.* **2012**, *112*, 2015−2041.

(36) Twarock, R.; Luque, A. Structural Puzzles in Virology Solved with An Overarching Icosahedral Design Principle. *Nat. Commun.* **2019**, *10*, 4414.

(37) Chakrabarty, R.; Mukherjee, P. S.; Stang, P. J. Supramolecular Coordination: Self-Assembly of Finite Two- and Three-Dimensional Ensembles. *Chem. Rev.* **2011**, *111*, 6810−6918.

(38) Cook, T. R.; Zheng, Y. R.; Stang, P. J. Metal-Organic Frameworks and Self-Assembled Supramolecular Coordination Complexes: Comparing and Contrasting the Design, Synthesis, and

Functionality of Metal-Organic Materials. *Chem. Rev.* **2013**, *113*, 734−777.

(39) Stang, P. J. Abiological Self-Assembly via Coordination: Formation of 2D Metallacycles and 3D Metallacages with Well-Defined Shapes and Sizes and Their Chemistry. *J. Am. Chem. Soc.* **2012**, *134*, 11829−11830.

(40) Baxter, P.; Lehn, J.-M.; DeCian, A.; Fischer, J. Multicomponent Self-Assembly: Spontaneous Formation of a Cylindrical Complex from Five Ligands and Six Metal Ions. *Angew. Chem., Int. Ed. Engl.* **1993**, *32*, 69−72.

(41) Ruben, M.; Rojo, J.; Romero-Salguero, F. J.; Uppadine, L. H.; Lehn, J.-M. Grid Type Metal Ion Architecture: Functional Supramolecular Arrays. *Angew. Chem., Int. Ed.* **2004**, *43*, 3644−3662.

(42) Stang, P. J.; Cao, D. H. Transition Metal Based Cationic Molecular Boxes. Self-Assembly of Macrocyclic Platinum(II) and Palladium(II) Tetranuclear Complexes. *J. Am. Chem. Soc.* **1994**, *116*, 4981−4982.

(43) Olenyuk, B.; Whiteford, J. A.; Fechtenkötter, A.; Stang, P. J. Self-assembly of Nanoscale Cuboctahedra by Coordination Chemistry. *Nature* **1999**, *398*, 796−799.

(44) Fujita, M.; Yazaki, J.; Ogura, K. Preparation of a Macrocyclic Polynuclear Complex, $[(en)Pd(4,4,-bpy)]_4(NO_3)_8$, Which Recognizes an Organic Molecule in Aqueous Media. *J. Am. Chem. Soc.* **1990**, *112*, 5645−5647.

(45) Caulder, D. L.; Powers, R. E.; Parac, T. N.; Raymond, K. N. The Self-Assembly of a Predesigned Tetrahedral M_4L_6 Supramolecular Cluster. *Angew. Chem., Int. Ed.* **1998**, *37*, 1840−1843.

(46) Ahmad, N.; Chughtai, A. H.; Younus, H. A.; Verpoort, F. Discrete Metal-Carboxylate Self-Assembled Cages: Design, Synthesis and Applications. *Coord. Chem. Rev.* **2014**, *280*, 1−27.

(47) Hosono, N.; Kitagawa, S. Modular Design of Porous Soft Materials via Self-Organization of Metal-Organic Cages. *Acc. Chem. Res.* **2018**, *51*, 2437−2446.

(48) Jin, P.; Dalgarno, S. J.; Atwood, J. L. Mixed Metal-Organic Nanocapsules. *Coord. Chem. Rev.* **2010**, *254*, 1760−1768.

(49) Xu, L.; Wang, Y.-X.; Yang, H.-B. Recent Advances in The Construction of Fluorescent Metallocycles and Metallocages via Coordination-Driven Self-Assembly. *Dalton Trans.* **2015**, *44*, 867−890.

(50) Rota Martir, D.; Zysman-Colman, E. Photoactive Supramolecular Cages Incorporating Ru(II) and Ir(III) Metal Complexes. *Chem. Commun.* **2019**, *55*, 139−158.

(51) Croué, V.; Goeb, S.; Sallé, M. Metal-Driven Self-Assembly: The Case of Redox-Active Discrete Architectures. *Chem. Commun.* **2015**, *51*, 7275−7289.

(52) Xu, L.; Wang, Y.-X.; Chen, L.-J.; Yang, H.-B. Construction of Multiferrocenyl Metallacycles and Metallacages via Coordination-Driven Self-Assembly: From Structure to Functions. *Chem. Soc. Rev.* **2015**, *44*, 2148−2167.

(53) Clever, G. H.; Punt, P. Cation-Anion Arrangement Patterns in Self-Assembled Pd_2L_4 and Pd_4L_8 Coordination Cages. *Acc. Chem. Res.* **2017**, *50*, 2233−2243.

(54) Chen, L.-J.; Yang, H.-B.; Shionoya, M. Chiral Metallosupramolecular Architectures. *Chem. Soc. Rev.* **2017**, *46*, 2555−2576.

(55) Bistri, O.; Reinaud, O. Supramolecular Control of Transition Metal Complexes in Water by a Hydrophobic Cavity: A Bio-Inspired Strategy. *Org. Biomol. Chem.* **2015**, *13*, 2849−2865.

(56) Saalfrank, R. W.; Stark, A.; Peters, K.; von Schnering, H. G. The First "Adamantoid" Alkaline Earth Metal Chelate Complex: Synthesis, Structure, and Reactivity. *Angew. Chem., Int. Ed. Engl.* **1988**, *27*, 851−853.

(57) Fujita, M.; Oguro, D.; Miyazawa, M.; Oka, H.; Yamaguchi, K.; Ogura, K. Self-Assembly of Ten Molecules into Nanometer-Sized Host Frameworks. *Nature* **1995**, *378*, 469−471.

(58) Nishioka, Y.; Yamaguchi, T.; Kawano, M.; Fujita, M. Asymmetric [2 + 2] Olefin Cross Photoaddition in a Self-Assembled Host with Remote Chiral Auxiliaries. *J. Am. Chem. Soc.* **2008**, *130*, 8160−8161.

(59) Kusukawa, T.; Fujita, M. Self-Assembled M_6L_4-Type Coordination Nanocage with 2,2-Bipyridine Ancillary Ligands. Facile Crystallization and X-ray Analysis of Shape-Selective Enclathration of Neutral Guests in the Cage. *J. Am. Chem. Soc.* **2002**, *124*, 13576−13582.

(60) Caulder, D. L.; Raymond, K. N. Supramolecular Self-Recognition and Self-Assembly in Gallium(III) Catecholamide Triple Helices. *Angew. Chem., Int. Ed. Engl.* **1997**, *36*, 1440−1442.

(61) Kersting, B.; Meyer, M.; Powers, R. E.; Raymond, K. N. Dinuclear Catecholate Helicates: Their Inversion Mechanism. *J. Am. Chem. Soc.* **1996**, *118*, 7221−7222.

(62) Fox, O. D.; Dalley, N. K.; Harrison, R. G. A Metal-Assembled, pH-Dependent, Resorcinarene-Based Cage Molecule. *J. Am. Chem. Soc.* **1998**, *120*, 7111−7112.

(63) Cram, D. J. Molecular Container Compounds. *Nature* **1992**, *356*, 29−36.

(64) Fujita, M.; Tominaga, M.; Hori, A.; Therrien, B. Coordination Assemblies from a Pd(II)-Cornered Square Complex. *Acc. Chem. Res.* **2005**, *38*, 369−378.

(65) Hayes, R.; Bernard, S. A.; Imberti, S.; Warr, G. G.; Atkin, R. Solvation of Inorganic Nitrate Salts in Protic Ionic Liquids. *J. Phys. Chem. C* **2014**, *118*, 21215−21225.

(66) Thøgersen, J.; Réhault, J.; Odelius, M.; Ogden, T.; Jena, N. K.; Jensen, S. J. K.; Keiding, S. R.; Helbing, J. Hydration Dynamics of Aqueous Nitrate. *J. Phys. Chem. B* **2013**, *117*, 3376−3388.

(67) Drew, H. D. K.; Pinkard, F. W.; Preston, G. H.; Wardlaw, W. Supposed Isomerism among the Pallado-Diammines. *J. Chem. Soc.* **1932**, 1895−1909.

(68) Kumar, A.; Mukherjee, P. S. Multicomponent Self-Assembly of Pd^{II}/Pt^{II} Interlocked Molecular Cages: Cage-to-Cage Conversion and Self-Sorting in Aqueous Medium. *Chem. - Eur. J.* **2020**, *26*, 4842−4849.

(69) Hanopolskyi, A. I.; De, S.; Białek, M. J.; Diskin-Posner, Y.; Avram, L.; Feller, M.; Klajn, R. Reversible Switching of Arylazopyrazole within a Metal-Organic Cage. *Beilstein J. Org. Chem.* **2019**, *15*, 2398−2407.

(70) Mal, P.; Schultz, D.; Beyeh, K.; Rissanen, K.; Nitschke, J. R. An Unlockable-Relockable Iron Cage by Subcomponent Self-Assembly. *Angew. Chem., Int. Ed.* **2008**, *47*, 8297−8301.

(71) Zhang, D.; Ronson, T. K.; Nitschke, J. R. Functional Capsules via Subcomponent Self-Assembly. *Acc. Chem. Res.* **2018**, *51*, 2423−2436.

(72) Bolliger, J. L.; Belenguer, A. M.; Nitschke, J. R. Enantiopure Water-Soluble $[Fe_4L_6]$ Cages: Host-Guest Chemistry and Catalytic Activity. *Angew. Chem., Int. Ed.* **2013**, *52*, 7958−7962.

(73) Meng, W.; Clegg, J. K.; Thoburn, J. D.; Nitschke, J. R. Controlling the Transmission of Stereochemical Information through Space in Terphenyl-Edged Fe$_4$L$_6$ Cages. *J. Am. Chem. Soc.* **2011**, *133*, 13652−13660.

(74) Tidmarsh, I. S.; Faust, T. B.; Adams, H.; Harding, L. P.; Russo, L.; Clegg, W.; Ward, M. D. Octanuclear Cubic Coordination Cages. *J. Am. Chem. Soc.* **2008**, *130*, 15167−15175.

(75) Whitehead, M.; Turega, S.; Stephenson, A.; Hunter, C. A.; Ward, M. D. Quantification of Solvent Effects on Molecular Recognition in Polyhedral Coordination Cage Hosts. *Chem. Sci.* **2013**, *4*, 2744−2751.

(76) Kishi, N.; Li, Z.; Yoza, K.; Akita, M.; Yoshizawa, M. An M_2L_4 Molecular Capsule with an Anthracene Shell: Encapsulation of Large Guests up to 1 nm. *J. Am. Chem. Soc.* **2011**, *133*, 11438−11441.

(77) Yamashina, M.; Sei, Y.; Akita, M.; Yoshizawa, M. Safe Storage of Radical Initiators within a Polyaromatic Nanocapsule. *Nat. Commun.* **2014**, *5*, 4662.

(78) Yazaki, K.; Akita, M.; Prusty, S.; Chand, D. K.; Kikuchi, T.; Sato, H.; Yoshizawa, M. Polyaromatic Molecular Peanuts. *Nat. Commun.* **2017**, *8*, 15914.

(79) Lewis, J. E. M.; Crowley, J. D. *Exo*-and *Endo*-hedral Interactions of Counteranions with Tetracationic Pd_2L_4 Metallosupramolecular Architectures. *Supramol. Chem.* **2014**, *26*, 173−181.

(80) Preston, D.; McNeill, S. M.; Lewis, J. E. M.; Giles, G. I.; Crowley, J. D. Enhanced Kinetic Stability of [Pd$_2$L$_4$]$^{4+}$ Cages through Ligand Substitution. *Dalton Trans.* **2016**, *45*, 8050−8060.

(81) Lewis, J. E. M.; Elliott, A. B. S.; McAdam, C. J.; Gordon, K. C.; Crowley, J. D. "Click" to Functionalise: Synthesis, Characterisation and Enhancement of the Physical Properties of a Series of *Exo*- and *Endo*-Functionalised Pd$_2$L$_4$ Nanocages. *Chem. Sci.* **2014**, *5*, 1833−1843.

(82) Yazaki, K.; Sei, Y.; Akita, M.; Yoshizawa, M. Polycationic-Shelled Capsular and Tubular Nanostructures and Their Anionic-Guest Binding Properties. *Chem. - Eur. J.* **2016**, *22*, 17557−17561.

(83) Domarco, O.; Kieler, C.; Pirker, C.; Dinhof, C.; Englinger, B.; Reisecker, J. M.; Timelthaler, G.; García, M. D.; Peinador, C.; Keppler, B. K.; Berger, W.; Terenzi, A. Subcellular Duplex DNA and G-Quadruplex Interaction Profiling of a Hexagonal Pt^{II} Metallacycle. *Angew. Chem., Int. Ed.* **2019**, *58*, 8007−8012.

(84) Rama, T.; Blanco-Gómez, A.; Neira, I.; Domarco, O.; García, M. D.; Quintela, J. M.; Peinador, C. Integrative Self-Sorting of Bipyridinium/Diazapyrenium-Based Ligands into Pseudo[1]-Rotaxanes. *Chem. - Eur. J.* **2017**, *23*, 16743−16747.

(85) Neira, I.; Alvariño, C.; Domarco, O.; Blanco, V.; Peinador, C.; García, M.; Quintela, J. Tuning of the Self-Threading of Ring-in-Ring Structures in Aqueous Media. *Chem. - Eur. J.* **2019**, *25*, 14834−14842.

(86) Roy, B.; Zangrando, E.; Mukherjee, P. S. Self-Assembly of a Redox Active Water Soluble Pd$_6$L$_8$ 'Molecular Dice'. *Chem. Commun.* **2016**, *52*, 4489−4492.

(87) Cai, L.-X.; Li, S.-C.; Yan, D.-N.; Zhou, L.-P.; Guo, F.; Sun, Q.-F. Water-Soluble Redox-Active Cage Hosting Polyoxometalates for Selective Desulfurization Catalysis. *J. Am. Chem. Soc.* **2018**, *140*, 4869−4876.

(88) Percástegui, E. G.; Mosquera, J.; Nitschke, J. R. Anion Exchange Renders Hydrophobic Capsules and Cargoes Water-Soluble. *Angew. Chem., Int. Ed.* **2017**, *56*, 9136−9140.

(89) Percástegui, E. G.; Mosquera, J.; Ronson, T. K.; Plajer, A. J.; Kieffer, M.; Nitschke, J. R. Waterproof Architectures through Subcomponent Self-Assembly. *Chem. Sci.* **2019**, *10*, 2006−2018.

(90) Grommet, A. B.; Hoffman, J. B.; Percástegui, E. G.; Mosquera, J.; Howe, D. J.; Bolliger, J. L.; Nitschke, J. R. Anion Exchange Drives Reversible Phase Transfer of Coordination Cages and Their Cargoes. *J. Am. Chem. Soc.* **2018**, *140*, 14770−14776.

(91) Zhang, D.; Ronson, T. K.; Lavendomme, R.; Nitschke, J. R. Selective Separation of Polyaromatic Hydrocarbons by Phase Transfer of Coordination Cages. *J. Am. Chem. Soc.* **2019**, *141*, 18949−18953.

(92) Thomas, J. A. Locking Self-Assembly: Strategies and Outcomes. *Chem. Soc. Rev.* **2007**, *36*, 856−868.

(93) Lincoln, S. A.; Merbach, A. E. Substitution Reactions of Solvated Metal Ions. *Adv. Inorg. Chem.* **1995**, *42*, 1−88.

(94) Richens, D. T. Ligand Substitution Reactions at Inorganic Centers. *Chem. Rev.* **2005**, *105*, 1961−2002.

(95) Davis, A. V.; Raymond, K. N. The Big Squeeze: Guest Exchange in an M$_4$L$_6$ Supramolecular Host. *J. Am. Chem. Soc.* **2005**, *127*, 7912−7919.

(96) Hong, C. M.; Morimoto, M.; Kapustin, E. A.; Alzakhem, N.; Bergman, R. G.; Raymond, K. N.; Toste, F. D. Deconvoluting the Role of Charge in a Supramolecular Catalyst. *J. Am. Chem. Soc.* **2018**, *140*, 6591−6595.

(97) He, Y. P.; Yuan, L. B.; Chen, G. H.; Lin, Q. P.; Wang, F.; Zhang, L.; Zhang, J. Water-Soluble and Ultrastable Ti$_4$L$_6$ Tetrahedron with Coordination Assembly Function. *J. Am. Chem. Soc.* **2017**, *139*, 16845−16851.

(98) Kang, Y.-H.; Liu, X.-D.; Yan, N.; Jiang, Y.; Liu, X.-Q.; Sun, L.-B.; Li, J.-R. Fabrication of Isolated Metal-Organic Polyhedra in Confined Cavities: Adsorbents/Catalysts with Unusual Dispersity and Activity. *J. Am. Chem. Soc.* **2016**, *138*, 6099−6102.

(99) Byrne, K.; Zubair, M.; Zhu, N.; Zhou, X.-P.; Fox, D. S.; Zhang, H.; Twamley, B.; Lennox, M. J.; Düren, T.; Schmitt, W. Ultra-Large Supramolecular Coordination Cages Composed of Endohedral Archimedean and Platonic Bodies. *Nat. Commun.* **2017**, *8*, 15268.

(100) Tonigold, M.; Volkmer, D. Comparative Solvolytic Stabilities of Copper(II) Nanoballs and Dinuclear Cu(II) Paddle Wheel Units. *Inorg. Chim. Acta* **2010**, *363*, 4220−4229.

(101) Liu, G.; Di Yuan, Y.; Wang, J.; Cheng, Y.; Peh, S. B.; Wang, Y.; Qian, Y.; Dong, J.; Yuan, D.; Zhao, D. Process-Tracing Study on the Postassembly Modification of Highly Stable Zirconium Metal-Organic Cages. *J. Am. Chem. Soc.* **2018**, *140*, 6231−6234.

(102) Roberts, D. A.; Pilgrim, B. S.; Nitschke, J. R. Covalent Post-Assembly Modification in Metallosupramolecular Chemistry. *Chem. Soc. Rev.* **2018**, *47*, 626−644.

(103) Zeng, H.; Stewart-Yates, L.; Casey, L. M.; Bampos, N.; Roberts, D. A. Covalent Post-Assembly Modification: A Synthetic Multipurpose Tool in Supramolecular Chemistry. *ChemPlusChem* **2020**, *85*, 1249−1269.

(104) Nam, D.; Huh, J.; Lee, J.; Kwak, J. H.; Jeong, H. Y.; Choi, K.; Choe, W. Cross-Linking Zr-Based Metal-Organic Polyhedra via Postsynthetic Polymerization. *Chem. Sci.* **2017**, *8*, 7765−7771.

(105) Parthiban, S.; Kwon, J.-Y. Amorphous Boron-Indium-Zinc-Oxide Active Channel Layers for Thin-Film Transistor Fabrication. *J. Mater. Chem. C* **2015**, *3*, 1661−1665.

(106) Liu, H. K.; Sun, W. Y.; Ma, D. J.; Yu, K. B.; Tang, W. X. The First X-Ray Structurally Characterized M$_3$L$_2$ cage-like Complex with Tetrahedral Metal Centres and Its Encapsulation of a Neutral Guest Molecule. *Chem. Commun.* **2000**, *3*, 591−592.

(107) Taylor, C. G. P.; Piper, J. R.; Ward, M. D. Binding of Chemical Warfare Agent Simulants as Guests in a Coordination Cage: Contributions to Binding and a Fluorescence-Based Response. *Chem. Commun.* **2016**, *52*, 6225−6228.

(108) Aoki, S.; Suzuki, S.; Kitamura, M.; Haino, T.; Shiro, M.; Zulkefeli, M.; Kimura, E. Molecular Recognition of Hydrocarbon Guests by a Supramolecular Capsule Formed by the 4:4 Self-Assembly of Tris(Zn^{2+}-Cyclen) and Trithiocyanurate in Aqueous Solution. *Chem. - Asian J.* **2012**, *7*, 944−956.

(109) Irving, H.; Mellor, D. H. The Stability of Metal Complexes of 1,10-Phenanthroline and Its Analogues. Part I. 1,10-Phenanthroline and 2,2′-Bipyridyl. *J. Chem. Soc.* **1962**, 5222−5237.

(110) Irving, H.; Williams, R. J. P. The Stability of Transition-Metal Complexes. *J. Chem. Soc.* **1953**, 3192−3210.

(111) Shannon, R. D. Revised Effective Ionic Radii and Systematic Studies of Interatomic Distances in Halides and Chalcogenides. *Acta Crystallogr., Sect. A: Cryst. Phys., Diffr., Theor. Gen. Crystallogr.* **1976**, *32*, 751−767.

(112) Eigen, M. Fast Elementary Steps in Chemical Reaction Mechanisms. *Pure Appl. Chem.* **1963**, *6*, 97−116.

(113) Hunter, C. A.; Anderson, H. L. What is Cooperativity? *Angew. Chem., Int. Ed.* **2009**, *48*, 7488−7499.

(114) von Krbek, L. K. S.; Schalley, C. S.; Thordarson, P. Assessing Cooperativity in Supramolecular Systems. *Chem. Soc. Rev.* **2017**, *46*, 2622−2637.

(115) Ibukuro, F.; Kusukawa, T.; Fujita, M. A Thermally Switchable Molecular Lock. Guest-Templated Synthesis of a Kinetically Stable Nanosized Cage. *J. Am. Chem. Soc.* **1998**, *120*, 8561−8562.

(116) Charbonniere, L. J.; Bernardinelli, G.; Piguet, C.; Sargeson, A. M.; Williams, A. F. Synthesis, Structure and Resolution of a Dinuclear Co^{III} Triple Helix. *J. Chem. Soc., Chem. Commun.* **1994**, 1419−1420.

(117) Burke, M. J.; Nichol, G. S.; Lusby, P. J. Orthogonal Selection and Fixing of Coordination Self-Assembly Pathways for Robust Metallo-organic Ensemble Construction. *J. Am. Chem. Soc.* **2016**, *138*, 9308−9315.

(118) Leigh, D. A.; Lusby, P. J.; McBurney, R. T.; Morelli, A.; Slawin, A. M. Z.; Thomson, A. R.; Walker, D. B. Getting Harder: Cobalt(III)-Template Synthesis of Catenanes and Rotaxanes. *J. Am. Chem. Soc.* **2009**, *131*, 3762−3771.

(119) Symmers, P. R.; Burke, M. J.; August, D. P.; Thomson, P. I. T.; Nichol, G. S.; Warren, M. R.; Campbell, C. J.; Lusby, P. J. Non-Equilibrium Cobalt(III) "Click" Capsules. *Chem. Sci.* **2015**, *6*, 756−760.

(120) Zarra, S.; Clegg, J. K.; Nitschke, J. R. Selective Assembly and Disassembly of a Water-Soluble Fe$_{10}$L$_{15}$ Prism. *Angew. Chem., Int. Ed.* **2013**, *52*, 4837−4840.

(121) Umemoto, K.; Yamaguchi, K.; Fujita, M. Molecular Paneling via Coordination: Guest-Controlled Assembly of Open Cone and Tetrahedron Structures from Eight Metals and Four Ligands. *J. Am. Chem. Soc.* **2000**, *122*, 7150−7151.

(122) Tashiro, S.; Tominaga, M.; Kusukawa, T.; Kawano, M.; Sakamoto, S.; Yamaguchi, K.; Fujita, M. Pd^{II}-Directed Dynamic Assembly of a Dodecapyridine Ligand into End-Capped and Open Tubes: The Importance of Kinetic Control in Self-Assembly. *Angew. Chem., Int. Ed.* **2003**, *42*, 3267−3270.

(123) Dyson, H. J.; Wright, P. E.; Scheraga, H. A. The Role of Hydrophobic Interactions in Initiation and Propagation of Protein Folding. *Proc. Natl. Acad. Sci. U. S. A.* **2006**, *103*, 13057−13061.

(124) Baldwin, R. L.; Rose, G. D. How the Hydrophobic Factor Drives Protein Folding. *Proc. Natl. Acad. Sci. U. S. A.* **2016**, *113*, 12462−12466.

(125) Aliprandi, A.; Mauro, M.; De Cola, L. Controlling and Imaging Biomimetic Self-Assembly. *Nat. Chem.* **2016**, *8*, 10−15.

(126) Krieg, E.; Bastings, M. M. C.; Besenius, P.; Rybtchinski, B. Supramolecular Polymers in Aqueous Media. *Chem. Rev.* **2016**, *116*, 2414−2477.

(127) Jordan, J. H.; Gibb, B. C. Molecular Containers Assembled through The Hydrophobic Effect. *Chem. Soc. Rev.* **2015**, *44*, 547−585.

(128) Jiao, T.; Wu, G.; Zhang, Y.; Shen, L.; Lei, Y.; Wang, C.-Y.; Fahrenbach, A. C.; Li, H. Self-Assembly in Water with N-Substituted Imines. *Angew. Chem., Int. Ed.* **2020**, *59*, 18350−18367.

(129) Zhang, K.-D.; Ajami, D.; Rebek, J. Hydrogen-Bonded Capsules in Water. *J. Am. Chem. Soc.* **2013**, *135*, 18064−18066.

(130) Da Silva, J. P.; Kulasekharan, R.; Cordeiro, C.; Jockusch, S.; Turro, N. J.; Ramamurthy, V. Capsular Complexes of Nonpolar Guests with Octa Amine Host Detected in the Gas Phase. *Org. Lett.* **2012**, *14*, 560−563.

(131) Kulasekharan, R.; Ramamurthy, V. New Water-Soluble Organic Capsules Are Effective in Controlling Excited-State Processes of Guest Molecules. *Org. Lett.* **2011**, *13*, 5092−5095.

(132) Gibb, C. L. D.; Gibb, B. C. Well-Defined, Organic Nanoenvironments in Water: The Hydrophobic Effect Drives a Capsular Assembly. *J. Am. Chem. Soc.* **2004**, *126*, 11408−11409.

(133) Giles, M. D.; Liu, S.; Emanuel, R. L.; Gibb, B. C.; Grayson, S. M. Dendronized Supramolecular Nanocapsules: pH Independent, Water-Soluble, Deep-Cavity Cavitands Assemble via the Hydrophobic Effect. *J. Am. Chem. Soc.* **2008**, *130*, 14430−14431.

(134) Gibb, C. L. D.; Gibb, B. C. Templated Assembly of Water-Soluble Nano-Capsules: Inter-Phase Sequestration, Storage, and Separation of Hydrocarbon Gases. *J. Am. Chem. Soc.* **2006**, *128*, 16498−16499.

(135) Liu, S.; Russell, D. H.; Zinnel, N. F.; Gibb, B. C. Guest Packing Motifs within a Supramolecular Nanocapsule and a Covalent Analogue. *J. Am. Chem. Soc.* **2013**, *135*, 4314−4324.

(136) Yoshizawa, M.; Catti, L. Bent Anthracene Dimers as Versatile Building Blocks for Supramolecular Capsules. *Acc. Chem. Res.* **2019**, *52*, 2392−2404.

(137) Fujita, M.; Ibukuro, F.; Hagihara, H.; Ogura, K. Quantitative Self-Assembly of a [2]Catenane from Two Preformed Molecular Rings. *Nature* **1994**, *367*, 720−723.

(138) Hori, A.; Akasaka, A.; Biradha, K.; Sakamoto, S.; Yamaguchi, K.; Fujita, M. Chirality Induction through the Reversible Catenation of Coordination Rings. *Angew. Chem., Int. Ed.* **2002**, *41*, 3269−3272.

(139) Fujita, M.; Fujita, N.; Ogura, K.; Yamaguchi, K. Spontaneous Assembly of Ten Components into Two Interlocked, Identical Coordination Cages. *Nature* **1999**, *400*, 52−55.

(140) Cullen, W.; Hunter, C. A.; Ward, M. D. An Interconverting Family of Coordination Cages and a Meso-Helicate; Effects of Temperature, Concentration, and Solvent on the Product Distribution of a Self-Assembly Process. *Inorg. Chem.* **2015**, *54*, 2626−2637.

(141) Hof, F.; Craig, S. L.; Nuckolls, C.; Rebek, J. Molecular Encapsulation. *Angew. Chem., Int. Ed.* **2002**, *41*, 1488−1508.

(142) Pluth, M. D.; Raymond, K. N. Reversible Guest Exchange Mechanisms in Supramolecular Host-Guest Assemblies. *Chem. Soc. Rev.* **2007**, *36*, 161−171.

(143) Schneider, H.-J. Binding Mechanisms in Supramolecular Complexes. *Angew. Chem., Int. Ed.* **2009**, *48*, 3924−3977.

(144) Schmuck, C. Guest Encapsulation within Self-Assembled Molecular Containers. *Angew. Chem., Int. Ed.* **2007**, *46*, 5830−5833.

(145) Mecozzi, S.; Rebek, J., Jr. The 55% Solution: A Formula for Molecular Recognition in the Liquid State. *Chem. - Eur. J.* **1998**, *4*, 1016−1022.

(146) Biedermann, F.; Nau, W. M.; Schneider, H.-J. The Hydrophobic Effect Revisited—Studies with Supramolecular Complexes Imply High-Energy Water as a Noncovalent Driving Force. *Angew. Chem., Int. Ed.* **2014**, *53*, 11158−11171.

(147) Biedermann, F.; Uzunova, V. D.; Scherman, O. A.; Nau, W. M.; De Simone, A. Release of High-Energy Water as an Essential Driving Force for the High-Affinity Binding of Cucurbit[n]urils. *J. Am. Chem. Soc.* **2012**, *134*, 15318−15323.

(148) Biedermann, F.; Schneider, H.-J. Experimental Binding Energies in Supramolecular Complexes. *Chem. Rev.* **2016**, *116*, 5216−5300.

(149) Yoshizawa, M.; Kusukawa, T.; Kawano, M.; Ohhara, T.; Tanaka, I.; Kurihara, K.; Niimura, N.; Fujita, M. Endohedral Clusterization of Ten Water Molecules into a "Molecular Ice" within the Hydrophobic Pocket of a Self-Assembled Cage. *J. Am. Chem. Soc.* **2005**, *127*, 2798−2799.

(150) Metherell, A. J.; Cullen, W.; Williams, N. H.; Ward, M. D. Binding of Hydrophobic Guests in a Coordination Cage Cavity Is Driven by Liberation of "High-Energy" Water. *Chem. - Eur. J.* **2018**, *24*, 1554−1560.

(151) Jungwirth, P.; Cremer, P. S. Beyond Hofmeister. *Nat. Chem.* **2014**, *6*, 261−263.

(152) Zhang, Y. J.; Cremer, P. S. The Inverse and Direct Hofmeister Series for Lysozyme. *Proc. Natl. Acad. Sci. U. S. A.* **2009**, *106*, 15249−15253.

(153) Assaf, K. I.; Nau, W. M. The Chaotropic Effect as an Assembly Motif in Chemistry. *Angew. Chem., Int. Ed.* **2018**, *57*, 13968−13981.

(154) Jordan, J. H.; Gibb, C. L. D.; Wishard, A.; Pham, T.; Gibb, B. C. Ion-Hydrocarbon and/or Ion-Ion Interactions: Direct and Reverse Hofmeister Effects in a Synthetic Host. *J. Am. Chem. Soc.* **2018**, *140*, 4092−4099.

(155) Yoshizawa, M.; Tamura, M.; Fujita, M. AND/OR Bimolecular Recognition. *J. Am. Chem. Soc.* **2004**, *126*, 6846−6847.

(156) Fox, O. D.; Leung, J. F. Y.; Hunter, J. M.; Dalley, N. K.; Harrison, R. G. Metal-Assembled Cobalt(II) Resorc[4]Arene-Based Cage Molecules That Reversibly Capture Organic Molecules from Water and Act as NMR Shift Reagents. *Inorg. Chem.* **2000**, *39*, 783−790.

(157) Harrison, R. G.; Burrows, J. L.; Hansen, L. D. Selective Guest Encapsulation by a Cobalt-Assembled Cage Molecule. *Chem. - Eur. J.* **2005**, *11*, 5881−5888.

(158) Biros, S. M.; Bergman, R. G.; Raymond, K. N. The Hydrophobic Effect Drives the Recognition of Hydrocarbons by an Anionic Metal-Ligand Cluster. *J. Am. Chem. Soc.* **2007**, *129*, 12094−12095.

(159) Clegg, J. K.; Cremers, J.; Hogben, A. J.; Breiner, B.; Smulders, M. M. J.; Thoburn, J. D.; Nitschke, J. R. A Stimuli Responsive System of Self-Assembled Anion-Binding Fe$_4$L$_6$$^{8+}$ Cages. *Chem. Sci.* **2013**, *4*, 68−76.

(160) Ronson, T. K.; Giri, C.; Kodiah Beyeh, N.; Minkkinen, A.; Topić, F.; Holstein, J. J.; Rissanen, K.; Nitschke, J. R. Size-Selective Encapsulation of Hydrophobic Guests by Self-Assembled M$_4$L$_6$ Cobalt and Nickel Cages. *Chem. - Eur. J.* **2013**, *19*, 3374−3382.

(161) Smulders, M. M. J.; Zarra, S.; Nitschke, J. R. Quantitative Understanding of Guest Binding Enables the Design of Complex Host-Guest Behavior. *J. Am. Chem. Soc.* **2013**, *135*, 7039−7046.

(162) Riddell, I. A.; Smulders, M. M. J.; Clegg, J. K.; Nitschke, J. R. Encapsulation, Storage and Controlled Release of Sulfur Hexafluoride from a Metal-Organic Capsule. *Chem. Commun.* **2011**, *47*, 457−459.

(163) Roukala, J.; Zhu, J.; Giri, C.; Rissanen, K.; Lantto, P.; Telkki, V. V. Encapsulation of Xenon by a Self-Assembled Fe$_4$L$_6$ Metallosupramolecular Cage. *J. Am. Chem. Soc.* **2015**, *137*, 2464−2467.

(164) Du, K.; Zemerov, S. D.; Hurtado Parra, S.; Kikkawa, J. M.; Dmochowski, I. J. Paramagnetic Organocobalt Capsule Revealing Xenon Host-Guest Chemistry. *Inorg. Chem.* **2020**, *59*, 13831−13844.

(165) Mal, P.; Breiner, B.; Rissanen, K.; Nitschke, J. R. White Phosphorus Is Air-Stable within a Self-Assembled Tetrahedral Capsule. *Science* **2009**, *324*, 1697−1700.

(166) Bolliger, J. L.; Ronson, T. K.; Ogawa, M.; Nitschke, J. R. Solvent Effects upon Guest Binding and Dynamics of a Fe^{II}$_4$L$_4$ Cage. *J. Am. Chem. Soc.* **2014**, *136*, 14545−14553.

(167) Whitehead, M.; Turega, S.; Stephenson, A.; Hunter, C. A.; Ward, M. D. Quantification of Solvent Effects on Molecular Recognition in Polyhedral Coordination Cage Hosts. *Chem. Sci.* **2013**, *4*, 2744−2751.

(168) Turega, S.; Cullen, W.; Whitehead, M.; Hunter, C. A.; Ward, M. D. Mapping the Internal Recognition Surface of an Octanuclear Coordination Cage Using Guest Libraries. *J. Am. Chem. Soc.* **2014**, *136*, 8475−8483.

(169) Cullen, W.; Thomas, K. A.; Hunter, C. A.; Ward, M. D. pH-Controlled Selection between One of Three Guests from a Mixture Using a Coordination Cage Host. *Chem. Sci.* **2015**, *6*, 4025−4028.

(170) Cullen, W.; Turega, S.; Hunter, C. A.; Ward, M. D. pH-Dependent Binding of Guests in the Cavity of a Polyhedral Coordination Cage: Reversible Uptake and Release of Drug Molecules. *Chem. Sci.* **2015**, *6*, 625−631.

(171) Taylor, C. G. P.; Argent, S. P.; Ludden, M. D.; Piper, J. R.; Mozaceanu, C.; Barnett, S. A.; Ward, M. D. One Guest or Two? A Crystallographic and Solution Study of Guest Binding in a Cubic Coordination Cage. *Chem. - Eur. J.* **2020**, *26*, 3054−3064.

(172) Kim, T. Y.; Digal, L.; Gardiner, M. G.; Lucas, N. T.; Crowley, J. D. Octahedral [Pd$_6$L$_8$]$^{12+}$ Metallosupramolecular Cages: Synthesis, Structures and Guest-Encapsulation Studies. *Chem. - Eur. J.* **2017**, *23*, 15089−15097.

(173) Galan, A.; Ballester, P. Stabilization of Reactive Species by Supramolecular Encapsulation. *Chem. Soc. Rev.* **2016**, *45*, 1720−1737.

(174) Rizzuto, F. J.; von Krbek, L. K. S.; Nitschke, J. R. Strategies for Binding Multiple Guests in Metal-Organic Cages. *Nat. Rev. Chem.* **2019**, *3*, 204−222.

(175) Smulders, M. M. J.; Nitschke, J. R. Supramolecular Control over Diels-Alder Reactivity by Encapsulation and Competitive Displacement. *Chem. Sci.* **2012**, *3*, 785−788.

(176) Yoshizawa, M.; Kusukawa, T.; Fujita, M.; Yamaguchi, K. Ship-in-a-Bottle Synthesis of Otherwise Labile Cyclic Trimers of Siloxanes in a Self-Assembled Coordination Cage. *J. Am. Chem. Soc.* **2000**, *122*, 6311−6312.

(177) Furusawa, T.; Kawano, M.; Fujita, M. The Confined Cavity of a Coordination Cage Suppresses the Photocleavage of α-Diketones to Give Cyclization Products through Kinetically Unfavorable Pathways. *Angew. Chem., Int. Ed.* **2007**, *46*, 5717−5719.

(178) Horiuchi, S.; Murase, T.; Fujita, M. Noncovalent Trapping and Stabilization of Dinuclear Ruthenium Complexes within a Coordination Cage. *J. Am. Chem. Soc.* **2011**, *133*, 12445−12447.

(179) Takezawa, H.; Akiba, S.; Murase, T.; Fujita, M. Cavity-Directed Chromism of Phthalein Dyes. *J. Am. Chem. Soc.* **2015**, *137*, 7043−7046.

(180) Samanta, D.; Gemen, J.; Chu, Z.; Diskin-Posner, Y.; Shimon, L. J. W.; Klajn, R. Reversible Photoswitching of Encapsulated Azobenzenes in Water. *Proc. Natl. Acad. Sci. U. S. A.* **2018**, *115*, 9379−9384.

(181) Samanta, D.; Galaktionova, D.; Gemen, J.; Shimon, L. J. W.; Diskin-Posner, Y.; Avram, L.; Král, P.; Klajn, R. Reversible Chromism of Spiropyran in the Cavity of a Flexible Coordination Cage. *Nat. Commun.* **2018**, *9*, 641.

(182) Samanta, D.; Mukherjee, S.; Patil, Y. P.; Mukherjee, P. S. Self-Assembled Pd$_6$ Open Cage with Triimidazole Walls and the Use of Its Confined Nanospace for Catalytic Knoevenagel- and Diels-Alder

Reactions in Aqueous Medium. *Chem. - Eur. J.* **2012**, *18*, 12322−12329.

(183) Howlader, P.; Mondal, B.; Purba, P. C.; Zangrando, E.; Mukherjee, P. S. Self-Assembled Pd(II) Barrels as Containers for Transient Merocyanine Form and Reverse Thermochromism of Spiropyran. *J. Am. Chem. Soc.* **2018**, *140*, 7952−7960.

(184) Saha, R.; Devaraj, A.; Bhattacharyya, S.; Das, S.; Zangrando, E.; Mukherjee, P. S. Unusual Behavior of Donor-Acceptor Stenhouse Adducts in Confined Space of a Water-Soluble Pd^{II}$_8$ Molecular Vessel. *J. Am. Chem. Soc.* **2019**, *141*, 8638−8645.

(185) Li, K.; Zhang, L. Y.; Yan, C.; Wei, S. C.; Pan, M.; Zhang, L.; Su, C. Y. Stepwise Assembly of Pd$_6$(RuL$_3$)$_8$ Nanoscale Rhombododecahedral Metal-Organic Cages via Metalloligand Strategy for Guest Trapping and Protection. *J. Am. Chem. Soc.* **2014**, *136*, 4456−4459.

(186) Wu, K.; Li, K.; Hou, Y. J.; Pan, M.; Zhang, L. Y.; Chen, L.; Su, C. Y. Homochiral D_4-Symmetric Metal-Organic Cages from Stereogenic Ru(II) Metalloligands for Effective Enantioseparation of Atropisomeric Molecules. *Nat. Commun.* **2016**, *7*, 10487.

(187) Hou, Y.-J.; Wu, K.; Wei, Z.-W.; Li, K.; Lu, Y.-L.; Zhu, C.-Y.; Wang, J.-S.; Pan, M.; Jiang, J.-J.; Li, G.-Q.; Su, C.-Y. Design and Enantioresolution of Homochiral Fe(II)-Pd(II) Coordination Cages from Stereolabile Metalloligands: Stereochemical Stability and Enantioselective Separation. *J. Am. Chem. Soc.* **2018**, *140*, 18183−18191.

(188) Yamashina, M.; Matsuno, S.; Sei, Y.; Akita, M.; Yoshizawa, M. Recognition of Multiple Methyl Groups on Aromatic Rings by a Polyaromatic Cavity. *Chem. - Eur. J.* **2016**, *22*, 14147−14150.

(189) Matsuno, S.; Yamashina, M.; Sei, Y.; Akita, M.; Kuzume, A.; Yamamoto, K.; Yoshizawa, M. Exact Mass Analysis of Sulfur Clusters upon Encapsulation by a Polyaromatic Capsular Matrix. *Nat. Commun.* **2017**, *8*, 749.

(190) Yamashina, M.; Akita, M.; Hasegawa, T.; Hayashi, S.; Yoshizawa, M. A Polyaromatic Nanocapsule as a Sucrose Receptor in Water. *Sci. Adv.* **2017**, *3*, No. e1701126.

(191) Kusaba, S.; Yamashina, M.; Akita, M.; Kikuchi, T.; Yoshizawa, M. Hydrophilic Oligo(Lactic Acid)s Captured by a Hydrophobic Polyaromatic Cavity in Water. *Angew. Chem., Int. Ed.* **2018**, *57*, 3706−3710.

(192) Yamashina, M.; Kusaba, S.; Akita, M.; Kikuchi, T.; Yoshizawa, M. Cramming versus Threading of Long Amphiphilic Oligomers into a Polyaromatic Capsule. *Nat. Commun.* **2018**, *9*, 4227.

(193) Niki, K.; Tsutsui, T.; Yamashina, M.; Akita, M.; Yoshizawa, M. Recognition and Stabilization of Unsaturated Fatty Acids by a Polyaromatic Receptor. *Angew. Chem., Int. Ed.* **2020**, *59*, 10489−10492.

(194) Yamashina, M.; Sartin, M. M.; Sei, Y.; Akita, M.; Takeuchi, S.; Tahara, T.; Yoshizawa, M. Preparation of Highly Fluorescent Host-Guest Complexes with Tunable Color upon Encapsulation. *J. Am. Chem. Soc.* **2015**, *137*, 9266−9269.

(195) Klosterman, J. K.; Yamauchi, Y.; Fujita, M. Engineering Discrete Stacks of Aromatic Molecules. *Chem. Soc. Rev.* **2009**, *38*, 1714−1725.

(196) Ono, K.; Klosterman, J. K.; Yoshizawa, M.; Sekiguchi, K.; Tahara, T.; Fujita, M. ON/OFF Red Emission from Azaporphine in a Coordination Cage in Water. *J. Am. Chem. Soc.* **2009**, *131*, 12526−12527.

(197) Murase, T.; Otsuka, K.; Fujita, M. Pairwise Selective Formation of Aromatic Stacks in a Coordination Cage. *J. Am. Chem. Soc.* **2010**, *132*, 7864−7865.

(198) Osuga, T.; Murase, T.; Fujita, M. Triple-Decker Au$_3$-Ag-Au$_3$-Ag-Au$_3$ Ion Cluster Enclosed in a Self-Assembled Cage. *Angew. Chem., Int. Ed.* **2012**, *51*, 12199−12201.

(199) Sawada, T.; Yoshizawa, M.; Sato, S.; Fujita, M. Minimal Nucleotide Duplex Formation in Water through Enclathration in Self-Assembled Hosts. *Nat. Chem.* **2009**, *1*, 53−56.

(200) Dong, V. M.; Fiedler, D.; Carl, B.; Bergman, R. G.; Raymond, K. N. Molecular Recognition and Stabilization of Iminium Ions in Water. *J. Am. Chem. Soc.* **2006**, *128*, 14464−14465.

(201) Pluth, M. D.; Bergman, R. G.; Raymond, K. N. Making Amines Strong Bases: Thermodynamic Stabilization of Protonated Guests in a Highly-Charged Supramolecular Host. *J. Am. Chem. Soc.* **2007**, *129*, 11459−11467.

(202) Fiedler, D.; Bergman, R. G.; Raymond, K. N. Stabilization of Reactive Organometallic Intermediates inside a Self-Assembled Nanoscale Host. *Angew. Chem., Int. Ed.* **2006**, *45*, 745−748.

(203) Tiedemann, B. E. F.; Raymond, K. N. Dangling Arms: A Tetrahedral Supramolecular Host with Partially Encapsulated Guests. *Angew. Chem., Int. Ed.* **2006**, *45*, 83−86.

(204) Sgarlata, C.; Mugridge, J. S.; Pluth, M. D.; Tiedemann, B. E. F.; Zito, V.; Arena, G.; Raymond, K. N. External and Internal Guest Binding of a Highly Charged Supramolecular Host in Water: Deconvoluting the Very Different Thermodynamics. *J. Am. Chem. Soc.* **2010**, *132*, 1005−1009.

(205) Sgarlata, C.; Mugridge, J. S.; Pluth, M. D.; Zito, V.; Arena, G.; Raymond, K. N. Different and Often Opposing Forces Drive the Encapsulation and Multiple Exterior Binding of Charged Guests to a M_4L_6 Supramolecular Vessel in Water. *Chem. - Eur. J.* **2017**, *23*, 16813−16818.

(206) Zarra, S.; Smulders, M. M. J.; Lefebvre, Q.; Clegg, J. K.; Nitschke, J. R. Guanidinium Binding Modulates Guest Exchange within an $[M_4L_6]$ Capsule. *Angew. Chem., Int. Ed.* **2012**, *51*, 6882−6885.

(207) Kubik, S. Anion Recognition in Water. *Chem. Soc. Rev.* **2010**, *39*, 3648−3663.

(208) Gale, P. A.; Howe, E. N. W.; Wu, X. Anion Receptor Chemistry. *Chem.* **2016**, *1*, 351−422.

(209) Busschaert, N.; Caltagirone, C.; Van Rossom, W.; Gale, P. A. Applications of Supramolecular Anion Recognition. *Chem. Rev.* **2015**, *115*, 8038−8155.

(210) Liu, Y.; Sengupta, A.; Raghavachari, K.; Flood, A. H. Anion Binding in Solution: Beyond the Electrostatic Regime. *Chem.* **2017**, *3*, 411−427.

(211) Custelcean, R. Anion Encapsulation and Dynamics in Self-Assembled Coordination Cages. *Chem. Soc. Rev.* **2014**, *43*, 1813−1824.

(212) Langton, M. J.; Serpell, C. J.; Beer, P. D. Anion Recognition in Water: Recent Advances from a Supramolecular and Macromolecular Perspective. *Angew. Chem., Int. Ed.* **2016**, *55*, 1974−1987.

(213) Rice, C. R.; Slater, C.; Faulkner, R. A.; Allan, R. L. Self-Assembly of an Anion-Binding Cryptand for the Selective Encapsulation, Sequestration, and Precipitation of Phosphate from Aqueous Systems. *Angew. Chem., Int. Ed.* **2018**, *57*, 13071−13075.

(214) Custelcean, R.; Bosano, J.; Bonnesen, P. V.; Kertesz, V.; Hay, B. P. Computer-Aided Design of a Sulfate-Encapsulating Receptor. *Angew. Chem., Int. Ed.* **2009**, *48*, 4025−4029.

(215) Martrell, A. E.; Smith, R. M. *Critical Stability Constants*; Springer: New York, 1982.

(216) Custelcean, R.; Bonnesen, P. V.; Duncan, N. C.; Zhang, X.; Watson, L. A.; Van Berkel, G.; Parson, W. B.; Hay, B. P. Urea-Functionalized M_4L_6 Cage Receptors: Anion-Templated Self-Assembly and Selective Guest Exchange in Aqueous Solutions. *J. Am. Chem. Soc.* **2012**, *134*, 8525−8534.

(217) Yi, S.; Brega, V.; Captain, B.; Kaifer, A. E. Sulfate-Templated Self-Assembly of New M_4L_6 Tetrahedral Metal Organic Cages. *Chem. Commun.* **2012**, *48*, 10295−10297.

(218) Zhang, D.; Ronson, T. K.; Mosquera, J.; Martinez, A.; Guy, L.; Nitschke, J. R. Anion Binding in Water Drives Structural Adaptation in an Azaphosphatrane-Functionalized $Fe^{II}_4L_4$ Tetrahedron. *J. Am. Chem. Soc.* **2017**, *139*, 6574−6577.

(219) Zhang, D.; Ronson, T. K.; Mosquera, J.; Martinez, A.; Nitschke, J. R. Selective Anion Extraction and Recovery Using a $Fe^{II}_4L_4$ Cage. *Angew. Chem., Int. Ed.* **2018**, *57*, 3717−3721.

(220) Plajer, A. J.; Percástegui, E. G.; Santella, M.; Rizzuto, F. J.; Gan, Q.; Laursen, B. W.; Nitschke, J. R. Fluorometric Recognition of Nucleotides within a Water-Soluble Tetrahedral Capsule. *Angew. Chem., Int. Ed.* **2019**, *58*, 4200−4204.

(221) Wang, W.; Wang, Y. X.; Yang, H. B. Supramolecular Transformations within Discrete Coordination-Driven Supramolecular Architectures. *Chem. Soc. Rev.* **2016**, *45*, 2656−2693.

(222) Scherer, M.; Caulder, D. L.; Johnson, D. W.; Raymond, K. N. Triple Helicate—Tetrahedral Cluster Interconversion Controlled by Host-Guest Interactions. *Angew. Chem., Int. Ed.* **1999**, *38*, 1587−1592.

(223) Wang, S.; Sawada, T.; Ohara, K.; Yamaguchi, K.; Fujita, M. Capsule-Capsule Conversion by Guest Encapsulation. *Angew. Chem., Int. Ed.* **2016**, *55*, 2063−2066.

(224) Wang, S.; Sawada, T.; Fujita, M. Capsule-Bowl Conversion Triggered by a Guest Reaction. *Chem. Commun.* **2016**, *52*, 11653−11656.

(225) Casini, A.; Woods, B.; Wenzel, M. The Promise of Self-Assembled 3D Supramolecular Coordination Complexes for Biomedical Applications. *Inorg. Chem.* **2017**, *56*, 14715−14729.

(226) Kim, T. Y.; Vasdev, R. A. S.; Preston, D.; Crowley, J. D. Strategies for Reversible Guest Uptake and Release from Metallosupramolecular Architectures. *Chem. - Eur. J.* **2018**, *24*, 14878−14890.

(227) Mitragotri, S.; Burke, P.; Langer, R. Overcoming the Challenges in Administering Biopharmaceuticals: Formulation and Delivery Strategies. *Nat. Rev. Drug Discovery* **2014**, *13*, 655−672.

(228) Zhou, J.; Yu, G.; Huang, F. Supramolecular Chemotherapy Based on Host-Guest Molecular Recognition: A Novel Strategy in the Battle against Cancer with a Bright Future. *Chem. Soc. Rev.* **2017**, *46*, 7021−7053.

(229) Sepehrpour, H.; Fu, W.; Sun, Y.; Stang, P. J. Biomedically Relevant Self-Assembled Metallacycles and Metallacages. *J. Am. Chem. Soc.* **2019**, *141*, 14005−14020.

(230) Samanta, S. K.; Isaacs, L. Biomedical Applications of Metal Organic Polygons and Polyhedra (MOPs). *Coord. Chem. Rev.* **2020**, *410*, 213181.

(231) Yu, J.; Patel, S. A.; Dickson, R. M. In Vitro and Intracellular Production of Peptide-Encapsulated Fluorescent Silver Nanoclusters. *Angew. Chem., Int. Ed.* **2007**, *46*, 2028−2030.

(232) Horcajada, P.; Gref, R.; Baati, T.; Allan, P. K.; Maurin, G.; Couvreur, P.; Férey, G.; Morris, R. E.; Serre, C. Metal-Organic Frameworks in Biomedicine. *Chem. Rev.* **2012**, *112*, 1232−1268.

(233) Zhang, Z.; Sang, W.; Xie, L.; Dai, Y. Metal-Organic Frameworks for Multimodal Bioimaging and Synergistic Cancer Chemotherapy. *Coord. Chem. Rev.* **2019**, *399*, 213022.

(234) De coupade, C.; Fittipaldi, A.; Chagnas, V.; Michel, M.; Carlier, S.; Tasciotti, E.; Darmon, A.; Ravel, D.; Kearsey, J.; Giacca, M.; Cailler, F. Novel Human-Derived Cell-Penetrating Peptides for Specific Subcellular Delivery of Therapeutic Biomolecules. *Biochem. J.* **2005**, *390*, 407−418.

(235) Lindsay, M. A. Peptide-Mediated Cell Delivery: Application in Protein Target Validation. *Curr. Opin. Pharmacol.* **2002**, *2*, 587−594.

(236) Leroueil, P. R.; Hong, S. Y.; Mecke, A.; Baker, J. R.; Orr, B. G.; Banaszak Holl, M. M. Nanoparticle Interaction with Biological Membranes: Does Nanotechnology Present a Janus Face? *Acc. Chem. Res.* **2007**, *40*, 335−342.

(237) Fang, Y.; Lian, X.; Huang, Y.; Fu, G.; Xiao, Z.; Wang, Q.; Nan, B.; Pellois, J.-P.; Zhou, H.-C. Investigating Subcellular Compartment Targeting Effect of Porous Coordination Cages for Enhancing Cancer Nanotherapy. *Small* **2018**, *14*, 1802709.

(238) Therrien, B. Transporting and Shielding Photosensitisers by Using Water-Soluble Organometallic Cages: A New Strategy in Drug Delivery and Photodynamic Therapy. *Chem. - Eur. J.* **2013**, *19*, 8378−8386.

(239) Furrer, M. A.; Schmitt, F.; Wiederkehr, M.; Juillerat-Jeanneret, L.; Therrien, B. Cellular Delivery of Pyrenyl-Arene Ruthenium Complexes by a Water-Soluble Arene Ruthenium Metalla-Cage. *Dalton Trans.* **2012**, *41*, 7201−7211.

(240) Therrien, B.; Süss-Fink, G.; Govindaswamy, P.; Renfrew, A. K.; Dyson, P. J. The "Complex-in-a-Complex" Cations $[(acac)_2M \subset Ru_6-(p\text{-}iPrC_6H_4Me)_6(tpt)_2(dhbq)_3]^{6+}$: A Trojan Horse for Cancer Cells. *Angew. Chem., Int. Ed.* **2008**, *47*, 3773−3776.

(241) Yi, J. W.; Barry, N. P. E.; Furrer, M. A.; Zava, O.; Dyson, P. J.; Therrien, B.; Kim, B. H. Delivery of Floxuridine Derivatives to Cancer Cells by Water-Soluble Organometallic Cages. *Bioconjugate Chem.* **2012**, *23*, 461−471.

(242) Schmitt, F.; Freudenreich, J.; Barry, N. P. E.; Juillerat-Jeanneret, L.; Süss-Fink, G.; Therrien, B. Organometallic Cages as Vehicles for Intracellular Release of Photosensitizers. *J. Am. Chem. Soc.* **2012**, *134*, 754−757.

(243) Zhao, D.; Tan, S.; Yuan, D.; Lu, W.; Rezenom, Y. H.; Jiang, H.; Wang, L. Q.; Zhou, H. C. Surface Functionalization of Porous Coordination Nanocages via Click Chemistry and Their Application in Drug Delivery. *Adv. Mater.* **2011**, *23*, 90−93.

(244) Zheng, Y. R.; Suntharalingam, K.; Johnstone, T. C.; Lippard, S. J. Encapsulation of Pt(IV) Prodrugs within a Pt(II) Cage for Drug Delivery. *Chem. Sci.* **2015**, *6*, 1189−1193.

(245) Zheng, Y.-R.; Suntharalingam, K.; Bruno, P. M.; Lin, W.; Wang, W.; Hemann, M. T.; Lippard, S. J. Mechanistic Studies of the Anticancer Activity of an Octahedral Hexanuclear Pt(II) Cage. *Inorg. Chim. Acta* **2016**, *452*, 125−129.

(246) Yue, Z.; Wang, H.; Bowers, D. J.; Gao, M.; Stilgenbauer, M.; Nielsen, F.; Shelley, J. T.; Zheng, Y.-R. Nanoparticles of Metal-Organic Cages Designed to Encapsulate Platinum-Based Anticancer Agents. *Dalton Trans.* **2018**, *47*, 670−674.

(247) Roy, B.; Ghosh, A. K.; Srivastava, S.; D'Silva, P.; Mukherjee, P. S. A Pd$_8$ Tetrafacial Molecular Barrel as Carrier for Water Insoluble Fluorophore. *J. Am. Chem. Soc.* **2015**, *137*, 11916−11919.

(248) Bhat, I. A.; Jain, R.; Siddiqui, M. M.; Saini, D. K.; Mukherjee, P. S. Water-Soluble Pd$_8$L$_4$ Self-Assembled Molecular Barrel as an Aqueous Carrier for Hydrophobic Curcumin. *Inorg. Chem.* **2017**, *56*, 5352−5360.

(249) Samanta, S. K.; Moncelet, D.; Briken, V.; Isaacs, L. Metal-Organic Polyhedron Capped with Cucurbit[8]uril Delivers Doxorubicin to Cancer Cells. *J. Am. Chem. Soc.* **2016**, *138*, 14488−14496.

(250) Samanta, S. K.; Quigley, J.; Vinciguerra, B.; Briken, V.; Isaacs, L. Cucurbit[7]uril Enables Multi-Stimuli-Responsive Release from the Self-Assembled Hydrophobic Phase of a Metal Organic Polyhedron. *J. Am. Chem. Soc.* **2017**, *139*, 9066−9074.

(251) Samanta, S. K.; Moncelet, D.; Vinciguerra, B.; Briken, V.; Isaacs, L. Metal Organic Polyhedra: A Click-and-Clack Approach Toward Targeted Delivery. *Helv. Chim. Acta* **2018**, *101*, No. e1800057.

(252) Dong, J.; Pan, Y.; Wang, H.; Yang, K.; Liu, L.; Qiao, Z.; Yuan, Y. D.; Peh, S. B.; Zhang, J.; Shi, L.; Liang, H.; Han, Y.; Li, X.; Jiang, J.; Liu, B.; Zhao, D. Self-Assembly of Highly Stable Zirconium(IV) Coordination Cages with Aggregation Induced Emission Molecular Rotors for Live-Cell Imaging. *Angew. Chem., Int. Ed.* **2020**, *59*, 10151−10159.

(253) Burke, B. P.; Grantham, W.; Burke, M. J.; Nichol, G. S.; Roberts, D.; Renard, I.; Hargreaves, R.; Cawthorne, C.; Archibald, S. J.; Lusby, P. J. Visualizing Kinetically Robust Co$^{III}_4$L$_6$ Assemblies in Vivo: SPECT Imaging of the Encapsulated [^{99m}Tc]TcO$_4^-$ Anion. *J. Am. Chem. Soc.* **2018**, *140*, 16877−16881.

(254) Yamashina, M.; Tsutsui, T.; Sei, Y.; Akita, M.; Yoshizawa, M. A Polyaromatic Receptor with High Androgen Affinity. *Sci. Adv.* **2019**, *5*, No. eaav3179.

(255) Hatakeyama, Y.; Sawada, T.; Kawano, M.; Fujita, M. Conformational Preferences of Short Peptide Fragments. *Angew. Chem., Int. Ed.* **2009**, *48*, 8695−8698.

(256) Fujita, D.; Suzuki, K.; Sato, S.; Yagi-Utsumi, M.; Yamaguchi, Y.; Mizuno, N.; Kumasaka, T.; Takata, M.; Noda, M.; Uchiyama, S.; Kato, K.; Fujita, M. Protein Encapsulation within Synthetic Molecular Hosts. *Nat. Commun.* **2012**, *3*, 1093.

(257) Mosquera, J.; Szyszko, B.; Ho, S. K. Y.; Nitschke, J. R. Sequence-Selective Encapsulation and Protection of Long Peptides by a Self-Assembled Fe$^{II}_8$L$_6$ Cubic Cage. *Nat. Commun.* **2017**, *8*, 14882.

(258) Pazos, E.; Mosquera, J.; Vázquez, M. E.; Mascareñas, J. L. DNA Recognition by Synthetic Constructs. *ChemBioChem* **2011**, *12*, 1958−1973.

(259) Oleksi, A.; Blanco, A. G.; Boer, R.; Usón, I.; Aymamí, J.; Rodger, A.; Hannon, M. J.; Coll, M. Molecular Recognition of a Three-Way DNA Junction by a Metallosupramolecular Helicate. *Angew. Chem., Int. Ed.* **2006**, *45*, 1227−1231.

(260) Cardo, L.; Sadovnikova, V.; Phongtongpasuk, S.; Hodges, N. J.; Hannon, M. J. Arginine Conjugates of Metallo-Supramolecular Cylinders Prescribe Helicity and Enhance DNA Junction Binding and Cellular Activity. *Chem. Commun.* **2011**, *47*, 6575−6577.

(261) Howson, S.; Bolhuis, A.; Brabec, V.; Clarkson, G. J.; Malina, J.; Rodger, A.; Scott, P. Optically Pure, Water-Stable Metallo-Helical 'Flexicate' Assemblies with Antibiotic Activity. *Nat. Chem.* **2012**, *4*, 31−36.

(262) Brabec, V.; Howson, S. E.; Kaner, R. A.; Lord, R. M.; Malina, J.; Phillips, R. M.; Abdallah, Q. M. A.; McGowan, P. C.; Rodger, A.; Scott, P. Metallohelices with Activity against Cisplatin-Resistant Cancer Cells; Does the Mechanism Involve DNA binding? *Chem. Sci.* **2013**, *4*, 4407−4416.

(263) Zhao, A.; Howson, S. E.; Zhao, C.; Ren, J.; Scott, P.; Wang, C.; Qu, X. Chiral Metallohelices Enantioselectively Target Hybrid Human Telomeric G-Quadruplex DNA. *Nucleic Acids Res.* **2017**, *45*, 5026−5035.

(264) Zhao, C.; Song, H.; Scott, P.; Zhao, A.; Tateishi-Karimata, H.; Sugimoto, N.; Ren, J.; Qu, X. Mirror-Image Dependence: Targeting Enantiomeric G-Quadruplex DNA Using Triplex Metallohelices. *Angew. Chem., Int. Ed.* **2018**, *57*, 15723−15727.

(265) Xi, S.-F.; Bao, L.-Y.; Lin, J.-G.; Liu, Q.-Z.; Qiu, L.; Zhang, F.-L.; Wang, Y.-X.; Ding, Z.-D.; Li, K.; Gu, Z.-G. Enantiomers of Tetrahedral Metal-Organic Cages: A New Class of Highly Efficient G-Quadruplex Ligands with Potential Anticancer Activities. *Chem. Commun.* **2016**, *52*, 10261−10264.

(266) Xi, S.-F.; Bao, L.-Y.; Xu, Z.-L.; Wang, Y.-X.; Ding, Z.-D.; Gu, Z.-G. Enhanced Stabilization of G-Quadruplex DNA by [Ni$_4$L$_6$]$^{8+}$ Cages with Large Rigid Aromatic Ligands. *Eur. J. Inorg. Chem.* **2017**, 3533−3541.

(267) Zhu, J.; Haynes, C. J. E.; Kieffer, M.; Greenfield, J. L.; Greenhalgh, R. D.; Nitschke, J. R.; Keyser, U. F. Fe$^{II}_4$L$_4$ Tetrahedron Binds to Nonpaired DNA Bases. *J. Am. Chem. Soc.* **2019**, *141*, 11358−11362.

(268) Dong, Z.; Luo, Q.; Liu, J. Artificial Enzymes Based on Supramolecular Scaffolds. *Chem. Soc. Rev.* **2012**, *41*, 7890−7908.

(269) Pauling, L. Nature of Forces between Large Molecules of Biological Interest. *Nature* **1948**, *161*, 707−709.

(270) Zhang, X.; Houk, K. N. Why Enzymes Are Proficient Catalysts: Beyond the Pauling Paradigm. *Acc. Chem. Res.* **2005**, *38*, 379−385.

(271) Raynal, M.; Ballester, P.; Vidal-Ferran, A.; Van Leeuwen, P. W. N. M. Supramolecular Catalysis. Part 2: Artificial Enzyme Mimics. *Chem. Soc. Rev.* **2014**, *43*, 1734−1787.

(272) Hooley, R. J. Taking on the Turnover Challenge. *Nat. Chem.* **2016**, *8*, 202−204.

(273) Kaphan, D. M.; Levin, M. D.; Bergman, R. G.; Raymond, K. N.; Toste, F. D. A Supramolecular Microenvironment Strategy for Transition Metal Catalysis. *Science* **2015**, *350*, 1235−1238.

(274) Wang, Z. J.; Clary, K. N.; Bergman, R. G.; Raymond, K. N.; Toste, F. D. A Supramolecular Approach to Combining Enzymatic and Transition Metal Catalysis. *Nat. Chem.* **2013**, *5*, 100−103.

(275) van Leeuwen, P. W. N. M.; Raynal, M. In *Supramolecular Chemistry in Water*; Wiley-VCH: Weinheim, Germany, 2019; Chapter 14.

(276) Ito, H.; Kusukawa, T.; Fujita, M. Wacker Oxidation in an Aqueous Phase through the Reverse Phase-Transfer Catalysis of a Self-Assembled Nanocage. *Chem. Lett.* **2000**, *29*, 598−599.

(277) Fuertes-Espinosa, C.; García-Simón, C.; Pujals, M.; Garcia-Borràs, M.; Gómez, L.; Parella, T.; Juanhuix, J.; Imaz, I.; Maspoch, D.; Costas, M.; et al. Supramolecular Fullerene Sponges as Catalytic Masks for Regioselective Functionalization of C$_{60}$. *Chem.* **2020**, *6*, 169−186.

(278) Severinsen, R. J.; Rowlands, G. J.; Plieger, P. G. Coordination Cages in Catalysis. *J. Inclusion Phenom. Macrocycl. Chem.* **2020**, *96*, 29−42.

(279) Tan, C.; Chu, D.; Tang, X.; Liu, Y.; Xuan, W.; Cui, Y. Supramolecular Coordination Cages for Asymmetric Catalysis. *Chem. - Eur. J.* **2019**, *25*, 662−672.

(280) Fang, Y.; Powell, J. A.; Li, E.; Wang, Q.; Perry, Z.; Kirchon, A.; Yang, X.; Xiao, Z.; Zhu, C.; Zhang, L.; Huang, F.; Zhou, H.-C. Catalytic Reactions within the Cavity of Coordination Cages. *Chem. Soc. Rev.* **2019**, *48*, 4707−4730.

(281) Sinha, I.; Mukherjee, P. S. Chemical Transformations in Confined Space of Coordination Architectures. *Inorg. Chem.* **2018**, *57*, 4205−4221.

(282) Raynal, M.; Ballester, P.; Vidal-Ferran, A.; Van Leeuwen, P. W. N. M. Supramolecular Catalysis. Part 1: Non-Covalent Interactions as a Tool for Building and Modifying Homogeneous Catalysts. *Chem. Soc. Rev.* **2014**, *43*, 1660−1733.

(283) Catti, L.; Zhang, Q.; Tiefenbacher, K. Advantages of Catalysis in Self-Assembled Molecular Capsules. *Chem. - Eur. J.* **2016**, *22*, 9060−9066.

(284) Wang, K.; Jordan, J.; Hu, X.-Y.; Wang, L. Supramolecular Strategies for Controlling Reactivity within Confined Nanospace. *Angew. Chem., Int. Ed.* **2020**, *59*, 13712−13721.

(285) Wiester, M. J.; Ulmann, P. A.; Mirkin, C. A. Enzyme Mimics Based upon Supramolecular Coordination Chemistry. *Angew. Chem., Int. Ed.* **2011**, *50*, 114−137.

(286) Murase, T.; Fujita, M. Pericyclic Reactions in an Aqueous Molecular Flask. *Chem. Rec.* **2010**, *10*, 342−347.

(287) Takezawa, H.; Kanda, T.; Nanjo, H.; Fujita, M. Site-Selective Functionalization of Linear Diterpenoids through U-Shaped Folding in a Confined Artificial Cavity. *J. Am. Chem. Soc.* **2019**, *141*, 5112−5115.

(288) Takezawa, H.; Shitozawa, K.; Fujita, M. Enhanced Reactivity of Twisted Amides inside a Molecular Cage. *Nat. Chem.* **2020**, *12*, 574−578.

(289) Kang, J.; Rebek, J. Acceleration of a Diels-Alder Reaction by a Self-Assembled Molecular Capsule. *Nature* **1997**, *385*, 50−52.

(290) Breslow, R. Biomimetic Chemistry and Artificial Enzymes: Catalysis by Design. *Acc. Chem. Res.* **1995**, *28*, 146−153.

(291) Leenders, S. H. A. M.; Gramage-Doria, R.; De Bruin, B.; Reek, J. N. H. Transition Metal Catalysis in Confined Spaces. *Chem. Soc. Rev.* **2015**, *44*, 433−448.

(292) Guzmán-Percástegui, E.; Hernández, D. J.; Castillo, I. Calix[8]arene Nanoreactor for Cu(I)-Catalysed C-S Coupling. *Chem. Commun.* **2016**, *52*, 3111−3114.

(293) Deraedt, C.; Astruc, D. Supramolecular Nanoreactors for Catalysis. *Coord. Chem. Rev.* **2016**, *324*, 106−122.

(294) Wang, Q. Q.; Gonell, S.; Leenders, S. H. A. M.; Dürr, M.; Ivanovic-Burmazovic, I.; Reek, J. N. H. Self-Assembled Nanospheres with Multiple Endohedral Binding Sites Pre-Organize Catalysts and Substrates for Highly Efficient Reactions. *Nat. Chem.* **2016**, *8*, 225−230.

(295) Martí-Centelles, V.; Spicer, R. L.; Lusby, P. J. Non-Covalent Allosteric Regulation of Capsule Catalysis. *Chem. Sci.* **2020**, *11*, 3236−3240.

(296) Jiao, J.; Li, Z.; Qiao, Z.; Li, X.; Liu, Y.; Dong, J.; Jiang, J.; Cui, Y. Design and Self-Assembly of Hexahedral Coordination Cages for Cascade Reactions. *Nat. Commun.* **2018**, *9*, 4423.

(297) Holloway, L. R.; Bogie, P. M.; Lyon, Y.; Ngai, C.; Miller, T. F.; Julian, R. R.; Hooley, R. J. Tandem Reactivity of a Self-Assembled Cage Catalyst with Endohedral Acid Groups. *J. Am. Chem. Soc.* **2018**, *140*, 8078−8081.

(298) Bogie, P. M.; Holloway, L. R.; Ngai, C.; Miller, T. F.; Grewal, D. K.; Hooley, R. J. A Self-Assembled Cage with Endohedral Acid Groups Both Catalyzes Substitution Reactions and Controls Their Molecularity. *Chem. - Eur. J.* **2019**, *25*, 10232−10238.

(299) Jiao, J.; Tan, C.; Li, Z.; Liu, Y.; Han, X.; Cui, Y. Design and Assembly of Chiral Coordination Cages for Asymmetric Sequential Reactions. *J. Am. Chem. Soc.* **2018**, *140*, 2251−2259.

(300) Fiedler, D.; Leung, D. H.; Bergman, R. G.; Raymond, K. N. Selective Molecular Recognition, C-H Bond Activation, and Catalysis in Nanoscale Reaction Vessels. *Acc. Chem. Res.* **2005**, *38*, 349−358.

(301) Hong, C. M.; Bergman, R. G.; Raymond, K. N.; Toste, F. D. Self-Assembled Tetrahedral Hosts as Supramolecular Catalysts. *Acc. Chem. Res.* **2018**, *51*, 2447−2455.

(302) Ward, M. D.; Hunter, C. A.; Williams, N. H. Coordination Cages Based on Bis(Pyrazolylpyridine) Ligands: Structures, Dynamic Behavior, Guest Binding, and Catalysis. *Acc. Chem. Res.* **2018**, *51*, 2073−2082.

(303) Yoshizawa, M.; Takeyama, Y.; Kusukawa, T.; Fujita, M. Cavity-Directed, Highly Stereoselective [2 + 2] Photodimerization of Olefins within Self-Assembled Coordination Cages. *Angew. Chem., Int. Ed.* **2002**, *41*, 1347−1349.

(304) Yoshizawa, M.; Takeyama, Y.; Okano, T.; Fujita, M. Cavity-Directed Synthesis within a Self-Assembled Coordination Cage: Highly Selective [2 + 2] Cross-Photodimerization of Olefins. *J. Am. Chem. Soc.* **2003**, *125*, 3243−3247.

(305) Yoshizawa, M.; Tamura, M.; Fujita, M. Diels-Alder in Aqueous Molecular Hosts: Unusual Regioselectivity and Efficient Catalysis. *Science* **2006**, *312*, 251−255.

(306) Nishioka, Y.; Yamaguchi, T.; Yoshizawa, M.; Fujita, M. Unusual [2 + 4] and [2 + 2] Cycloadditions of Arenes in the Confined Cavity of Self-Assembled Cages. *J. Am. Chem. Soc.* **2007**, *129*, 7000−7001.

(307) Horiuchi, S.; Murase, T.; Fujita, M. Diels-Alder Reactions of Inert Aromatic Compounds within a Self-Assembled Coordination Cage. *Chem. - Asian J.* **2011**, *6*, 1839−1847.

(308) Fang, Y.; Murase, T.; Fujita, M. Cavity-Promoted Diels-Alder Reactions of Unsubstituted Naphthalene: Fine Reactivity Tuning by Cavity Shrinkage. *Chem. Lett.* **2015**, *44*, 1095−1097.

(309) Horiuchi, S.; Nishioka, Y.; Murase, T.; Fujita, M. Both [2 + 2] and [2 + 4] Additions of Inert Aromatics via Identical Ternary Host-Guest Complexes. *Chem. Commun.* **2010**, *46*, 3460−3462.

(310) Yamaguchi, T.; Fujita, M. Highly Selective Photomediated 1,4-Radical Addition to *o*-Quinones Controlled by a Self-Assembled Cage. *Angew. Chem., Int. Ed.* **2008**, *47*, 2067−2069.

(311) Rétey, J. Enzymic Reaction Selectivity by Negative Catalysis or How Do Enzymes Deal with Highly Reactive Intermediates? *Angew. Chem., Int. Ed. Engl.* **1990**, *29*, 355−361.

(312) Yoshizawa, M.; Miyagi, S.; Kawano, M.; Ishiguro, K.; Fujita, M. Alkane Oxidation via Photochemical Excitation of a Self-Assembled Molecular Cage. *J. Am. Chem. Soc.* **2004**, *126*, 9172−9173.

(313) Murase, T.; Nishijima, Y.; Fujita, M. Unusual Photoreaction of Triquinacene within Self-Assembled Hosts. *Chem. - Asian J.* **2012**, *7*, 826−829.

(314) Murase, T.; Takezawa, H.; Fujita, M. Photo-Driven Anti-Markovnikov Alkyne Hydration in Self-Assembled Hollow Complexes. *Chem. Commun.* **2011**, *47*, 10960−10962.

(315) Cullen, W.; Takezawa, H.; Fujita, M. Demethylenation of Cyclopropanes via Photoinduced Guest-to-Host Electron Transfer in an M_6L_4 Cage. *Angew. Chem., Int. Ed.* **2019**, *58*, 9171−9173.

(316) Dalton, D. M.; Ellis, S. R.; Nichols, E. M.; Mathies, R. A.; Toste, F. D.; Bergman, R. G.; Raymond, K. N. Supramolecular $Ga_4L_6^{12-}$ Cage Photosensitizes 1,3-Rearrangement of Encapsulated Guest via Photoinduced Electron Transfer. *J. Am. Chem. Soc.* **2015**, *137*, 10128−10131.

(317) Guo, J.; Xu, Y. W.; Li, K.; Xiao, L. M.; Chen, S.; Wu, K.; Chen, X. D.; Fan, Y. Z.; Liu, J. M.; Su, C. Y. Regio- and Enantioselective Photodimerization within the Confined Space of a Homochiral Ruthenium/Palladium Heterometallic Coordination Cage. *Angew. Chem., Int. Ed.* **2017**, *56*, 3852−3856.

(318) Guo, J.; Fan, Y. Z.; Lu, Y. L.; Zheng, S. P.; Su, C. Y. Visible-Light Photocatalysis of Asymmetric [2 + 2] Cycloaddition in Cage-Confined Nanospace Merging Chirality with Triplet-State Photosensitization. *Angew. Chem., Int. Ed.* **2020**, *59*, 8661−8669.

(319) Horiuchi, S.; Murase, T.; Fujita, M. A Remarkable Organometallic Transformation on a Cage-Incarcerated Dinuclear Ruthenium Complex. *Angew. Chem., Int. Ed.* **2012**, *51*, 12029−12031.

(320) Fiedler, D.; Pagliero, D.; Brumaghim, J. L.; Bergman, R. G.; Raymond, K. N. Encapsulation of Cationic Ruthenium Complexes into a Chiral Self-Assembled Cage. *Inorg. Chem.* **2004**, *43*, 846−848.

(321) Leung, D. H.; Fiedler, D.; Bergman, R. G.; Raymond, K. N. Selective C-H Bond Activation by a Supramolecular Host-Guest Assembly. *Angew. Chem., Int. Ed.* **2004**, *43*, 963−966.

(322) Leung, D. H.; Bergman, R. G.; Raymond, K. N. Scope and Mechanism of the C-H Bond Activation Reactivity within a Supramolecular Host by an Iridium Guest: A Stepwise Ion Pair Guest Dissociation Mechanism. *J. Am. Chem. Soc.* **2006**, *128*, 9781−9797.

(323) Kohyama, Y.; Murase, T.; Fujita, M. Metal-Organic Proximity in a Synthetic Pocket. *J. Am. Chem. Soc.* **2014**, *136*, 2966−2969.

(324) Bender, T. A.; Morimoto, M.; Bergman, R. G.; Raymond, K. N.; Toste, F. D. Supramolecular Host-Selective Activation of Iodoarenes by Encapsulated Organometallics. *J. Am. Chem. Soc.* **2019**, *141*, 1701−1706.

(325) Yoshizawa, M.; Sato, N.; Fujita, M. Selective Enclathration of Linear Alkanols by a Self-Assembled Coordination Cage. Application to the Catalytic Wacker Oxidation of ω-Alkenols. *Chem. Lett.* **2005**, *34*, 1392−1393.

(326) Fiedler, D.; Bergman, R. G.; Raymond, K. N. Supramolecular Catalysis of a Unimolecular Transformation: Aza-Cope Rearrangement within a Self-Assembled Host. *Angew. Chem., Int. Ed.* **2004**, *43*, 6748−6751.

(327) Fiedler, D.; Van Halbeek, H.; Bergman, R. G.; Raymond, K. N. Supramolecular Catalysis of Unimolecular Rearrangements: Substrate Scope and Mechanistic Insights. *J. Am. Chem. Soc.* **2006**, *128*, 10240−10252.

(328) Hastings, C. J.; Fiedler, D.; Bergman, R. G.; Raymond, K. N. Aza Cope Rearrangement of Propargyl Enammonium Cations Catalyzed by a Self-Assembled "Nanozyme". *J. Am. Chem. Soc.* **2008**, *130*, 10977−10983.

(329) Brown, C. J.; Bergman, R. G.; Raymond, K. N. Enantioselective Catalysis of the Aza-Cope Rearrangement by a Chiral Supramolecular Assembly. *J. Am. Chem. Soc.* **2009**, *131*, 17530−17531.

(330) Pluth, M. D.; Bergman, R. G.; Raymond, K. N. Proton-Mediated Chemistry and Catalysis in a Self-Assembled Supramolecular Host. *Acc. Chem. Res.* **2009**, *42*, 1650−1659.

(331) Pluth, M. D.; Bergman, R. G.; Raymond, K. N. Acid Catalysis in Basic Solution: A Supramolecular Host Promotes Orthoformate Hydrolysis. *Science* **2007**, *316*, 85−88.

(332) Pluth, M. D.; Bergman, R. G.; Raymond, K. N. Supramolecular Catalysis of Orthoformate Hydrolysis in Basic Solution: An Enzyme-like Mechanism. *J. Am. Chem. Soc.* **2008**, *130*, 11423−11429.

(333) Pluth, M. D.; Bergman, R. G.; Raymond, K. N. The Acid Hydrolysis Mechanism of Acetals Catalyzed by a Supramolecular Assembly in Basic Solution. *J. Org. Chem.* **2009**, *74*, 58−63.

(334) Ha, N.-C.; Kim, M.-S.; Lee, W.; Choi, K. Y.; Oh, B.-H. Detection of Large pK_a Perturbations of an Inhibitor and a Catalytic Group at an Enzyme Active Site, a Mechanistic Basis for Catalytic Power of Many Enzymes. *J. Biol. Chem.* **2000**, *275*, 41100−41106.

(335) Száraz, S.; Oesterhelt, D.; Ormos, P. pH-Induced Structural Changes in Bacteriorhodopsin Studied by Fourier Transform Infrared Spectroscopy. *Biophys. J.* **1994**, *67*, 1706−1712.

(336) Westheimer, F. H. Coincidences, Decarboxylation, and Electrostatic Effects. *Tetrahedron* **1995**, *51*, 3−20.

(337) Hastings, C. J.; Pluth, M. D.; Bergman, R. G.; Raymond, K. N. Enzymelike Catalysis of the Nazarov Cyclization by Supramolecular Encapsulation. *J. Am. Chem. Soc.* **2010**, *132*, 6938−6940.

(338) Hastings, C. J.; Bergman, R. G.; Raymond, K. N. Origins of Large Rate Enhancements in the Nazarov Cyclization Catalyzed by Supramolecular Encapsulation. *Chem. - Eur. J.* **2014**, *20*, 3966−3973.

(339) Hart-Cooper, W. M.; Clary, K. N.; Toste, F. D.; Bergman, R. G.; Raymond, K. N. Selective Monoterpene-like Cyclization Reactions Achieved by Water Exclusion from Reactive Intermediates in a Supramolecular Catalyst. *J. Am. Chem. Soc.* **2012**, *134*, 17873−17876.

(340) Negoi, A.; Wuttke, S.; Kemnitz, E.; Macovei, D.; Parvulescu, V. I.; Teodorescu, C. M.; Coman, S. M. One-Pot Synthesis of Menthol Catalyzed by a Highly Diastereoselective Au/MgF₂ Catalyst. *Angew. Chem., Int. Ed.* **2010**, *49*, 8134−8138.

(341) da Silva, K. A.; Robles-Dutenhefner, P. A.; Sousa, E. M. B.; Kozhevnikova, E. F.; Kozhevnikov, I. V.; Gusevskaya, E. V. Cyclization of (+)-Citronellal to (−)-Isopulegol Catalyzed by H₃PW₁₂O₄₀/SiO₂. *Catal. Commun.* **2004**, *5*, 425−429.

(342) Zhao, C.; Sun, Q. F.; Hart-Cooper, W. M.; Dipasquale, A. G.; Toste, F. D.; Bergman, R. G.; Raymond, K. N. Chiral Amide Directed Assembly of a Diastereo- and Enantiopure Supramolecular Host and Its Application to Enantioselective Catalysis of Neutral Substrates. *J. Am. Chem. Soc.* **2013**, *135*, 18802−18805.

(343) Hart-Cooper, W. M.; Zhao, C.; Triano, R. M.; Yaghoubi, P.; Ozores, H. L.; Burford, K. N.; Toste, F. D.; Bergman, R. G.; Raymond, K. N. The Effect of Host Structure on the Selectivity and Mechanism of Supramolecular Catalysis of Prins Cyclizations. *Chem. Sci.* **2015**, *6*, 1383−1393.

(344) Kaphan, D. M.; Toste, F. D.; Bergman, R. G.; Raymond, K. N. Enabling New Modes of Reactivity via Constrictive Binding in a Supramolecular-Assembly-Catalyzed Aza-Prins Cyclization. *J. Am. Chem. Soc.* **2015**, *137*, 9202−9205.

(345) Bierschenk, S. M.; Bergman, R. G.; Raymond, K. N.; Toste, F. D. A Nanovessel-Catalyzed Three-Component Aza-Darzens Reaction. *J. Am. Chem. Soc.* **2020**, *142*, 733−737.

(346) Zhao, C.; Toste, F. D.; Raymond, K. N.; Bergman, R. G. Nucleophilic Substitution Catalyzed by a Supramolecular Cavity Proceeds with Retention of Absolute Stereochemistry. *J. Am. Chem. Soc.* **2014**, *136*, 14409−14412.

(347) Murase, T.; Nishijima, Y.; Fujita, M. Cage-Catalyzed Knoevenagel Condensation under Neutral Conditions in Water. *J. Am. Chem. Soc.* **2012**, *134*, 162−164.

(348) Samanta, D.; Mukherjee, P. S. Multicomponent Self-Sorting of a Pd₇ Molecular Boat and Its Use in Catalytic Knoevenagel Condensation. *Chem. Commun.* **2013**, *49*, 4307−4309.

(349) Bhat, I. A.; Devaraj, A.; Howlader, P.; Chi, K. W.; Mukherjee, P. S. Preparation of a Chiral Pt₁₂ Tetrahedral Cage and Its Use in Catalytic Michael Addition Reaction. *Chem. Commun.* **2018**, *54*, 4814−4817.

(350) Bhat, I. A.; Devaraj, A.; Zangrando, E.; Mukherjee, P. S. A Discrete Self-Assembled Pd₁₂ Triangular Orthobicupola Cage and Its Use for Intramolecular Cycloaddition. *Chem. - Eur. J.* **2018**, *24*, 13938−13946.

(351) Howlader, P.; Das, P.; Zangrando, E.; Mukherjee, P. S. Urea-Functionalized Self-Assembled Molecular Prism for Heterogeneous Catalysis in Water. *J. Am. Chem. Soc.* **2016**, *138*, 1668−1676.

(352) Howlader, P.; Mukherjee, P. S. Face and Edge Directed Self-Assembly of Pd₁₂ Tetrahedral Nano-Cages and Their Self-Sorting. *Chem. Sci.* **2016**, *7*, 5893−5899.

(353) Cullen, W.; Misuraca, M. C.; Hunter, C. A.; Williams, N. H.; Ward, M. D. Highly Efficient Catalysis of the Kemp Elimination in the Cavity of a Cubic Coordination Cage. *Nat. Chem.* **2016**, *8*, 231−236.

(354) Cullen, W.; Metherell, A. J.; Wragg, A. B.; Taylor, C. G. P.; Williams, N. H.; Ward, M. D. Catalysis in a Cationic Coordination Cage Using a Cavity-Bound Guest and Surface-Bound Anions: Inhibition, Activation, and Autocatalysis. *J. Am. Chem. Soc.* **2018**, *140*, 2821−2828.

(355) Taylor, C. G. P.; Metherell, A. J.; Argent, S. P.; Ashour, F. M.; Williams, N. H.; Ward, M. D. Coordination-Cage-Catalysed Hydrolysis of Organophosphates: Cavity- or Surface-Based? *Chem. - Eur. J.* **2020**, *26*, 3065−3073.

(356) Mozaceanu, C.; Taylor, C. G. P.; Piper, J. R.; Argent, S. P.; Ward, M. D. Catalysis of an Aldol Condensation Using a Coordination Cage. *Chemistry* **2020**, *2*, 22−32.

(357) Koblenz, T. S.; Wassenaar, J.; Reek, J. N. H. Reactivity within a Confined Self-Assembled Nanospace. *Chem. Soc. Rev.* **2008**, *37*, 247−262.

(358) Brown, C. J.; Miller, G. M.; Johnson, M. W.; Bergman, R. G.; Raymond, K. N. High-Turnover Supramolecular Catalysis by a

Protected Ruthenium(II) Complex in Aqueous Solution. *J. Am. Chem. Soc.* **2011**, *133*, 11964−11966.

(359) Leung, D. H.; Bergman, R. G.; Raymond, K. N. Highly Selective Supramolecular Catalyzed Allylic Alcohol Isomerization. *J. Am. Chem. Soc.* **2007**, *129*, 2746−2747.

(360) Bender, T. A.; Bergman, R. G.; Raymond, K. N.; Toste, F. D. A Supramolecular Strategy for Selective Catalytic Hydrogenation Independent of Remote Chain Length. *J. Am. Chem. Soc.* **2019**, *141*, 11806−11810.

(361) Otte, M.; Kuijpers, P. F.; Troeppner, O.; Ivanović-Burmazović, I.; Reek, J. N. H.; De Bruin, B. Encapsulation of Metalloporphyrins in a Self-Assembled Cubic M_8L_6 Cage: A New Molecular Flask for Cobalt-Porphyrin-Catalysed Radical-Type Reactions. *Chem. - Eur. J.* **2013**, *19*, 10170−10178.

(362) Otte, M.; Kuijpers, P. F.; Troeppner, O.; Ivanović-Burmazović, I.; Reek, J. N. H.; De Bruin, B. Encapsulated Cobalt-Porphyrin as a Catalyst for Size-Selective Radical-Type Cyclopropanation Reactions. *Chem. - Eur. J.* **2014**, *20*, 4880−4884.

(363) Kuijpers, P. F.; Otte, M.; Dürr, M.; Ivanović-Burmazović, I.; Reek, J. N. H.; De Bruin, B. A Self-Assembled Molecular Cage for Substrate-Selective Epoxidation Reactions in Aqueous Media. *ACS Catal.* **2016**, *6*, 3106−3112.

(364) Salles, A. G.; Zarra, S.; Turner, R. M.; Nitschke, J. R. A Self-Organizing Chemical Assembly Line. *J. Am. Chem. Soc.* **2013**, *135*, 19143−19146.

(365) Wang, Z. J.; Brown, C. J.; Bergman, R. G.; Raymond, K. N.; Toste, F. D. Hydroalkoxylation Catalyzed by a Gold(I) Complex Encapsulated in a Supramolecular Host. *J. Am. Chem. Soc.* **2011**, *133*, 7358−7360.

(366) Malay, A. D.; Miyazaki, N.; Biela, A.; Chakraborti, S.; Majsterkiewicz, K.; Stupka, I.; Kaplan, C. S.; Kowalczyk, A.; Piette, B. M. A. G.; Hochberg, G. K. A.; et al. An Ultra-Stable Gold-Coordinated Protein Cage Displaying Reversible Assembly. *Nature* **2019**, *569*, 438−442.

(367) Golub, E.; Subramanian, R. H.; Esselborn, J.; Alberstein, R. G.; Bailey, J. B.; Chiong, J. A.; Yan, X.; Booth, T.; Baker, T. S.; Tezcan, F. A. Constructing Protein Polyhedra via Orthogonal Chemical Interactions. *Nature* **2020**, *578*, 172−176.